5-2011

Roles of Non-thermal Plasma in Gas-phase Glycerol Dehydration Catalyzed by Supported Silicotungstic Acid

Lu Liu
lliu11@utk.edu

To the Graduate Council:

I am submitting herewith a dissertation written by Lu Liu entitled "Roles of Non-thermal Plasma in Gas-phase Glycerol Dehydration Catalyzed by Supported Silicotungstic Acid." I have examined the final electronic copy of this dissertation for form and content and recommend that it be accepted in partial fulfillment of the requirements for the degree of Doctor of Philosophy, with a major in Biosystems Engineering.

Xiaofei Ye, Major Professor

We have read this dissertation and recommend its acceptance:

Douglas G. Hayes, Joseph J. Bozell, Igor Alexeff

Accepted for the Council:
Dixie L. Thompson

Vice Provost and Dean of the Graduate School

(Original signatures are on file with official student records.)

To the Graduate Council:

I am submitting herewith a dissertation written by Lu Liu entitled “Roles of Non-thermal Plasma in Gas-phase Glycerol Dehydration Catalyzed by Supported Silicotungstic Acid” I have examined the final electronic copy of this dissertation for form and content and recommend that it be accepted in partial fulfillment of the requirements for the degree of Doctor of Philosophy, with a major in Biosystems Engineering.

Xiaofei P. Ye, Major Professor

We have read this dissertation
and recommend its acceptance:

Douglas G. Hayes

Joseph J. Bozell

Igor Alexeff

Accepted for the Council:

Carolyn R. Hodges

Vice Provost and Dean of the Graduate School

(Original Signatures are on file with official student records.)

Roles of Non-thermal Plasma in Gas-phase Glycerol Dehydration Catalyzed by Supported Silicotungstic Acid

A Dissertation Presented for
the Doctor of Philosophy
Degree
The University of Tennessee, Knoxville

Lu Liu
May 2011

Acknowledgements

I would like to thank my advisor, Dr. X. Philip Ye, who conceived and guided the research in this dissertation. Also, this dissertation would not have been completed without the valuable input from my committee members, Dr. Joseph Bozell, Dr. Douglas Hayes, and Dr. Igor Alexeff. I also wish to express my thanks to my lifelong friends, Dr. Leming Cheng, and Dr. Javier Gomez del Rio; without their companionship and continuous encouragement, I would not have been able to proceed this far. Most importantly, I feel a great appreciation to my parents and Brian; their understanding and support helped me maintain the strength to face and overcome the difficulties in the process of researching and writing this document.

To my family

Abstract

Acrolein is an indispensable chemical intermediate with a rising demand in recent years. The concern of the increase of propylene prices due to the shrinking supply of nonrenewable crude oil makes the acid-catalyzed gas-phase glycerol dehydration to acrolein a prime candidate for research. The analysis showed that the sustainable acrolein production from glycerol was both technically and economically viable. Alumina2700® (Al) and Silica1252® (Si) loaded with silicotungstic acid (HSiW) possessed distinct features while provided equally good acrolein yield (73.86mol% and 74.05mol%, respectively) optimally.

Due to the unique non-equilibrium characteristics, non-thermal plasma (NTP) could promote a variety of chemical reactions; however, its application in a dehydration process remained blank. This study used the reaction of glycerol dehydration to acrolein to probe whether NTP could 1) improve acrolein yield during dehydration, 2) suppress the coke formation and regenerate the catalyst, and 3) modify the properties of the catalyst.

The dielectric barrier discharge configuration was used to generate NTP; various NTP field strengths and also their interaction with temperature and the catalyst were investigated. The results showed that NTP improved the glycerol conversion and that NTP with a proper field strength increased acrolein selectivity. The optimal acrolein yields of 83.6 mol% and 83.1 mol% were achieved with 3.78 kV/cm NTP and 4.58 kV/cm NTP at 275°C for HSiW-Al and HSiW-Si, respectively.

The application of NTP-O_2 (5% oxygen in argon, 4.58 kV/cm) during glycerol dehydration significantly suppressed coke formation on HSiW-Si. NTP-O_2 could regenerate the deactivated HSiW-Si at low temperatures by removing both soft and hard coke at various rates. NTP-O_2 with higher field strength, at medium operation temperature (150ºC) and in argon atmosphere was more effective for coke removal/catalyst regeneration.

Applying NTP to the catalyst fabrication showed some capabilities in modifying catalyst properties, including enlarging surface area, preserving mesopores, increasing acid strength and Brønsted acidity. NTP with argon as the discharge gas performed better in these modifications than NTP with air as the discharge gas.

Table of Contents

List of Tables

List of Figures

Abbreviations (in alphabetical order)

Al	Alumina
Ar	Argon
BET	Brunauer-Emmett-Teller (surface area measurement method)
COA	Co-fed oxygen alone
DBD	Dielectric barrier discharge
FID	Flame ionization detector
FTIR	Fourier transform infrared spectroscopy
GC	Gas chromatography
GHSV	Gas-hourly-space-velocity
He	Helium
HPA	Heteropoly acid
HSiW	Silicotungstic acid
HSiW-Al	Alumina supported silicotungstic acid
HSiW-Si	Silica (1252) supported silicotungstic acid
LN	Liquid nitrogen
N_2	Nitrogen
NTP	Non-thermal plasma
NTP-O_2	Non-thermal plasma with oxygen-containing gas as the discharge gas
PID	Proportional–integral–derivative
PBR	Packed-bed reactor
Si	Silica
TCD	Thermal conductivity detector
TOS	Time-on-stream
TPD	Temperature programmed desorption
TS	Transition state
TPO	Temperature programmed oxidation
VOC	Volatile organic carbons
XRD	X-ray diffraction

Introduction

Non-thermal plasma (NTP) has unique features that have the capability to produce unconventional chemical processes. A variety of processes can only be activated or promoted by NTP. No one yet knows how far the frontiers of NTP chemistry can extend. NTP's application in the dehydration process remained unexplored, thus far. Therefore, it was worthwhile to make such an exploration, and possibly to pioneer research in this area.

Acrolein production via glycerol dehydration recently has attracted much attention due to overproduction of glycerol from biodiesel production. Acrolein is an important reactant or intermediate in many industrial applications; thus, there is an ever-growing demand for it, if it can be produced affordably. The dehydration process certainly has its merits, and possesses commercial and industrialization potential. The glycerol-based production of acrolein is a promising research direction, which also can ultimately boost a sustainable route of acrylic acid production.

Using glycerol dehydration to produce acrolein can also be used as a test case to probe the non-thermal plasma chemistry in the dehydration process. This was the solution to satisfying the research interests in both areas; hence this dissertation presents my contribution to both areas.

In Chapter 1, the background information is introduced concerning acrolein, including its chemical and physical properties, uses, and synthesis history. A comparatively review was made regarding petroleum-based acrolein production and the bio-based acrolein production from glycerol, justifying that there is a promising future for a process of glycerol conversion to acrolein.

In Chapter 2, non-thermal plasma is introduced, in both physical and chemical aspects. Plasma physics, such as how to generate NTP (in this study) and how to characterize NTP, are briefly covered. The recent progress in NTP application to chemical processes is also reviewed.

Chapter 3 explicates how the catalysts were finally selected to be used in the NTP-related study. Catalyst characterization and reaction kinetics are compared to evaluate what catalyst support that silicotungstic acid was loaded on provided a better catalytic performance in terms of glycerol dehydration.

Chapter 4 presents the kinetic study of glycerol dehydration conducted using the catalysts determined in Chapter 3. NTP was applied using argon as the discharge gas. The effects of temperature, the NTP application, and the interaction of the two that influenced the glycerol dehydration reaction are also discussed.

Chapter 5 presents the study of the possible roles of non-thermal oxygen plasma (NTP-O_2) in glycerol dehydration to acrolein. The problem of catalyst deactivation was the primary focus; NTP-O_2 was studied regarding the suppression of coke formation during the dehydration reaction and the regeneration of the deactivated catalyst.

Chapter 6 probes the feasibility of fabricating better acidic heterogeneous catalysts by integrating the NTP discharge during the catalyst fabrication. Of interest was how the catalyst properties and the kinetic performance of the fabricated catalysts would be different under the application of NTP discharge during fabrication.

The main conclusions obtained from this research are provided in Overall Summary. All the supplementary information and the associated calculations mentioned in the main text are provided in the appendices.

Chapter 1

A comparative review of petroleum-based and bio-based acrolein production

Abstract

Acrolein is an important chemical intermediate for many common industrial chemicals, leading to an array of useful end-products. This chapter comparatively reviews all the synthetic methods, including the former (aldol condensation) and contemporary (partial oxidation of propylene) manufacturing methods, the partial oxidation of propane, and most importantly, the bio-based glycerol-dehydration route. Emphasis is placed on the current manufacturing method from propylene and the bio-based route from glycerol, an abundantly available and relatively inexpensive raw material due to the biodiesel production. This review provides the technical details and addressees the incentives of industrialization, in the aim of justifying the transition towards the bio-based route.

Keywords: glycerol, dehydration, aldol condensation, propylene, propane, partial oxidation.

1.1 Introduction

1.1.1 Acrolein---an important and versatile chemical intermediate

Acrolein (IUPAC name: prop-2-enal), the simplest unsaturated aldehyde, is a colorless (or yellow) liquid (b.p. 53°C) at room temperature with a pungent and piercing odor. The conjugation of the carbonyl group with a vinyl group provides acrolein with a high degree of reactivity. As a necessary intermediate, acrolein is uniquely indispensable in the chemical industry. Acrolein is the starting material to produce acrylic acid and ester, glutaraldehyde, methionine, polyurethane and polyester resin (Figure 1-1).

It is worth emphasizing a couple of these chemicals with very high industrial value. Acrylic acid is a valuable chemical commodity with a lucrative market. The polymeric form of acrylic acid can be formulated into super-absorbant materials, such as diapers, hard plastic materials like acrylates, and paints and coatings. As one of the fastest growing commodity chemicals, acrylic acid is in increasingly higher demand every year; statistics show that approximately 4% growth in the demand of acrylic acid is expected each year globally. A shortage of acrylic acid supply was reported in 2010 due to the closure of some plants despite the growing demand.

While the majority of crude acrolein goes to the manufacture of acrylic acid, the major percentage (e.g. approximately 80% in 2002 [1]) of refined acrolein is consumed in the synthesis of methionine. Methionine is a sulfur containing amino acid that is required by animals but is not sufficient in natural food sources. The production capacity had been expanding steadily since 1977. Currently, the world's largest methionine facility was built in 2006 in Antwerp, Belgium, with an annual capacity of 120,000 tons per year [2]. The global demand for methionine was approximately 450,000-500,000 tons per year, with an annual growth rate of over 5% projected, especially in Asia, according to a business newsletter in the Japan's Corporate News [3].

The remainder of manufactured acrolein is used in the production of many chemicals, including glutaraldehyde, 1,2,6-hexanetriol, quinoline, pentaerythritol, cycloaliphatic epoxy resins, oil-well derivatives, and water treatment chemicals [4] (Figure 1-1). Also, acrolein can be directly used as a very effective broad spectrum aquatic biocide by injection into water, controlling the undesired microbial and the growth of aquatic weeds [5].

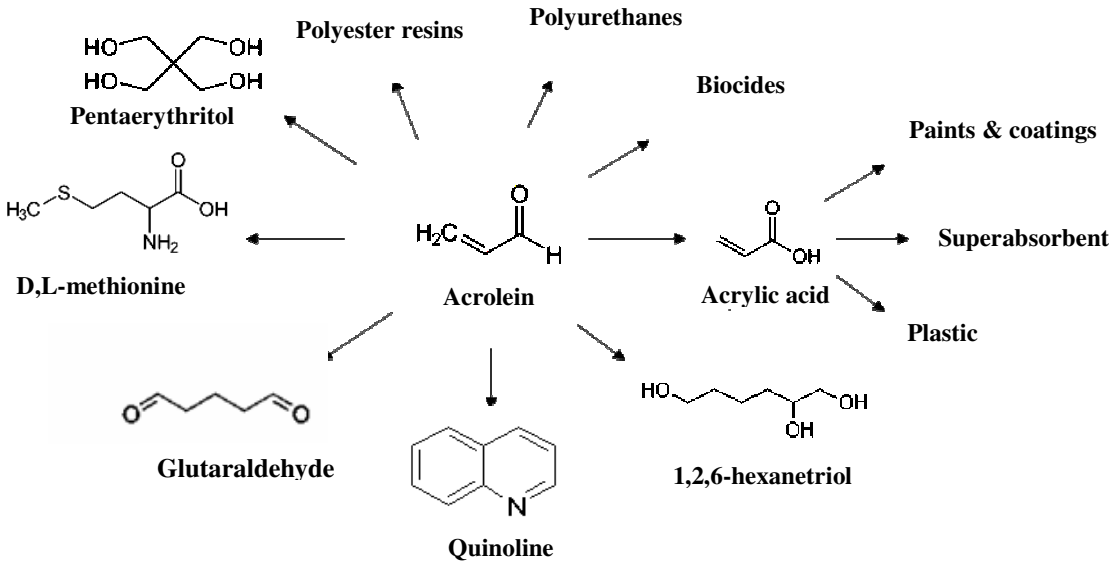

Figure 1-1: Chemicals derived from acrolein [1, 2, 4, 5]

1.1.2 Overview of acrolein synthesis methods

There has always been a demand for acrolein in industry. Efforts and improvements in the production of acrolein have been continuously made over several decades (Figure 1-2). Acrolein can be synthesized by catalytic aldol condensation of acetaldehyde and formaldehyde, which was also the first industrial process [6]. Partial oxidation of propylene catalyzed by multi-component metal catalysts has also been used as a manufacturing method. Much effort had been expended by industry and academia to optimize the processes and to develop highly efficient catalysts. Acrolein can be produced from partial oxidation of propane, although it is more difficult to control selectivity; thus, the yield has not reached a satisfactory level thus far. Several other petroleum-based synthetic routes were used successfully to synthesize acrolein. Ai *et al*. synthesized acrolein via the reaction of formaldehyde and ethanol at 240-320ºC using nickel phosphate or the silica-supported metal (tungsten, zinc, nickel, or magnesium) oxide [7]. Acrolein can also be obtained by the oxidation of allyl alcohol, or decomposition of allyl ether. However, these two routes have significant drawbacks for application at a larger scale, including low availability and high expense of the reactants, high energy consumption, low selectivity, etc.

Acrolein can also be produced via bio-based routes. As early as the 1900s, acrolein formation was encountered during alcoholic fermentation from grains [8, 9] with certain bacterial strains, such as *Bacillus, Klebsiella and Lactobacillus* [10]. In the case of alcoholic fermentation, acrolein was an undesirable compound, and the target of these studies had always been minimizing or preventing the associated acrolein production. Only recently have the researchers started to investigate the possibility of tuning this “undesired” route into possible chemical production. Vollenweider *et al.* gave a clear statement of the potential of the solely biotechnological route of acrolein production [11]; however, so far the bacterial catalytic method has not gathered any notable momentum at any production level. It also had been noticed centuries ago that burning fat resulted in an unpleasant odor; this pungent odor was from acrolein. The collection of acrolein during glycerol distillation [12], where glycerol pyrolysis occurred, was probably the prototype of the double dehydration process, producing acrolein from glycerol. Acrolein formation from glycerol becomes faster and much more selective with the presence of an acid, compared to pyrolysis alone. The acid-catalyzed glycerol dehydration is now categorized as a bio-based route, because glycerol is largely

available from biodiesel production, which is originated from renewable biological resources. This bio-based glycerol route became appealing and started to show its industrial value as the development of acid catalysis. The bio-based route specifically refers to glycerol dehydration to acrolein hereafter.

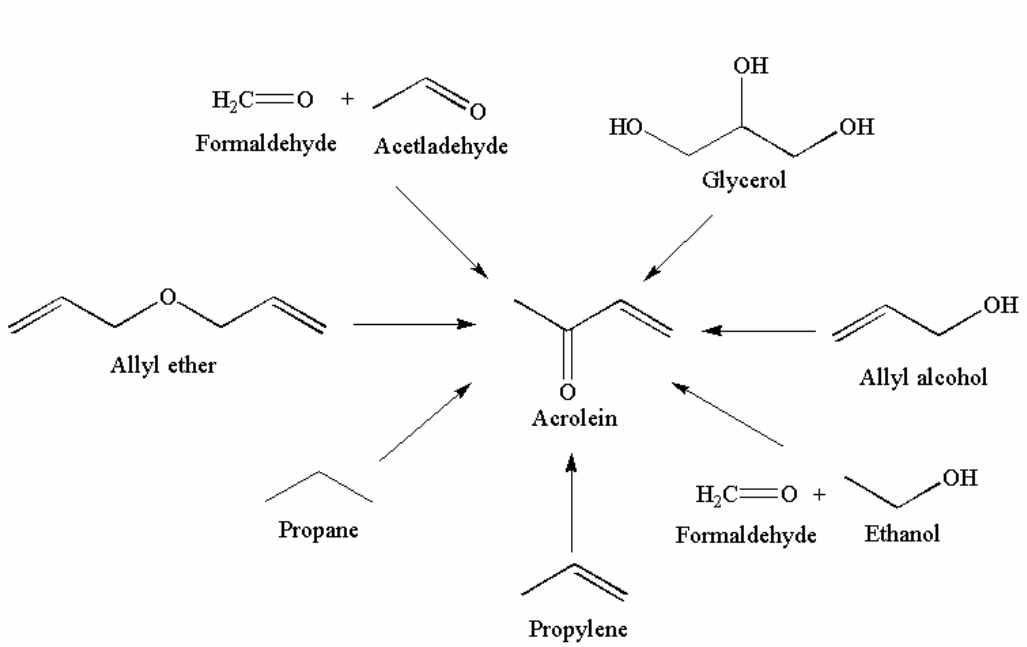

Figure 1-2: Summary of the primary synthesis methods of acrolein [6] [13] [12].

1.1.3 Going toward the bio-based route

Before justifying the transition towards the bio-based route, it is necessary to examine the history of the development of acrolein production. Degussa launched the first industrial acrolein production in 1942, producing acrolein via aldol condensation of acetaldehyde and formaldehyde [6]. Aldol condensation method was the industrial practice for a couple of decades. In the mid-1900s, the petroleum industry became prosperous, and propylene became a largely abundant and rather cheap raw material. Using partial oxidation of propylene to produce acrolein attracted the industries' and researchers' attention. In 1958, Shell started the first pilot plant operation of gas-phase propylene partial oxidation. Later, SOHIO's (Standard Oil of Ohio) discovered bismuth molybdate catalysts, and achieved the high-output and cost-effective acrolein production. The partial oxidation of propylene has been the predominant manufacturing method worldwide ever since. The carbon-carbon double bond makes propylene readily undergo a variety of reactions, leading to a spectrum of value-added

chemicals. Polypropylene, acrylonitrile, propylene oxide, and isopropyl alcohol are the examples of the commercial chemicals derived from propylene. The growing demand in many processes continuously drives up the propylene price. On the contrary, propane is the byproduct from both natural gas production and oil refining, but it only commercially consumed as fuel. In addition to being produced from multiple sources, propane does not have many applicable usages; as the result, propane is much cheaper than propylene [14] . The studies have been carried on for decades on acrolein synthesis from propane. However, the acrolein yield via partial oxidation of propane has not reached a point that is worthwhile to be commercialized. Furthermore, propane is a petroleum derivative after all, which does not fundamentally change production dependency on petroleum.

It is not difficult to find that an inexpensive source of raw materials usually provides the primary momentum for chemical process development. The availability and sustainability of the raw materials are important considerations. With the continuously growing problem of the non-sustainability of petroleum, a synthesis pathway from a renewable resource is much more desirable.

The world's energy and raw material demands keep increasing, imposing a large burden on the fossil fuel resources. Unfortunately, fossil fuel resources are not sustainable and are very likely to be mostly depleted in a few decades. Also, the significant amount of CO_2 emission from fossil fuel usage is also increasing steadily, which might cause irreversible damage to the environment and climate. One solution to these problems is to utilize renewable resources and gradually transfer the global economy toward a more sustainable future. Biodiesel is a good example of such transformation; due to the simple operation, commercial production has already been launched on a small scale all over the world. Biodiesel production and production capacity worldwide are increasing every year with the regulatory and socioeconomic pressure of renewable energy. One mole of glycerol is generated along with each mole of triglyceride conversion to biodiesel. As the result of the growth of biodiesel, large amounts of glycerol are produced and therefore available to the market place (Figure 1-3). Various sources [15-17] have reported that the price of glycerol has been lowered by its large availability, and even credits are given for reselling the crude glycerol.

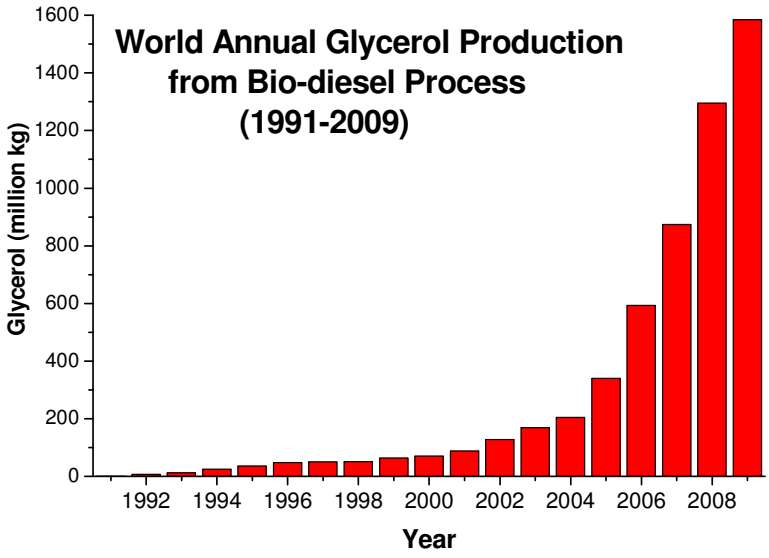

Figure 1-3: Annual glycerol production worldwide resulting from biodiesel production. The values were calculated based on the stoichiometric relation between glycerol and biodiesel, the annual production of which were referred from various sources [18-20]. The density of biodiesel used was 0.88 kg/L.

Because of the glycerol glut, acrolein, one of the value-added chemical derivatives of glycerol, has attracted great attention in recent years. Recent development of acid-catalyzed dehydration achieved good acrolein yield and great potential use of this method as a substitutive or complementary method to the propylene oxidation route in the future.

1.2 Technical aspects of synthetic acrolein approaches

1.2.1 Aldol condensation of acetaldehyde and formaldehyde

The first industrial acrolein production used aldol condensation of acetaldehyde and formaldehyde. The overall equation is shown in Equation 1-1. Degussa first initiated the acrolein production using this synthesis method in 1941.

$$CH_2O + CH_3 - CHO \rightarrow CH_2 = CH - CHO + H_2O \qquad \textbf{Equation 1-1}$$

Although this industrial process has since been replaced by propylene partial oxidization due to the prosperous development of petroleum industry in the mid-1900s, researchers never completely gave up the interest in this synthesis pathway. The key to

improving the acrolein production using this approach lies in finding a catalyst with a very high catalytic performance. The catalysts that were studied included mixed silica-alumina catalysts with various SiO_2/Al_2O_3 ratios [21], oxide silica gel supported basic or amphoteric oxides [22], oxide (ZnO, MgO, MoO_3, B_2O_3, and P_2O_5) loaded on various zeolites (ZSM-5, Y-faujasite, Al_2O_3 and SiO_2) [23], hydrotalcite-like materials [24], ion-exchange montmorillonite-rich materials [25], and clinoptilolite-rich natural zeolites [26]. Among them, the best yield (over 90% based on acetaldehyde) reported so far was achieved by Ai *et al.* using Si-Na, Si-Li Si-Mg, and Si-Zn oxide [22]. The aldol condensation occurred mainly on medium-strength acidic sites, while coking occurred mainly on the strong acid sites. Some people believed that formaldehyde can be produced from any carbon and hydrogen source, while acetaldehyde can be synthesized from biomass fermentation; therefore, the two necessary reactants of acrolein production via aldol-condensation are more readily available than propylene [23]. However, the problem is that complete conversion had never been attained, which complicates the downstream separation, since the product and reactants had similar physical properties, such as boiling temperature. The basic-acidic dual sites both contribute to acrolein production, and the ratio of the basic and acidic sites and the ratio of the acid site with different acid strengths could be optimized for the best acrolein yield [24].

The future of this method lies in whether a catalyst with very high catalytic activity can be developed, so that the nearly complete conversion can be attained. Otherwise, the downstream separation would be too challenging and difficult, because the product and reactant had similar physical properties, such as boiling temperature.

1.2.2 Current manufacturing method: partial oxidation of propylene

The partial oxidation of propylene to acrolein is shown in Equation 1-2. The manufacturing process for this reaction is usually operated at 300-450ºC in a multi-tubular reactor, composed of tubes with diameters of about 2.5 centimeters and lengths of 3-5 meters with packed beds of multi-component metal catalysts [27]. The multi-component metal catalysts for partial oxidation of propylene usually can be expressed in a general formula, Mo-Bi-X^{II}-X^{III} (-X^{I}-Y-Z)-O, where Mo-Bi-X^{II}-X^{III} are the basic structures containing four necessary metal components: Mo, Bi, X^{II} (one of the following elements: Co, Ni, Me, Mg, Pb), X^{III} (one of the elements Fe, Cr, Ce, Al). Bismuth molybdates are located on the surface

of the catalyst particles, serving as the major active sites; however, great activity occurs only with the simultaneous presence of divalent (e.g., Co^{2+}) and trivalent (e.g. Fe^{3+}) metal components. Optionally, X^I could be one of the alkaline metals, Y could be one of Sb, Te, W, V, Nb, and Z could be P or B. Steam is commonly co-fed with the reactant gases in the industrial process due to its benefits to the acrolein production. Water competitively occupies the strong oxidation sites, preventing further oxidation of acrolein to CO_2 [28]; the rate of acrolein formation is increased as a result [29, 30]. Also, water possibly creates new sites for propylene adsorption to the catalyst surface, thus enhancing the partial oxidation. The service life of these industrial catalysts is usually around 2-5 years. As one of the classical petrochemical processes, partial oxidation of propylene received continuous attention for the development since 1960. The leading development was contributed by industry, which disclosed improvements of the catalysts and processes in patents. Table 1-1 summarizes the most promising disclosures in chronological order.

$$H_2C = CH - CH_3 + O_2 \rightarrow H_2C = CH - CHO + H_2O$$ **Equation 1-2**

Table 1-1 The summary of acrolein production by partial oxidation of propylene

Catalyst	Feed composition [1] (I: propylene)	Contact time (sec)	Temperature (°C)	Conversion	Selectivity[2]	References
$Mo_5VW_{1.5}Te_{0.5}Sb_2Sn$/Bi oxide	I:O:steam=1:1.6:6	3	450		66.5% (yield)	[31]
Te-Ce oxide (Te:Ce=9:1)	I:air=1:10	2.2	440		60% (yield)	[32]
Te-V-W-As/Sn-(Sb) oxide	I:O:steam=1:6:3	4.9	370	65.6%	69.9%	[33]
Sn-Sb-U oxide	I:O:N 5:7.5:87.5	3.5	430	89%	81%	[34]
$SnSb_2VFe_{0.5}Bi_{0.01}$ oxide	I:O:N:steam=1:12:67:15	3	270	62.3%	72.8%	[35]
$Cr_2Al_{0.7}Mo_7Te_{0.35}$ oxide	I:air:steam=4:50:46	4	384	95%	83.3%	[36]
$Ni_{10}Co_{0.3}FeBiPMo_{12}O_{57}$	I:air:steam=1:10:4.1	1.8	360	90%	93.1% (acrolein +acrylic acid)	[37]
$Ni_{10}Co_{0.3}FeBiPMo_{12}O_{51}$	I:air:steam=2.1:16:10			95%	75%	[38]
$NiCo_3Fe_2BiAs_{15}K_{0.2}Mo_{12}O_{48.35}$	I:air:steam=1:10:5		305	94%	93%	[39]
$NiCo_3Fe_2BiP_2K_{0.2}Mo_{12}O_{49.6}$	I:air:steam=1:10:5	15	305	96%	88%	[40]
$Mo_{12}Bi_{0.1\text{-}7}Mg_{0.5\text{-}12}Fe_{0.1\text{-}7}Mn_{0\text{-}5}O_{25\text{-}80}$	I:air:steam=4.5:53:42.5	9	370	94.8%	73.7%	[41]
$Ni_{10.5}FeBiMo_2O_{54}$	I:air:steam=1:10:6	4		95.80%	69.90%	[42]
Mo-Bi-Fe-Mn-X oxide (X = K, Rb, and/or Cs)	I:air:steam=6:42.8:51.2	2.4	340	91.30%	80.40%	[43]
Mo-Co-Fe-Bi-X-O (X= Sn or Sn with Al, Ni, W, Cr, In, Nb)		2.4		90.80%	81.50%	[44]
B-W-Co-Bi-Fe-Mo-Si-M-O (M = alkali metal)	I:air:steam=4:56:40	6		99.60%	73.70%	[45]
Te-Ti-Mo-(P)-X-O (X=one of the elements Zn, Cd, Al, Ce, Zr, Mn, Fe, Co, Ni, Ag)			445-475	63-92%	70-95%	[46]
$Mo_{10}Co_8Fe_2Bi_{0.9}V_{0.05}K_{0.05}$ oxide	I:air:steam=1:10:4		330	89%	97.30%	[47]
$Mo_{10}BiFe_2Co_8Zr_{0.1}Ca_{0.1}Ti_{0.2}$ oxide	I:air:steam=1:10:4		310	98.6%	91.8%	[48]
$Mo_{12}Te_2Sb_2Zr_{0.5}Zn_{0.5}V_{0.5}$ oxide	I:air:steam=1:10:4		350	98.3%	88.3%	[48]
$Co_4BiFeW_2Mo_{10}Si_{1.35}K_{0.06}$ oxide	I:O:steam:N=7:12.6:10:70.4	2.25	320	96.20%	86.60%	[49]
Co-K-Mo-W-(P) oxide	I:air:steam=1:10:8		350	84.9-86.9%	83.1-87.7%	[50]
$Mo_{12}W_{0.3}BiFeZn_{0.1}Co_{4.5}K_{0.06}Al_{0.1}Si_5O_x$			310	99.30%-99.5%	90.10%-92.30%	[51-53]
$Mo_{12.25}Bi_1Fe_3Co_8Cs_{0.1}$			360	96.00%	88.75%	[54]
Bi-Mo-Fe-Ni-Si oxide	I:O:N= 1:1-20:1-20	3	360	87.30%	96.50%	[55]
Mo-Bi-Fe-Co-(Ni)-X oxide (X=Cs and/or K)				>97%	87.63%	[56]

[1] molar ratio is used (mol/mol)

[2] Selectivity is defined as the molar ratio between the carbon in the acrolein produced in the reaction and the carbon in the converted propylene.

It is generally agreed that partial oxidization of propylene to acrolein is initiated from the coordination of the propylene C-C double-bond site to the active catalyst site, leading to the formation of an allyl intermediate surface species (Figure 1-4). This is the rate-determining step, which occurs at the bridge O center (Scheme 1) or the carbonyl site (Scheme 2) depending on the nature of the specific catalysts involved [57]. The C-O bond is then formed with the O insertion, followed by a second hydrogen abstraction. Generally, the lattice oxygen on the catalyst surface contributes to the specific selectivity, while the adsorbed oxygen radical/molecule contributes to the total oxidation, leading to CO_x [58]. The gaseous molecular oxygen served as the supplier to reoxidize the catalyst, making sure of the sufficient availability of lattice oxygen [59]. CO_x could also be formed from both propylene and acrolein precursors due to the rather large mobility of the lattice oxygen. Therefore, the mobility of the lattice oxygen, determined by the structure of catalyst, is critical to both propylene conversion and acrolein selectivity [60]. Acrylic acid formation occurs from the consecutive oxidation of the adsorbed acrolein precursor.

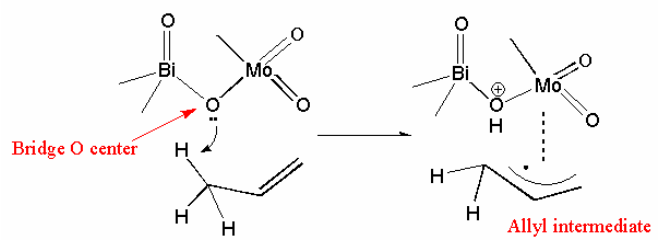

Scheme 1

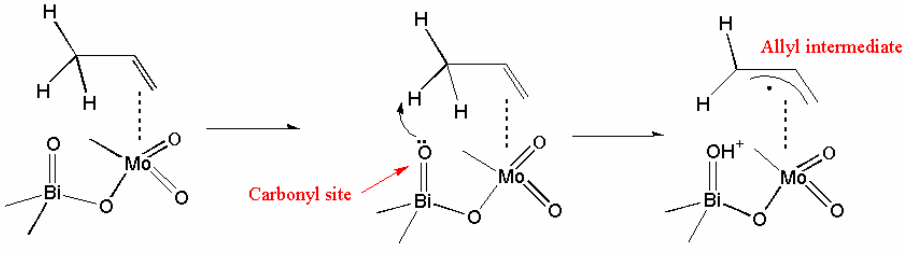

Scheme 2

Figure 1-4: Mechanisms of formation of allyl intermediate (initial/rate-determining steps of partial oxidation of propylene) [60, 61].

Gas phase partial oxidation of propylene to acrolein is highly exothermic [30]. As a result, one of the major issues for the reactor design of acrolein production is how to efficiently release the heat generated during the reaction. Heat release is essential to maintain

the isothermal reaction condition and prevent temperature runoff and explosion. In addition to the commonly used multi-tubular reactor, approaches to improve heat release are worth acknowledging. Patience and Mill discovered the potential utilization of a circulating fluidized bed reactor and gave the initial modeling and assessment of its commercial scale application [62]. Leib *et al.* later used a neural network model to simulate the performance of the fluidized bed reactor, providing more industrial application flexibility [63]. The circulating fluidized bed reactor allowed the usage of higher propylene concentrations with lower restrictions of the upper explosion limit, gave a higher heat and mass transfer rate, higher turndown ratio, and simplified the operation of catalyst addition and removal. However, the requirement of a high attrition resistant catalyst and insufficient kinetic and transport fundamental information hindered its commercialization until now. Song *et al.* improved the multi-tubular reactor by employing the heat transfer effect of CO_2 during the reactor operation, and increased the productivity by 14%. Heat transfer effects caused by the inert gas were studied both theoretically and experimentally. The addition of CO_2 provided a larger safe range of reactant inlet and coolant temperatures [64, 65]. Redingshofer *et al.* introduced a catalytic wall reactor, for which a specific temperature could be much better maintained during operation [30, 66]. They suggested the use of this type of "wall reactor" to conduct the kinetic and mechanistic study of highly exothermic reactions to achieve more reliable results. O'Neil *et al.* developed a distributive membrane reactor, which, they found, could increase the acrolein yield and suppress CO_x production by lowering the partial pressure of oxygen [67].

1.2.3 Partial oxidation of propane

Due to the inexpensive price and ready availability of propane, researchers were motivated to investigate the possibility of producing acrolein via partial oxidation of propane. This is very challenging because the bonds are strong in alkanes. Usually, the alkanes are thermodynamically more stable than the desired oxygenates; it is very easy for them to be over-oxidized to CO_x, the only products more stable than the feedstock propane. The overall formula of propane partial oxidation to acrolein is presented in Equation 1-3.

$$H_3C - CH_2 - CH_3 + \frac{3}{2}O_2 \rightarrow H_2C = CH - CHO + 2H_2O \qquad \textbf{Equation 1-3}$$

Three possible sets of elementary reaction combinations could result in the overall formula of partial oxidation to acrolein [67, 68]. The first possible mechanism is the simultaneous hydrogen abstraction and oxygen insertion (Mechanism 1 in Figure 1-5). The second possible mechanism is a sequential process with propane dehydrogenation to propylene followed by oxygen insertion into propylene forming acrolein (Mechanism 2 in Figure 1-5). The final possibility is sequential oxygen insertion into the propane molecule followed by dehydrogenation of the C-C bond into acrolein (Mechanism 3 in Figure 1-5), which is unrealistic from a thermodynamic stability point of view: on one hand, once a methyl group in the alkane is oxidized, the second methyl group is more easily oxidized [69]; on the other hand, the C-H bond in the carbonyl group is weaker than the H-C bond of ethyl group where a hydrogen extraction is desired for acrolein production.

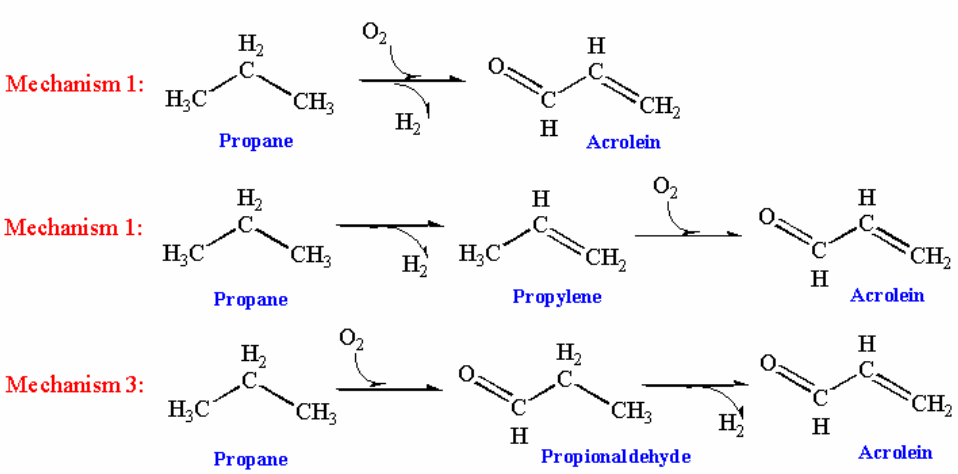

Figure 1-5: The three possible mechanisms of partial oxidation of propane to acrolein

Most of the studies agreed on the "sequential" mechanism (Mechanism 2 in Figure 1-5) of propane-to-propylene-to-acrolein in general with slight variations in the intermediate species generated prior to the formation of acrolein. A variety of metal catalysts have been used in the past, such as Ag-Bi-Mo-V-O[70], Bi-Ba-Te-O [71], V-P-O [72], Ni-Mo-O [72], and $MoPO/SiO_2$ [68]. A variety of methods/tools were utilized to elucidate the proposed mechanisms, such as *in situ* infrared or Raman spectroscopic methods [68, 73], evaluating individual steady-state reactions with different reactants [73], using some probe molecules to understand the reactions [74], etc. Yi *et al.* proposed that there was a transient state

[$CH_3CH(O)CH_3$] before the formation of propylene during the "first step", and also a transient state of [$CH=CHCH_2(O)$] leading to acrolein formation during the "second step". Zhang *et al*. believed that during the period where propylene exists as a form of π-allyl species, which interchanged with a transient σ-allyl species to subsequently form acrolein [75]. Kaddouri *et al*. proposed that a π-type precursor was formed before propane proceeding to acrolein formation in the Ni-Mo-O system, while propane proceeded directly to acrolein in V-P-O system [72]. Stern and Grasselli claimed that the first-order reaction with respect to propane applied to the first step (primarily the oxidation of propane to propylene) [76]. The first-order reaction with respect to propylene also applied to the second step where propylene was oxidized to acrolein. In both steps, the oxidation agent was the nucleophilic lattice oxygen of the catalyst, which could be rapidly replenished by O_2 in the gas phase. However, not all investigators agreed with this "sequential mechanism". For example, Savary *et al*. suggested that acrolein and propylene were independently produced directly from propane based on their study results of propane selective oxidation obtained over $AV_2P_2O_{10}$ (A=Ca, Cd, Ba, Pb) in 1996 [77]. Zhang and Catlow published their study results from molecular dynamics modeling [75]. Based on their density functional calculation, the acrolein production was directly formed from propane instead of from the chemical intermediate propylene: the first H was extracted from the methyl group via heterolytic splitting, followed by six other consecutive elementary reactions. This could be a specific catalytic behavior of the prototype catalyst $FeSbO_4$ that they used, or possibly it could be more generally applicable. It would be interesting to test the general applicability of this mechanism using other catalysts.

The reported acrolein production by partial oxidation of propane has not yet reached a level comparable to the acrolein production via partial oxidation of propylene, although lots of efforts have been made on this process. The following studies achieved relatively higher acrolein yield. The first more successful effort was made by Kim *et al*. in 1989 [78]. They reported that the addition of Ag dopant on bismuth vanadomolybdates ($Ag_xBi_{1-y/3}V_{1-y}Mo_yO_4$) led to the selective production of acrolein after their test of a series of monovalent metal ion-doped (Li, Na, K, Rb, Ag, Tl) bismuth vanadomolybdates [78, 79]. Conversion varied slightly within 13%-20%, while the selectivity of acrolein increased from about 20% to over 60% as the reaction temperature increased from 380ºC to 540ºC. There was a slight

decreasing trend for acrolein selectivity but a steady increasing trend for propane conversion as the C_3H_8-to-O_2 molar ratio was increased. Higher space velocity resulted in lower conversion and higher selectivity. A stable selectivity over 60% was observed when the space velocity was larger than 2000 cm^3 $g\text{-}cat^{-1}$ h^{-1} [80]. The optimal catalyst formula is $Ag_{0.01}Bi_{0.85}V_{0.54}Mo_{0.45}O_4$ for maximal acrolein selectivity. Acrolein selectivity of 64% was achieved with this formula under the experimental condition (500ºC, molar ratio of C_3H_8:O_2 0.55, space velocity 3000 cm^3 g^{-1} h^{-1}), although the conversion was only 13%. In 2004, Jiang *et al*. found that addition of phosphorus into Mo-V-Te-O catalysts ($MoV_{0.3}Te_{0.23}P_{0.15}O_n$) improved both the propane conversion (46.6%) and acrolein selectivity (47%); as a result, the yield reached 21.9% [81]. Zhu and co-workers [82] specifically examined the function of vanadium using a Mo-V-Te-O catalyst, although this catalyst did not allow other researchers to achieve a good yield [83-86]. They found that high concentrations of surface V^{5+} favored propane conversion and propylene selectivity, while low bulk V^{4+} favored acrolein selectivity. By controlling pH during preparation, the ratio of the pair V^{4+}/V^{5+}could be altered. The best result achieved was 21.4mol% acrolein yield (44.2% conversion and 48.4mol% selectivity). Many other catalysts have been studied, such as bismuth-containing mixed oxides ($Ba_{5.55}Bi_{2.3}Te_3O_{18}$, $Ba_{5.55}Bi_{0.3}Mg_3Te_3O_{18}$, etc) [71], bifunctional catalysts (metal oxide Ce-Te-Mo-O for selective oxidation and halogen F, Cl for dehydrogenation) [87], B-P mixed oxides [88], Bi_2O_3-MoO_3 [71], $Fe_2(MoO_4)_3$ [71], VTeO/SBA-15 and V-Te-O/SiO_2 [83], $MgCr_2O_4$ [89], BiCeVMoO [90], and Ce-Ag-Mo-P-O [91], although the results were even less satisfying.

If the mechanism consisting of two simultaneous reactions (both hydrogen abstraction and oxygen insertion simultaneously) (Mechanism 1 in Figure 1-5) is correct, then it is rather difficult, if not impossible, to achieve a decent acrolein yield. Since the two reactions use preferred catalysts with different functional properties, different temperatures, reactant ratios, resident time, etc., a sophisticated catalyst needs to be developed which can assimilate all of the active components with different catalytic functions; however, the active components for each of the both reactions need to be properly isolated to prevent the counter effect [74]. Studies showed that neither simple precipitation nor mechanical mixing of the catalysts with two functional phases could make the catalyst meet the requirements of both reactions [69, 74]. It was suggested that future development of a catalyst with a complex center that can

achieve acrolein via a one-step surface process, but how to do this is an open question. If the mechanism consisting of two sequential reactions occurs for partial oxidation of propane to acrolein (Mechanism 1 in Figure 1-5), one solution is to execute the overall reaction in two sequential steps that occur in separate reactors or in separate layers of the catalysts: propane to propylene, and then propylene to acrolein. Each sub-reaction can be improved separately [74]. Sinev *et al*. pioneered the effort to integrate these two steps [69]. They used VSbBiBa/Al_2O_3 and MoBiXoFe complex oxides, which were supposedly good catalysts for propane dehydrogenation and propylene partial oxidation, respectively, in two separate layers. A yield of 11.3 mol% (18% conversion and 62.8 mol% selectivity) was obtained, which was higher than the mathematical multiplication of the yields achieved in the two individual reactions (propane-to-propylene and propylene-to-acrolein). This result suggested that an intermediate formed from propane over VSbBiBa/Al_2O_3. This intermediate was more readily catalyzed into acrolein than propylene by MoBiXoFe. O'Neill *et al*. proposed a dual-bed membrane reactor [67], which could reduce the partial pressure of O_2 in each of the consecutive separated catalyst beds, and thus promote each reaction step towards higher acrolein yield. However, the optimum acrolein yield according to their theoretical modeling calculation could only reach about 19mol%.

1.2.4 Promising bio-based route---glycerol dehydration

The bio-based route using glycerol dehydration has become a very promising route for acrolein production in recent years, due to the sufficient availability of glycerol caused by biodiesel production. The overall equation is shown in Equation 1-4.

$$H_2C(OH)CH(OH)CH_2OH \rightarrow CH_2=CH-CHO+2H_2O \qquad \textbf{Equation 1-4}$$

The presence of acid can greatly improve glycerol conversion and/or acrolein selectivity. The possible mechanism is that an acid (an electron accepter, hydronium ion for example) helps the formation of carbocations (enol I and enol II) as shown in Figure 1-6 A&B. The acidity and the surface/pore structure of the catalyst have some influence in the final ratio of the two carbocations. Nevertheless, the 2^o carbocation would always be predominant, since it is thermodynamically much more stable than 1^o carbocation and its

formation rate is faster. Then 2° carbocation can attract an electron from the neighboring carbon and form the enol, which would quickly transform into 3-hydroxypropanal. Dehydration could occur once again on 3-hydroxypropanal, leading to acrolein formation (Figure 1-6 A1). Similarly, the 1° carbocation could form acetol also through a less stable enol compound (Figure 1-6 B1). In addition to intramolecular enol formation, intermolecular condensation to form glycerol oligomers could occur, which is often favored at lower temperature [92].

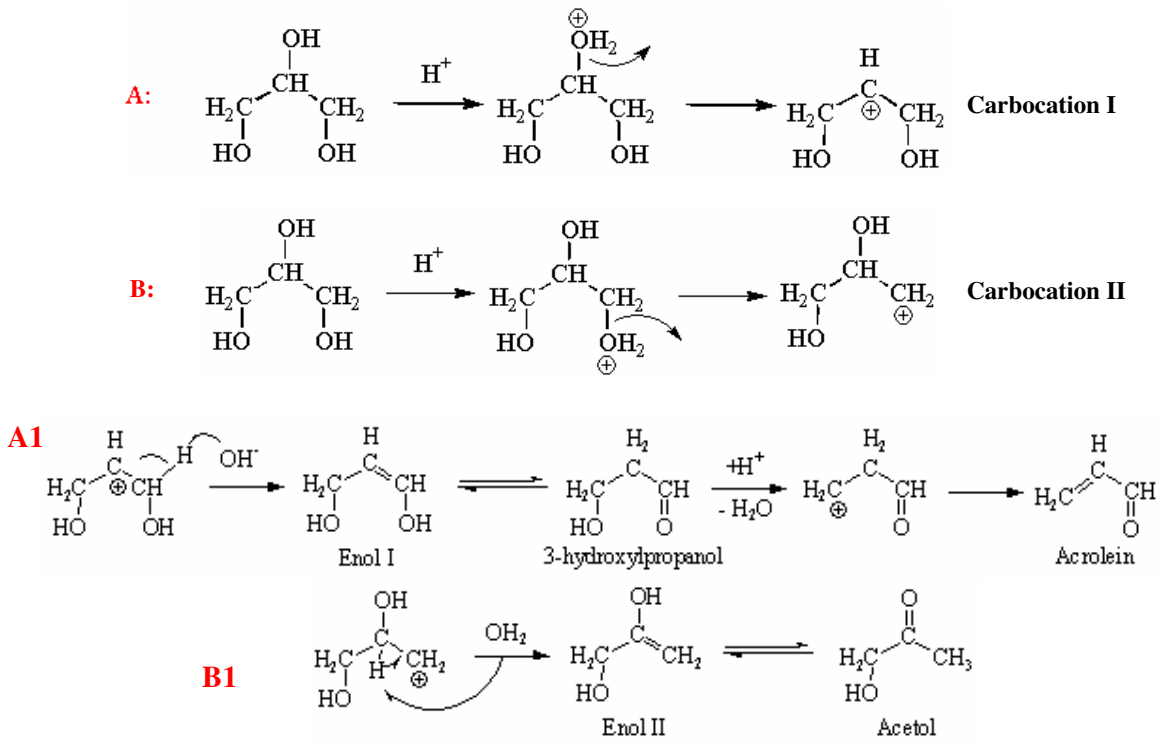

Figure 1-6: Ionic pathways of glycerol dehydration; A) to acetol, and B) to acrolein.

Even with the presence of the acid, the activation energy barrier is still considerable. As the result, the studies of converting glycerol to acrolein conducted in liquid phase under atmospheric pressure all failed to achieve a satisfying acrolein yield even in the presence of mineral acid or mineral salts [93-96]. Therefore, energizing the reactant glycerol molecule is the foremost problem that needs to be solved in this bio-based method. Commonly, there are two different approaches to satisfy the energy requirement: 1) pressurizing the reaction vessel and conducting the reactions under sub-critical/supercritical condition; 2) increasing the reaction temperature and conducting the gas-phase reaction.

1.2.4.1 Glycerol conversion to acrolein in sub-critical/ supercritical water

In 1987, Ramayya *et al*. conducted a liquid phase glycerol dehydration under high pressure [97]. Nearly 100 mol% acrolein selectivity was achieved, but glycerol conversion was low (<40%). They used 0.005M H_2SO_4 as the catalyst and 0.5M glycerol solution as the reactant feed. With the fixed pressure at 34.5 MPa, they found a higher temperature favored the glycerol conversion but not necessarily acrolein selectivity.

In 2001, Bühler *et al*. studied the reactions of glycerol under sub-/super-critical water conditions. This study covered the temperature range of 349 to 475°C at 25, 35, and 45 MPa and the residence time ranging from 32 to 165 s [98]. Clearly, high temperature favors the gas-phase products such as H_2, CO, and CO_2, and the production was more enhanced at temperatures above 450°C. Longer resident times, lower temperature, and higher pressures seemed preferable for acrolein production; however, strong trends of the acrolein yield in terms of these conditional parameters were not observed.

The corrosion of the reactor is a problem under sub-/super-critical water conditions, and the corrosion is more severe with the usage of mineral acids or even $ZnCl_2$ as catalysts. $ZnSO_4$ is usually much less corrosive, which justified the usage of $ZnSO_4$ as the acid catalyst by Ott *et al*. [99]. They found that in the sub-critical condition, glycerol conversion increased as the quantity of $ZnSO_4$ increased. The best result in their study (75 mol% selectivity and 50% conversion), after searching within the temperature range of 300 to 390°C and the pressure range of 25 to 34 MPa, was obtained by reaction of 1wt% glycerol at 360°C and 25 MPa in the presence of 470 g g^{-1} $ZnSO_4$. They also found that the residence time was important under sub-critical conditions, but not to the same degree under supercritical conditions. They believed that the reaction underwent an ionic pathway (as shown in Figure 1-6) under sub-critical conditions, while the reaction underwent a radical pathway (Figure 1-7) under supercritical conditions. As the result, the reaction conducted under sub-critical condition was more selectively lead to acrolein production. However, Watanabe and co-workers held a different opinion, claiming that supercritical condition was better for acrolein production [100]. The glycerol conversion obtained at the temperature above the critical point (400°C) was significantly higher than that obtained at the temperatures below the critical point (300°C and 350°C). In their study, results at various temperatures (300°C, 350°C,

400°C), pressures (25 MPa, 30 MPa, and 34.5 MPa), glycerol concentrations (0.25 mol/L, 0.05 mol/L), and H_2SO_4 concentrations (1mmol/L, 5mmol/L), the maximum acrolein production yield obtained was 81 mol% selectivity at 92 % conversion at 400°C and 30 MPa with the feed of 0.005 mol/L H_2SO_4 and 0.05 mol/L glycerol solution, and the residence time was 10.23 s [100]. This result showed that the selectivity decreased and the conversion increased as the residence time increased. In the supercritical region, glycerol conversion increased with increasing pressure.

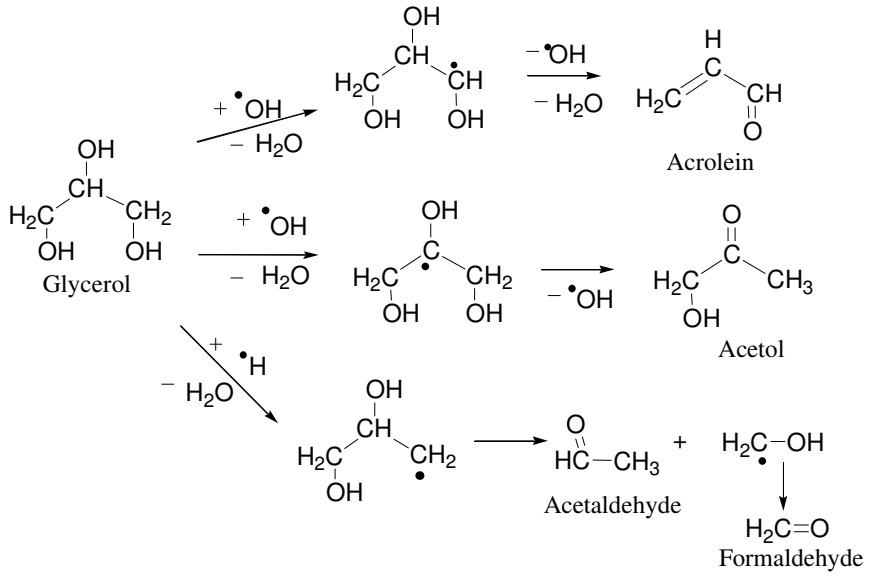

Figure 1-7: Radical pathway of glycerol conversion to acrolein, acetol, acetaldehyde and formaldehyde [98]

Several drawbacks lie within the sub-critical/supercritical reaction. First, it seems there is a constraint associated with the glycerol feed concentration. The feed glycerol solution should be controlled below 5 wt%, and a higher concentration could result in easier plugging by coke deposits at the reaction wall, pipes, or the connector. This situation may cause a severe safety problem, since the reaction is operated at high pressure. Second, sub-/supercritical water itself already imposes a burden on the system materials, and in the presence of the acid catalyst, corrosion issue would be more severe for the reaction process. As a result, after a period of time, due to corrosion and plugging, the entire reactor and pipeline would need to be replaced, which certainly increases the cost. Third, since it is a homogenous catalytic reaction, the downstream separation of the acid from the product and

later the recycling or disposal process of the acid are also big issues for the practical scale-up of the liquid phase reaction.

1.2.4.2 Gas phase reaction

The other approach of conducting glycerol conversion to acrolein was operating a gas-phase reaction. Gas-phase approach has several advantages compared to the sub-/supercritical water method. First, gas-phase reaction is simpler. The atmospheric operation does not cause much corrosion to the reactor, and does not need the expensive pressure controlling system; it may even utilize, to a large degree, the current manufacturing equipment with a minimal adjustment to promptly launch the bio-based production. Second, the gas phase reaction is usually accomplished in a packed-bed reactor using heterogeneous catalysts, so the downstream separation of acid from the product is minimized. These advantages favor gas-phase approach to sub-critical/supercritical approach when comes to the industrialization consideration. With all these advantages, there are significantly larger number of the studies used the gas-phase method in comparing to that using the sub-/supercritical water method.

The solid catalyst plays the important role in determining whether good acrolein production can be achieved. Several catalyst properties taken together determine the catalytic performance: 1) surface area, 2) pore size, 3) acid strength, 4) and the nature of the acid sites. Usually a larger surface area provides a great amount of active sites for the catalytic conversion, which usually leads to higher yield of the desired catalytic product. Mesoporosity has been noted as the most appropriate for glycerol dehydration. Tsukuda *et al.* conducted a parallel comparison of supported HSiW with silica of different pore sizes (3 nm, 6 nm, and 10 nm). The fabricated catalyst with the largest mesopore size exhibited not only higher acrolein selectivity, but also maintained the space yield for longer on-stream time. Chai *et al*. divided the acidity (H_0) into three major groups: $H_0 \leq -8.2$, $-8.2 \leq H_0 \leq -3.0$, and $-3.1 \leq H_0 \leq +6.8$, where H_0 is obtained by the Hammett acidity function. The solid acids with strengths in the range $-8.2 \leq H_0 \leq -3.0$ were most likely to have good acrolein production; or else the catalyst either does not provide sufficient acidity to selectively catalyze acrolein formation or is too acidic to easily suffer from surface coke formation. Brønsted acid sites are superior to Lewis acid sites for acrolein production; however, several studies show that Lewis acid sites could be converted to Brønsted acid sites in the presence of water vapor [101].

1.2.4.2.1 Catalysts

1) Supported mineral acids

Of the supported mineral acids, phosphoric acid has been so far reported as the most favorable. The studies have been conducted on various supporting materials, such as α-Al_2O_3, activated bentonite, and activated carbon. Common mineral acids are usually water soluble; therefore, they can not be solid acids by themselves. Previous studies used them as solid acids after they were supported by some catalyst frameworks. Boronic acid, sulfuric acid, and phosphoric acid supported by silica [102], alumina [103], zeolite [104] have been studied in the past. The supported phosphoric acid thus far provided the best result. In 1993, Neher *et al*. [9] stated that they had produced 1,2- and 1,3-propandiol from glycerol. The first step described in their patent is the dehydration of glycerol using an alumina-supported phosphoric acid for the production of acrolein. The acrolein yield was reported as 70.5 mol%. Suzuki patented the semi-batch reaction using H_3PO_4/α -Al_2O_3 with dropwise addition of glycerol solution, and reported 42% conversion and 89 mol% selectivity [105].

2) Zeolites

Zeolites are crystallized aluminosilicates, consisting of a three-dimensional framework of tetrahedral SiO_4 or AlO_4. The general formula of zeolite can be represented as $M_x/n[(AlO_2)_x(SiO_2)_y]wH_2O$. The zeolite has well defined yet controllable pore sizes, good thermal stability, and tunable distribution of Brønsted and Lewis acidities [106]. Li and co-workers patented their idea of using acidic zeolites to catalyze glycerol dehydration to acrolein. The highest acrolein yield was reported as 82.1 mol% using ZSM-11 as catalyst at 320°C [107]. Corma and co-workers operated glycerol conversion in a microdowner unit in the presence of ZSM-5 zeolites. At the optimal condition, they reported 62.1 mol% acrolein selectivity and 100% glycerol conversion [108]. Goehlich *et al*. conducted their screening test of several zeolites using a microactivity test unit. They found a low amount of phosphoric acid loading boosted the acrolein selectivity [109]. Neher *et al*. achieved 71-75 mol% selectivity using HZSM-5 to catalyze the liquid phase reaction (250-300°C) at 70 bar; however, the corresponding glycerol conversion was only 15-19%. Chao *et al*. disclosed their development of a catalyst using HZSM-5 with a SiO_2/Al_2O_3 molar ratio of 25-360, together

with the active metal components. The selectivity of 75.2 mol% and a complete conversion was claimed. Kim and co-workers examined the effect of the SiO_2 to Al_2O_3 molar ratio (ranged from 23-1000) in ZSM-5, and the results showed that HZSM-5 with the SiO_2/Al_2O_3 ratio of 150 provided the highest glycerol dehydration activity [110]. Jia and co-workers investigated the performance of a nano-crystalline zeolite. In their examination of the particle-size effect and Al/Si ratio, they concluded that the nano-crystalline zeolite with small pore size and large Al content was the most promising.

3) Metal/mixed oxide catalysts

In general, for mixed or metal oxides, the preparation procedures (calcination parameters in particular) modify the acid/base properties, making significant differences in their catalytic performance in the reactions. Chai *et al*. investigated Nb_2O_5, and found that it exhibited the best catalytic performance when calcined at 600°C. Ulgen and Holderich reported 72.1 mol% acrolein selectivity at 88.7 mol% conversion using ZrO_2 supported WO_3 with loading of 15.43 wt% [92]. In 2008, Okuno *et al*. disclosed their findings that crystalline metallosilicates containing one of the metal elements Al, Ga, or Fe with certain ratios to Si were good catalyst candidates for glycerol dehydration to acrolein [111]. Artia patented their solid acid catalyst, a crystal of a rare earth metal salt of phosphoric acid, by adding a phosphate ion to a solution of water, a hydroxide of one rare earth metal and/or its dehydration condensation product, followed by a co-firing procedure [112]. Liu *et al*. detailed their study of rare earth (La, Ce, Nd, Sm, Eu, Gd, Tb, Ho, Er, Tm, Yb, Lu) pyrophosphates. Although the unsupported rare earth pyrophosphates did not have large surface areas (<50 m^2/g), many of them already displayed promising catalytic performance. The calcination temperature and precipitation pH condition are two important parameters during catalyst fabrication that provide a large tunable range in terms of the final catalytic performance in the glycerol dehydration reaction. Also, enlarging the catalyst surface area with supporting materials provides an opportunity for further potential improvement.

4) Heteropoly acid (HPA)

HPA feature strong Brønsted acidity, approaching the super-acid region (a super acid is defined as an acid with strength greater than that of 100% H_2SO_4 [113]). Compared to the

conventional acids, HPAs are economical and environmentally friendly, and they have well-defined structures and tunable acidity levels [113-115]. The most common commercially available HPAs are $H_3PW_{12}O_{40}$, $H_4PW_{11}VO_{40}$, $H_4SiW_{12}O_{40}$, H_3PMo_{12}, and $H_4SiMo_{12}O_{40}$. The problems with direct usage of HPAs are as follows. First, they are water soluble, as are all the mineral acids [113-115]. Direct usage in the reaction with a large amount of polar substances would result in substantial loss of the HPA during the course of the reaction. Second, although featuring a strong acidity, HPAs usually have low specific surface areas [116, 117]. As the result, in a lot of HPA applications, HPAs were loaded on certain supporting materials (e.g. [118-120]). Strong acidity of HPAs can be retained after being loaded on the support surface, while larger surface areas can be achieved, as determined by the supporting materials [116, 117, 121]. In other words, the supporting materials intrinsically tune HPAs, imposing new features on the HPAs. With proper selection, the supported HPAs can be very good candidates for solid acid catalysts for glycerol dehydration to acrolein.

There is an optimal HPA loading for a given support. Under-loading necessarily leads to less desired acidity or acid strength, while overloading weakens the proton sites and makes acid distribution less uniform. Several studies have looked into this type of catalyst, and several commercially available HPAs with different supporting materials have been studied in the past, as listed in Table 1-2. Although some studies found that crystal-phase of HSiW formed on a silica surface when the loading was larger than 20 wt% prior to the crystal-phase formation, Tsukuda and co-workers obtained good acrolein production results using silica-supported HPAs with 30 wt% acid loading. Three different size mesoporous silicas were compared, 3 nm, 6 nm, and 10 nm pore diameters with surface areas of 733 m^2g^{-1}, 466 m^2g^{-1}, and 310 m^2g^{-1}, respectively. HSiW is finely dispersed on the silica with 3 nm pore. However, since the HSiW molecule itself is about 1.2 nm, there is only a very small opening for the reactants to enter and product to leave the site. Consequently, it is easier for the deposited coke to clog the entrance. HSiW crystalline structures started to aggregate on 6 nm silica pores, and more so on the 10 nm pores; yet still they provided appropriate pore size, surface area, and acid strength to achieve high acrolein yield. All three catalysts exhibited almost identical acrolein yields initially; the ones with larger pores showed overall higher yield, because the conversion decreased slower, which was attributed to less coke formation [102]. The study of HSiW loaded on activated carbon with surface area of 1068 $m^2\ g^{-1}$ showed that

10 wt% loading of HSiW provided the best catalytic performance [122]. The acid strength of HSiW was reduced upon loading to activated carbon less than 5 wt% [123], while higher loading caused more aggregation of HSiW molecules resulting in the decrease of the pore size and thus more severe deactivation. Dubois *et al*. patented their work using the salt of a HPA, and the yields were between 49.8 mol% and 93.1 mol% and the conversion was between 78.6%-100% [124, 125].

Atia *et al*. conducted a factorial type of comparison study on both the HPAs and the catalyst supports. They found that the same trends occurred as in the case of alumina supported HSiW: larger mesoporous alumina supported HSiW showed a better catalytic performance for acrolein production. They found that either 10 wt% or 20 wt% loading made no significant difference on catalytic conversion. HSiW was a better acid than $H_3PMo_{12}O_4$, $H_3PW_{12}O_{40}$(HPW), or $(NH_4)_3PMo_{12}O_{40}$ on silica, alumina, and aluminosilicate, which possibly was the combination effect of acid strength, thermal stability, oxidation potential, and hydrolytic stability [123]. Alumina- and aluminosilicate-supported acids showed a rather long and stable catalytic life.

Chai *et al*. used anti-sintering ZrO_2 nano-crystals to support HPW. Optimal loading of HPW was between 10-20 wt% [126]. Interaction between ZrO_2 and HPW increased the thermal stability of HPW. The ZrO_2 supported HPW calcined at 650°C gave the best catalytic performance, and also had the potential to be regenerated with a conventional oxygen burning method. Other than using supported HPAs, the usage of the salt of HPAs plays the similar role in modifying the surface area, porosity, and thermal stability, which varied greatly by the nature of the counter-cations [123]. Alhansah *et al*. conducted a study of the HPA salts with cesium, which had been reported as the most promising counter-cation for acid catalytic reaction. HPW-Cs salt showed better performance than HSiW-Cs salt, and both of them showed high acrolein selectivity. The doping of Pt group metals to HPW-Cs salt slowed the deactivation rate without lowering the acrolein selectivity. The best catalyst, as they discovered, was 52 wt% Pd-doped $Cs_{2.5}H_{0.5}PW_{12}O_{40}$ [127].

Table 1-2 summarizes the recent achievements in the gas-phase glycerol dehydration in terms of acrolein production.

Table 1-2: Recent progress of acrolein production via gas-phase glycerol dehydration

Catalysts	particle sizes (um)	surface area (m^2/g)	Glycerol conversion (%)	Acrolein selectivity (mol%)	Carrier gas	Glycerol concentration	Glycerol feed information	Temperature (°C)	TOS [1]	Ref.
Nb_2O_5 (calcined @400 ℃)	N.A.[2]	99	88	51	30 mL/min N_2	36.20 wt%	80 h^{-1}	315	9-10h	[128]
ZSM5 (Si/Al = 100)	40-120	70	100	62.1				350	9-10h	[108]
15%H_3PO_4/SiO_2(6 nm)	75-650	N.A.	69.9	48.2	30mL/min He	10 wt%		325	5 h	[102]
15%H_3BO_3/SiO_2(6 nm)	75-650	N.A.	1.5	27.3	30mL/min He	10 wt%		325	5 h	
30% $H_3PW_{12}O_{40}/SiO_2$	75-650	N.A.	99.7	65.1	30mL/min He	10 wt%		325	5 h	
30% $H_4SiW_{12}O_{40}/SiO_2$	N.A.	N.A.	98.3	86.2	30mL/min He	10 wt%		275	5 h	
30% $H_3MoW_{12}O_{40}/SiO_2$	N.A.	N.A.	98.4	33.4	30mL/min He	10 wt%		275	5 h	
$H_4SiW_{12}O_{40}$	N.A.	<5	26.7	59	30mL/min He	10 wt%		275	5 h	
15.43% WO_3/ZrO_2	500-1000	59	88	72.1	2.5mL/min O_2	20 wt%	330 h^{-1}	280	8 h	[92]
20%HPMo/A_5	N.A.	N.A.	97.3	45	30mL/min He	10 wt%		275	several hours	[101]
20%HPW/A5	N.A.	N.A.	99.2	51.7				275	several hours	
20%HSiW/A5	N.A.	N.A.	98.4	63.6				275	several hours	
10%HSiW/Al_2O_3-SiO_2 (4nm)	N.A.	N.A.	100	75				275	several hours	
HSiW20/A_{12}	N.A.	N.A.	99	74	30 mL/min N_2	36.20 wt%	400 h^{-1}	315	9-10h	
30%$H_3PW_{12}O_{40}/SiO_2$ (calcined@350 ℃)	350-840 (20-40mesh)	141	25	59	31 mL/min N_2	36.20 wt%	400 h^{-1}	315	9-10h	[126]
30%$H_3PW_{12}O_{40}/SiO_2$ (calcined@650 ℃)	350-840 (20-40mesh)	162	20	54	32 mL/min N_2	36.20 wt%	400 h^{-1}	315	9-10h	
15%$H_3PW_{12}O_{40}/ZrO_2$ (calcined@650 ℃)	350-840u (20-40mesh)	133	76	71	33 mL/min N_2	36.20 wt%	400 h^{-1}	315	9-10h	
10%$H_4SiW_{12}O_{40}$/AC	350-840 (20-40mesh)	N.A.	92.6	75.1	20 mL/min He	10 wt%		330	5 h	[122]
$Nd_4(P_2O_7)_3$ (ph=6, calcinate @ 500 ℃)	N.A.	N.A.	96.4	82.7	30 mL/min N_2	36.2 wt%	227 h^{-1}	320	7-8h	
CsPW	45-180	130	41 (100)	94 (98)	15 mL/min N_2	10 wt%	227 h^{-1}	275	5h (1h)	[127]
$Cs_2HPW_{12}O_{40}$	45-181	70	21(91)	94 (97)	15 mL/min N_2	10 wt%	227 h^{-1}	275	5h (1h)	
0.5%Pd/CsPW	45-182	84	79 (97)	96 (83)	15 mL/min H_2	10 wt%	227 h^{-1}	275	5h (1h)	
0.5%Ru/C + CsPW (1:10)	45-183	117	50 (95)	92 (94)	15 mL/min H_2	10 wt%	227 h^{-1}	275	5h (1h)	
20%HPW/SiO_2	45-184	205	60 (100)	95 (97)	15 mL/min N_2	10 wt%	227 h^{-1}	275	5h (1h)	

Table 1-2 continued

Catalysts	particle sizes	surface area (m2/g)	Glycerol conversion (%)	Acrolein selectivity (mol%)	Carrier gas	Glycerol concentration	Glycerol feed information	Temperature (°C)	TOS	Ref.
2%Pd/20%HPW/SiO_2	45-185	200	72 (100)	94 (85)	15 mL/min H_2	10 wt%	227 h^{-1}	275	5h (1h)	[127]
$VOPO_4$ (Calcinate@800ºC)	N.A.	10	100	64	18 mL/min N_2 mixed with O_2	20 wt%	227 h^{-1}	300	10 h	[129]
SAPO-11	N.A.	89	88(65)	62(55)	50mL/min He	5 wt%	43 (90) h^{-1}	280	after 1hr	[130]
SAPO-34	N.A.	359	59(42)	72(65)	50mL/min He	105 wt%	44 (90) h^{-1}	280	after 1hr	
$La_4(P_2O_7)_3$	N.A.	N.A.	76.2	78.5	30mL/min N_2	36.2 wt.%	227 h^{-1}	320	7-8hr	[131]
$Ce_4(P_2O_7)_3$	N.A.	N.A.	44.8	42.9	30mL/min N_2	36.2 wt.%	228 h^{-1}	320	7-8hr	
$Nd_4(P_2O_7)_3$	N.A.	N.A.	87.2	79.9	30mL/min N_2	36.2 wt.%	229 h^{-1}	320	7-8hr	
$Sm_4(P_2O_7)_3$	N.A.	N.A.	89.7	77.8	30mL/min N_2	36.2 wt.%	230 h^{-1}	320	7-8hr	
$Eu_4(P_2O_7)_3$	N.A.	N.A.	83.1	78.5	30mL/min N_2	36.2 wt.%	231 h^{-1}	320	7-8hr	
$Gd_4(P_2O_7)_3$	N.A.	N.A.	88.2	78.9	30mL/min N_2	36.2 wt.%	232 h^{-1}	320	7-8hr	
$Tb_4(P_2O_7)_3$	N.A.	N.A.	87.6	78.8	30mL/min N_2	36.2 wt.%	233 h^{-1}	320	7-8hr	
$Ho_4(P_2O_7)_3$	N.A.	N.A.	84.4	77.2	30mL/min N_2	36.2 wt.%	234 h^{-1}	320	7-8hr	
$Er_4(P_2O_7)_3$	N.A.	N.A.	86.7	79.7	30mL/min N_2	36.2 wt.%	235 h^{-1}	320	7-8hr	
$Tm_4(P_2O_7)_3$	N.A.	N.A.	87	77.8	30mL/min N_2	36.2 wt.%	236 h^{-1}	320	7-8hr	
$Yb_4(P_2O_7)_3$	N.A.	N.A.	48.4	63.7	30mL/min N_2	36.2 wt.%	237 h^{-1}	320	7-8hr	
$Lu_4(P_2O_7)_3$	N.A.	N.A.	58.5	64.4	30mL/min N_2	36.2 wt.%	238 h^{-1}	320	7-8hr	

[1] Time-on-stream

[2] Not available

1.2.4.2.2 Reaction conditions

In Cheng and Ye's diffuse reflectance FTIR study, they found that higher temperature would cause the formation of polymeric condensation compounds, and would also facilitate the formation of acetate and surface-bound carbonate products, resulting in smaller carbon chain products, such as CH_3CHO, CH_4, CO, and CO_2 [132]. In Yoda and Ootawa's FTIR study of glycerol dehydration on H-MFI zeolite, the dehydration yielded exclusively acrolein under 87ºC [133]. Zeolite has been used as catalyst for the kinetic study by Kim and co-workers [110]. They investigated a broad range of SiO_2/Al_2O_3 ratios, which covered the ratio of the zeolite that Yoda and Ootawa used. However, acetol formation was detected. This finding reinforces the possibility that low temperature was favored for acrolein production. The reason might be that the decomposition of acrolein into formaldehyde and acetaldehyde occurs much faster at higher temperatures, causing the partial loss of acrolein when examining the downstream product. Pathak *et al*. claimed that the condensable products (such as acrolein, acetol, etc) were dominant at low temperatures, while at high temperatures more incondensable products (such as CO_2, H_2, etc) were present [134]. Kuba and Dubois used their catalyst screening program to screen rapidly various reaction conditions for glycerol conversion to acrolein [135]. The results showed catalysts deactivated much faster at higher temperatures. Although glycerol conversion increased with the increase of the reaction temperature, glycerol started to decompose at a temperature of 300ºC, known as glycerol pyrolysis; this is not favorable for the desired dehydration product. Also, several studies reported that glycerol conversion attained almost complete conversion before reaching 290°C (for example, 275°C in Atia's study and 240°C in Ulgen and Hoelderich's study), so a further increase of the reaction temperature would not necessary lead to higher acrolein yields. A relatively better acrolein selectivity occurred at 275°C for all the catalysts investigated by Atia *et al*. [101]. According to Ulgen and Hoelderich, however, lower temperature favors the intermolecular dehydration leading to the glycerol oligomerization. At higher temperatures, they found the maximum selectivity occurs at 280°C [92].

The surface reaction network of the chemisorbed glycerol is very likely to be influenced by the presence of water vapor [110]. The undesired sequential reactions from acrolein might be suppressed by the water vapor. With the presence of water, some Lewis acid sites might be converted into Brønsted acid sites, which are preferred for acrolein formation [132].

1.2.4.2.3 Problems to be solved

Promising progress has been achieved regarding the acrolein yield, which is already competitive with the current manufacturing methods derived from propylene [108]. To make this bio-based process into a completely satisfactory substitution to the propylene method, one problem yet needs to be solved: how to extend the service life of the highly efficient solid acid catalysts to the timescale of months to years. Catalyst deactivation problem was reported in almost every single study on glycerol dehydration to acrolein [92, 101-103, 110, 122, 126, 127, 129-131, 133, 135-142]. The negative influence of catalyst deactivation usually reflected in the decrease of glycerol conversion along the reaction time course, which lowered the overall acrolein yield. For example, compared to glycerol conversion at 1 hour TOS, the conversion at 5 hours TOS was reduced by 40%-59% for the caesium heteropoly salts in Alhanash and co-workers' study [127]; In the study by Kim *et al.* [110], the ZSM-5 catalysts with various Si/Al ratios showed a reduction of 46% to 69% in glycerol conversion at 10-12 hours TOS compared to 2 hours TOS, and also some reduction in acrolein selectivity.

Catalyst deactivation is caused by coke formation on the catalyst surface, thereby blocking the pores and preventing the reactant contact with the active sites. Glycerol conversion would decrease as the result. Also, part of the coke is formed from acrolein or glycerol, so its formation reduced the acrolein yield. Stronger acid sites, or more specifically, strong Brønsted acid sites, are favored by acrolein formation, but they unfortunately also lead to more severe coking and therefore more severe catalyst deactivation [127].

Some efforts were made regarding the catalyst deactivation problem. Although not as catalytically good as supported HPAs, one advantage of the zeolite or other metal oxide catalysts that have been calcined at a higher temperature than 450°C or 500°C is that a conventional coke removal method using oxygen burning can be applied. Chai stated that 20% O_2 blended with N_2 at the reaction temperature 315°C was sufficient for a complete regeneration [128]; however, no data was provided to show this result at such a low temperature, at which hard coke could not be cleaned according to classical theories. Some studies claimed that co-feeding small amounts of oxygen helped to suppress the side products and the coke formation [143, 144]. Artia *et al*. disclosed their glycerol dehydration process using zeolite as the acid catalyst [145]. The idea of their operation was that after 12 hours of the glycerol dehydration reaction, the glycerol feed was halted, and O_2-containing gas was flashed through the reactor at 360°C for 8 hours. The regained acrolein yield (63 mol%) could be seen in the product sampled after 3 hour of the restarted reaction [146]. Yan *et al*. (2009) tried to ameliorate the coking problem by operating the reaction at a lower pressure than atmospheric, to aid in the evaporation of glycerol and to prevent condensation of reactants/products on the catalyst surface. The catalyst's life is also extended at a lower pressure. Alhanash *et al*. tried to ease the coking problem by doping the solid acid catalyst with a platinum-group metal and the addition of H_2 to the carrier gas. The addition of hydrogen possibly hydrogenated the coke precursor, which is the reverse reaction of coke formation [127].

1.3 Discussion of the economic and industrial potential

The technical details and the current development of the bio-based method as well as other acrolein synthesis methods have been reviewed. Compared with aldol condensation and partial oxidation of propane, the bio-based method from glycerol is a more sustainable and viable alternative to the current manufacturing method. In this section, the industrial application potential and the economic virtues of the bio-based method were further demonstrated via comparative discussion between the propylene-based method and the bio-based method.

The process flow diagram for the partial oxidation of propylene to acrolein is presented in Figure 1-8 [147-149]. In this process, compressed air, propylene and steam are heated to 250^{o}C prior to entering the packed bed reactor; a typical molar ratio of these three components is 1:10:5. The reactor is operated at 250-320^{o}C and 150-250 kPa, and the gaseous mixture is quenched with sufficient water and partially cooled to remove the byproduct acrylic acid and a trace amount of acetic acid. The quench tower in Figure 1-8 is for this purpose. Then the gaseous mixture, including the products, remaining reactants, and inert gas, is sent to an absorber, where the noncondensable gases (unreacted propylene, O_2, N_2, and CO_x) are removed as the off-gas and the dilute acrolein liquid stream were sent to the subsequent stripping column. In the stripping column, the majority of water is condensed at the bottom, while the raw acrolein is obtained as distillate. The refined acrolein (> 95%) is obtained after two subsequent separation towers (extraction column and distillation tower) to remove the lighter organic impurities.

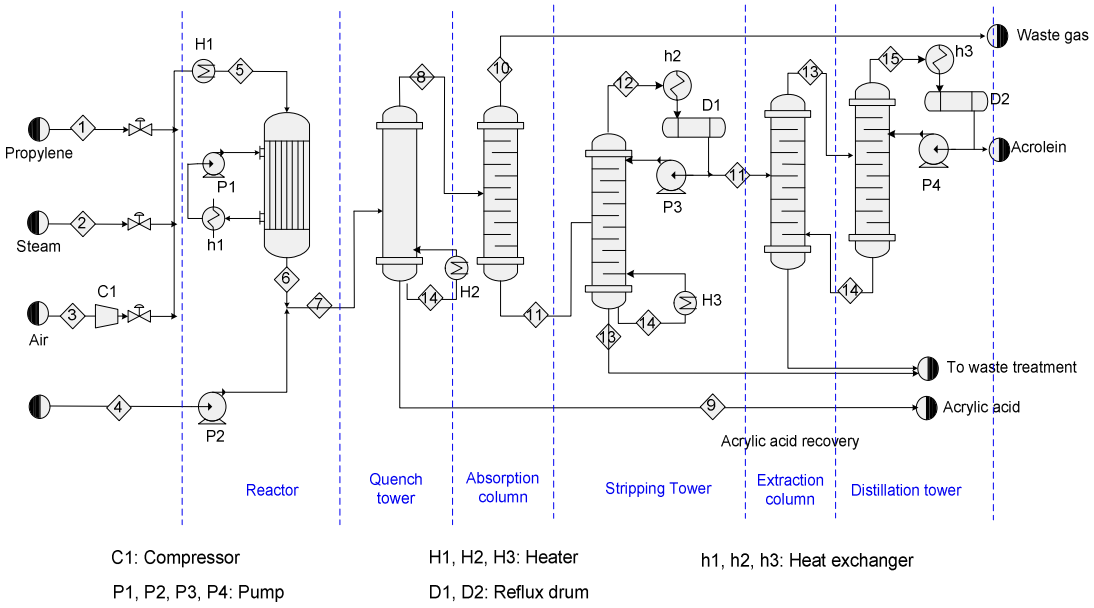

Figure 1-8: Process flow diagram for production of acrolein from propylene [148, 150, 151].

Figure 1-9 is a proposed industrial gas-phase glycerol dehydration process flow diagram. Glycerol is heated to 275°C, and fed into a mixing and agitation tank, into which

high-temperature steam is also fed. The output (4.663mol% glycerol/steam) is fed into the packed-bed reactor (275°C). If crude glycerol is used, the pretreatment needs to be added to remove any solids, fouled organics, salts, free fatty acids, color and odor. Glycerol-water vapor, together with the onsite generated nitrogen, is fed into the reactor packed with the alumina supported silicotungstic acid and operated at 275°C and atmospheric pressure (101 kPa). The gaseous mixture at the reactor outlet includes incondensable gases (N_2 and carbon oxide), water vapor, acrolein, low-boiling compounds (acetaldehyde and propionaldehyde) and high-boiling point compounds (acetol, acetic acid, acrylic acid, phenol, glycerol, etc.). From this point on, the treatment can be directly adopted from the propylene-based process. The gaseous mixture is washed with a limited amount of water in the quench tower to remove the high-boiling compounds. Then acrolein is absorbed with a large amount of water in the absorption tower, and the incondensable gases (N_2, CO_x, etc) are removed. The diluted acrolein solution is then worked up to crude acrolein in the stripper, and then purified via two steps of distillation through the extraction column and the distillation tower.

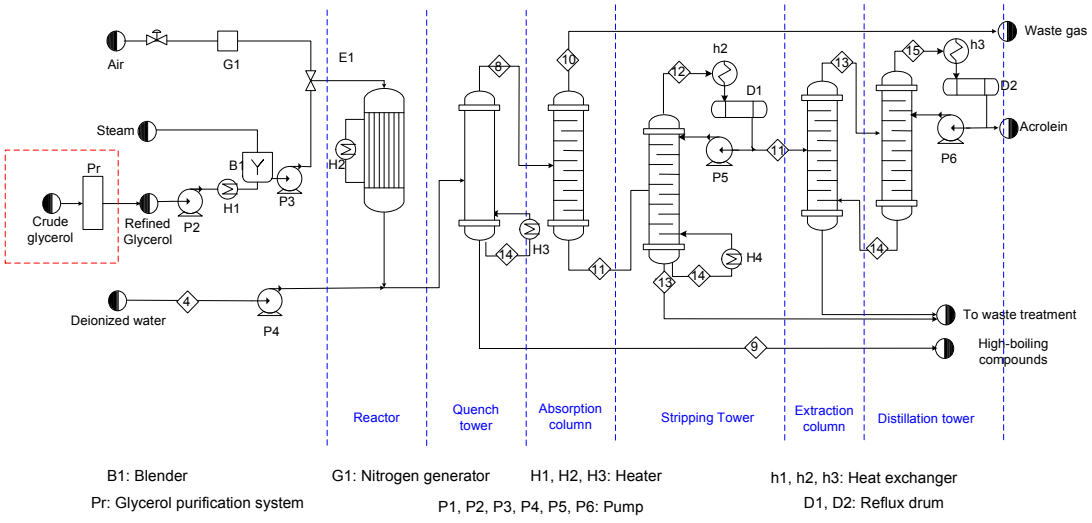

Figure 1-9: Proposed process flow diagram for production of acrolein from glycerol. The red rectangle is applied if crude glycerol is used as starting material.

To analyze the economical feasibly of bio-based acrolein production, the concept of production costs plus profit (PCPP) was used. Figure 1-10 lists the elements in calculation of PCPP, which is a proxy for the market price of the end product. As is demonstrated in the

table, PCPP is composed of direct operating costs, taxes, insurance fees and plant overhead, the allowance for marketing, administration and R&D, and the capital charge.

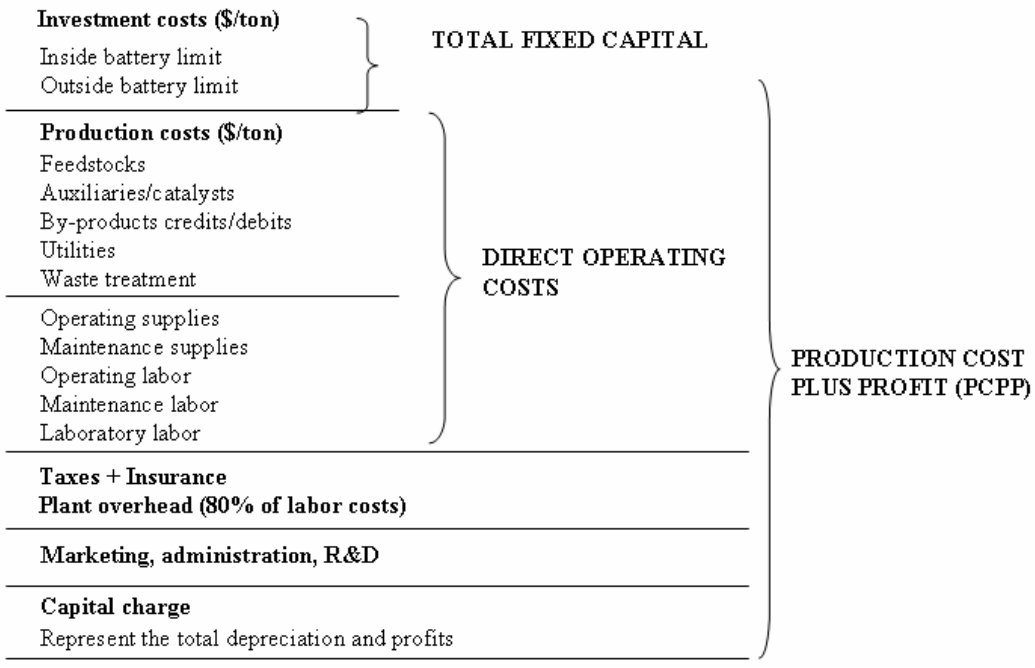

Figure 1-10: The components of the production costs plus profits (PCPP) (reproduced from Hermann *et al.* [152])

To simplify the comparison of the two processes, the following equations (Equations 1-5 and 1-7) are to be used in the calculation. Two parts compose the direct operating cost: the variable cost and the fixed cost, each of which contains several elements, respectively:

$$\Pi = \lambda \cdot Y - C_v - C_{fix} \qquad \textbf{Equation 1-5}$$

where Π is the profit, λ is the market price of the product acrolein in the unit of \$/ton, Y is the annual mass production of acrolein in the unit of ton, C_v is the variable cost in the unit of \$, which includes the cost for feedstock, catalyst, energy, and labor, etc., and C_{fix} is fixed cost in the unit of \$, which includes all the others costs, such as investment, capital, marketing, administration, etc.

$$C_v = C_{catalyst} + C_{feedstock} + C_{energy} + C_{other} \quad \textbf{Equation 1-6}$$

where C_v is the variable cost, $C_{catalyst}$ is the cost for the catalyst, $C_{feedstock}$ is the cost for feedstock, C_{energy} is the cost for energy consumption, C_{other} includes all the other components in the viable cost, which is assumed to be the same for both processes.

The difference of variable cost between propylene-based process and bio-based acrolein can thus be expressed in Equation 1-7.

$$\begin{aligned} & \Delta C_v = \Delta C_{catalyst} + \Delta C_{feedstock} + \Delta C_{energy} + \Delta C_{other} \\ \textbf{=>} \quad & = (C^g_{catalyst} - C^p_{catalyst}) + (C^g_{feedstock} - C^p_{feedstock}) + (C^g_{energy} - C^p_{energy}) \end{aligned} \quad \textbf{Equation 1-7}$$

where △ denotes the difference between propylene-based method and bio-based method, the superscript "p" denotes propylene-based process, and the superscript "g" denotes bio-based process.

Table 1-3 comparatively lists the major components with their specifications in the two production processes (based on Figure 1-8 and Figure 1-9). Comparing these two processes, it is not difficult to observe that there are many similarities existing between these two production schemes. The multiple packed-bed reactor (PBR) system is well applicable to both production methods. The partial oxidation of propylene to acrolein is highly exothermic (~ -356 kJ/mol), while the glycerol dehydration to acrolein is endothermic (~ 43 kJ/mol) (Appendix II); therefore, an efficient heat exchanger is needed for the multiple-PBRs in the propylene-based production to promptly release the heat, while the multiple-PBRs in bio-based production need a furnace to maintain the reaction operating at a elevated temperature. The PBR for propylene-based production usually operates at 150-250 kPa, and it usually costs more in comparison to the PBR in the bio-based acrolein production, which operates at atmospheric pressure. Considering these factors, it is reasonable to make the assumption that the fixed costs for the reactors are equivalent for both processes.

Table 1-3: Comparative list of the reactor and separation columns of propylene-based production and bio-based production [1]

	Propylene-based process	Bio-based process
Pretreatment steps	• Heating propylene and air	• Purification (if crude glycerol is used as starting materials • Heating glycerol, mixing glycerol with steam
PBR [2] reactor	• Multiple reactors packed with multi-components metal • Operating at ~320^{o} C, strong exothermic reaction • Operating at the 150-250 kPa • Require careful temperature control; good cooling system	• Multiple reactors packed with alumina supported heteropoly acid • Operating at ~280^{o} C, endothermic reaction • Operating at atmospheric pressure • Good heat isolation, need heating supply
1st column	• Quenching the products • Removing the high-boiling compounds, mainly acrylic acid and acetic acid	• Quenching the products • Removing the high-boiling compounds, including acetol, acetic acid, acrylic acid, phenol and glycerol
2nd column	• Entrance: propylene, CO_x, steam, acrolein, acetaldehyde, propionaldehyde • Obtaining the diluted acrolein solution devoid of incondensable gases	• Feed: acrolein, acetaldehyde, propionaldehyde, steam, CO_x, N_2. • Obtaining the diluted acrolein solution devoid of incondensable gases
3rd column	• Entrance: acrolein, water, acetaldehyde, propionaldehyde. • Distillate: crude acrolein	• Entrance: acrolein, water, acetaldehyde, propionaldehyde. • Distillate: crude acrolein
4th column	• Entrance: acrolein, acetaldehyde, propionaldehyde. • Distillate: acrolein containing less impurity	• Entrance: acrolein, acetaldehyde, propionaldehyde. • Distillate: acrolein containing less impurity
5th column	Obtaining refined acrolein; adding stabilizer.	Obtaining refined acrolein; adding stabilizer

[1] This table corresponds to the schemes presented in Figure 1-8 and Figure 1-9.

[2] PBR stands for packed-bed reactor.

(The difference in the energy cost will be considered in C_{energy} as part of C_v.) The post-processing steps are essentially the same for both synthesis methods, so the cost regarding this part can be considered the same. The major differences exist prior to the reactors, as categorized under "Pretreatment steps" in Table 1-3. Comparing to the propylene-based acrolein production, the following unit equipment is additionally needed for the bio-based production. A nitrogen generator is needed for bio-based acrolein production ($23,340 quoted by Gazcon onsite nitrogen generation for the following specifications: up to 250 L/min, 99% purity, up to 5 bar outlet pressure, 24 hour/day operation). Also a mixing/agitation tank is needed to blend hot glycerol with steam. If crude glycerol is used, a pretreatment step can be added to remove any solid, foul organics, salts, and free fatty acids (FFAs), color and odor. Several commercial products are available for this application, such as HEED® or HEEPM™ system (http://www.eetcorp.com/heepm/glycerinspecs.htm) from EET Cooperation (Harriman, TN, USA), Glycerol-Refining-System from Crown Ion Works (http://www.crowniron.com/technologies/oleo_glycerine.cfm) (Minneapolis, MN, USA) and ROHMIHAAS's AMBERSEP™ BD50 from DOW (http://www.amberlyst.com/glycerol.htm). A conservative assumption is made that the fixed cost (C_{fix}) plus C_{other} of bio-based acrolein production from crude glycerol and from refined glycerol is 1.3 and 1.1 times of propylene-based acrolein production.

Table 1-4 shows that the several major components in the variable cost C_v that differ greatly between propylene-based and bio-based methods for a 10,000-ton acrolein production. The quantities for steam only refer to what is used in the reaction. Also, the energy listed in the table only refers to the part of energy required to heat up the reactant(s) and required for the reaction (assuming the energy consumption of all the other processes are the same for both production methods). The consumption of deionized water used in the quenching and absorbing processes and the solvent used in the extraction step (Figures 1-8 & 1-9) in propylene-based production and bio-based production is equivalent; therefore, their costs are not included in Table 1-4. The quantities of the feedstocks required for both processes are calculated based on the stoichiometric relation under the assumption of 80 mol% acrolein yield, and the quantity calculated for crude glycerol was based on the glycerol purity of 80 %. In terms of the last two variations in the variable cost (Equation 1-7), the bio-based method using refined glycerol costs $12.95 million (MM)-$16.13 MM, which is 0.82-1.02 times the cost of these parts of the propylene-based method; the bio-based method using

crude glycerol cost $2.71 MM-5.83 MM, which is 17.2%-40.5% of that of propylene-based method.

Table 1-4: Comparison of propylene-based and bio-based acrolein production (10,000 ton/year) regarding feedstock and energy consumption

Raw Material	Price	Propylene process (/year)	Bio-based process (/year)	
			From refined glycerol	From crude glycerol
Propylene	$1664 /ton [1]	9,375 ton [2]	-	-
Refined glycerol	$595.25- 749.57 /ton [3]	-	20,536 ton [4]	-
Crude glycerol	$77.16-198.42 /ton [3]	-	-	25,669 ton [5]
Steam	$7.31 /ton	20,089 ton [6]	82,142 ton [7]	82,142 ton [7]
Energy	$0.05/kWh	0	$2.67*10^6$ kWh [8]	$2.67*10^6$ kWh [8]
	Total	$15.74 MM [9]	$12.95-16.13 MM [10]	$2.71-5.83 MM [11]

[1] the price reported in February 2011 by ICIS [153]
[2] calculated based on the 10,000-ton annual acrolein production and 80 mol% acrolein yield: [10,000 ton/(56 g/mol)*(42 g/mol)]/80%=9,375 ton
[3] the price reported in September 2010 by ICIS [154], except for that the lower end of crude-glycerol price [155]
[4] calculated based on the 10,000-ton annual acrolein production, 80 mol% acrolein yield, and the stoichiometry of glycerol dehydration to acrolein: [10,000 ton/(56 g/mol)*(92 g/mol)]/80%= 20,536 ton
[5] calculated based on the same assumptions as 4 and the assumption that the crude glycerol contains 80% glycerol: [10,000 ton/(56 g/mol)*(92 g/mol)]/80%/80%=25,669 ton
[6] calculated based on the feed molar ratio of propylene-air-steam as 1:10:5 and the calculated propylene requirement: 9,375 ton/(42 g/mol)*(18 g/mol)*5=20,089 ton
[7] calculated based on the calculated requirement for glycerol and the assumption that the feed has a concentration of 20 wt% glycerol: 20,536 ton/20%= 82,142 ton
[8] calculated based on the heat requirement (43 kJ/mol) for the endothermic dehydration reaction (Appendix II) and the annual working hours of 8000 hours/year: [(10^5 ton/year*(10^6 g/1 ton)/(56 g/mol)]/80%*(43kJ/mol)*(0.000278 kWh/1kJ)=$2.67*10^6$ kWh/year
[9] ($1664 /ton)*(9,375 ton)+($7.31 /ton)*(20,089 ton)=$15.74*10^6$=$15.74 M
[10] low: ($595.25 /ton)*(20,536 ton)+($7.31 /ton)*(82,142 ton)+($0.05 /kWh)*($2.67*10^6$ kWh)=$12.95*10^6$=$12.95 M
high: ($749.57 /ton)*(20,536 ton)+($7.31 /ton)*(82,142 ton)+($0.05 /kWh)*($2.67*10^6$ kWh)=$16.13*10^6$=$16.13 M
[11] low: ($77.16 /ton)*(25,669 ton)+($7.31 /ton)*(82,142 ton)+($0.05 /kWh)*($2.67*10^6$ kWh)=$2.99*10^6$=$2.71 M
high: ($198.42 /ton)*(25,669 ton)+($7.31 /ton)*(82,142 ton)+($0.05 /kWh)*($2.67*10^6$ kWh)=$5.83*10^6$=$5.83 M

Consider bismuth molybdate as an example of the multi-component metal catalyst. In general, the acid catalyst is much cheaper than a multicomponent metal catalyst. For example, the retail price (Sigma-Aldrich) of the active compounds bismuth molybdate costs over twice as much as silicotungstic acid (Table 5-1). It is reasonable to assume that the relative cost difference remains the same, even though both catalysts would be available at a

much lower price on the industrial scale. The average lifetime of a multicomponent catalyst is 1-2 years. According to the statement made by Atia *et al.* on the catalyst lifetime and the regeneration [123], it is reasonable to make an assumption that each batch of the catalyst can last for about a half year. The catalyst quantity required in a 10,000 ton annual acrolein production via the propylene process is 7,083 kg, assuming 80mol% acrolein yield and 100 h^{-1} [1] gas-hourly-space velocity (GHSV). With these assumptions, the total cost of the acid catalyst is 1.01 times that of the multicomponent catalyst for an annual production of 10,000 ton acrolein (Table 1-5). Any improvement in GHSV and catalyst lifetime would reduce the ratio of catalyst cost of the glycerol process to that of the propylene process. If an assumption is made that the industrial catalyst price falls within the range of \$50/kg-500/kg for the propylene process (\$0.483MM -4.83MM per year), the cost of the catalyst for the glycerol-based method is \$0.488 MM-4.88 MM per year. Then the difference of the catalyst cost between the bio-based method and the propylene-based ($\Delta C_{catalyst}$) is \$0.005 MM-0.05 MM.

Table 1-5: Catalyst comparison of propylene-based and the glycerol-based acrolein production (10,000 ton/year)

	Propylene process	**Glycerol process**
Active catalyst	bismuth molybdate	silicotungstic acid
Retail price	\$3.53/g	\$1.62/g
Life time	1.5 year	0.5 year
Quantities	9,657 kg [1]	7,083 kg [2]
Total cost factor (/year) [3]	**1**	**1.01**
Total cost (/year)	\$0.48 MM -4.83 MM [4]	\$0.49 MM-4.88 MM [5]

[1] calculated for 10,000 ton acrolein production. Acrolein yield of 80mol% was assumed. The density of the bismuth-molybdate-based catalyst was used as 5670 kg/m^3, and GHSV was used as 800 h^{-1}
[2] calculated for 10,000 ton acrolein production. Acrolein yield of 80mol% was assumed. The density the silicotungstic-acid-based catalyst was used as 520 kg/m^3, and GHSV was used as 100 h^{-1}
[3] Due to the fact that the industrial catalyst price of propylene process is unknown, this factor reflects the relative relationship between the catalysts of propylene-based process and bio-based process.
[4] calculated based on the assumption that the price of the industrial catalyst for propylene-based production falls within the range of \$50/kg-500/kg
[5] lower limit: \$0.483 MM*1.01=\$0.288 MM; upper limit: \$4.83 MM*1.01=\$4.88 MM

Based on Equation 1-7, the difference of the variable cost ($\Delta C_{v,}$) between the bio-based acrolein production from refined glycerol and the propylene based method is -\$2.78MM [(12.75-15.74)MM+(0.488-0.483)MM] to 0.44MM [(16.13-15.74)MM+(4.88-4.83)MM];

while ΔC_v from crude glycerol is -$13.03MM [(2.71-15.74)MM+(0.488-0.483)MM] to -$9.86MM [(5.83-15.74)MM+(4.88-4.83)MM].

The current acrolein price is $2673 per ton (quoted 2010-3-31); equivalently, the total annual market sales of 10,000-ton acrolein would be $26.73MM (from a propylene-based process). If the profit is assumed to be 20% of the total annual market acrolein sales (λY), the summation of the variable cost and the fixed cost is $21.38 MM [$26.73MM*(1-20%)] for current propylene production. If the same profit ($5.34 MM) is assumed, based on Equation 1-5 and the variation on the variable and the fixed cost discussed above, the total annual market acrolein sales via the bio-based route from refined glycerol should be $24.50MM ($(15.74-2.78)MM+1.1*$(21.38-15.74)MM+$5.34MM) to $27.72MM ($(15.74+0.44)MM+1.1*$(21.38-15.74)MM+$5.34MM). Consequently, the market price of acrolein from refined glycerol is $2304-2626 per ton. The total annual market acrolein sales via the bio-based route from crude glycerol should be $15.38MM ($(15.74-$13.03)MM+1.3*$(21.38-$15.74)MM+$5.34MM) to $18.55MM ($(15.74-$9.86)MM+1.3*$(21.38-15.74)MM+$5.34 MM). It results in the market price of acrolein from crude glycerol is $1538-1855 per ton.

Based on the estimation above, at the current developmental stage of gas-phase glycerol dehydration, the acrolein price provided by the bio-based route using refined glycerol as the feedstock is equivalent to the current manufacturing method; the price is significantly reduced (31-42% reduction) if the production begins with crude glycerol. It is worth noting that the estimation was based on the modest assumption that represents the current average developmental stage of this bio-based method (GHSV 100h^{-1} and 80mol% acrolein yield). Compared with over a half-century development of the propylene methods, extensive research on the gas-phase glycerol dehydration began just several years ago. The research is underway to improve the acrolein yield and, more importantly, on-stream-time. A longer on-stream-time allows larger GHSV for a given operation period. Any improvement in GHSV, the acrolein yield (higher than 80 mol%) and/or catalyst life time would further lower the acrolein price produced from glycerol.

The glycerol market has been very volatile in the past few years. Therefore, a sensitivity analysis was conducted to calculate the bio-based acrolein price with a wide price

range of glycerol (both refined and crude) (Figure 1-11). The price of bio-based acrolein from crude glycerol is still much cheaper than propylene-base acrolein even if the price of crude glycerol reaches $250/ton. In addition, the price of the catalyst for partial oxidation of propylene is used as one axis, due to the difficulty in obtaining the exact price. As stated previously, the price of the Bi-Mo-O catalyst falls within this range ($50-$500/kg).

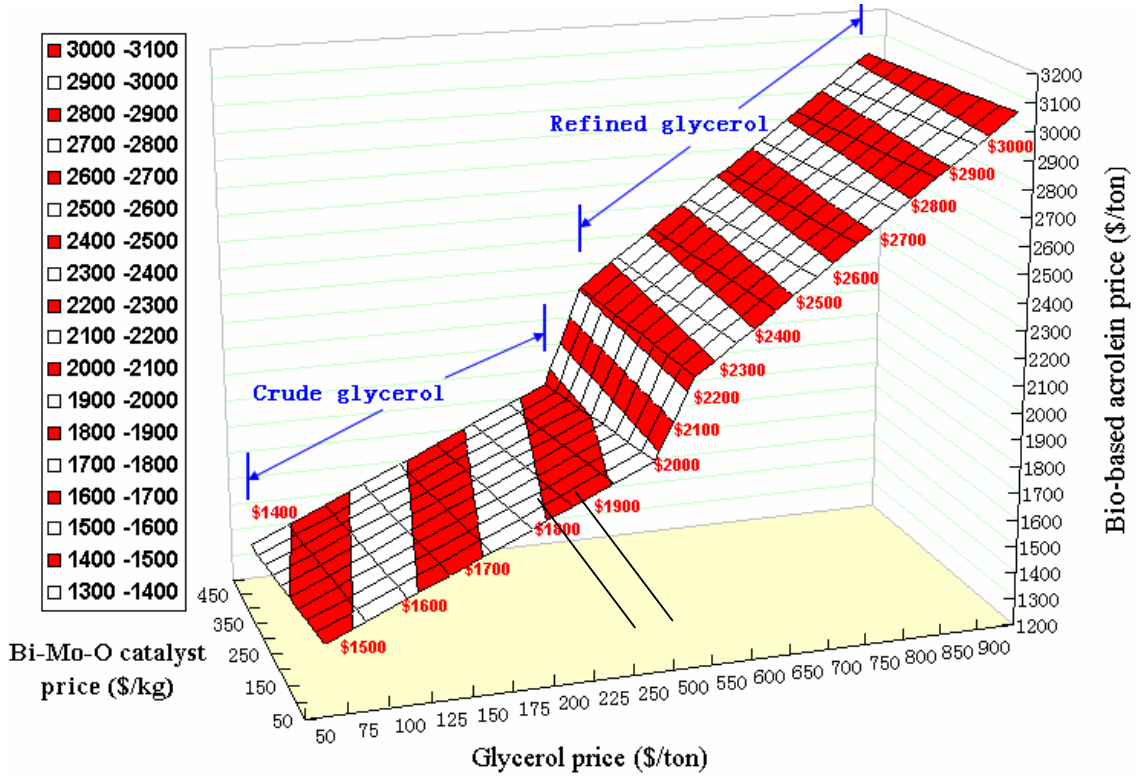

Figure 1-11: The calculated price of bio-based acrolein as the functions of the price of refined/crude glycerol and the price of the catalyst for propylene oxidation

In addition, it is also worth mentioning that government policies and regulations are usually in favor of the sustainable bio-based production. For example, the Renewable Energy and Job Creation Act (H.R. 6049) that passed in Sept. 2008 provides approximately $18 billion of tax incentives for investment in renewable energy, carbon capture and sequestration demonstration projects, energy efficiency and conservation. Numerous tax-credit programs have long existed supporting biodiesel production. Several proposals are on the way, which provide some possibilities such as a 30-cents-per-pound tax credit for bio-based chemical production in large-scale plants, and even a higher rate for small-scale producers [156]. In this calculation, the tax expenses were assumed to be the same for both processes. However,

the fact is that this part of the expense would be much lower for the bio-based processes because of the varieties of tax credits. Therefore, the bio-based acrolein production cost could be further lowered.

Other than launching a complete new individual bio-based acrolein production plant, a couple of optional strategies are available. As mentioned before, both gas-phase reactions shared some operation similarity. The current manufacturing method uses a packed-bed reactor operating in the range of 300-400°C. These conditions should not require much modification to switch to a gas-phase glycerol dehydration method: the gas pipelines can be readily connected to a different carrier gas source, and after changing the heat exchanger to a furnace, the packed-bed reactor is ready to operate after changing the oxidation catalyst to the dehydration acid catalyst. The post-processing layouts may be directly utilized in the bio-based production with minimal adjustment. Therefore, the installation cost, including the cost of major equipment, the installation, engineering and field expenses, and the contractor's fee, can be minimized. Consequently, it is a very tempting scenario for the current acrolein manufacturer to launch the bio-based acrolein production on their current plant setting, the decision-making of which might be already on their discussion table.

Also, instead of completely replacing the propylene method, the bio-based acrolein production from glycerol, serving as a complementary method, may be more likely to be the industrial tide in the near future. An integrated process combining the two methods, operating simultaneously, can fully take advantage of the exothermic characteristic of one reaction and the endothermic character of the other, saving some of the production cost. The disclosure of a combined process of glycerol dehydration and propylene oxidation indicates that a transitional stage has begun to launch a glycerol-conversion method industrially [157].

As mentioned in Section 1.1.1, acrylic acid production is a major consumption of acrolein; the production is growing each year due to the market demand for acrylic acid. It is worth nothing that there is barely any technical barrier, uncertainty or challenge existing in converting bio-based acrolein to acrylic acid. The gas-phase catalytic oxidation of acrolein to acrylic acid is an industrially well developed process. The facility is usually built on the site of the acrolein plant to minimize the handling and transportation of acrolein. Usually the oxidation of acrolein to acrylic acid is catalyzed by V–Mo–(W) mixed oxides in a packed-bed

reactor at an elevated temperature (240-300°C); acrolein conversion is typically around 99% and selectivity to acrylic acid around 95 mol% [158-161]. The current industrial practice (technology and facilities) can be directly adapted in realizing this process to produce bio-based acrylic acid.

The attractions are enormous, including the ecological benefits, the steadily rising demand for the petrochemical products in competition with the draining petroleum resource, and the expansion and growth of the bio-based industry. The price advantage of glycerol as a feedstock has already been demonstrated; what makes the glycerol approach more attractive is that with the continuous growth of biodiesel production and the continuous shrinkage of non-renewable petroleum resource, an increasing trend of the price difference can almost be ensured. The analyses and conclusions not only agree with some previously forecasted statements [99, 108], but also are in line with the current industrial movement [162, 163]. Arkema, the fifth largest acrylics manufacturer, is building a demonstration plant of bio-based acrolein/acrylic acid production within 3 years [164]. The world's third largest manufacturer, Nippon Shokubai, received $225,000 funding from the Japanese government in 2009, and has been launching the R&D of this bio-based route from glycerol to acrolein/acrylic acid ever since. Their pilot plant will be ready in mid-2011 [165].

1.4 Conclusions

The chemical industry must energize its proven technological capabilities to change fundamentally how chemical intermediates and products are made. The continuation of a vibrant chemical industry requires a radical change in strategy akin to the introduction of the alternative feedstocks that have greater sustainability and (potentially) lower cost. From aldol condensation, to partial oxidation of propylene, and then to the research interest in propane oxidation, history bears witness to the incentive of the industrialization of a synthetic approach, justifying the actions taken toward a bio-based route. The bio-based route (producing acrolein from the biodiesel byproduct glycerol) has already met some promising milestones at this point, however, challenges remain. Research efforts underway today that focuses on the bio-based route might be a necessity for the survival and growth of acrolein (acrylic acid) manufacturers tomorrow.

Chapter 2

Non-thermal plasma physics & chemistry:

fundamentals & applications

Plasma is an ionized gas: at least one electron is not bound to an atom or molecule in the system, making that atom or molecule a positively charged ion, although the system remains electrically neutral. Analogous to gases, the plasma temperature is determined by the average energy of all the plasma particles and their relevant degrees of freedom. The existence of various types of plasma particles with various degrees of freedoms allows the plasma to remain away from thermodynamic equilibrium. Plasma of this type is known as non-thermal plasma (NTP), where there are "very hot" electrons and the "cool" heavy particles (neutral species, ions, etc). Usually in NTP, ionization and chemical processes are directly determined by the electron temperature, instead of the thermal process or the overall gas temperature. NTP features high energy efficiency; the discharge power can be controlled efficiently and selectively.

2.1 NTP physics

Electric breakdown of a neutral gas in the presence of an external electric field is the fundamental basis of non-thermal plasma. The applied voltage must exceed the breakdown voltage for the gases to form plasma. An expression for this voltage is given below, at which point the gases lose their dielectric properties and become conductors. The governing equation of the breakdown voltage related to the gap distance and the pressure [166] is shown in Equation 2-1, and the plotted relationship between breakdown voltage and the distance and the gas pressure is presented in Figure 2-1.

$$V = \frac{B \cdot (p \cdot d)}{\ln\left[A \cdot p \cdot d / (\ln \frac{1}{\gamma} + 1) \right]}$$ **Equation 2-1**

where V is the breakdown voltage, p is the gas pressure, d is the distance between two electrodes; A and B are constants that depend on the composition of the gas; γ is Townsend coefficient characterized by the secondary electron emission (The values for several gases are listed in Table 2-1.)

Table 2-1: List of the constants A and B (Equation 2-1) for the empirical calculation of the Paschen curve and the minimum sparking potential, or the easiest breakdown condition, for various gases [166, 167]

	H_2	He	N_2	O_2	Argon	Air	H_2O
A (cm^{-1} $Torr^{-1}$)	5	3	10	-	12	15	13
B ($V\ cm^{-1}$ $Torr^{-1}$)	130	34	310	-	180	365	290
$V_{min\ (V)}$	273	156	251	450	137	327	
pd at V_{min} (Torr · cm)	1.15	4.0	0.67	0.7	0.9	0.567	

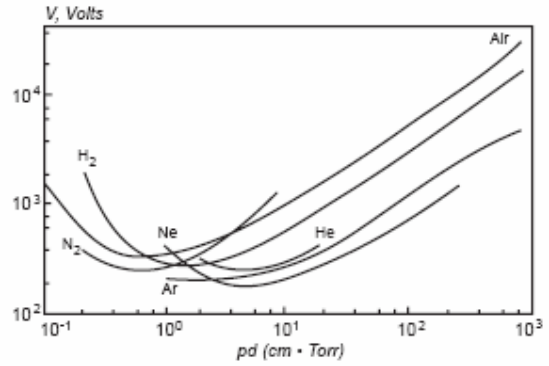

Figure 2-1: Breakdown Paschen curves for different atomic and molecular gases (reprint with permission [166])

The energetic electrons transform kinetic energy into potential energy of the excited species by energizing the atoms and molecules. The energy transfer by electrons is very efficient, and more than 90% of the kinetic energy can be transferred. The effective stationary breakdown voltage is approximately 50% higher than the theoretically calculated Paschen field [168].

Depending on the discharge formation mechanism, the pressure range, electric source and the electrode configuration, non-thermal plasma can be categorized as follows: corona discharge, glow discharge, dielectric barrier discharge (DBD), radio-frequency discharge, and microwave discharge. DBD can generate non-thermal plasma in the most simple and flexible way in terms of the configuration, operating medium and operating parameters [169]. It is highly efficient and has low power consumption [166]. More importantly, the scale-up of this NTP technology to a large dimension is comparatively straightforward [169, 170]. These features make DBD attractive to a variety of applications. Usually, the gas breakdown occurs in a number of individual tiny breakdown channels (or ionized plasma channels), referred to

as microdischarges. The plasma energy is transferred between the accelerated electrons, the atoms, and molecules both within and outside of the microdischarge. Generating DBD non-thermal plasma can be as simple as applying a high voltage AC between two electrodes that are separated by at least one dielectric barrier. The dielectric barrier in a DBD serves two functions. First, it limits the amount of transported charges and energy in a single microdischarge, so the discharge can be extinguished when the voltage drop falls below the breakdown voltage. Second, it allows parallel filaments to form in close proximity, so that the microdischarges are well distributed over the entire electrode surface. Figure 2-2 demonstrates several configurations that have been used frequently to generate a DBD discharge [169, 171-174]. There are three basic layouts: the dielectric barrier on the ground or high-voltage electrode, the barriers on both electrodes, and the barrier in the middle of the discharge gap without contacting either electrode. Each of the three layouts can be assembled in either a planar configuration (Figure 2-2 A,B,C) or a cylindrical configuration (Figure 2-2 D,E,F).

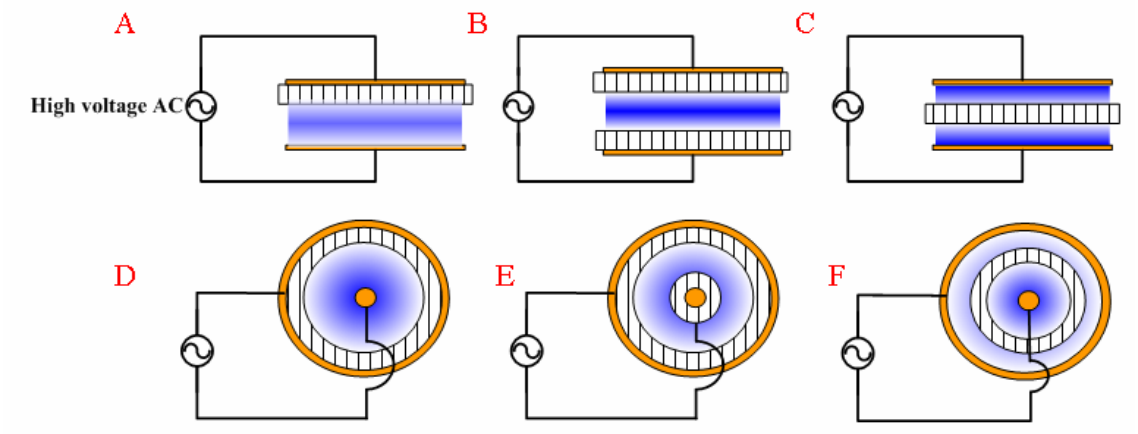

Figure 2-2 Common planar and cylindrical configurations of dielectric barrier discharge [8]

The plasma characteristics can be manipulated by adjusting the operating parameters, such as the applied voltage and frequency, temperature and pressure, changing the operating medium, such as the gas properties, and modifying the discharge zone configurations, such as the electrode materials and the geometrical orientation [169].

The microdischarge current with spike-like patterns usually has a discharge duration of a few nanoseconds, which is too short for the current probe to acquire an accurate reading. Therefore, it is difficult to determine the dissipated power via the ordinary method by integrating the voltage multiplied with the current over the unit time interval (Equation 2-2) [175].

$$P = \frac{1}{t}\int_0^t U(t')I(t')dt \qquad \textbf{Equation 2-2}$$

where P is the power, t is a unit time interval, $U(t')$ is the voltage across the discharge area at the time point t', and $I(t')$ is the current at the time point.

Manley developed in 1943 [175] the technique of using the Lissajous figure as an alternative approach to determine the dissipated power, which has become a well-accepted alternative method for DBD plasma power determination ever since. The usage of closed voltage/charge Lissajous figures bypasses the necessity to resolve the individual microdischarge current peak, and uses the time-integrated current instead. A Lissajous figure is obtained by connecting a capacitor (usually several nF) [174, 176] in the circuit in series to the plasma discharge. The average power dissipated across the discharge area is obtained by the multiplication of the area of the Lissajous close parallelogram, the discharge frequency, and the capacitance (Equation 2-3):

$$P = \frac{1}{t}\oint U(Q)dQ = C_M f \oint U dU_c \qquad \textbf{Equation 2-3}$$

where t is a unit time interval, U is the voltage across the discharge area, Q is the electric charge, f is the frequency, C_M is the capacitance of the capacitor, and U_c is the voltage across the capacitor.

The field strength is a common parameter used to specify the plasma configuration in plasma kinetic studies. It is defined as the discharge voltage divided by the discharge gap, or the distance between two electrodes (Equation 2-4) [177-179]:

$$Field\_Strength = V/d$$ **Equation 2-4**

where V is discharge voltage, usually in the unit of kV, and d is the distance between the electrodes.

2.2 NTP chemistry

In non-thermal plasma, electrons have very high temperatures on the order of 10^4-10^5 K (1-10 eV), but the overall gas temperature can remain as low as room temperature [180, 181]. Electrons first gain energy from the electrical field [182]. The highly energized electrons fill the system, and collide with other particles in the system. Because of the large mass difference between electrons and the other particles (molecules, ions, etc.), the collisions are inelastic. The energy transferred from electrons to these particles retains potential energy instead of kinetic energy. Therefore, instead of wasting energy for increasing the gas temperature (kinetic movement of the gas particles), the energy is more efficiently and specifically utilized in chemical processes, such as ionization and bond dissociation [166]. A broad range of reactive species can be generated by non-thermal plasma, including vibrationally excited species as in conventional chemistry, electronically exited species, super-excited neutral molecules, free radicals, as well as positive and negative ions. For example, the major active neutral species produced in air by discharge are $O_2(^1\Delta_g)$, $O(^3P)$, $O(^1D)$, $O(^1S)$, $N_2(A^3\Sigma_u)$, $N_2(a'^1\Sigma_u)$, $N_2(B^3\Pi_g)$, $N_2(C^3\Pi_u)$, $N(^4S)$, $N(^2P)$, $N(^2D)$, NO, and $NO^*(A^2\Pi^+)$. In addition, when humidity is significant, highly reactive species are formed: $H_2O.^+$, H., .OH, or HO_2 and cluster ions containing H_2O [166]. The important reactions in NTP include excitation, dissociation, attachment, ionization, recombination, charge transfer, and decomposition [183]. The most common plasma reactions of molecular gases are summarized in Table 2-2.

Table 2-2: Main plasma reactions in molecular/atomic gases [166, 170]

Reaction name	General Equations
Excitation	$e + A \rightarrow A^* + e$ $e + A_2 \rightarrow A_2^* + e$
Ionization	$e + A \rightarrow A^+ + 2e$ $e + A_2 \rightarrow A_2^+ + 2e$
Dissociative ionization	$e + A_2 \rightarrow A^+ + A + 2e$
Penning ionization	$M^* + A \rightarrow A^+ + M + e$ $M^* + A_2 \rightarrow A_2^+ + M + e$ M^*:metastable species
Dissociation	$e + A_2 \rightarrow 2A + 2e$
Penning ionization	$M^* + A_2 \rightarrow 2A + M$
Attachment	$e + A_2 \rightarrow A_2^-$
Dissociative attachment	$e + A_2 \rightarrow A^- + A$
Charge exchange	$A^+ + B \rightarrow A + B^+$
Recombination	$e + A_2^+ \rightarrow A_2$ $A^+ + B^- \rightarrow AB$ $A + B + M \rightarrow AB + M$

NTP can excite most chemical species, including those that cannot be excited in conventional chemistry or even in photochemistry; NTP can efficiently increase the internal energy of the reactants and facilitate them to overcome the reaction barrier [184]. During collision, the highly energetic electrons can transfer energy efficiently to the reactants for their bond dissociation, ionization, recombination, and so on. High electron temperature, but low overall gas temperature, determines the unusual chemistry in non-thermal plasmas. High-energy efficiency, high specific productivity, and high selectivity can be achieved in plasma for a variety of chemical processes [166, 183-185].

2.3 NTP applications

High electron temperature, but low overall gas temperature, determines the unusual chemistry of non-thermal plasmas. Here are some areas where NTP application has been studied.

Lots of research activities have been developed using NTP in converting greenhouse gases into value-added products. NTP-assisted partial oxidation of methane into methanol has attracted much research interest due to the increasing demand of methanol in the biodiesel production. DBD configuration is considered as one of the most promising techniques to achieve a one-step synthesis. This NTP-assisted, one-step methanol synthesis would not only reduce both capital and operational costs, but also would significantly reduce the greenhouse gas emission, if the technology were successfully developed. Recent developments and issues regarding NTP-assisted methanol production have been reviewed [186, 187]. NTP has also been applied to reforming methane to syngas, the recent development of which was reviewed by Chen *et al.* [184]. Synergistic effect between catalysts and NTP has been claimed in many studies. For example, Pietruszka and Heintze claimed that NTP chemically activated reactants, and thus accelerated the processes of reactant adsorption and product desorption [188]. Kraus *et al.* made a similar statement that the discharge-active methane was easier to adsorb onto the catalyst surface [174]. Although the technology in this application has yet to mature, the NTP approach has already shown some promise in improving the reactivity and yield and in preventing catalyst deactivation due to coke deposition, sulfur presence, and high temperature [189] [190]. Plasma-chemical processes allow the dissociation of CO_2, which is the basis of the value-added CO_2 utilization. A non-thermal plasma system is well known for its energy efficiency in CO_2 dissociation; the discharge energy can be selectively focused on the dissociation processes. The principle and kinetics have been detailed in Chapter 5 of Fridman's book [166]. The plasma assisted reaction between CO_2 and hydrogen can lead to methanol production. More importantly, the reforming of CO_2 and methane simultaneously to higher hydrocarbons, aldehydes, and carboxylic acids can be achieved with NTP reactors. The NTP technologies for reforming of CO_2 and methane have been comprehensively reviewed by Liu *et al.* [180] and Istadi and Amin [191].

NTP has long been used as an efficient tool for the removal of atmospheric pollutants, such as volatile organic compounds (VOCs) from ambient air and nitrogen oxides in the flue gas and engine exhaust. Common VOCs, such as benzene, xylene, toluene, formaldehyde, formic acid, trichloroethylene, and dichloromethane, have been studied in the past with the NTP catalytic technology [185]. Basically, the oxidative species excited by NTP oxidize VOCs into CO_x, (eventually CO_2); the presence of catalysts improved the VOCs adsorption,

and caused the formation of some surface oxygen species, which actively participated in the surface oxidation reactions. The synergistic effect between the catalyst and NTP greatly improved the removal thoroughness, energy efficiency, and mineralization rate [185]. NTP has also been used in the removal of the NO_x from the engine exhaust [192-196]. The synergistic combination of NTP's oxidative potential, proper catalysts, and the reducing agent ammonia, hydrocarbon or CO, allows the conversion of NO_x to molecular nitrogen efficiently at low temperatures.

NTP technology has also been applied to treat wastewater. For example, a NTP system is incorporated by a sewage treatment plant in southern Ontario to control the odor in 120,000 cfm air emissions [135]. NTP plays this role in several ways. The NTP discharge can physically disrupt biological cells. UV induced photo-chemistry in the NTP system helped destroy microorganisms. In a gas-liquid discharge environment, the active species formed in the gas-phase can diffuse into the liquid, and the liquid molecule can evaporate and affect the gas-phase reactions. For example, $H_2O.^+$, which is formed via a charge-transfer mechanism in NTP, diffuses into the liquid-phase bulk water, and subsequently forms hydroxyl radicals. The hydroxyl radical can recombine with water to form H_2O_2 [166]. Also, the negative oxygen ions formed in the air under the NTP discharge can also induce the formation of .OH radicals and H_2O_2, both of which are strong oxidants to kill microorganisms. Last but not least, ozone formed by discharge in the air diffuses into water, and ozone itself is a strong oxidant that damages microorganism. A technical review by Locke *et al.* in this area is available for the details [197].

NTP has been studied both theoretically and experimentally in the reduction of the oxides of metals [198-201] and other elements [202]. The key to this metallurgical process is the high-efficiency of generating H atoms by NTP. The H atoms formed via surface dissociation initiate the metal reduction at the surface, and then the H atoms diffuse into the crystal structure; as the result, the metal reduction starts on the surface and propagate further into the solid body [166]. One direct application is to use this technology for the reduction of metal catalysts instead of using thermal reduction. Some studies have already shown the advantages of NTP reduction in comparison to thermal reduction [203-205].

The utilization of plasma techniques during catalyst preparation has been reported in the literature, and the developments in this field were well summarized in the reviews by van Durme *et al.* [185], Liu *et al.* [206], and Kizling [207]. The unique functions of NTP include the generation of ultra-fine particles, the deposition of catalytically active species, enhanced preparation such as fast metal reduction, and surface modification.

Various NTP applications can be found in the area of surface modification. In the textile industry, NTP treatment can successfully increase the hydrophilic character of almost all types of fibers by introducing water compatible functional groups, such as –COOH, –OH and $–NH_2$ [208]. It was reported that the DBD technique could modify surface morphology, increase the frictional coefficient of the fiber, and improve the cohesion force of soybean protein fibers [209]. DBD plasma has been commonly used in polymer surface modification [210-217]. Utilization of non-thermal plasma in chemical vapor deposition is advantageous compared to the conventional route in that the energy barrier can be easily overcome with NTP to prevent the high-temperature disruption of heat-sensitive substrate materials. NTP can generate chemically active species, leading to film formation, and also NTP can bombard the surface with the active species, introducing new properties to the surface materials. The technical details in this area have been reviewed by Alexandrov and Hitchman [218]. A wide range of organic compounds have been applied for plasma polymerization, such as hydrocarbons, acetone, ethylene oxide, hexamethyldisiloxane, and so on [219]. Via NTP with different discharge gases, specific functional groups can be implanted on the material surface. Ge *et al.* [220] used DBD to modify nanometer scale carbon materials properties, and found that different discharge conditions caused different surface behaviors. They proved that by manipulating the discharge configuration, carbon black can be adapted according to one's needs. Gessner [221] found that functional groups can be deposited onto glass or a polymer surface with the DBD plasma treatment.

There have also been some applications of NTP in inorganic chemistry; and some examples are given as follows. The non-thermal plasma assisted synthesis of ammonia was reported [222]. The production of hydrogen cyanide was catalyzed through the vibrationally excited nitrogen molecule N_2^* under NTP condition, and then continued via chain reaction [223, 224]. Non-thermal plasma helped overcome the energy barrier required for breaking the

strong N-N bond, and achieved higher conversion to NO. The vibrationally excited N_2 molecules and the resulting dissociative recombination of N atoms activated by NTP are the key contributors for the reaction to proceed [166]. Non-thermal plasma could vibrationally excite CO molecules and act effectively in the synthesis of metal carbonyls. The process was especially valuable for the synthesis of $Cr(CO)_6$, $Mo(CO)_6$, $Mn_2(CO)_{10}$, $W(CO)_6$, since they could not be alternatively produced by independent of solvents [166]. Non-thermal plasma was applied in hydride formation, such as reacting solid Si with the plasma-activated H in forming SiH_4. Non-thermal plasma was also applied in the decomposition of halides [166].

In summary, the non-equilibrium characteristics of non-thermal plasma allow a variety of chemical processes. Good selectivity can still be achieved if the difference in the bond disassociation energies exists. Approximately, a difference of 4.2 kJ/mol in bond dissociation energy is sufficient to lead to a selectivity ratio of 9 to 1 at room temperature, while a 42 kJ/mol difference in the bond disassociation energies can ensure selective bond breaking under plasma conditions [183]. High energy efficiency, high conversion, and high selectivity can be achieved in non-thermal plasma for a variety of chemical processes. Non-thermal plasma application has been extended to more and more areas; however, the limit of NTP application remains unclear, creating a challenge for future researchers. The applications of NTP and the studies regarding NTP chemistry have been extensively reviewed; with the knowledge, it is concluded that whether non-thermal plasma can play a part in dehydration process has never been studied.

Objectives

Bio-based acrolein production is one of the most promising processes in developing the chemical platform of glycerol in support of biodiesel production. This study is to contribute to the development of this bio-based approach. Instead of focusing on searching for new solid acid catalysts, a different approach is taken by integrating non-thermal plasma (NTP) into the process. Extensive literature review shows that NTP application in dehydration has never been reported. This study uses this particular dehydration process (glycerol dehydration to acrolein) to discover the potential of NTP in dehydration.

The main objective is to discover whether and to what extent NTP application can improve the process of converting glycerol to acrolein. The main objective is divided into three sub-objectives. The first one is to study the NTP effect during the acid-catalyzed dehydration reaction. The second is to solve the catalyst deactivation problem using the NTP technique. The third is to study whether applying NTP to the catalyst preparation could contribute to fabricating better acid catalysts for glycerol dehydration reaction.

Chapter 3

Glycerol dehydration to acrolein catalyzed by supported silicotungstic acid

Abstract

The value of the bio-based acrolein production route via glycerol dehydration has been addressed in Chapter 1. In this Chapter, differently supported silicotungstic acid (HSiW) catalysts were studied to better understand the effect of supporting materials and the acid, and to reduce the number of the catalysts for the non-thermal plasma (NTP) study. Three supports (Al2700, Si1252, and Si1254) loaded with HSiW were studied for the glycerol dehydration at 275°C. The catalyst deactivation was most severe for Si1254 supported HSiW, which even negatively influenced the acrolein selectivity. Between Si1252 supported HSiW and Al2700 supported HSiW, the former one showed higher acrolein selectivity and faster deactivation, while the latter one featured relatively much longer lifetime.

Keywords: glycerol conversion, acrolein selectivity, catalyst deactivation, supported silicotungstic acid

3.1 Introduction

Heteropoly acids (HPAs) feature strong Brønsted acidity and have flexibility to be modulated. They are also economical and environmentally friendly. Because of numerous virtues, HPAs have attracted more and more attention and have been successfully applied to many acid-catalyzed reactions. Silicotungstic acid (HSiW), one of HPAs, has been previously proven as one of the most effective acid catalysts that have been studied for acrolein production from glycerol [101, 102, 139].

Alumina (Al_2O_3) and silica (SiO_2) are two of the most common supporting materials used in the industry for providing large surface area to accommodate the desired chemical reaction. Several research groups [101, 102, 139] have studied these two supports for glycerol dehydration to acrolein. However, it seems that a consensus has not yet been reached regarding which one is superior. Tsukuda *et al.* [102] found that a proper mesopore size was important for acrolein production, and that among the three investigated supports with different pore sizes, the two silica supports with larger pore sizes (6 nm and 10 nm; surface area: 466 m^2/g and 310 m^2/g) both provided high glycerol conversion and high acrolein selectivity. Atia *et al.* [101] claimed that alumina-supported acid showed higher catalytic

activity and acrolein selectivity than silica-supported acid, although the reported selectivity did not exceed what Tsukuda reported. As a result, both alumina and silica were used for the kinetics study. Grace Davison (Slough, UK) is one of the largest world-wide providers of the high quality catalyst support in large varieties to numerous industrial practices. It is useful and informative to directly conduct the study upon some commercially available products. Screening was conducted among all the available supporting materials based on the physical properties (pore size, particle size and surface area) and the knowledge obtained from literature. The following three different supports, Al2700, Si1252, and Si1254, were selected to be used in the study. The objective in this section was to compare how the differently supported catalysts differ in their characteristics and catalytic performance in glycerol conversion to acrolein, and to finalize one (or two, at most) catalyst(s) for non-thermal plasma kinetic study.

3.2 Materials and Methods

Catalyst preparation

Mesoporous Al_2O_3 (Davicat® Al2700) and two types of mesoporous SiO_2 (Davicat® Si1252 and Davicat® Si1254) were supplied by Grace-Davison (Slough, UK). The specification data provided by the manufacturer are listed in Table 3.1. Silicotungstic acid ($H_4SiW_{12}O_{40}\cdot 24H_2O$, hereafter abbreviated as HSiW) was purchased from Sigma Aldrich (St. Louis, MO, USA).

Table 3-1: Manufacturer data of material properties of the catalyst support

Name	Si 1252	Si 1254	Al 2700
Shape	granules	granules	beads
Particle size (mm)	1-3	1-3	1.2-2.4
Average pore diameter (nm)	11	6	N/A
Pore volume (cc/g)	1.02	0.81	1.10
Surface area (m^2/g)	390	540	150
Density (g/cm^3)	0.43	0.38	0.40

HSiW was loaded onto the catalyst support by the impregnation method. The support was calcined at 300^o C for 2 hours before use. HSiW of 10% weight percentage (wt%) of the support was dissolved in deionized water to make a 0.04g/mL solution. The calcined support

was added to the HSiW solution. Constant stirring was applied to the mixture at room temperature for 24 hours to ensure the equilibrium of adsorption-desorption processes. The resultant mixture was dried first at 55°C for 24 hours with the application of constant stirring. Then the mixture was dried at 105°C until complete dryness (~6 hours). The mixture was calcined at 300°C before the 2nd impregnation for another 10 wt% acid loading. The procedure was repeated until the desired amount of loading was achieved. 30 wt% loading for alumina and 20 wt% loading for silica were selected based on the optimal loading from previous studies [101, 102]. Therefore, in total, three catalysts were used in the study, and they were Si1254 with 20 wt% HSiW loading (HSiW-Si1254), Si1252 with 20 wt% HSiW loading (HSiW-Si1252), and Al2700 with 30 wt% loading.

Catalyst characterization

Characterization of surface area, acid dispersion on the support surface, and acid strength was performed for the fresh catalysts, HSiW-Al2700, HSiW-Si1252 and HSiW-Si1254. Also, temperature programmed oxidation (TPO) analysis and surface area measurement were conducted for each of the three catalysts collected after 7.5 hours time-on-stream (TOS) to examine the coke deposition on each catalyst. The characterization methods are detailed as follows.

The surface area of the catalyst was determined via single-point Brunauer-Emmett-Teller (BET) measurement using a Pulsar ChemBET TPR/TPR station from Quantachrome Instrument (Boynton Beach, FL, USA). The catalyst (0.100g) was degassed at 300° C in the nitrogen atmosphere. The physisorption started when the sample cell was immersed into a liquid nitrogen bath, and then desorption occurred at room temperature. In order to quickly bring the temperature of the cell back to room temperature, the cell was immersed into water as soon as it was removed from the liquid nitrogen bath to facilitate the heat transfer. Both adsorption and desorption processes were detected by a thermal conductivity detector (TCD) and recorded on the computer. The volume of the desorbed nitrogen, together with room temperature and atmosphere pressure, was used to calculate the surface area of the catalyst via the following equation (Equation 3-1):

$$SA = {SA_{total}}/{w} = \frac{P \cdot V \cdot N \cdot A_{cs} \cdot (1 - P/P_o)}{R \cdot T \cdot w}$$ **Equation 3-1**

where SA is surface area, P and P_o are the equilibrium pressure and the saturation pressure of the adsorbates at the temperature of adsorption, V is the total volume of the adsorbed (or desorbed) nitrogen, N is Avogadro's number ($6.023*10^{23}$ molecules/mol), A_{cs} is the cross-sectional area of the N_2 molecule (0.162 nm^2), R is the gas constant, T is the temperature at which the desorption takes place, and w is the weight of the catalyst in the glass cell.

With the knowledge of the specific surface area, the surface coverage of HSiW on Si1252, Si1254, and Al can be calculated via Equation 3-2 [101]. This parameter provides the information of the coverage of the active acid sites on a given catalyst surface [20][101]:

$$D_{surface} = \frac{L\%}{(1 - L\%) \cdot M_{HSiW} \cdot A_{BET}}$$ **Equation 3-2**

where $D_{surface}$ denotes the surface coverage of HSiW on the support, $L\%$ is the acid loading weight percentage, M_{HSiW} is the molecular weight of HSiW (3310.66 g/mol) loaded on the silica, and A_{BET} is the surface area of the support, respectively [20].

The acid strengths of the solid catalysts were evaluated via temperature programmed desorption (TPD) using Pulsar ChemBET TPR/TPR station (flow diagram available in Appendix VII). The samples were preheated to 100°C and remained at 100°C for 1 hour with ultra-pure helium gas flowing through at 70 mL min^{-1}. The TCD signal had been stabilized by the end of this one-hour period. Then the inlet gas was changed from helium to ammonia, also at 70 mL min^{-1}, and kept ammonia flowing through the sample cell for 30 min at 100°C to ensure that the catalyst inside of the sample cell was saturated with ammonia. The inlet gas was switched back to helium (70 mL min^{-1}), and the helium flushed through the cell at 100°C for 2 hours to remove the physisorbed ammonia. The temperature of 100°C was used during the adsorption process to ensure that it was high enough to remove the physisorbed gaseous particles and low enough not to affect the subsequent chemisorption. The TPD was measured from 100°C to 600°C with the temperature elevation rate of 10°C min^{-1}. A TPD profile graph was obtained with temperature as the X-axis and the TCD signal (proportional to the amount of evacuated NH_3) as the Y-axis. In principle, NH_3 is absorbed onto the catalyst surface; NH_3

adsorbed on stronger acid sites will be more difficult to desorb (remove) from those sites, and will only do so when a higher temperature is applied. As the result, as the temperature elevates, the amount of the preferentially evacuated NH_3 will provide a measure of acid strength of the solid catalyst.

Powder X-ray diffraction (XRD) patterns were recorded on a Philips X'Pert PRO PW3050 X-ray diffractometer using Cu $K\ \alpha$ radiation (0.154 nm) and a graphite generator. The tube voltage and the current were 45 kV and 40 mA, respectively. The scan rate was 0.5º/min, and the scan range was 2º–80º with the step size of 0.04º.

The spent catalyst was characterized via TPO technique using Pulsar ChemBET TPR/TPR station (flow diagram available in Appendix VII). Prior to the formal TPO measurement, the spent catalyst (0.100g) was dried at 105ºC in a convection oven for 12 hours, and preheated at 300°C under nitrogen flow for 3 hours. The cell was cooled to room temperature, and then the inlet gas was switched to the oxygen-containing gas (5% oxygen blended with helium) flowing through at 70 mL/min. The TPO was measured from 25°C to 900°C at a temperature elevation rate of 10°C min^{-1}. The principle of this technique is the oxidation reaction between oxygen and the carbonaceous species (coke) deposited on catalyst surface. Coke has a distribution of carbonaceous species with different structural complexities, which require different temperatures to activate the oxidation reaction. The coke species with larger molecule weight and more complex structure would require a higher reaction temperature to be oxidized by oxygen. As the temperature elevates, the oxygen preferentially reacts with the surface coke species, and the consumed amount of oxygen gives a measure of the coke profile regarding the relative amount and hardness of the coke deposited on the surface during the reaction. Some surface coke can be directly oxidized into CO_2 and flushed off the catalyst surface; while some surface coke needed several steps before eventually being converted into CO_2. Therefore, the outlet effluent gas from the sample included the inert background gas helium, the remaining oxygen and CO_2. The ideal solution of monitoring the oxidation reaction was to let the effluent gas pass through a separation column before entering the detector, so that each gas could be quantified individually. However, there was no separation column built into the machine.

Glycerol dehydration

A schematic of the experimental layout is presented in Figure 3-1. Glycerol dehydration was carried out in a down-flow packed-bed reactor (PBR), which was oriented vertically. The base of the reactor was a quartz tube (length 300 mm, ID 19.35 mm, OD 25.3 mm). A 313 W heating tape (Omega Scientific, USA) was used to heat the PBR; this 4-foot tape was evenly wrapped around the outside wall of the quartz tube. The heating tape was controlled by proportional-integral-derivative (PID) temperature controller to maintain the desired temperature of the catalyst bed. The PBR had an external layer of thermal insulation material to minimize the heat loss to the surroundings. A volume of 7 mL of catalyst (~3.7g for HSiW-Si1254, ~3.2g for HSiW-Si1252, ~3.6 g for HSiW-Al2700) were packed at the lower end of the PBR, leaving sufficient travel length for carrier gas and glycerol feed to be preheated to the desired temperature before reaching the catalyst bed. Gas-hourly-space-velocity (GHSV), as defined in Equation 3-3, was used by most of the previous publications in glycerol dehydration. As the result, the catalyst was controlled by volume instead of weight to standardize the comparison of the kinetic performance under different conditions in this study with the same GHSV.

$$\mathbf{GHSV = u_{glycerol} / V_{catalyst}} \qquad \textbf{Equation 3-3}$$

where GHSV is gas-hourly-space-velocity (h^{-1}), $u_{glycerol}$ is volumetric flow rate of glycerol in the gas phase, and $V_{catalyst}$ is the catalyst bed volume

The glycerol solution (20 wt% of glycerol in water) was fed by a syringe pump with 6.02 g/hour feeding rate, which was equivalent to 84.4 h^{-1} GHSV of glycerol. Argon was used as the carrier gas, and its flow rate was regulated at 60 mL/min. The products after reaction traveled through a condenser with flowing tap water, and the majority of the liquid product was condensed in a 50 mL vial immersed in an ice-water cold bath (1st condensation stage). Any products that were unable to be condensed in the first condensation stage were collected in a 20 mL vial that was immersed in a liquid nitrogen bath (2nd condensation stage).

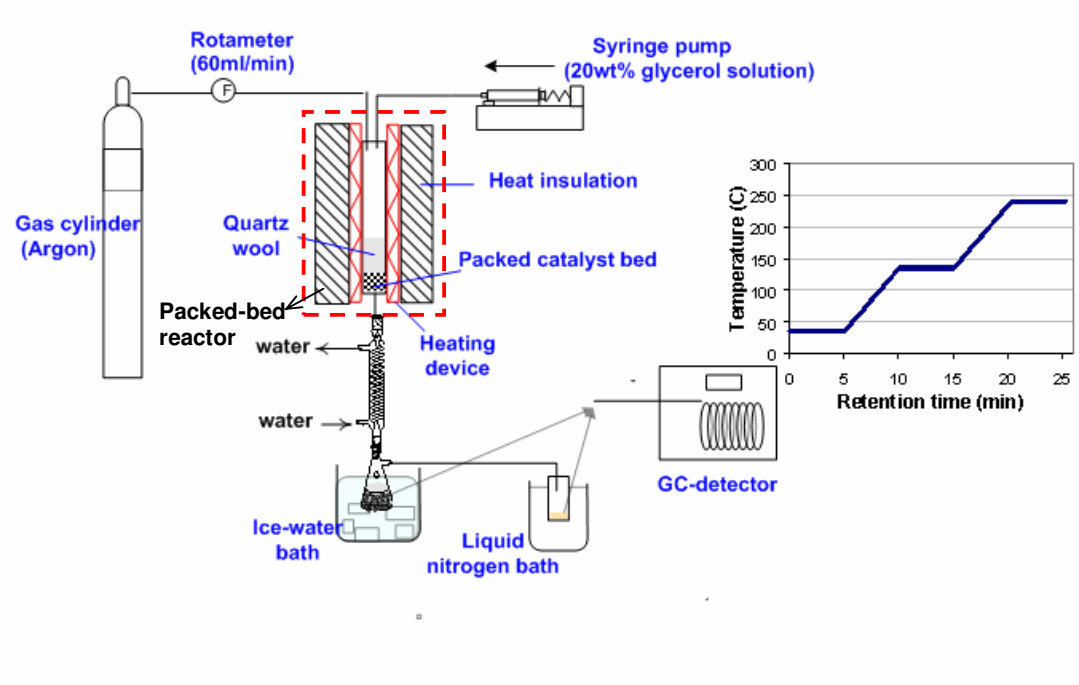

Figure 3-1: Apparatus for glycerol dehydration

After each 1.5 hour interval, the vials from the two condensation stages were replaced with a new set of vials. Each of the samples collected from the two condensation stages was individually analyzed via GC-FID, and the total concentration of a specific chemical was calculated via Equation 3-4:

$$C = \frac{C_1 \cdot W_1 + C_2 \cdot W_2}{W_1 + W_2}$$ **Equation 3-4**

where C is the concentration (g/g) of a quantified chemical, which was then used to calculate the conversion or selectivity, C_1 and C_2 are the concentrations of that chemical in the sample collected from the 1st and 2nd condensation stage, respectively, and W_1 and W_2 are the weight of the sample from the 1st and 2nd condensation stage, respectively.

The samples were analyzed by GC-FID with a VB-WAX capillary column (0.25 mm i.d., 25 m in length) (Valco Instrument Co. Inc., USA). The GC inlet temperature was set at 240° C, and the developed GC oven temperature program is also shown in Figure 3-1 and is described as follows. The oven temperature was initially maintained at 35° C (the set point)

for 5 minutes, ramped to 135^{o} C at the rate of 20^{o} C/min, maintained at 135^{o} C for 5 minutes, ramped to 240^{o} C at the rate of 20^{o} C/min, and maintained the temperature at 240^{o} C for 5 minutes. All the products were well separated with this temperature program. Figure 3-2 shows a typical GC chromatogram (A) of the collected samples from the 1st condensation stage and a typical chromatogram (B) of the diluted sample from 2nd condensation stage. The standard calibration curve using external calibration was obtained for each of the following chemicals: acetaldehyde, propionaldehyde, acrolein, acetol, glycerol, respectively, and such calibration curves were used to calculate the amount of these chemicals in the collected sample. An internal calibration method was also developed using butanol as the internal standard; the internal calibration was only performed periodically to ensure the performance of the external calibration method.

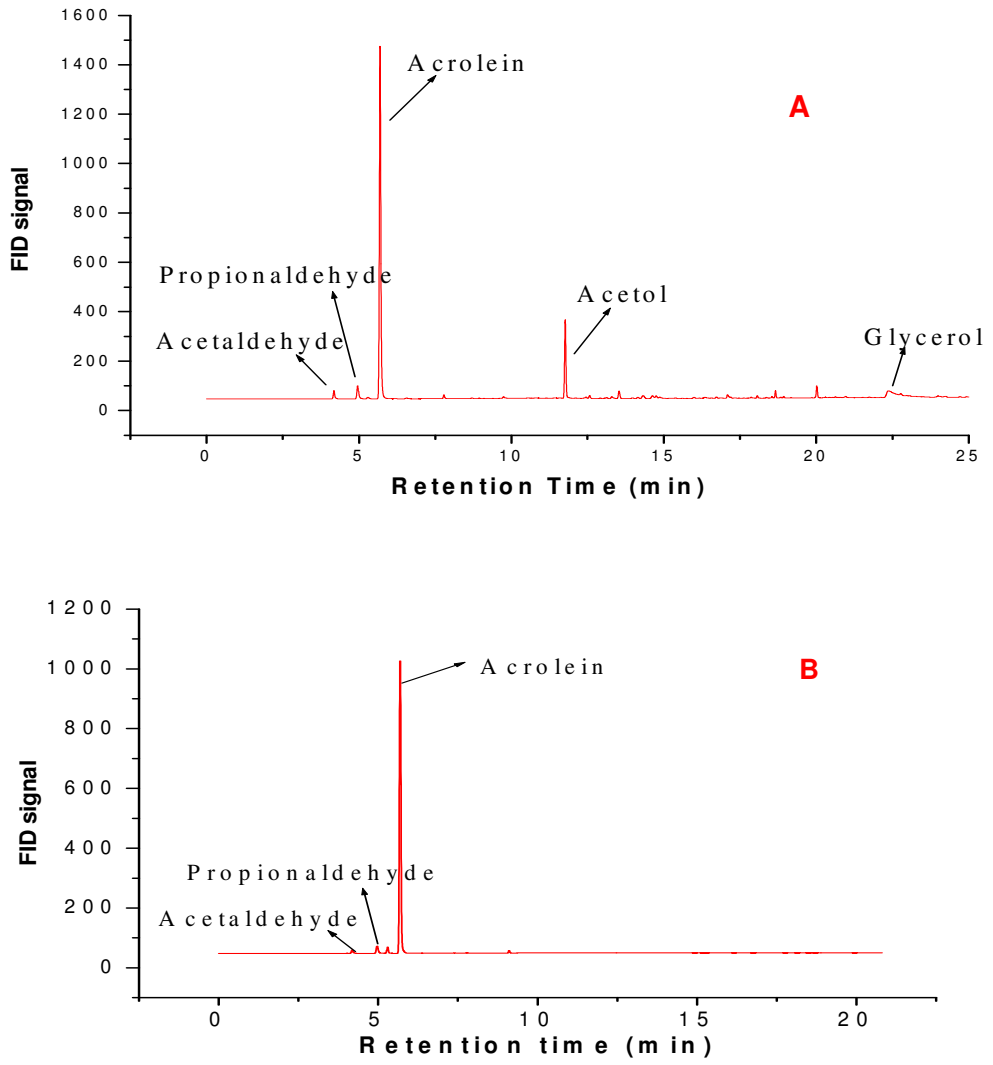

Figure 3-2: The typical GC chromatograph of the sample collected in the 1st condensation stage (A) and the sample collected in the 2nd condensation stage (B)

The following kinetic parameters were used to evaluate the catalytic performance, and the corresponding calculations are shown in Equation 3.5-Equation 3.8.

Glycerol conversion (%) was calculated via Equation 3-5:

$$X_{glycerol} = \frac{n_{reacted}}{n_{feed}} \times 100\% = \frac{n_{feed} - n_{quantified}}{n_{feed}} \times 100\%$$ **Equation 3-5**

where $X_{glycerol}$ is glycerol conversion (%), $n_{reacted}$ is the moles of glycerol reacted, and n_{feed} is the moles of glycerol in the feed， $n_{quantified}$ is the remaining glycerol in the collected sample quantified by GC.

Acrolein yield (mol%) was calculated via Equation 3-6:

$$Y_{acrolein} = \frac{n_{acrolein}}{n_{feed}} \times 100\%$$ **Equation 3-6**

where $Y_{acrolein}$ is the yield of acrolein (mol%), $n_{acrolein}$ is the moles of acrolein in the sample, and n_{feed} is the moles of glycerol in the feed.

Product selectivity (mol%), or the selectivity to any of the quantified products, was calculated via Equation 3-7:

$$S_{product} = \frac{n_{c-product}}{n_{c-gly-reacted}} \times 100\%$$ **Equation 3-7**

where $S_{product}$ is the selectivity to a specific product (mol%), $n_{c\text{-}product}$ is the moles of carbon in the specific product, and $n_{c\text{-}gly\text{-}reacted}$ is the moles of carbon in the converted glycerol.

Carbon balance (%) was calculated via Equation 3-8:

$$C\% = \frac{\sum_1^n (Carbon_{unreacted\_glycerol\_i} + (\sum Carbon_{product})_i) + W_{coke}}{Carbon_{feed}} \times 100\%$$ **Equation 3-8**

where n represents the total number of samples that were collected for each 7.5 time-on-stream (TOS) kinetic run (a sample was collected every 1.5 hours TOS); i denotes the i^{th}

sample; $Carbon_{unreacted\_glycerol\_i}$ is the carbon content, in units of g, of the unreacted glycerol in the i^{th} sample; $Carbon_{product}$ is the carbon content (g) of a specific product (acrolein, acetaldehyde, propionaldehyde, and acetol) in a sample; W_{coke} is the carbon content in the coke of the entire reaction time span; $Carbon_{feed}$ is the total carbon content (g) injected over the reaction time span. As mentioned before, coke is a distribution of carbonaceous species. It is almost impossible to know the exact carbon content of the coke, although carbon certainly accounts for the majority of the weight of the coke. In this study, the calculation of coke amount was based on the assumption that carbon accounted for all the catalyst weight gain.

Two kinetic runs were carried out for each of the three catalysts (HSiW-Si1252, HSiW-Si1254, and HSiW-Al2700) at 275° C. Since no confounding effect between catalyst and reaction temperature has ever been reported, the results from the experiments at 275° C should be sufficient to make an objective comparison and draw a valid conclusion. The time-one-stream was 7.5 hours for every single kinetic run, and the samples were collected and analyzed every 1.5 hours. The kinetic data presented were the average of the last 6 hours, unless specified otherwise. The sample collected from the first 1.5 hours TOS was excluded because of the concern that the catalytic reaction was not yet stabilized.

3.3 Results and Discussion

The measured surface areas after acid loading were 300±10m^2/g, 395±10m^2/g, and 140±3m^2/g for Si1252, Si1254, and alumina (Al), respectively. Compared to the surface area of the corresponding support, the loss of the surface area was 23% for Si1252, 27% for Si1254, and 6.7% for Al after acid loading.

Figure 3-3 presents the XRD results. Only broad peaks were observed for the alumina support, showing that the alumina is in an amorphous phase. There was a huge decline at the starting point, which was likely due to an intensive signature peak at low angles (<2 °). (Unfortunately, due to the instrumentation restrictions, lower angle X-ray was not performed.) The peak around 1° is associated with the mesoporous structure, which agreed with the fact that the alumina support used in the study was γ alumina. HSiW loading did not introduce additional peaks, showing that HSiW was well dispersed on Al. Si1254 and Si1252

have similar XRD patterns except for within the very small angle region, suggesting both silica supports are in an amorphous form with only pore size differences. The XRD patterns of supported HSiW were all very similar to that of the corresponding support, and no very distinctive peak assignable to HSiW was observed, suggesting that HPA was well dispersed on the surface of Si1252 and Si1254. The calculated surface coverage of HSiW (Equation 3.2) was 0.1912, 0.2517 and 0.9247 μmol/m^2 for HSiW-Si1254, HSiW-Si1252, and HSiW-Al, respectively. The results showed that even with a high HSiW surface density (HSiW-Al, 0.9247 μmol/m^2), no crystalline structure of HSiW can be observed on alumina supported acid. This could be due to the strong interaction between the Al surface and HSiW, which forced the acid molecules to diffuse faster into pores, and localize evenly on the entire surface. Overall, the XRD patterns showed that HSiW was well dispersed on all three supports.

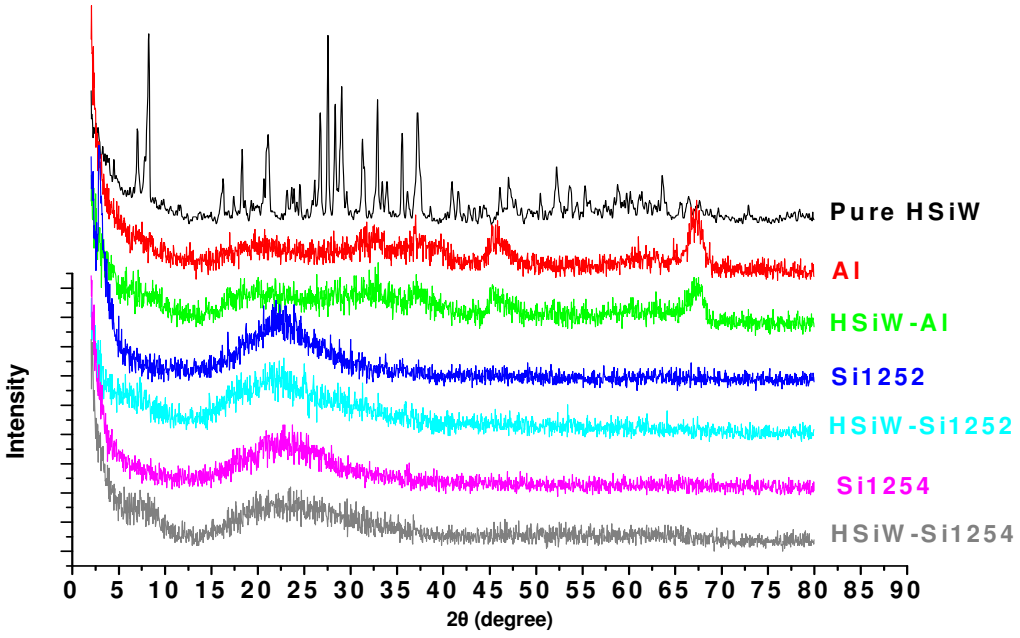

Figure 3-3: XRD patterns of silicotungstic acid (HSiW), Al and Al-supported HSiW, Si1252 and Si1252-supported HSiW, Si1254 and Si1254-supported HSiW.

Figure 3-4 shows the NH_3-TPD profiles for HSiW-Al2700, HSiW-Si1252, and HSiW-Si1254. The gaseous base (NH_3) molecules absorbed on a strong acid site are more difficult

to desorb than those adsorbed on a weak acid site. As the temperature further increases along the program, NH_3 previously adsorbed on a stronger site is evacuated, and detected by TCD. On a TPD graph, the Y-axis is the TCD signal intensity, positively correlated to the number of acid sites with certain acid strength, which was indicated by the position at the X-axis. Higher temperature on the X-axis associates with stronger acid strength. Therefore, from a TPD profile, one can infer the relative amount of different acid sites. Both HSiW-Si1252 and HSiW-Si1254 showed a relatively larger amount of strong acid sites (the region above 550ºC) than HSiW-Al, although the acid loading was 30 wt% on Al and only 20 wt% on Si1252 and Si1254. The possible reason for this fact is that Al has some basicity; the strong interaction between support and the acid caused partial distortion of HSiW, which caused some acidity loss (to be discussed more in detail in Chapter 6). On the contrary, silica has no surface basicity and very weak acidity [225]; therefore, it did not strongly interact with HSiW and did not cause as much HSiW distortion as Al [101, 114]. HSiW-Al had a relatively larger amount of weaker acid sites (the region 200 ºC-500ºC) than the other two silica-supported catalysts.

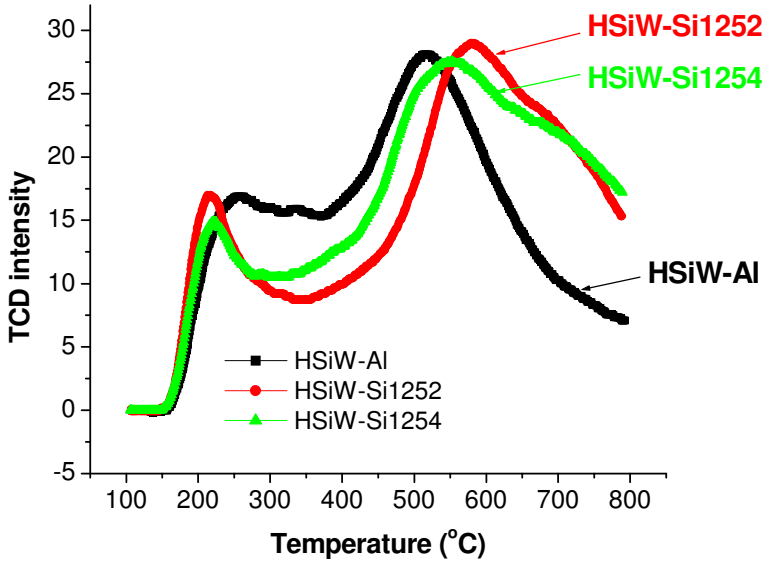

Figure 3-4: NH_3-TPD profile of silica-supported and alumina-supported HSiW.

Table 3.2 summarizes the catalytic activity of HSiW loaded onto the three different supports with different sizes of mesopores at 275°C. The result shows that all the catalysts were able to reach good conversion (over 98%) (the number in the parenthesis in Table 3.2) at 1.5 hours time-on-stream (TOS), but the average glycerol conversion descended in the

order of HSiW-Al > HSiW-Si1252 > HSiW-Si1254. The decrease in the average conversion was caused by the catalyst deactivation. The selectivity to the desired product, acrolein, descended in the order of HSiW-Si1252, HSiW-Al, HSiW-Si1254. Therefore, HSiW-Al and HSiW-Si1252 are similar in the average acrolein yield during 7.5 hours: 74.1 mol% (HSiW-Al) and 73.9 mol% (HSiW-Si1252), while HSiW-Si1254 only reached the acrolein yield of 66.2 mol%. HSiW-Al had the highest selectivity to the byproducts, acetaldehyde, propionaldehyde and acetol, while HSiW-Si1254 had the least. At 275°C, Acetol was the major gaseous byproduct; acetaldehyde and propionaldehyde were all less than 2mol% for all three catalysts at 275°C. HSiW-Si1254 is more selective to coke formation: HSiW-Si1254 had the largest catalyst weight gain after 7.5 hours TOS (19.4%), which was more than double that of HSiW-Al (8.65%).

Table 3-2: Reaction of glycerol at 275° C over differently supported silicotungstic acid

	Conversion (%)	Selectivity (mol%)				Coke [4]	Yield (mol%)
		Acrolein	Acetaldehyde	Propion-aldehyde	Acetol		
HSiW-Si1252	92.9 [1] ± 0.6 [2] (98.7±0.7) [3]	79.5±0.2	1.1± 0.24	1.1± 0.04	7.6±0.3	14.27% ± 0.5%	73.9
HSiW-Si1254	89.0± 1.2 (98±0.8)	74.4±0.7	0.8± 0.05	0.9± 0.1	4.2±0.9	19.4% ± 0.94%	66.2
HSiW-Al	96.2± 0.3 (98±1.1)	77.0±0.9	1.9± 0.13	1.4± 0.05	11.6±0.9	8.65% ±0.92%	74.1

1: Mean calculated based on the average conversion (selectivity) over 1.5-7.5 hours time-on-stream (TOS) of two kinetic repetitions.

2: Standard error.

3: The values were obtained at 1.5 hour TOS.

4. Calculated by the catalyst weight gain after 7.5 hour reaction divided by the fresh catalyst weight.

The decreasing trend in glycerol conversion over the reaction course was observed for both silica-supported catalysts, but not for HSiW-Al (Figure 3-5). The glycerol conversion of HSiW-Si1254 decreased faster than that of HSiW-Si1252, indicating that HSiW-Si1254 deactivated faster than HSiW-Si1252. For all of these catalysts, acrolein selectivity remained relatively stable after 1.5 hour TOS; as a result, the acrolein yield along the time course had the similar trend as the glycerol conversion. HSiW-Al provided a generally consistent yield after 1.5 hour TOS; HSiW-Si1252 attained an equivalent yield, if not higher, than HSiW-Al, even though HSiW-Si1252 did not have as good conversion as HSiW-Al (Table 3.2). The acrolein yield on HSiW-Si1254 was the least satisfying, because of both the fastest conversion decrease along TOS and lowest acrolein selectivity among the three catalysts.

Figure 3-5 B also shows the justification for why the first 1.5 hour TOS was excluded in calculating the average kinetic data: acrolein yield at 1.5 hours TOS was low (Figure 3-5 B), because catalysts had not yet reached equilibrium.

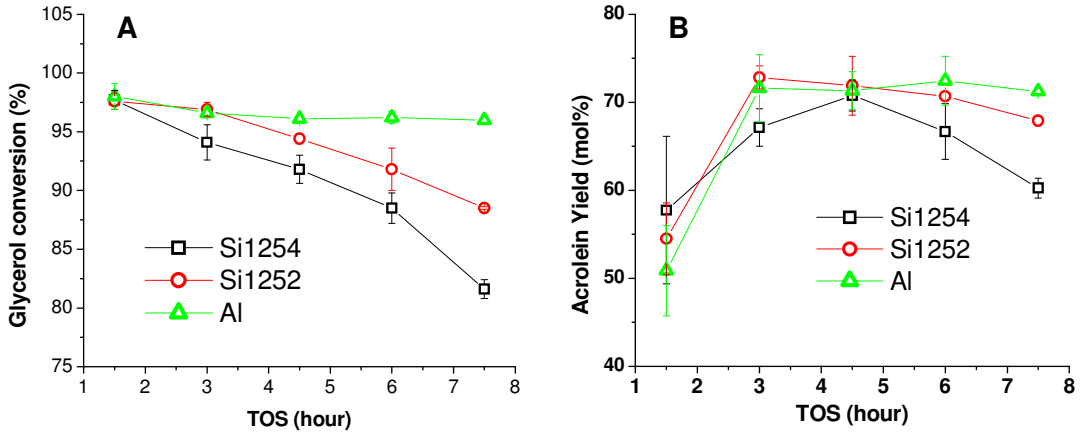

Figure 3-5: Glycerol conversion (A) and acrolein yield (B) as functions of time-on-stream (TOS); each data point was the average of two repetitive kinetic runs; each value stands for the average conversion/yield over 1.5-7.5 hours. Error bars were obtained using standard deviation calculation. GHSV: 84.4 h^{-1}; 60 mL/min argon carrier gas flow; reaction temperature: 275° C.

There was no obvious trend in acetaldehyde selectivity as a function of TOS (Figure 3-6 A), and there may be a subtle decreasing trend for the propionaldehyde selectivity (Figure 3-6 B). The responses of acetol formation to the TOS and the reaction temperature are shown in Figure 3-6 C. Acetol selectivity showed an increasing trend along TOS, although the increase tended to level off at longer TOS. On the contrary, it was observed that the GC peak of phenol decreased along TOS, showing that the selectivity to phenol was decreasing as the reaction proceeded. However, the fact that phenol is not totally soluble in water would introduce extra error in the calibration; as the result, only qualitative observation of the trend with respect of TOS was made for phenol instead of conducting quantitative measurement.

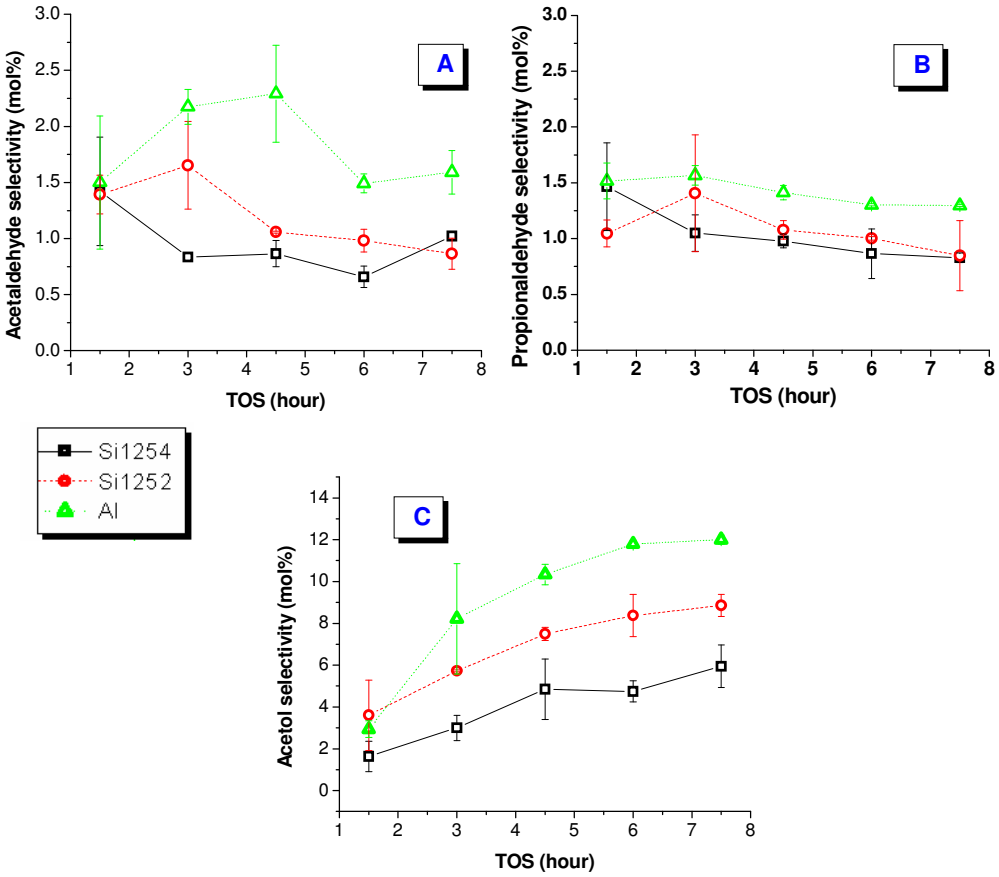

Figure 3-6: The selectivity of acetaldehyde (A), propionaldehyde (B), and acetol (C) as functions of time-on-stream (TOS); each data point was the average of two repetitive kinetic runs; each value stands for the average conversion/yield over 1.5-7.5 hours; error bars were obtained using standard deviation calculation. GHSV: 84.4 h^{-1}; 60 mL/min argon carrier gas flow; reaction temperature: 275° C.

"Hard" and "soft" are often used to describe the deposited carbonaceous species on the catalyst surface in relative terms: "softer" coke has relatively smaller molecular size (lower degree of polymerization) and less structural complexity, while "harder" coke has larger molecular size and a more complex structure. Figure 3-7 shows the result of the TPO runs of the spent catalysts after 7.5 hours TOS. In a TPO graph, the X-axis is temperature while the Y-axis is the TCD signal that is related to the amount of a certain coke on the catalyst surface. Therefore, any point on the TPO curve indicates a relative amount (position in Y-axis) of the coke with certain degree of hardness (position in X-axis). The signal of harder coke locates at the higher-temperature end of a TPO graph, and vice versa. HSiW-Al only

showed one peak in lower temperature region (~480ºC); HSiW-Si1252 showed a small peak around 480ºC, and a larger peak around 650ºC; HSiW-Si1254 showed a large peak around 520ºC, and a peak around 850 ºC. It is clear that HSiW-Al has the least coking: the TPO curves shifted to the "softer coke" end compared to the other two silica-supported HSiW. HSiW-Si1254 was considered as the least favorite regarding the coking issue, because some of the coke formed on the surface was very "hard". HSiW-Si1254 not only showed a higher amount of coke deposit (Table 3-2) than HSiW-Si1252, but also the coke composition was more distributed toward the hard coke region (larger degree of polymerization, more complex, cross-linked structure, and higher hydrogen deficiency). On the contrary, the alumina-supported catalyst not only showed the least catalyst weight gain, but also the deposited coke was more fully composed of softer coke (Figure 3-7).

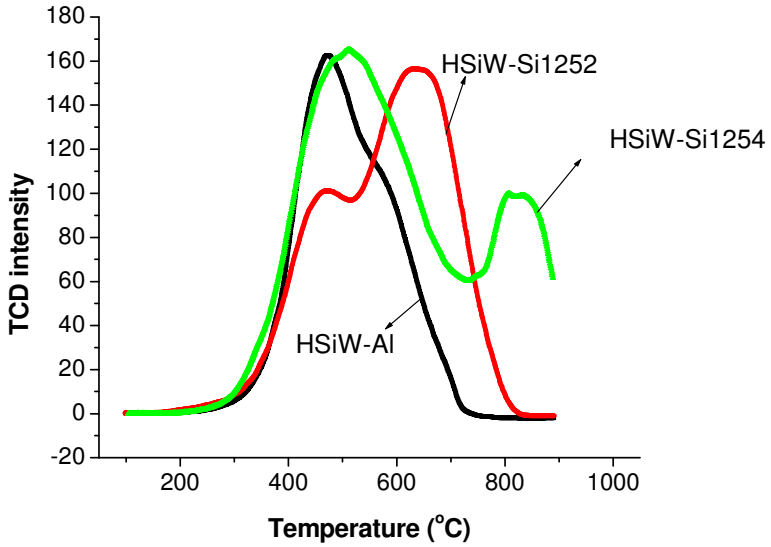

Figure 3-7: Temperature programmed oxidation (TPO) of the spent catalysts after 7.5 hours of reaction. The experiment was conducted on Pulsar with 70 mL/min 5% O_2 blended in helium. The heating rate was 10 ºC/min.

The size of glycerol molecule is 0.3-0.5 nm [226, 227]. The average pore diameter of Si1254 is 6 nm, smallest among the three catalyst support; HSiW-Si1254 would have even smaller pores (the diameter of a HSiW molecule is 1.1 nm) [228]. Therefore, it is most likely that HSiW-Si1254 provided highest mass-transfer resistance [102]. Some of glycerol molecules might have aggregated at the mouth of pore entrance, facilitating intermolecular condensation, forming linear, cyclic, and branched glycerol oligomers [130]. Polymerization

of the glycerol oligomers could be a significant contributor of coke formation [130]. Furthermore, with narrower pores, HSiW-Si1254 might suffer some desorption problem [108]: the unreacted glycerol molecules that entered the pore and the product molecules (e.g. acrolein) that formed in the pore might have more easily been trapped inside of smaller pores than larger pores. The trapped chemical compounds, most of which contained unsaturated bonds, could undergo secondary condensation to form larger compounds, leading to coke after continuous polymerization [130]. The observation that the acrolein selectivity consistently remained at a lower level compared to the other two catalysts (Table3-2) might be because that undesired consumption of glycerol as well as acrolein in coking formation occurred as soon as the reaction started and continued for the duration of the reaction.

HSiW-Si1254 exhibited a faster drop in glycerol conversion than HSiW-Si1252 and certainly HSiW-Al (Figure 3-5). The plausible explanation is provided as follows. When coke formed on the catalyst surface, it might have deposited near the mouth of catalyst pores, narrowing or completely blocking the pore entrance [229, 230]. The blockage of the entrances of the pores would make all the active sites within the pore inaccessible, significantly reducing the total number of the active sites. Consequently, the glycerol conversion suffered a significant decrease. HSiW-Si1254 had the smallest pores among the three catalysts; therefore, the likelihood of the occurrence of such a coke deposition mechanism was larger compared to HSiW-Si1252 and HSiW-Al.

Figure 3-8 summarizes the reaction pathway to the major products of the glycerol dehydration. Glycerol was converted into 3-hydroxypropanal (1) and acetol (2), depending on whether the protonation occurred on the primary or the secondary hydroxyl group [102, 136]. The highly unstable 3-hydroxypropanal would quickly convert into acrolein (3), and/or into formaldehyde and acetaldehyde via retro Aldol reaction (6) [102, 136]. Phenol could be formed from glycerol via dimerisation–cyclisation followed by dehydration (4), and/or could be formed via catalyzed polymerization of acrolein over acid sites (12) [130]. Propionaldehyde was possibly formed by the hydrogenation of acrolein followed by isomerization (8), and/or possibly formed from hydrogenation of acetol (9) [102, 136] followed by dehydration of 1,2-propandiol (11) [108, 130]. Acetone was another dehydration product of 1,2-propandiol (10) [108, 130]. The hydrogen that supplied the hydrogenation was

possibly formed from the dehydrogenation of oligomers during coke deposition, which occurred from the onset of the glycerol conversion process. Glycerol could form linear, cyclic, and branched glycerol oligomers via intermolecular condensation under acidic condition (5) [101, 130]. As shown in the figure, C2, C3 ketone and aldehyde were subjected to subsequent reactions forming oligomerization (including in (13)-(16) and (18)-(20)); the involved mechanism included Dels-Alder addition (e.g. acrolein + acrolein), aldol condensation (eg. propionaldehyde + acetone), dehydration, dehydrationation, and repetition and/or combination of them [101]. The oligomerization could occur between the same type of compounds or between different types of compounds. Furthermore, these oligomers can be further polymerized, either with themselves or with other groups of oligomers. The continuous addition and hydrogen removal form increasingly hard coke (included in (13)-(20)) [130].

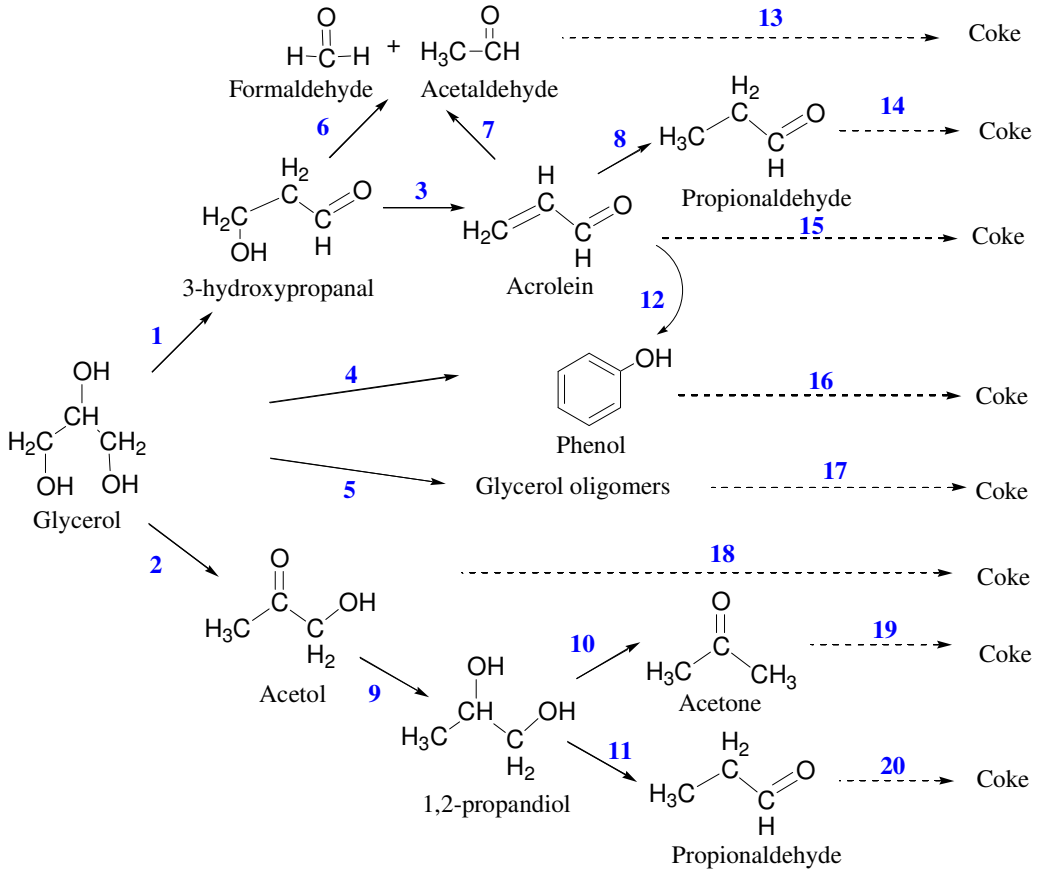

Figure 3-8: The reaction network of the gas-phase glycerol dehydration process [101, 102, 108, 130, 136].

3.4 Conclusions

The results showed that characteristics and catalytic performance of the supported silicotungstic acid were greatly influenced by the support on which HSiW was loaded.

The catalyst deactivation mainly affected the acrolein production in causing the decrease of glycerol conversion during the reaction course. During 7.5 hours TOS, HSiW-Al did not show any conversion decrease, HSiW-Si1252 showed some, and HSiW-Si1254 showed the fastest decrease of glycerol conversion along TOS. The weight gain of the spent catalyst and TPO profile confirmed that the coking occurred the most severely on HSiW-Si1254, and the least severely on HSiW-Al.

HSiW-Si1254 showed the lowest average glycerol conversion during 7.5 hours TOS due to the fastest catalyst deactivation, and the lowest average acrolein selectivity. Its performance in acrolein production was much less satisfying than HSiW-Si1252, the silica support with the larger pore size. Therefore, HSiW-Si1254 was excluded from the further studies.

HSiW-Si1252 and HSiW-Al showed similar acrolein yields, 73.9 mol% (92.9% glycerol conversion, 79.5 mol% acrolein selectivity) and 74.1 mol% (96.2% glycerol conversion, 77.0 mol% acrolein selectivity), respectively, during 7.5 hours TOS. HSiW-Al showed more stable performance over TOS (less coking), but it had a higher selectivity to the undesired gaseous byproducts (acetol, acetaldehyde, and propionaldehyde). Both HSiW-Si1252 and HSiW-Al have advantages and disadvantages; it was rather difficult to select one between them; therefore, both catalysts were used in the remainder of this study.

Chapter 4

Synergic effects of non-thermal plasma and solid acid catalyst in glycerol dehydration

Abstract

Non-thermal plasma (NTP) was integrated in glycerol dehydration with argon as the carrier and discharge gas. Various temperatures (220°C-320°C) and discharge field strengths (2.06 kV/cm-6.87 kV/cm) were studied for the individual and interactive effects regarding the conversion, the product selectivity, and coke formation. Results showed that the presence of NTP always improved the glycerol conversion, and NTP increased acrolein selectivity if properly conditioned. The optimal NTP field strength was 3.78 kV/cm (corresponding to 0.044 W) for HSiW-Al, and 4.58 kV/cm (0.0625 W) for HSiW-Si. The application of the optimal NTP improved acrolein yield by approximately 10 mol% on average when the reaction was operated at 275°C (the optimal temperature).

Keywords: non-thermal plasma, alumina, silica, silicotungstic acid, glycerol dehydration, acrolein, byproducts, conversion, selectivity, activation energy.

4.1 Introduction

The importance of the bio-based acrolein production has been addressed in Chapter 1. A great amount of effort has been made in the search for new acid catalysts. Some novel catalysts developed could be potentially rather expensive, or require topnotch skills to fabricate (yet still not showing significant improvement in lifetime), and therefore may be quite impractical. In the present research, a completely different path was taken in seeking the improvement of bio-based acrolein production by integrating a new element, non-thermal plasma (NTP), into the process. The deployment of this technique should not be very difficult, since there are already many NTP industrial applications and thus many potential installation issues have already been overcome.

NTP is a non-equilibrium state of matter where there exist “very hot” electrons, “hot” reactive species, and “cold” large neutral molecules [231]. Electrons are instantly energized upon the application of an electric field, and efficient transfer can occur of either kinetic energy to more electrons via elastic collisions or energy transfer for excitation and ionization of larger particles via inelastic collisions. A broad range of reactive species can be generated

in plasma, such as vibrationally excited species as in conventional chemistry, electronically exited species, and also the super-excited neutral molecules, positive and negative ions. The facilitation of dissociating chemical bonds and overcoming the activation barriers of desired processes has been reported by a great number of studies (e.g. [183, 232]). Due to high excitation ability and direct energy transfer efficiency, a great variety of reactions can take place at much milder conditions (temperature, pressure) under the application of a non-thermal plasma. NTP generated via dielectric barrier discharge (DBD) has been used in the methane reforming, combined with the usage of CO_2 [174, 190, 233, 234] or steam [234-237]. DBD plasma also has various applications in the treatment of volatile organic compounds of industrial air emission [238-246]. DBD has been applied in surface modification, and examples can be found such as in changing the nanostructure and surface morphology of the solid materials [220] [247, 248] [210-217], implanting functional groups (thus improving absorbability) [221] in terms of adhesion, hydrophilicity, adsorption, conductivity, and biocompatibility.

It is a completely new category of reaction in applying plasma for the glycerol dehydration. Examples in the literature are rather difficult to be found concerning plasma chemistry associated with dehydration. Nevertheless, the following rationalizations gave us ample reasons to explore this area.

The dehydration from glycerol to acrolein is an endothermic reaction (Appendix II); the reported activation energy without a catalyst is 305 kJ/mol [249]. The acid catalyst lowers the activation energy for the reaction to acrolein, while not necessarily for other side reactions. Therefore, it is very likely that the gap between the activation energy of different reactions may be enlarged (dependent on a specific catalyst), where the merits of NTP can be fully utilized to faciliate a certain reaction(s) conversion while not that of others. Since the reactants and many products have high heat capacities, the energy required to increase the gas temperature (to ensure a good catalytic performance) is considerable. Researchers have long striven to increase the energy efficiency of reactor heating so that the input energy can be entirely consumed in the reactions as much as possible. NTP usually allows reactions to occur at much lower temperatures, and could be a highly desirable solution. The non-equilibrium phase contains a large amount of highly energetic electrons. Through the

collision process, the electrons transfer their energy to the larger particles, such as molecules, ions, etc. Due to the significant difference in size and weight between electrons and the large particles, the transferred energy is not converted to kinetic energy; therefore, the overall gas temperature remains constant. Instead, it is all used in driving the chemical reactions, such as dissociating bonds, exciting species, and so on.

Plasma is an ionized gas containing a great number of free electrons and the positively charged ions that result from ionization. Glycerol dehydration is commonly accepted as an ionic pathway, through catalytic protonation and the intermediate carbocations. Not only protons can be formed in a NTP system in the presence of water, but also carbocations are very likely to be stabilized, which could possibly reduce the activation energy of the system.

Usually, a reactor is heated by the outside heating unit, and the heat is transferred from the heating source into the reactor wall and then inwards to the reactants inside. Although the assumption of uniform temperature in the radial direction is quite common in reaction engineering, in reality a temperature gradient exists. Depending on the thermodynamic properties of the substances in the system, the heat transfer rate varies, and, as a result, the temperature gradient may be more important in some reactor configurations than in others. It is highly possible that some of the reactant particles attain an optimal energy condition, while others do not. Compared to the sequential (indirect) process of conventional heating, energy transfer can be viewed as a parallel (direct) process in a NTP system. Energy can be efficiently transferred to the reactant particles by the direct collisions with the large amount of electrons in the system. As a result, the energy transfer can be much faster than conventional heat transfer; the reactants are likely to be homogenously energized. This direct energy transfer may significantly shift the chemical equilibrium towards product formation [166]. Also, since the energy was locally generated by the discharge field, the energy transfer loss should be considerably less than in conventional heating, which loses energy to the reactor wall and the environment.

Coke formation is a major problem that hinders bio-based routes of acrolein production. Catalytic activity is impaired by deactivated catalyst, which usually manifests as a conversion decrease (eg. [101, 126-128]) (also acrolein selectivity decreased in some microporous catalyst cases [102, 250]). It has been reported that the presence of a small

amount of oxidants in the system could inhibit the formation of carbonaceous surface species (coke precursors), and thus suppress coke formation. Hydroxyl radicals can be generated from water vapor by NTP, with its strong oxidizing ability. Therefore, it is reasonable to hypothesize that NTP application could suppress the coke formation during the reaction and thus improve the catalytic performance.

The objective was to study the glycerol dehydration to acrolein with and without non-thermal plasma application using silica1252 supported silicotungstic acid and alumina supported silicotungstic acid catalysts. Temperature and NTP field strength were two major effects to be studied.

4.2 Materials and Methods

Experimental apparatus

A schematic drawing of the experimental apparatus is presented in Figure 4-1. Glycerol dehydration was carried out in a down-flow packed-bed reactor (PBR) with NTP discharge as an option. The base of the reactor was a quartz tube (length 300 mm, ID 19.35mm, OD 25.3mm). A 313 W heating tape (Omega Scientific, USA) was used to heat the PBR; this 4-foot-long tape was evenly wrapped around the outside wall of the quartz tube. The heating tape was controlled by a proportional-integral-derivative (PID) controller to maintain a desired temperature for the catalyst bed. The very outside layer of the PBR was composed of a thick layer of heat insulation. A wire-to-cylinder type of DBD configuration was used to integrate the non-thermal plasma into the reaction zone. An Inconel^{TM} rod (1/16'') was inserted into the center of reactor, and it was connected to the high voltage port of the transformer. Copper tape (1/32'' thick) was wrapped around the outside wall of the reactor, and connected to ground. The rod and the tape served as two electrodes, while the quartz reactor wall served as the dielectric barrier. The circuit configuration is illustrated in Figure 4-1. The AC waveform was generated by an inverter (Solid state drive SSD110 model, PTI, Racine, WI) followed by a voltage transformer (55-HLH10102/D115, PTI, Racine, WI). The waveform of the NTP discharge was monitored (and could be recorded) via an oscilloscope (WaveLet^{TM} series, LeCroy, Chestnut Ridge, NY). The tunable inverter together with the oscilloscope allowed the adjustment of the frequency and voltage to the desired values. A capacitor (2 μF) was inserted in the circuit to create a phase lag to generate Lissajous figure

for power calculation, as discussed in Chapter 2. The discharge zone started from 1" upstream of the catalyst bed and terminated at the end of the catalyst bed (a cylindrical NTP zone with 0.75" in diameter and 2" in height), including both pre-bed discharge and on-bed discharge zones.

Based on the results in Chapter 3, 20 wt% HSiW-Si1252 (hereafter HSiW-Si) and 30 wt% HSiW-Al2700 (hereafter HSiW-Al) were used in the following tests. Approximately 7 mL HSiW-Al or HSiW-Si (exact volumes used slightly varied to ensure 84.4 h^{-1} gas-hourly-space-velocity at a specific reaction temperature) were packed at the lower end of the PBR, leaving sufficient travel length for carrier gas and glycerol feed to be preheated to the desired temperature before reaching the catalyst bed. The glycerol solution (20 wt% of glycerol in water) was fed by a syringe pump with 6.02 g/hour feeding rate, which was equivalent to 84.4 h^{-1} GHSV of glycerol. Argon was used as the carrier gas, and its flow rate was regulated to achieve 60 mL/min. The products after reaction traveled through a condenser with flowing tap water, and the majority of the liquid product was condensed in a 50 mL vial immersed in an ice-water cold bath (1^{st} condensation stage). Products that were unable to be condensed in the first condensation stage were collected in a 20 mL vial that was immersed in a liquid nitrogen bath (2^{nd} condensation stage). Each of the samples collected from the two condensation stages was individually analyzed via GC-FID, and the selectivity and conversion for a given time-on-stream (TOS) span were calculated based on the total concentration. Analytical and calculation details have been described in Chapter 3 Materials and Methods.

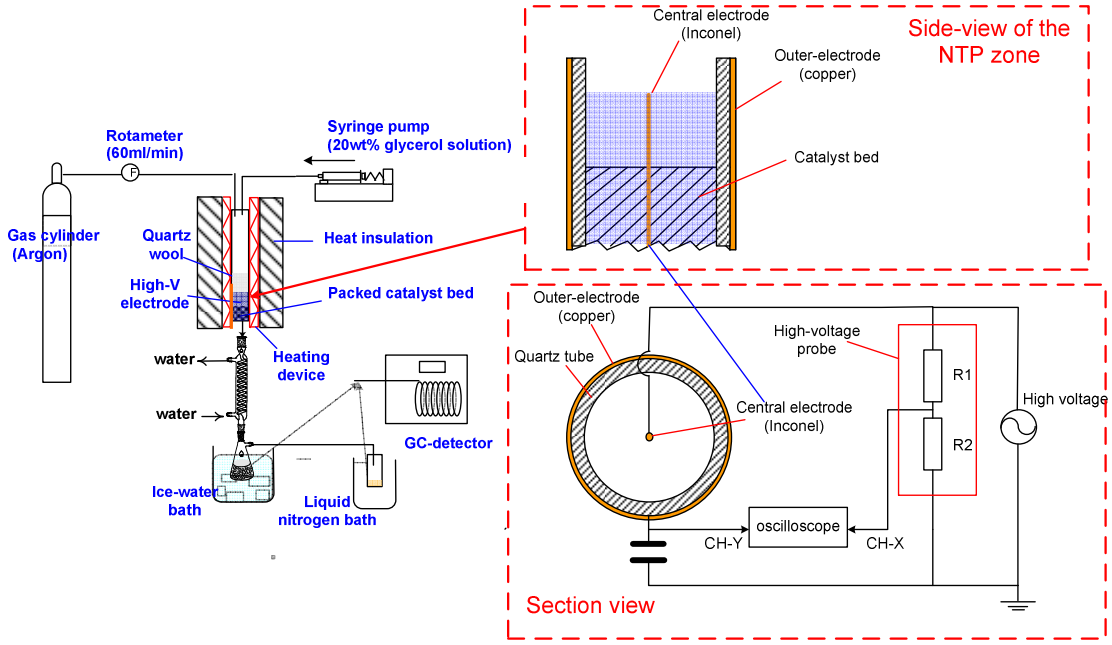

Figure 4-1: Packed bed reactor with NTP discharge as optional operation. The electrical configuration is displayed in the window with the section view of the reactor

Reaction conditions

The discharge voltage and frequency were monitored by oscilloscope and adjusted via the plasma generation device. To avoid any possible local heating due to too concentrated energy input, the discharge frequency was maintained at 1 kHz. The discharge voltages used in the study were 1.5 kV, 2.4 kV, 3.3 kV, 4.0 kV, 4.8 kV and 6 kV. Since the field strength is a more commonly used parameter to specify the plasma configuration in plasma kinetic studies, it will be used to specify the conditions in the text herein. The field strength corresponding to each discharge voltage used in the study is listed in Table 4-1.

Table 4-1: Plasma power and density corresponding to discharge voltage

Discharge Voltage (kV)	1.8	2.4	3.3	4.0	4.8	6.0
Field Strength (kV/cm)	2.06	2.75	3.78	4.58	5.50	6.87

The field strength effect was investigated by conducting glycerol dehydration with various NTP field strengths at 275°C; optimal NTP field strength was determined for HSiW-

Al and HSiW-Si. Also, glycerol dehydration was conducted with various NTP field strengths at 250°C, to investigate whether there was an interactive effect between NTP and temperature. Seven reaction temperatures, 220°C, 235°C, 250°C, 275°C, 290°C, 305°C, and 320°C, were investigated. The lower temperature limit is justified in Appendix I. The exclusive temperature effect of glycerol dehydration was obtained by operation of glycerol dehydration under the seven temperatures in absence of NTP. NTP at the optimal field strength was applied to glycerol dehydration operated at each of the seven temperatures to investigate whether the optimal NTP could improve the acrolein production at all the temperatures.

A set of "blank" experiments were conducted to investigate NTP with the absence of any acid catalyst. Instead of using HSiW-Al or HSiW-Si, 7 mL glass beads (3 mm diameter) were packed in the PBR, which can be viewed as the inert packing material (no catalytic capability). The tested conditions were 1) 275°C without NTP application (control), 2) 275°C with 3.78 kV/cm NTP application; 3) 275°C with 5.50 kV/cm NTP application.

To obtain the activation energy, three temperature levels (220°C, 235°C, 250°C) were conducted for both HSiW-Al and HSiW-Si with and without NTP at the optimal condition, and the experiments at three flow rates of glycerol solution (4.57 g/hr, 6.02 g/hr, and 9.135 g/hr) were conducted under each of the temperature conditions; the experiments under each condition were conducted in duplicate.

4.3 Results

4.3.1 NTP field-strength effect

Figure 4-2 shows the glycerol conversion and acrolein selectivity at 275°C and 250 °C as functions of NTP field strength when HSiW-Al was used. A continuously increasing trend of glycerol conversion was clearly shown as the NTP field strength increased. For the reactions at 250°C, the application of 3.78 kV/cm, 4.58 kV/cm, and 5.50 kV/cm increased the acrolein selectivity over the experiment operated without NTP, whereas the application of 6.87 kV/cm decreased the selectivity; for the reactions at 275°C, the 2.75 kV/cm and 3.78 kV/cm applications increased the selectivity, but the selectivity started to decrease as higher

field strength was applied. The acrolein selectivity was significantly lowered by applying 6.87kV/cm NTP to the reaction operated at 275°C.

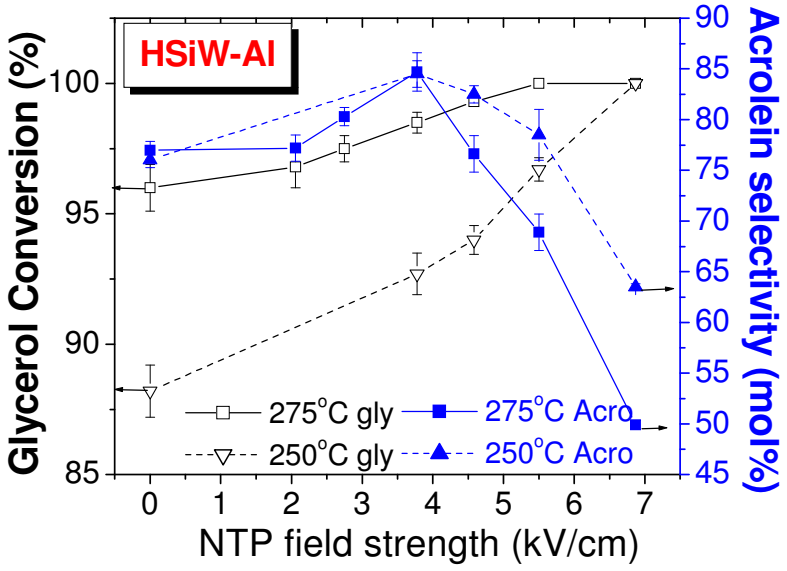

Figure 4-2: Glycerol conversion and acrolein selectivity as functions of NTP field strength during TOS of 1.5-7.5 hours on Al-supported HSiW (HSiW-Al). Gas-hourly-space-velocity of glycerol: 84.4 h^{-1}; Carrier gas argon flow rate: 60 mL/min

Figure 4-3 shows the glycerol conversion and acrolein selectivity as functions of NTP field strength at 275°C and 250°C when HSiW-Si was used. For the reactions at 250°C, the glycerol conversion clearly showed a continuously increasing trend as the NTP field strength increased. For the reactions at 275°C, only a slight conversion increase was observed when 2.08kV/cm NTP, 3.78 kV/cm NTP or 4.58 kV/cm NTP was applied ; and glycerol conversion decreased when 6 kV/cm NTP were applied. For the reactions conducted at 250°C, the NTP applications of 3.78 kV/cm, 4.58 kV/cm, and 5.50 kV/cm significantly increased the acrolein selectivity with the trend that acrolein selectivity increased with the increase of the field strength; however, the application of the further increased field strength, 6.87 kV/cm lowered the acrolein selectivity. For the reactions at 275°C, acrolein selectivity increased with the increase of the field strength until reaching 4.58 kV/cm; and then the selectivity started to decrease when 5.50 kV/cm NTP was applied, and the selectivity decreased significantly when 6.87 kV/cm was applied.

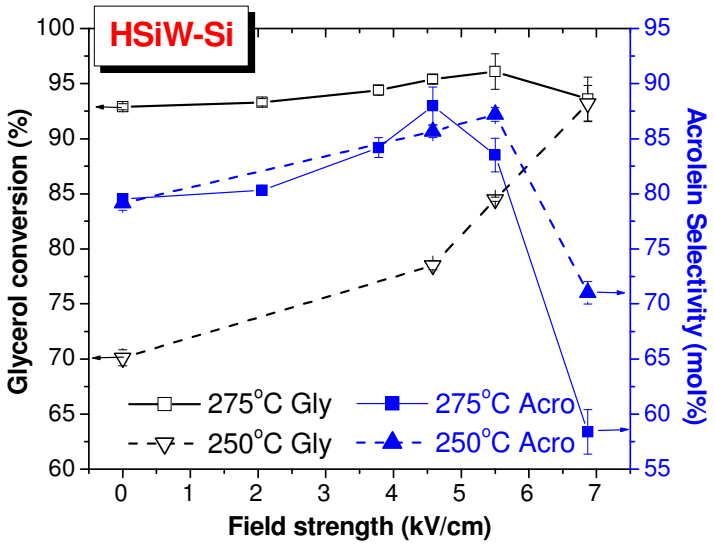

Figure 4-3: Glycerol conversion and acrolein selectivity as functions of NTP field strength during TOS of 1.5-7.5 hours on Si-supported HSiW (HSiW-Si). Gas-hourly-space-velocity of glycerol: 84.4 h^{-1}; Carrier gas argon flow rate: 60 mL/min

In general, glycerol conversion increased with the increase of NTP field strength, and the increase was more significant at 250°C than that at 275°C. In the case of HSiW-Si, a confounding factor, catalyst deactivation, was involved: more intense NTP would lead to the generation of more double-bonded compounds, subsequently forming coke and causing catalyst to deactivate. As a result, it countered the effect that NTP energized the glycerol molecules and thus improved the conversion.

Within a certain range of the NTP field strength, NTP application improved the acrolein selectivity. When the field strength was too low (such as 2.06 kV/cm), the intensity of NTP was not sufficient to cause breakdown and generate beneficial species (to be discussed later). When the field strength was too high, too many side reactions were activated, which decreased the selectivity to acrolein. The maximum acrolein selectivity occured at 3.78 kV/cm field strength for HSiW-Al and 4.58 kV/cm for the HSiW-Si. For HSiW-Si, the acrolein selectivity maximum occurred at 5.50 kV/cm when the reaction was conducted at 250°C, while it occurred at 4.58 kV/cm when it was conducted at 275°C. Also the selectivity decrease at the 6.87 kV/cm NTP condition was not as significant at 250°C as it

was at 275°C. These observations demonstrate that there was some interaction between NTP field strength and reaction temperature.

4.3.2 Temperature & NTP effects

Figure 4-4 displays the kinetic data obtained using HSiW-Al. Glycerol conversion and acrolein selectivity as function of temperature are shown in Figure 4-4 (A) for the regular (control) conditions and the NTP applied conditions, respectively. Acrolein yield provides a direct overall evaluation of acrolein production. To provide an overview of acrolein production at a given condition, the acrolein yields of all the corresponding conditions were also presented, as in Figure 4-4 (B). Seven temperatures were examined for the control conditions, NTP of 3.78 kV/cm and NTP of 4.58 kV/cm, respectively. The temperature effect could be extracted from the data obtained under the control conditions; these data points are denoted as "contol" in the figure. The conversion increased as the temperature increased from 220°C to 290°C. Glycerol was completely converted at 290°C and higher. Acrolein selectivity shows a mild increase as the reaction temperature increased within the range of 220°C to 275°C (77.0 mol% selectivity), while selectivity decreased sharply as the temperature further increased. As the result, the acrolein yield shows the trend of increasing first and then decreasing with the increase of the reaction temperature. The highest yield (74.1 mol%) was obtained at 275°C. The glycerol conversion at 220°C was increased over 7% by 3.78 kV/cm NTP, and was increased over 12% by 4.58 kV/cm NTP. The trajectories of the glycerol conversion for three NTP conditions merged to 100 (the complete conversion) at 290°C. Compared to the control condition, the selectivity to acrolein increased by employing 4.58 kV/cm NTP was 11.7 mol%, 7.9 mol%, and 3.2 mol% at 220°C, 235°C, and 250°C, respectively; the application of the 4.58 kV/cm NTP decreased the acrolein selectivity at 275°C, and decreased the acrolein selectivity more severely at higher temperature. The selectivity to acrolein increased by 3.78 kV/cm NTP was 9.6 mol%, 9.0 mol%, 8.2 mol%, 7.7 mol%, and 1.2 mol% at 220°C, 235°C, 250°C, 275°C, and 290°C, respectively; the application of 3.78 kV/cm NTP started to decrease the acrolein selectivity at 305°C and the temperatures above. The results showed that there was some interaction occurred between temperature and NTP field strength. The highest acrolein yield for the 3.78 kV/cm application was 83.6 mol% (275°C); the highest yield for the 4.58 kV/cm application was 76.6 mol% (250°C).

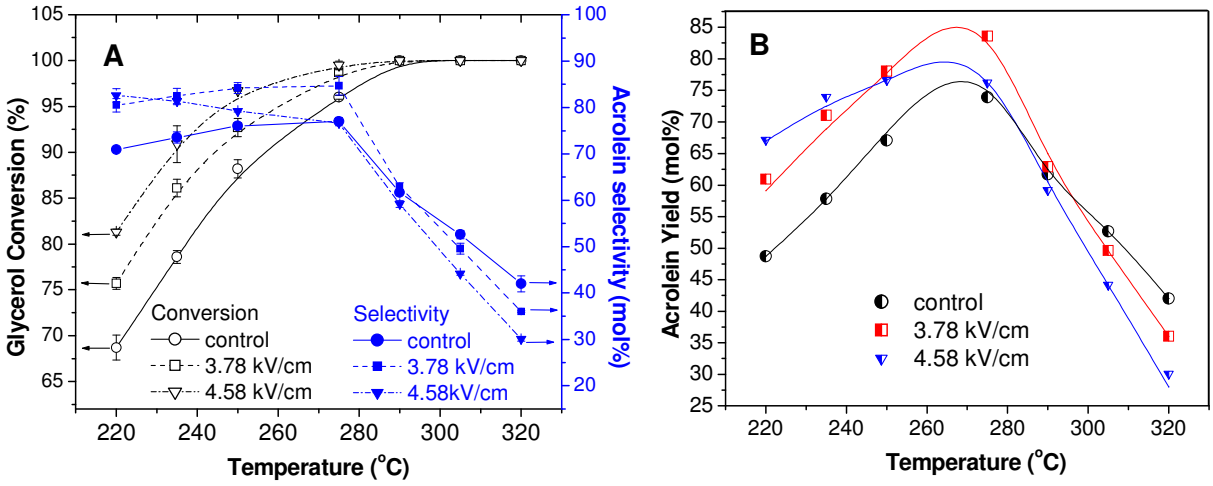

Figure 4-4: Glycerol conversion and acrolein selectivity (A) and acrolein yield (B) on Al supported HSiW as functions of temperature during TOS of 1.5-7.5 hours. GHSV: 84.4h^{-1}, 60mL/min argon flow

Figure 4-5 displays the kinetic data obtained using silica supported HSiW (HSiW-Si), including the conversion and selectivity presented in (A) and acrolein yield presented in (B). The glycerol conversion showed a significant increasing trend from 220°C to 290°C, but it seemed to show a slight decreasing trend as temperature was further increased above 290°C. Acrolein selectivity increased slightly from 220°C to 275°C; and, it significantly decreased at higher temperatures. The NTP application clearly increased the glycerol conversion at 220°C, 235°C, and 250°C. Not much difference in conversion was observed by applying NTP when the reaction was operated at 275°C and higher. Acrolein selectivity showed a relatively stable increase by NTP application at 220°C-275°C. At 290°C, NTP only slightly increased the acrolein selectivity; NTP application lowered the acrolein selectivity at 305°C and 320°C. The similar pattern as observed with HSiW-Al also occurred for HSiW-Si, with the optimal acrolein yield being 83.1 mol% with NTP application and 73.9 mol% without NTP at 275°C. Based on Figure 4-5B, it is concluded that the application of the optimal discharge (4.56 kV/cm) always increased acrolein yield when the reaction was conducted at 275°C or below.

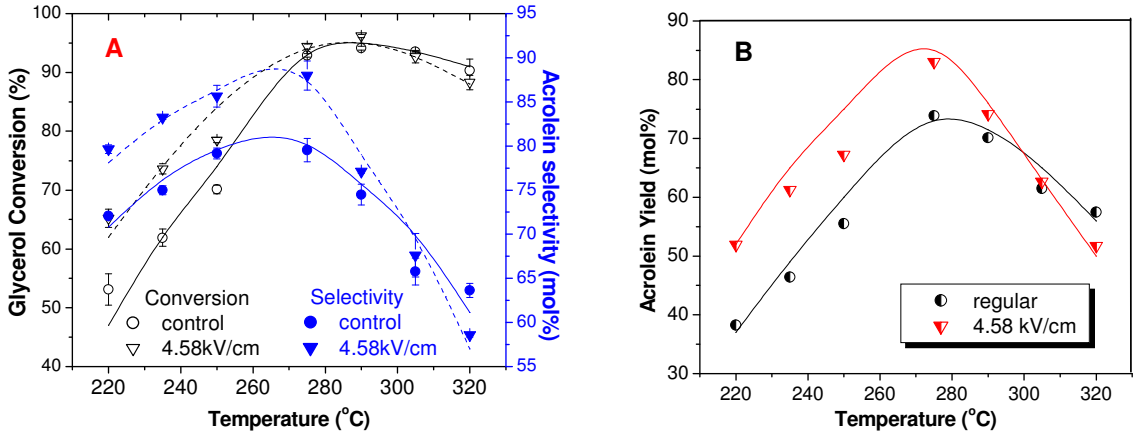

Figure 4-5: Glycerol conversion and acrolein selectivity (A) and acrolein yield (B) on Si supported HSiW as functions of temperature during TOS of 1.5-7.5 hours. GHSV: 84.4 h^{-1}, 60 mL/min argon flow

4.3.3 Byproducts

Acetaldehyde

Figure 4-6 presented the acetaldehyde (CH_3CHO) selectivity obtained with HSiW-Al and HSiW-Si under different temperature conditions without NTP and under different NTP fields strength conditions at 275°C. Acetaldehyde selectivity remained low (<1.2 mol%) when the reaction temperature was below 275°C, although a slight increasing trend was observed as the temperature increased. The acetaldehyde selectivity at 290°C was sharply higher than the selectivity at the lower temperatures, and kept increasing as temperature was further increased. The response of acetaldehyde selectivity to temperature shows that higher temperature favored the production of acetaldehyde and that there was a threshold of temperature only above which a significant increase in acetaldehyde selectivity occurred. Low field-strength NTP application barely caused any increase in the acetaldehyde selectivity, compared to the control condition. When 4.58 kV/cm NTP was applied to HSiW-Al and 5.50 kV/cm NTP was applied to HSiW-Si, the acetaldehyde selectivity started to show a significant increase compared to their counterparts under control condition. A sharp increase was observed when the 6.87 kV/cm NTP was applied for both HSiW-Al and HSiW-Si. The response of acetaldehyde selectivity to NTP shows that NTP application would increase acetaldehyde selectivity in general, but the increase was trivial at low field strength

NTP application and only became significant when the high field-strength NTP was applied. Also, by comparing the Figure 4-6 A and Figure 4-6 B, the selectivity to acetaldehyde in the HSiW-Al catalyzed glycerol dehydration was in general higher than that in the HSiW-Si catalyzed one, although they showed similar patterns in response to temperature and NTP field strength.

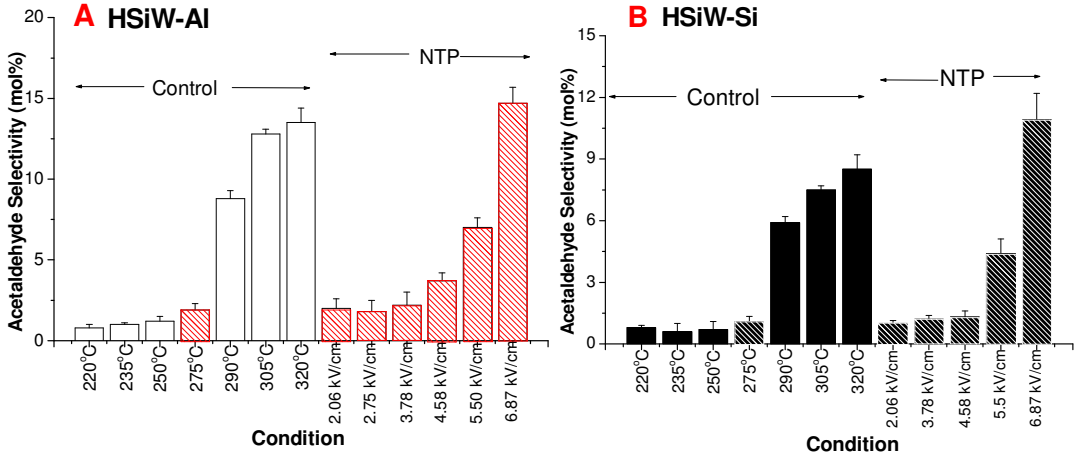

Figure 4-6: The selectivity of acetaldehyde under various reaction conditions using HSiW-Al (A) and HSiW-Si (B), respectively. The acetaldehyde selectivity obtained at 275°C (either with or without NTP) is cross-hatched.

Propionaldehyde

The selectivity of propionaldehyde (CH_3CH_2CHO) obtained from the differently conditioned reactions was presented in Figure 4-7. For the control conditions, the propionaldehyde selectivity barely changed in the temperature range from 220°C to 275°C, and it remained low. The selectivity increase only became significant at the temperature 290°C and above. A several-fold increase occurred at 290°C in the HSiW-Al catalyzed reaction, and occurred at 305°C in the HSiW-Si catalyzed reaction. Low field-strength NTP application did not change the selectivity appreciably. For HSiW-Al, the selectivity increase was initiated when 4.58 kV/cm NTP was applied to the reaction system, and a drastic increase occurred when 6.87 kV/cm NTP was applied. For HSiW-Si, the 5.50 kV/cm NTP

application caused a significant increase of propionaldehyde selectivity, and the 6.87 kV/cm application caused even more amount of propionaldehyde formed.

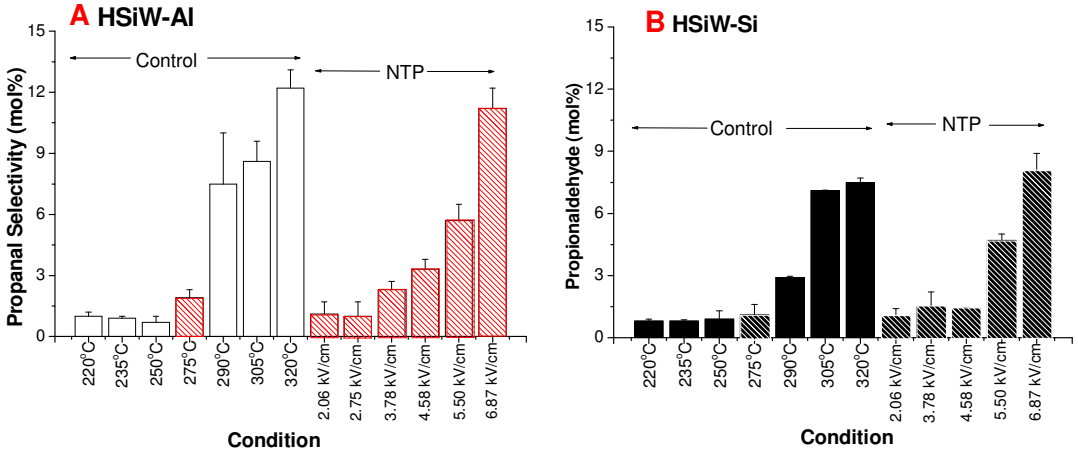

Figure 4-7: The selectivity to propionaldehyde under various reaction conditions using HSiW-Al (A) and HSiW-Si (B). The propionaldehyde selectivity obtained at 275°C (either with or without NTP) is cross-hatched.

Figure 4-8 displays the selectivity to acetol (CH_3COCH_2OH) under different reaction conditions using HSiW-Al (A) and HSiW-Si (B), respectively. The acetol selectivity showed a general increasing trend as the temperature increased from 220°C to 290°C; but the acetol selectivity sharply decreased as the temperature further increased. It was observed for both catalysts that the NTP application tended to lower the acetol selectivity. The overall trend was that the selectivity to acetol decreased with the increase of the NTP field strength, and the acetol selectivity was significantly lowered at high field-strength NTP applications.

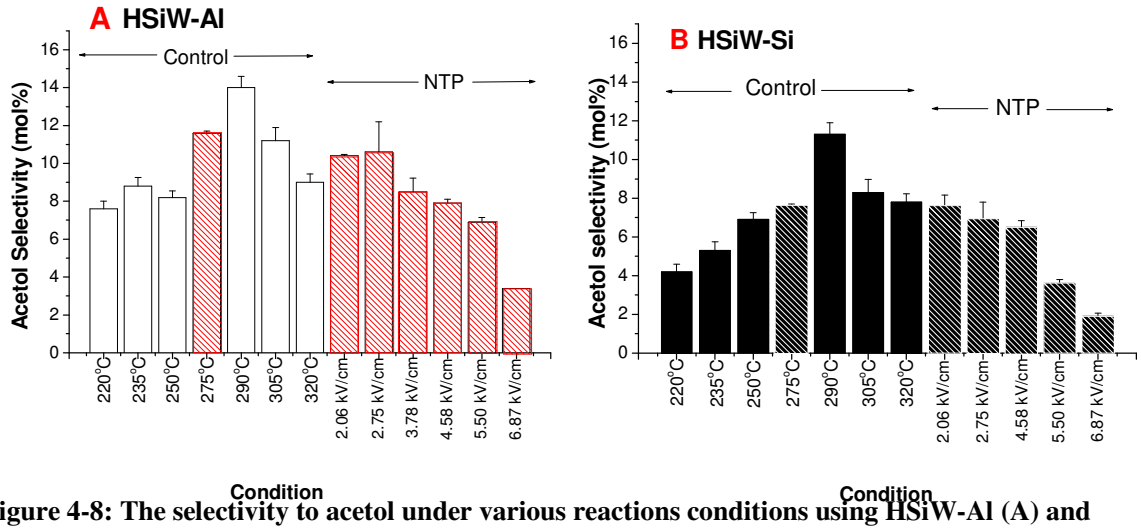

Figure 4-8: The selectivity to acetol under various reactions conditions using HSiW-Al (A) and HSiW-Si (B). The acetol selectivity obtained at 275°C (either with or without NTP) is cross-hatched.

Coke

The formation of coke, or the carbonaceous deposit, is the most undesirable side reaction, as it would cause the catalyst to deactivate and consequently the conversion to decrease. The nature of the acid catalyst and the reaction conditions are all influential factors determining the rate of coking and the type of the deposited coke. The amount of deposited coke during each of the differently conditioned reactions is listed in Table 4.2. The coking amount showed a slight decrease initially as the reaction temperature increased from 220°C; however, the coking amount significantly increased at high temperature.

Table 4-2: The coking amount deposited during a 7.5-hour time-on-stream period

		220 °C	235 °C	250 °C	275 °C	290 °C	305 °C	320 °C
HSiW-Al	**Control**	10.80%*	10.20%	8.48%	8.65%	8.56%	9.34%	12.34%
	3.78 kV/cm	9.98%	10.40%	7.60%	8.16%	8.01%	9.73%	13.78%
	Various voltages at 275°C	**2.06 kV/cm**	**2.75 kV/cm**	**4.58 kV/cm**	**5.50 kV/cm**	**6.87 kV/cm**		
		8.06%	8.11%	6.58%	5.60%	8.60%		
HSiW-Si	**Control**	15.38%	15.42%	14.86%	14.27%	14.35%	16.35%	17.46%
	4.58 kV/cm	14.40%	13.67%	14.45%	14.13%	14.19%	16.89%	18.65%
	Various voltages at 275°C	**2.06 kV/cm**	**3.78 kV/cm**	**5.50 kV/cm**	**6.87 kV/cm**			
		14.53%	14.98%	12.98%	13.85%			

*The amount of coke is calculated as the weight difference between the fresh catalyst and the spent catalyst after the 7.5-hour TOS reaction divided by the weight of the fresh catalyst; the number is expressed in percentages.

For all the data described in this section, overall mass balances (the summation of the samples directly collected from two condensation stages and the catalyst weight gain divided by the total consumption of the feed solution during the reaction time course) ranged from 87-96%. Carbon balances, calculated by summing the carbon content in the products and the catalyst weight gain divided by the carbon content in the glycerol feed over the reaction time duration, were around 85-99%.

4.3.4 Long-term stability test

A long-term stability test was conducted for NTP-assisted glycerol dehydration on HSiW-Al at 275^{o}C (Figure 4-9), the optimal condition for acrolein production. Glycerol dehydration was continuously operated for up to 50 hours without interruption. The glycerol conversion remained unchanged (~100%) for 22 hours TOS, and decreased to around 50% at 50 hours TOS. Acrolein selectivity remained relatively stable during the course of the 50-hours of TOS. A control condition (glycerol dehydration on HSiW-Al at 275^{o}C without NTP) was conducted as the comparison. The glycerol conversion under the NTP condition showed

a sign of slower decrease compared to the control condition, although the decrease under NTP condition was detected a couple of hours earlier than the control condition.

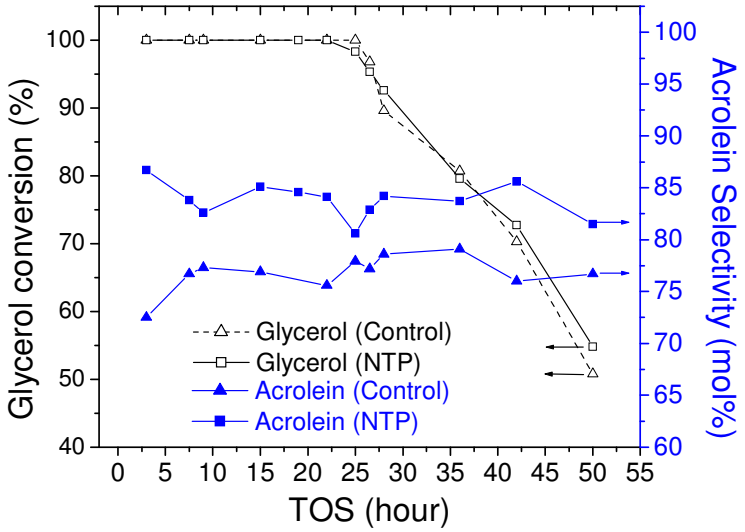

Figure 4-9: Long-term runs using HSiW-Al at 275° C with/without NTP. GHSV: 84.4 h^{-1}, 60 mL/min argon flow.

4.3.5 Blank test (no solid acid catalyst) with/without NTP

The result of the blank test (with the absence of the solid acid catalyst) was listed in Table 4-3. The acrolein yield without supported HSiW was 1.05 mol% (10.9% glycerol conversion, 9.6 mol% acrolein selectivity). With the application of 3.78 kV/cm, glycerol conversion was increased from 10.9% to 15.6%, and acrolein selectivity was increased from 9.6 mol% to 14.1 mol%. With the application of 5.50 kV/cm NTP, glycerol conversion was 21.7%, and acrolein selectivity was 17.5 mol%. Although NTP was much less significant in terms of catalyzing glycerol dehydration to acrolein compared to using HSiW-Si or HSiW-Al, it is evident that NTP made some improvement to both glycerol conversion and acrolein selectivity. Higher NTP field strength in this situation was more favored by acrolein production in this case, although the increase of the undesired acetaldehyde and propionaldehyde also occurred.

Table 4-3: Reaction of glycerol at 275° C without solid acid catalyst

	Conversion (%)	Selectivity (mol%)				Acrolein Yield (mol%)
		Acrolein	Acetaldehyde	Propionaldehyde	Acetol	
Control	10.9 [1] ± 0.3 [2]	9.6 ± 0.2	0.6 ± 0.0	NA [3]	15.6 ± 0.3	1.05
3.78 kV/cm NTP	15.6 ± 0.4	14.1 ± 0.5	0.6 ± 0.1	NA	16.4 ± 0.1	2.20
5.50 kV/cm NTP	21.7 ± 0.3	17.5 ± 0.5	1.0 ± 0.1	0.3 ± 0.0	17.6 ± 0.2	3.80

1: Mean of three repetitions.
2: Standard error.
3: Data not available (under detection limit).

4.4 Discussion

4.4.1 Temperature effect

Let us start the discussion concerning the effect of temperature only. Since the 20 wt% glycerol solution can be completely evaporated at temperatures above 210°C (Appendix I), the low conversion at low temperature observed for both catalysts can be attributed exclusively to the lack of energy. Energy insufficiency either resulted in that the glycerol molecules were not sufficiently activated for the reaction(s), or that the rate of the reaction(s) was not high enough to achieve a sufficient conversion within the given contact time. As the temperature increased, more glycerol molecules were energized to overcome the activation barrier, $1.44*10^5$ J/mol for HSiW-Al and $1.61*10^5$ J/mol for HSiW-Si (Appendix III). No sign of catalyst deactivation (in terms of glycerol conversion) was observed within 7.5 hours TOS for HSiW-Al. Therefore, the sensitivity of conversion to temperature straightforwardly reflected the fact that at higher temperature, more energy was charged to glycerol molecules, making them more reactive. For HSiW-Si, the fact that the average glycerol conversion never reached 100% was attributed to the deactivation of silica supported catalyst. The lower conversions at longer TOS of one continuous operation caused a decrease to the value of the average conversion during the 7.5 hours. A decline of glycerol conversion when the temperature was increased from 275°C to 320°C was possibly because that the catalyst deactivated faster at a higher temperature [102, 135].

Regarding the temperature effect on acrolein selectivity (refer to Figure 4-4 and 4-5), at lower temperature, protonated glycerol molecules tend to condense intermolecularly (Figure 4-10 I) [92]; therefore, an increasing trend was observed for the acrolein selectivity as the temperature increased from 220°C to 275°C. However, the acrolein selectivity at temperatures below 275°C was not much lower as compared to that at 275°C, because two other factors compensated the reduction in acrolein selectivity caused by glycerol consumption in intermolecular condensation (Figure 4-10 I). First, at low temperature, the formation of 2° carbocations is much easier than 1° carbocations [251]; hence the intramolecular dehydration tends to take the acrolein pathway rather than the acetol pathway (Figure 4-10 II). This statement agrees very well with Yoda and Ootawa's FTIR result that glycerol dehydration on H-MFI zeolite exclusively led to acrolein at 80°C [133]. Second, the side reactions to acetaldehyde and propionaldehyde were rather slow at low temperature; therefore, less acrolein would be consumed in producing these undesired products. At temperatures higher than 275°C, although the intramolecular condensation was reduced, several other side reactions, such as the formation of acetaldehyde and propionaldehyde, tended to be activated and accelerated under the higher temperature condition (Figures 4-6 and 4-7). As the result, the acrolein selectivity significantly decreased at the temperature 290°C and above.

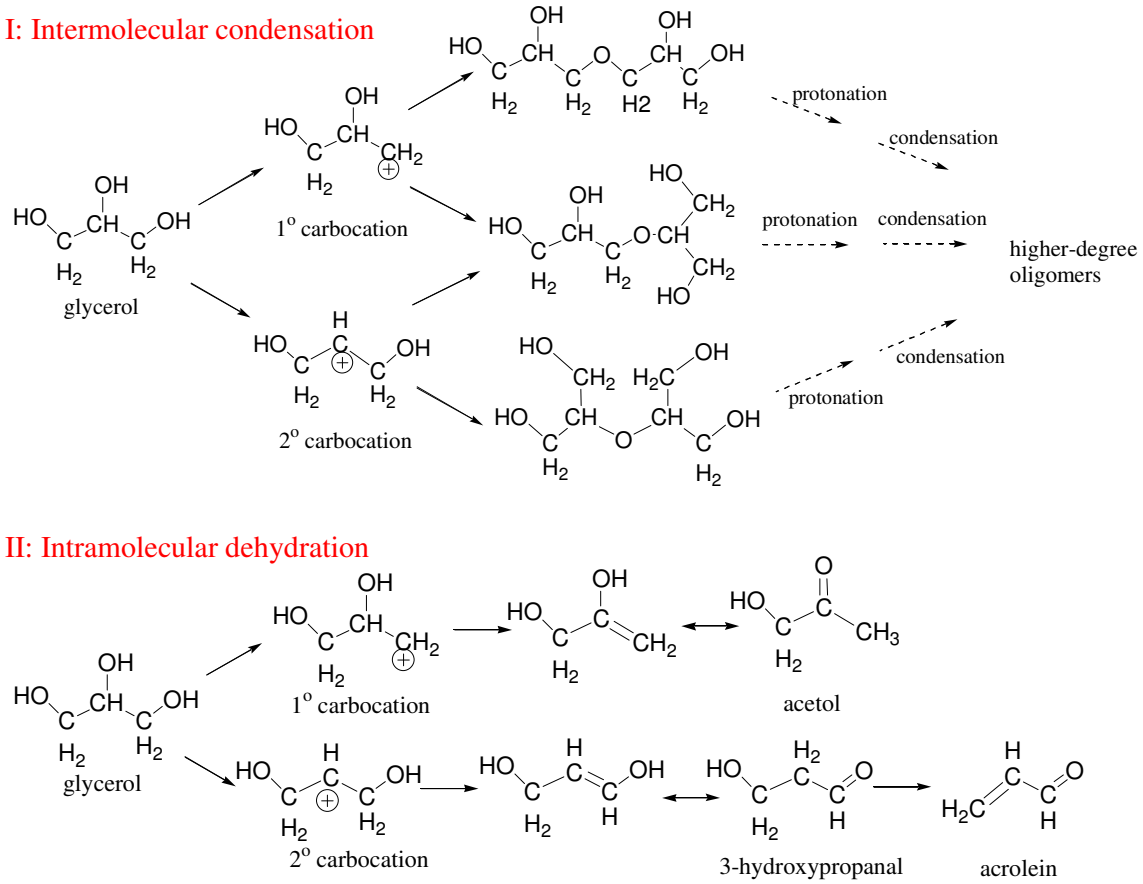

Figure 4-10: Illustration of intermolecular and intramolecular dehydration of glycerol

4.4.2 NTP effect

Some similarity can be found between the effects of NTP and that of temperature in glycerol conversion. It can be easily understood by viewing NTP as an energy input. Non-thermal plasma features efficient energy transfer via electron collisions [166]. In the NTP system, the breakdown occurred in the carrier gas argon. Highly excited electrons were generated from argon under NTP discharge (Equation 4-1). These electrons collided with glycerol molecules, and transferred energy directly to them (Equation 4-2). Also, the electrons collided with argon molecules, generating excited argon neutral, Ar^* (Equation 4-3); then energy was transferred from Ar^* to glycerol during the collision between these larger particles (Equation 4.4). Consequently, the "direct" or "indirect" energy transfer from

electrons excited glycerol molecules to "excited neutrals", $C_3H_8O_3^*$, making them more ready to follow this reaction path.

$$Ar \rightarrow Ar.^+ + e^- \qquad \textbf{Equation 4-1}$$

$$C_3H_8O_3 + e^- \rightarrow C_3H_8O_3^* + e^- \qquad \textbf{Equation 4-2}$$

$$Ar + e^- \rightarrow Ar^* + e^- \qquad \textbf{Equation 4-3}$$

$$C_3H_8O_3 + Ar^* \rightarrow C_3H_8O_3^* + Ar \qquad \textbf{Equation 4-4}$$

However, one should keep in mind that the NTP energy input and the formation of the more energized reactant was not only beneficial to the desired reaction (glycerol dehydration to acrolein). NTP's positive effect on glycerol conversion occurred in many reactions in the system instead of just in glycerol dehydration to acrolein.

The virtue of applying NTP in improving glycerol conversion might be achieved by operating the reaction at a higher temperature; however, the selectivity improvement made by NTP was never able to be achieved by optimization of the temperature condition alone. Figure 4-2--Figure 4.5 showed that NTP with proper field strength could improve acrolein selectivity; in addition, the result from the blank test (Table 4-3) confirmed that NTP alone improve acrolein selectivity to certain degree. The following discussion provides some insight regarding how NTP functioned in improving the selectivity to acrolein.

The induced acidity by NTP benefited the acrolein production. Two mechanisms possibly account for NTP acidity. First, the acidic behavior of NTP under high humidity could be stimulated by the non-resonant charge transfer processes (Equations 4-5 and 4-6) [166]. In the NTP system, the electrons were easily energized by the electrical field and freed from the argon molecules. A significant amount of positively charged argon ions, Ar^+, were formed as the result (Equation 4-1). During their collisions with water molecules, the argon ions transferred the positive charges and induced the formation of water ions, $H_2O.^+$ (Equation 4-5). The water ions subsequently reacted with neutral water molecules, and formed hydronium ions, H_3O^+ (Equation 4-6).

$$Ar.^+ + H_2O \rightarrow H_2O.^+ + Ar \qquad \textbf{Equation 4-5}$$

$H_2O.^+ + H_2O \rightarrow H_3O^+ + .OH$ **Equation 4-6**

Second, acidic behavior could also result from the ionization of water (Equation 4-7--Equation 4-9), as proposed by Liu *et al.* [252, 253]. The metastable neutral argon atoms (Ar*) were formed during electron collision events (Equation 4-7). These metastable argon atoms carried a significant amount of energy, and they could possibly ionize some water molecules when they collided with water (Equations 4-8 and Equation 4-9).

$Ar + e^- \rightarrow Ar^* + e^-$ **Equation 4-7**

$H_2O + Ar^* \rightarrow H_2O^* + Ar$ **Equation 4-8**

$H_2O^* \rightarrow H^+ + .OH + e^-$ **Equation 4-9**

The hydronium ion (or proton), formed possibly via the abovementioned mechanisms, could initialize the protonation of some glycerol molecules even prior to their contact with the acid sites of the catalyst (refer to Figure 1-4 in Chapter 1). Thus it could have resulted in an accumulative production toward acrolein.

NTP could positively interact with the catalyst and induce Brønsted acidity in the presence of water. It is already well known that the presence of water in the system can hydrate the acid catalyst, converting some of the Lewis acid sites to Brønsted acid sites [101, 132, 136], which favor acrolein formation [136]. HSiW has pure Brønsted acid sites; most, if not all, Lewis acid sites are located on the support. The electron bombardment would possibly induce the surface "defects" on the catalyst supports, hence potentially Brønsted acid sites. Also, with the efficient energy introduced by the NTP element, the dissociation of Al-O (or Si-O) and H-OH bonds is possibly facilitated (e.g. Equation 4-10). As a result, the dynamic interchange from Lewis acid to Brønsted acid sites would occur more frequently, which would advance acrolein production.

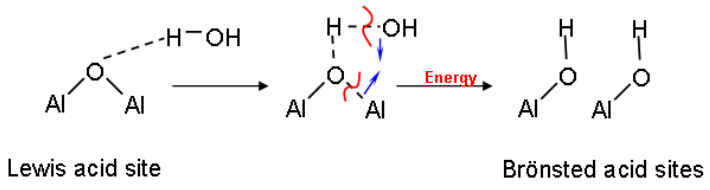

Equation 4-10

Usually, there are two approaches to facilitate a reaction. One is to provide the reactant(s) with the sufficient energy to overcome the activation barrier, and another is to lower the energy level of the transition state (TS). The former is normally achieved by conducting the reaction at a higher temperature, whereas the latter is normally achieved by using a catalyst. Depending on how effective the acid catalyst (especially Brønsted acidity) is for this particular reaction, the energy level of TS varies. Figure 4-10 illustrates the energy diagram of the overall reaction from glycerol to acrolein. The reaction barrier (or activation energy) E_a is the energy difference between the reactant and the transition-state species. The position A represents the transition state in the presence of HSiW-Al or HSiW-Si. NTP induced acidity possibly lowered the energy level of TS (from position A to position B in Figure 4-9). In addition, it is also likely that NTP increased the energy level of the starting material (from $C_3H_8O_3$ to $C_3H_8O_3^*$ as indicated in Figure 4-11). As the result, the new activation energy, E_a', was smaller than E_a. The result (the activation energy with NTP application was smaller than that without NTP application) agreed well with the proposed theory. The activation energy of HSiW-Al catalyzed glycerol dehydration at 3.78 kV/cm NTP was $1.37*10^5$ J/mol and the HSiW-Si catalyzed was $1.50*10^5$ J/mol (Appendix III). Both were smaller than the activation energies of their counterparts without NTP application ($1.44*10^5$ J/mol and $1.61*10^5$ J/mol for HSiW-Al and HSiW-Si, respectively).

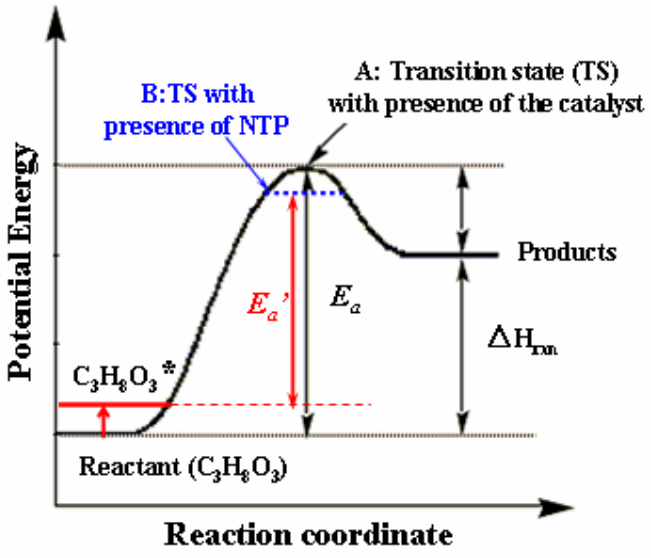

Figure 4-11: Illustration of the energy diagram for the overall reaction of glycerol dehydration to acrolein. E_a denotes the activation energy; $\triangle H_{rxn}$ denotes the enthalpy of reaction.

This illustration also helps understand how NTP functions in the glycerol dehydration process. In the respect to energizing the reactant, NTP is not selective; in the respect to lowering the TS energy level, NTP is selective to acrolein formation. The combination of HSiW-Al/HSiW-Si catalyst with NTP-induced acidity significantly lowered the energy barrier of the glycerol-to-acrolein reaction, but not of the others. This virtue was able to let NTP benefit the glycerol-to-acrolein reaction but not too much for the other reactions. Careful manipulation of the plasma properties is necessary so that the NTP can serve as the "selective" energy provider. At higher temperatures, the range to manipulate NTP to let it play a positive role in acrolein production is narrower than that at lower temperature. The example that the NTP exceeded the range and thus negatively affected the acrolein yield can be easily found in the results. For example, the 6.87 kV/cm application caused a drastic decrease of the acrolein yield in the HSiW-Al catalyzed reaction, while the 3.78 kV/cm NTP did not (Figure 4-2). The application of 4.58 kV/cm NTP to the reaction catalyzed at 320°C lowered the acrolein yield, but the same NTP application at 220°C did not (Figure 4-4).

The properly configured NTP significantly improved the acrolein yield when the reaction temperature was below 290°C (Figures 4-4 and 4-5). It is worth noting that such improvement did not require the sacrifice in energy consumption. The calculation showed that the energy consumption via NTP process was actually smaller than using conventional heating method (heating tape in this case) (Appendix IV).

The reason that the optimal NTP condition differed for HSiW-Si and HSiW-Al is probably due to geometrical factors and nature of the catalyst. HSiW-Si not only had more narrow pores, but also might be more densely packed because of granular shape, as compared to the HSiW-Al spherical beads. As a result, the mean-free-path of the electrons overall was shorter in the HSiW-Si system than in the HSiW-Al system, which may have weakened the discharge field, thus requiring more strength input to compensate the weakening effect.

4.4.3 Byproducts

Let us now take a look at the results of the major byproducts, acetaldehyde, propionaldehyde, acetol, and coke. The reactions leading to these byproducts could be either

competitive or sequential reactions to acrolein formation; therefore, the formation of these products negatively affects acrolein selectivity.

Acetaldehyde (Discussion related to Figure 4-6)

Nimlos *et al.* proposed that glycerol followed a pericyclic mechanism to form formaldehyde and vinyl alcohol, which was tautomerized to acetaldehyde (Figure 4-12 Path 1) [254]. The calculated reaction barrier of this pathway was much lower than the two dehydration pathways. If this mechanism were valid, the acetaldehyde selectivity would have been much higher than what was observed at low temperature. Therefore, this mechanism was eliminated in the case with the presence of the acid catalyst.

Several studies [102, 136] proposed that acetaldehyde was formed via the retro-Aldol reaction of 3-hydroxypropanal (Figure 4-12 Path 2). Acetaldehyde formation consumed a certain amount of 3-hydroxypropanal, which would otherwise have been converted to acrolein. Acrolein selectivity was significantly lowered at higher temperatures and higher field-strengths (Figures 4-2--4-5), which agreed well with the mechanism of acetaldehyde formation from 3-hydroxypropanal. Therefore, this mechanism was applicable.

Suprun *et al.* [130] proposed that acetaldehyde was formed from acetol via catalytic C-C bond cleavage, as shown in Figure 4-12 Path 3. Although the reverse trend between the selectivity of acetol and acetaldehyde was not observed in response to temperature change, it was observed in response of the field strength change. So the mechanism of producing acetaldehyde from acetol can be excluded if no NTP is applied, but can not be excluded under NTP conditions.

In summary, acetaldehyde was primarily formed from acrolein precursor 3-hydroxypropanal, and it might as well form from acetol when NTP is applied.

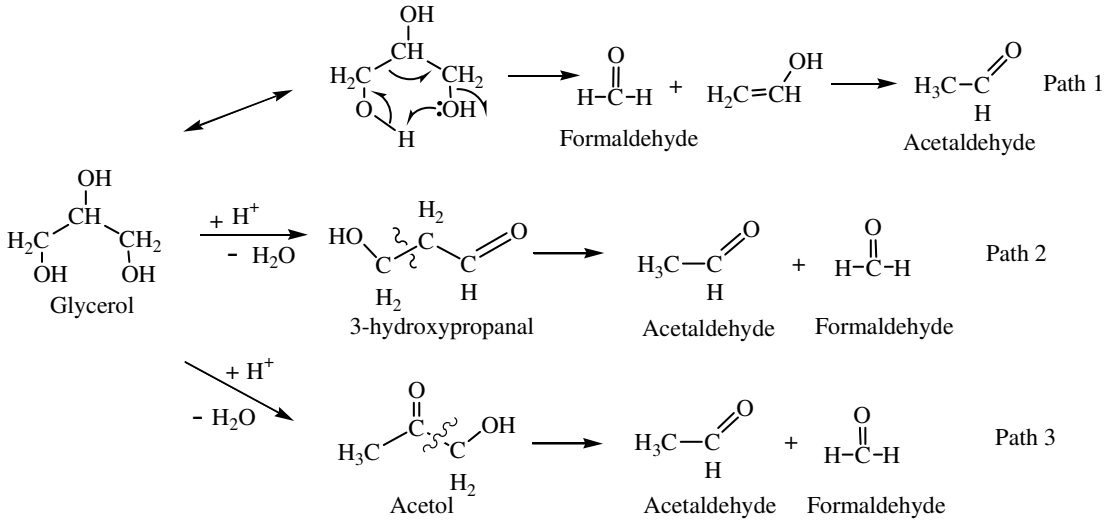

Figure 4-12: The plausible pathways of acetaldehyde formation

Propionaldehyde (Discussion related to Figure 4-7)

Although the selectivity of acetaldehyde and propionaldehyde responded similarly to temperature and NTP field strength, their formation mechanisms differed completely. Propionaldehyde could be formed from 1,2 addition of H_2 to the carbon-carbon double bonds (Figure 4-13 Path 1) or 1,4 addition of H_2 to the conjugated system to enol followed by isomerization (Figure 4-13 Path 1) [256]. The mechanism of deriving propionaldehyde from acrolein was adopted by Deleplanque *et al*. [141]. Corma *et al* and Suprun *et al.* proposed that propionaldehyde was formed exclusively from acetol [108, 130]. Figure 4-13 Path 3 depicts the mechanism of forming propionaldehyde from acetol. It was observed the co-occurrence of the decrease of acetol and the increase of propionaldehyde, especially in higher temperature operations and in the NTP applications. Hence the formation pathway from acetol was very likely for the process in this study. Also, the pathway from acrolein or 3-hydroxypropanal cannot be ruled out, since at high temperature and high NTP field strength, acrolein selectivity decreased while the propionaldehyde selectivity increased. Based on the agreement of the experimental data with the pathways provided by literature, the possible mechanism of propionaldehyde formation in this system is summarized in Figure 4-13, and the hydrogenation could occur to acrolein, acetol and/or 3-hydroxypropanal. The needed hydrogen was possibly formed from the dehydrogenation of oligomers during coke deposition, which occurred from the onset of the glycerol conversion process.

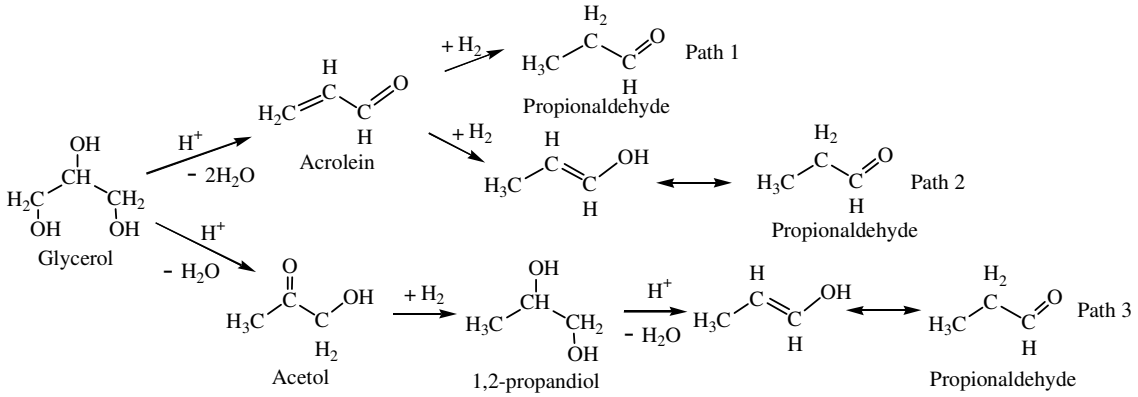

Figure 4-13: The plausible pathways of propionaldehyde formation

The thresholds of temperature and field strength were observed to cause a significant difference for the proportions of acetaldehyde and propionaldehyde in the product composition. This confirmed the earlier statement that NTP needs to be carefully configured to ensure that NTP was intense enough to provide the virtues of NTP in improving acrolein selectivity (NTP acidity) as well as glycerol conversion (efficient energy transfer), but not too intense to let the formation of the aldehydes pass the threshold and consume too much acrolein.

Acetol (Discussion related to Figure 4-8)

Different from the side reactions of acetaldehyde and propionaldehyde, the acetol pathway is a competing reaction with the acrolein pathway from the very beginning. The protonation of the OH on the 2° carbon leads eventually to acrolein, whereas the protonation of the OH on 1° carbon leads to acetol (Figure 4-10 II). Usually, Brønsted acid sites favor acrolein production; acetol formation was catalyzed via Lewis acid sites, if it was ever catalyzed [136]. HSiW introduced primarily Brønsted acid sites, and NTP induced solely Brønsted acidity, both of which were primarily functioning to lower the reaction barrier of acrolein formation. Consequently, acrolein formation was greatly catalyzed (but acetol formation was not), which competitively consumed a portion of glycerol that could have been converted to acetol. This explains the observation that the selectivity to acetol decreased under the NTP conditions in Figure 4-8. Several factors account for the lower acetol

selectivity at lower temperature. First, 2° carbocations are thermodynamically favored over 1° carbocations, in general [251]; at a lower temperature, the product distribution would contain more 2° carbocation-derived products, such as acrolein. Second, at lower temperatures, the intermolecular condensation of glycerol was favored [92]; this means that some of the formed 1° carbocations tended to interact with another molecule to form C-C single bonds, instead of interacting with the neighboring carbon within the same molecule to form a conjugated double bond. Hence the probability of acetol formation was lowered even more. (The mechanisms are illustrated previously in Figure 4-10.) Third, the rate of acetol formation itself was slower at a lower temperature. At temperatures above 305°C, the subsequent reactions from acetol were enhanced, such as the formation of acetaldehyde (Figure 4-13 Path 3) and propionaldehyde (Figure 4-13 Path 3) [108, 130, 136]. These subsequent reactions lowered the acetol selectivity at high temperature. The discussion above explained the observation that the selectivity to acetol in response to temperature in Figure 4-11.

Coke

The intermolecular condensation of glycerol was favored at low temperature, resulting in more glycerol oligomers formed [92, 108, 130]. The glycerol oligomers have relatively high boiling temperatures, and barely remained in the gas phase at the reaction temperature. These oligomers could not flow out of the packed-bed reactor as easily as the other gas-phase species; in other words, they received increased contact time with the catalyst to undergo the condensation reaction. The linear, cyclic and/or branched glycerol oligomers grew in size, contributing to the overall coking. As the temperature increased, intermolecular condensation was suppressed, and desorption of the products from the catalyst surface increased, reducing the contact time of the products and thus alleviating the polymerization of the products. As the result, less coke was formed when temperature increased from 220°C to 275°C/290°C. As temperature increased, intra-molecular dehydration [92] was enhanced, and more double-bonded compounds (acrolein and acetol) were formed. As temperature exceeded 290°C/305°C, aldehydes (or acetone [108, 130, 136]) were significantly increased, which often enhances coke formation [257]. The reaction rate of coke formation itself could have been significantly increased at high temperatures. These factors explained the observed

increasing trend of coke amount when temperature increased from 290°C to 320°C (Table 4.3).

With the discussion above, one would expect that more coke would be observed for the condition at the same temperature but with NTP application, since NTP increased the formation of acrolein, acetaldehyde, and propionaldehyde. However, comparing the data in the presence versus absence of NTP ("3.78 kV/cm" for HSiW-Al and "4.58 kV/cm" for HSiW-Si), it was found that the coke weight from NTP-applied reactions not only did not increase, but also showed some reduction tendency compared to their counterparts without NTP.

It was claimed that the existence of oxidants in the reaction system could suppress coke formation [92, 129]. Molecular oxygen co-fed into the system was effective in serving this function [92, 129], but water vapor was not [110]. Therefore, there must be another effective oxidative agent present in the NTP system that could partially suppress coke formation. The hydroxyl radical (.OH) can be produced via dissociative electron collisions with water by NTP (Equation 4-11).

$$H_2O + e^- \rightarrow H. + .OH + e^- \qquad \textbf{Equation 4-11}$$

The existence of the OH radicals in NTP with the presence of water vapor and the oxidative ability of .OHs have been well acknowledged in the environmental waste water treatment area [258, 259]. In the system, water was co-fed in a large quantity as a diluting agent of glycerol. Therefore, under the NTP discharge, it was very likely that some OH radicals were present in the reaction zone. The applied field strengths (3.78 kV/cm and 4.58 kV/cm) were relatively low, compared to the plasma intensities in waste water treatment applications [258, 259]. The concentration of .OH in the system was probably low, which possibly accounts for the fact that not very significant suppression was observed. Higher field strength NTP facilitated .OH generation, and the coke formation under the NTP application of 5.50 kV/cm was significantly less than the control condition. However, not much advantage in coke suppression was observed for the 6.87kV/cm NTP application, probably because under that intense NTP, more unsaturated cracking compounds or even some carbon radicals were formed, which would favor polymerization.

4.5 Conclusions

This chapter presented my study on the effects of the reaction temperature and NTP using argon as the discharge gas on the gas-phase glycerol dehydration on HSiW-Al and HSiW-Si.

As the reaction temperature increased, the glycerol conversion increased in general. At 290°C and above, glycerol was completely converted on HSiW-Al; complete conversion was never achieved on HSiW-Si because of the deactivation of HSiW-Si. In the temperature range of 220-275°C, the acrolein selectivity showed a slight increase when temperature increased from 220°C to 275°C, but significantly decreased when temperature was further increased to 290°C and above, because of significantly enhanced formation to acetaldehyde and propionaldehyde. Coke formation first decreased as the temperature increased; above 290°C, it significantly increased as the reaction temperature increased.

With the optimal NTP applied, a consistent improvement in the acrolein selectivity was observed when the reaction was operated at 275°C or below.

Some similarities were found between the effect of temperature and the effect of NTP in influencing certain kinetic parameters, and also there was some confounding effect between temperature and NTP. The result showed that NTP played the role of an efficient energy input, and also the role of providing additional acidity, which lowered the activation energy and improved acrolein selectivity. The optimal acrolein production was observed at 275°C, and under 3.78 kV/cm for HSiW-Al and 4.58 kV/cm for HSiW-Si, achieving acrolein yields of 83.6 mol% (98.7 % conversion, 84.7 mol% selectivity) and 83.1 mol% (94.4% conversion, 88.0 mol% selectivity) respectively. For HSiW-Si, such catalytic performances remained stable for over 20 hours TOS without showing deactivation.

Chapter 5

The positive roles of non-thermal O_2 plasma in coking suppression and catalyst regeneration

Abstract

The important chemical intermediate acrolein is produced by gas-phase glycerol dehydration catalyzed by solid acids. The major challenge of this method is how to extend catalyst service life, since the catalyst that leads to high acrolein selectivity usually deactivates rapidly. Silica supported silicotungstic acid (HSiW-Si) is a good example of such a catalyst. In the work described in this chapter, HSiW-Si was used to probe the potential of using non-thermal plasma with oxygen-containing gas as the discharge gas (NTP-O_2) to solve the catalyst deactivation problem. NTP-O_2 was found to be effective in both online coking suppression and off-line coke removal (catalyst regeneration).

Keywords: coking, carbonaceous species, deactivation, molecular oxygen, atomic oxygen, ozone, TPO, HSiW-Si.

5.1 Introduction

"Coke" is a general term used for any carbonaceous substances deposited on the catalyst surface during the reaction. These carbonaceous substances are a distribution of the polynuclear aromatic substances of aliphatic and alicyclic compounds usually formed via condensation, hydrogen abstraction, polymerization, and repetitions of these reactions [260]. The terms "soft" and "hard" are commonly used to describe coke, and these relative properties are associated with structural complexity and polymerization degree of the carbonaceous substances. Harder coke is more complex in structure and more difficult to be burned off. For example, a 5-carbon-ring aromatic compound is "harder" than an aphaliptic compound containing the same number of carbons; a 6-carbon-ring aromatic compound is "harder" than a 5-carbon-ring aromatic one.

Coke formed on the catalyst surface and blocked the active acid site, preventing the glycerol molecules from contacting and interacting with these sites. Glycerol conversion would decrease as the result. Also, part of the coke is formed from acrolein or glycerol, so its formation reduced the acrolein yield. Strong acid sites, or more specifically, strong Brønsted acid sites, are favored by acrolein formation, but they unfortunately also lead to more severe coking and therefore more severe catalyst deactivation [127].

The ideal solution to the deactivation problem is to suppress coke formation during the glycerol dehydration reaction. Alhanash *et al.* used platinum-doped catalyst and co-feeding H_2 [127] to reduce the coke formation. Using hydrogen unavoidably involves some safety issues. Whether the expensive usage of platinum is worthwhile is rather questionable, since deactivation still occurred within 10 hours time-on-stream (TOS) [127]. These issues would not make the bio-based acrolein process any more attractive to the acrolein manufacturers. Another direction of coke suppression is using O_2-containing gas as a carrier to maintain the products at an oxidized state [92, 129, 261] [141]. Although the catalyst deactivation was alleviated in all these studies, disagreement was found in whether acrolein yield would be negatively influenced. Ulgen and Hoelderich reported a slight increase in acrolein selectivity but a slight decrease in glycerol conversion [92] when using oxygen containing carrier gas. Wang *et al.* claimed that, with the presence of molecular oxygen, byproducts were significantly reduced [129]. Deleplanque *et al.* reported a reduction up to over 15 mol% in acrolein selectivity when using an O_2-containing carrier gas during glycerol dehydration [141]. Therefore, whether co-feeding oxygen is overall beneficial to the acrolein production is uncertain.

The Keggin structure (Appendix V), the most important feature of HPA, is retained intact during/after coke formation [115]. Deposited coke was reported to occur as an amorphous form, and its existence would not alter any crystalline structure of the catalyst [127, 129, 144]. In other words, supported HPA can be regenerated to regain the acid catalytic activity if the deposited coke is removed. Catalyst deactivation due to coking is quite common in industrial chemical production processes; the routine treatment is to flush the catalyst bed with oxygen-containing gas at elevated temperatures, usually 450-600°C, but depending on the catalyst characteristics and specific reactions, higher temperatures (600-800°C) may be required to remove the coke [139, 262, 263]. A problem encountered here is that the Keggin structure of HSiW can only be maintained up to 400°C [145] (one study claimed up to only 300°C [117]), depending on the characteristics of the supports. So the "regeneration" via the high-temperature combustion approach would remove the coke only at the cost of the reduction of the catalytic activity afterwards due to the significant loss of acidity. Therefore, the conventional decoking treatment is not appropriate for regenerating the supported HSiW for the acrolein production process.

Non-thermal plasmas (NTP) can initiate formation of ions, free radicals, and other highly reactive intermediates. In an O_2-containing atmosphere, NTP can convert the O_2 molecule into many highly reactive oxygen species, including the triplet ground-state oxygen atom $O(^3P)$, the metastable oxygen atom $O(^1D)$, metastable oxygen molecule $O_2(^1\Delta g)$, and ozone O_3. When humidity is present, additional highly reactive species are formed, such as $H_2O.^+$, free H atoms, and OH radicals. Most of these species are highly oxidative, and can oxidize substances that O_2 or air fails to oxidize under mild temperature conditions.

The original motivation of applying non-thermal plasma with oxygen-containing gas as the discharge gas (NTP-O_2) in this study came from the already industrialized practice in volatile organic compounds (VOCs) treatment. The presence of non-thermal plasma significantly improved the efficiency of VOC removal at ambient temperature (e.g., [185, 232, 238, 239, 264-267]). The common VOCs, toluene, benzene, and xylene, are aromatic compounds, and the removal is achieved by oxidizing them into CO or CO_2. The improvement of VOC removal is attributed to the highly reactive and oxidative species formed in NTP. Some similarities may be found between VOC removal and the decoking of the spent catalyst: the aromatic structure abundantly exists in coke and it is desired to oxidize them into CO_x or oxidize them into less complex structures. It is possible that these "highly reactive oxygen species" in NTP can play a role in the coke (especially coke precursor) suppression/removal in glycerol dehydration process.

There were several studies in the literature which further suggested that the NTP-O_2 would be a valid candidate for regenerating supported heteropoly acid (HPA). Cha *et al.* used DBD non-thermal plasma and successfully suppressed the formation of polycyclic aromatics and coke in the burning of propane gas [268]. Mawhinney *et al.* studied ozone oxidation of amorphous carbon with FTIR [269]; the surface reduction and morphological change of the adsorbent charcoal after the interaction with ozone was observed via SEM [270]. The efficiency of ozone removal by activated carbon (AC) was studied by Takeuchhi and Itoh: ozone molecules diffused into the AC micropores and reacted with carbon surface [271]. Khan and Al-Jalal studied atomic oxygen's role in decoking a coked zeolite [263]. Pieck *et al.* used ozone to regenerate a spent Pt-Re/alumina catalyst coked by the 8-hour reaction of cyclopentane with hydrogen at 500°C [272]. From the evidence above, NTP-O_2, which

contains both ozone and atomic oxygen, was very likely to contribute to solving the deactivation problem of a solid acid catalyst possessing thermal stability issues. Regenerating the deactivated catalyst is an important issue; depending on the catalyst's characteristics and the reaction it was used in, the deactivated catalysts can vary significantly in their coke profile, and thus vary in terms of how difficult they can be regenerated [273]. Therefore, it was necessary to expend some effort on regenerating the acid catalyst deactivated by glycerol dehydration process.

The objectives of this study were 1) to investigate whether the NTP-O_2 application in the glycerol dehydration process could suppress the formation of carbonaceous polyaromatic compounds, and ultimately suppress the coke formation; and 2) to investigate the NTP-O_2 effectiveness in the catalyst regeneration, so that the periodic coke removal can be incorporated into the bio-based acrolein production to increase its potential for industrialization.

5.2 Materials and Methods

5.2.1 Catalyst preparation

Our results showed that silica supported silicotungstic acid (HSiW-Si) would be a very good catalyst for acrolein production if it did not deactivate so fast. Therefore, HSiW-Si seemed to be an excellent candidate for the exploration of the potential of applying NTP-O_2 in 1) reducing coke formation during the reaction (in-situ coking suppression) and 2) regenerating the deactivated catalysts (periodic regeneration). Ultimately, the method developed in this study for glycerol dehydration to acrolein could be applied to other acid catalytic reactions using solid catalysts (especially HPAs) that have relatively low thermal stability.

HSiW was loaded on the catalyst support by the impregnation method. Silica support (Si) was calcined at 300^{o} C for 2 hours before use. HSiW of 10% weight percentage (wt%) of the support was dissolved in deionized water to make 0.04 g/mL solution. The calcined support was added to the HSiW solution. Constant stirring was applied to the mixture at room temperature for 24 hours to attain adsorption-desorption equilibrium. The resultant mixture was dried first at 55°C for 24 hours with the application of constant stirring. Then the mixture

was dried at 105°C for complete dryness. The mixture was calcined at 300°C before the 2nd impregnation. The procedures were repeated for another 10 wt% HSiW loading.

5.2.2 Online coking suppression during glycerol dehydration

The experiment in this subsection was designed to examine whether applying NTP-O_2 during the reaction was effective in coking suppression and was overall beneficial to acrolein production.

The configuration and orientation of the packed-bed, down-flow DBD reactor used for the kinetic experiment was previously described (Chapters 3 and 4). Oxygen-containing gas was achieved by a blending procedure. As is shown in Figure 5-1, oxygen (99.99%) and argon (99.99%) were well mixed as they flowed through a 400 mm tube filled with quartz wool. Each of the gas streams was individually controlled by a rotameter, and by adjusting the flow rate of each gas, the gases were proportionally fed to the blender, achieving a desired ratio (5% O_2 containing gas). The carrier gas, which was 5% (volumetric ratio) oxygen in argon, was fed into the reactor at 60 mL/min. The schematic of the entire system is illustrated in Figure 5.1. Glycerol conversion and product selectivity were obtained for comparison.

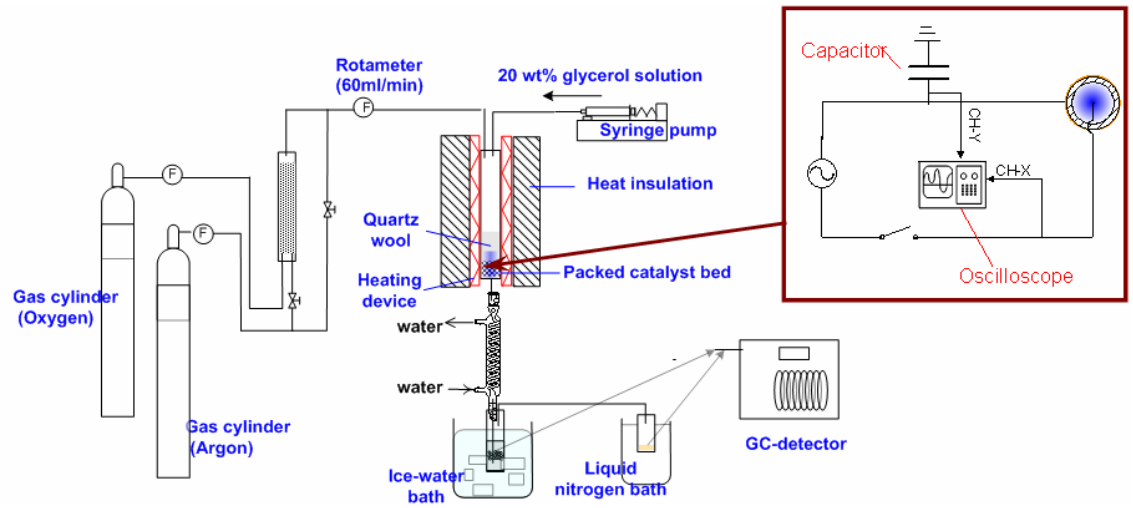

Figure 5-1: Apparatus for glycerol dehydration with the options of co-feeding oxygen and/or NTP

Glycerol dehydration at 275°C using pure argon as the carrier gas without NTP was used as the control test (referred to as "the control condition" hereafter). Glycerol dehydration kinetic experiments with oxygen-containing carrier gas (5% O_2 in argon) were conducted at 275°C with ("NTP-O_2") and without NTP discharge ("COA"), respectively. Table 5-1 lists these three conditions including 1) argon at 275°C, 2) 5% O_2 in argon at 275°C, and 3) 5% O_2 in argon with NTP discharge at 275°C; comparison was made among them. The total carrier gas flow rate was maintained at 60 mL/min. The electric field strength applied was 4.58 kV/cm, and the frequency used was 1 kHz for the NTP configuration. Two repetitions were conducted for each condition. The conversion and the selectivity of acrolein and the major gaseous byproduct were evaluated. Also the catalyst deactivation and coke formation were evaluated by glycerol conversion, catalyst weight gain, specific surface area, and temperature programmed oxidation (TPO).

Table 5-1: List of the experimental conditions for coking suppression [1]

	Temperature	Argon	5% O_2	NTP [2]	Denotation
Condition 1	275°C	Yes	No	No	Control
Condition 2	275°C	Yes	Yes	No	Co-fed oxygen alone (COA)
Condition 3	275°C	Yes	Yes	Yes	NTP-O_2

1: Catalyst: silica supported silicotungstic acid; glycerol solution: 20 wt%; gas-hourly-space-velocity: 84.4 h^{-1}; carrier gas flow rate: 60 mL/min, TOS: 7.5 hour.

2: NTP field strength: 4.58 kV/cm.

The principle of the TPO technique is that oxygen oxidizes the carbonaceous species (coke) that formed on the catalyst surface at an elevated temperature. Depending on the structural complexity of the coke, it is oxidized at different temperatures. "Harder" coke would require higher reaction temperature to be oxidized into CO_2. Therefore, as the temperature is increased, the oxygen preferentially reacts with the surface coke species, and the oxygen consumption provides a measure of the coke profile regarding the relative amount and hardness of the coke deposited on the surface during the reaction. The measurements were conducted using an oxygen-containing gas (5% oxygen blended with helium) at 70

mL/min. The spent catalyst (0.100g) was dried at 105ºC in a convection oven for 12 hours, and preheated at 300°C in nitrogen atmosphere prior to the TPO experiment. The temperature was programmed from 25°C to 900°C at a heating rate of 10°C min^{-1}. The effluent gases were subsequently passed through a liquid nitrogen trap before reaching the TCD detector; the oxidation product CO_2 was condensed, but the background gas helium and the unconsumed oxygen could pass through.

There were several reasons to use 5% O_2 blended with argon in the reaction instead of using pure oxygen and air. First, using a low dose of O_2 is to ensure operation under the explosion limit [274]. Second, the preliminary results showed that a heavy dose of oxygen would result in an even more significant loss of acrolein selectivity (decreased to below 50 mol% when using air at 275°C). Therefore, the oxygen-containing gas was configured as 5% oxygen blended in argon. Also, the use of argon rather than N_2 (the major component in air) made the result in Chapter 5 comparable to those of the previous chapters.

5.2.3 Offline coke removal and catalyst regeneration

The experiments of this subsection were designed for evaluating whether NTP-O_2 can be effective in removing the coke from the catalyst surface and regenerating the deactivate catalyst. The problem was approached from two vantage points.

5.2.3.1 Direct investigation of coke removal

In this section, the regeneration was investigated outside of the packed-bed reactor. The deactivated catalyst was taken out of the PBR. The experiments were focused on 1) monitoring the decoking process and 2) TPO characterization of the coke profile change after the treatment. This part of experiment was a direct evaluation in terms of coke removal.

Monitoring of the decoking process was completed using the system shown in Figure 5-2. The spent HSiW-Si was collected from a 7.5 hour kinetic experiment conducted at 275°C with argon as carrier gas (the kinetic result of the catalyst is presented in Table 3-2 and listed as HSiW-Si1252). The spent catalyst was placed in a home-made DBD cell with the wire-to-cylinder configuration; heat could be applied as an option using heating tape. The gas

flowed though the DBD cell, and traveled through a liquid nitrogen (LN) trap before reaching the TCD detector. Helium could not be condensed in the LN trap, and oxygen could pass through the LN trap, because 5% concentration was far below its saturation vapor pressure [275]. Five discharge field strengths (3.0 kV/cm, 4.8 kV/cm, 6.6 kV/cm, 8.4 kV/cm, and 10 kV/cm) were studied at ambient temperature (25°C), and the optimal NTP field strength was used to study the temperature effect (25°C, 100°C, 150°C, 200°C). Blank tests were conducted to obtain knowledge of the baseline, including data obtained by applying NTP to the discharge cell loaded with 200mg fresh catalyst at various discharge voltages using only helium and using oxygen-containing gas, respectively. The TCD signal can qualitatively reflect the decoking process. The gas was fed into the DBD cell at 30 mL per minute.

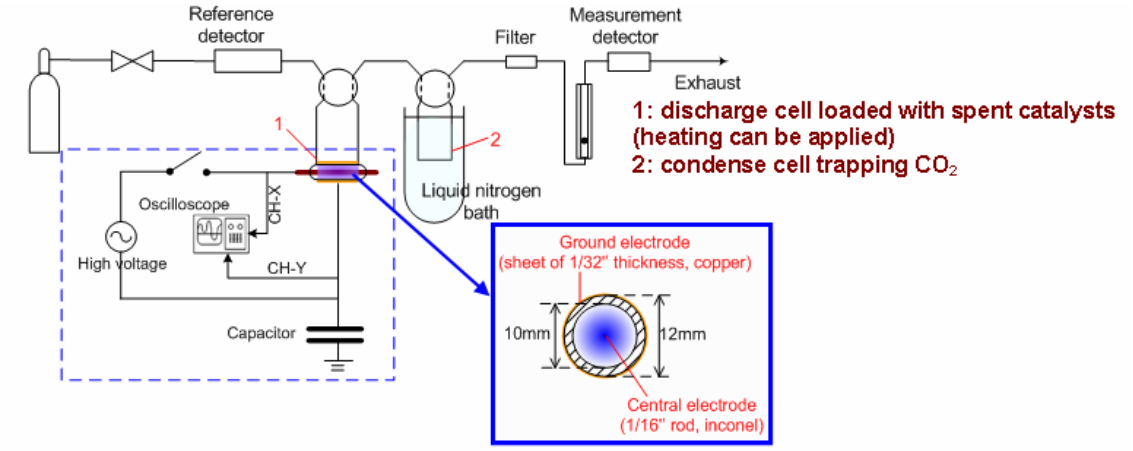

Figure 5-2: Schematic of catalyst regeneration device with NTP application

In addition to monitoring the decoking process, the coke removal was also evaluated by temperature programmed oxidation (TPO) characterization of the catalyst after a specific decoking treatment. The principle and experimental details of the TPO characterization technique were described in Section 5.2.2. The characteristic of the remaining coke on the catalyst surface after NTP-O_2 treatment was obtained in this manner. The coke removal effectiveness of each NTP-O_2 condition was evaluated based on the profile of coke distribution obtained via TPO.

5.2.3.2 Direct evaluation of catalyst regeneration

In the work described in this section, the catalyst was kept inside the packed-bed reactor and the regeneration with NTP-O_2 treatment was directly applied *in situ*. The experiments were focused on the glycerol dehydration performance after regeneration treatment. This was an indirect evaluation in terms of coke removal, but a direct evaluation in terms of whether the catalyst could be regenerated and the catalytic performance could be regained.

After 7.5 hours of glycerol dehydration in the down-flow PBR (84.4 h^{-1}GHSV, 60 mL min^{-1} argon gas, 275°C) the glycerol feed was stopped, the reactor temperature was lowered to 150°C, and the gas was switched to an oxygen-containing gas. Three different discharge gases were compared: 1) 20% oxygen blended in argon, 2) 20% oxygen blended in nitrogen, and 3) pure oxygen, which can be viewed as 20% oxygen in oxygen. (The noble gas argon should have similar behavior as helium as a NTP discharge gas.) The total gas flow rate was 30 mL/min. The NTP field-strength and operation temperature were based on the optimal condition found in the above-mentioned tests. After 2 hours, the plasma was stopped; the carrier gas was changed back to the original configuration, and the glycerol feed was restarted. The glycerol conversion and acrolein selectivity were obtained during a few hours TOS to test the generation effect. The regeneration-kinetic process was repeated for another time.

5.2.4 Combining online coking suppression and offline catalyst regeneration (coke removal)

Usually the effectiveness of coke removal greatly depends on the characteristics of the deposited coke. Therefore, in the research described in this section, instead of using spent HSiW-Si from a control dehydration process, the spent HSiW-Si from a NTP-O_2 assisted dehydration process was used to test the coke removal/catalyst regeneration. TPO characterization was conducted after 1.5 hours of coke removal NTP treatment in 5% oxygen/helium. Also, the continuous process incorporating both online coking suppression and offline catalyst regeneration was evaluated. The glycerol dehydration using oxygen-containing carrier gas was conducted with NTP applied; after the period of 7.5 hours TOS

reaction, NTP-O_2 regeneration treatment was applied for 2 hours. The kinetic reaction was resumed after the reaction to evaluate the regeneration result.

5.3 Results

5.3.1 Online coking suppression

Table 5-2 summarizes the results for glycerol conversion and the selectivity of acrolein and the major byproducts obtained under different reaction conditions. In comparison to the control condition (as previously defined in Table 5-1), the NTP-O_2 application significantly increased the glycerol conversion more than COA. COA caused a significant decrease in acrolein selectivity compared to the control condition, which agrees with Deleplanque's early report [141] demonstrating that co-fed oxygen alone lowers the acrolein selectivity. Part of acrolein was either converted to acrylic acid (~1-2mol% quantified by GC) and/or underwent further oxidation to CO_x. However, the acrolein selectivity under the NTP-O_2 condition did not show much difference compared to the control condition. Both COA and NTP-O_2 significantly reduced the selectivity to propionaldehyde. The acetol selectivity was significantly reduced in the COA condition, and more so in the NTP-O_2 condition. No significant decrease was observed in acetaldehyde selectivity for both COA and NTP-O_2 conditions compared to the control condition. Compared to the control condition, both COA and NTP-O_2 significantly reduced the coke formation, evidenced as significantly lowered catalyst weight increase after the reaction. This result shows that the introduction of NTP-O_2 can significantly suppress the coke formation without much sacrifice in acrolein selectivity, which was advantageous compared to the COA. A decrease in the carbon balance was probably due to the CO_2 and/or CO formation (from deep oxidation of the gaseous products), which unfortunately could not be measured in this experiment.

Table 5-2: Summary of the conversion and selectivity of the tested conditions

	Condition / Kinetics	275°C	275°C, O_2, NTP	275°C, O_2 (COA)
	Conversion (%)	92.9± 0.3	97.6± 0.1	95.9± 0.2
Selectivity (mol%)	**Acrolein**	79.5± 0.2	80.1± 0.5	72.2± 0.8
	Acetol	7.6± 0.3	3.6± 0.2	5.6± 0.2
	Acetaldehyde	1.1± 0.24	1.1± 0.11	1.0± 0.02
	Propionaldehyde	1.1± 0.04	0.4± 0.04	0.7± 0.07
	Coke (%)[3]	14.3± 0.5	7.0±0.6	9.9±1.0
	Carbon balance[4] **(%)**	96.0± 2.0	86.8±2.1	84.6± 0.6

1: The average of two kinetic repetitions; and each was the average conversion (selectivity) over time-on-stream (TOS) 1.5-7.5 hours.

2: Standard error of the mean of the two kinetic repetitions.

3: This percentage was calculated by the increased weight after the reaction divided by the weight of the fresh catalyst.

4: Carbon balance is calculated by the summation of carbon mass in the collected sample divided by the total carbon mass fed into the system. For simplicity, carbon C_n is usedas the formula of the coke for catalyst weight and accounted 100% of the increased catalyst weight as coke.

In addition to the clear reduction in the weight increase of the spent catalyst from either COA or NTP-O_2 as compared to that from the control condition (Table 5-2), the coking suppression is manifested in Figure 5-3 as well. Figure 5-3 A shows the deactivation in terms of glycerol conversion expressed as the difference between glycerol conversion at a specific TOS (X_n) and the conversion at 1.5 hours TOS (the first sampling point)(X_1) divided by X_1. Both NTP-O_2 and COA achieved coking suppression; the slopes of the conversion decrease were smaller than the control condition. Under the NTP-O_2 condition, suppression of coke formation was more effective in that the slope of the conversion decrease was even smaller. Figure 5-3 B is the TPO profile of the spent catalyst. Depending on its "hardness", the coke was preferentially oxidized into CO_2 by oxygen as the temperature increased. Carbon dioxide left the catalyst surface as the gaseous effluent, but CO_2 was condensed when the gaseous effluent passed through the liquid nitrogen trap. As for the two components in the effluent that were not condensed, helium amount remained the same before and after the sample cell, while the oxygen amount might change depending on whether and how much the coke could be oxidized. In a TPO graph, X-axis is temperature while the Y-axis is the signal of the detector. A point in the TPO curve indicates a relative amount (position in Y-axis) of the coke with certain hardness (position in X-axis). Harder coke locates on the higher-temperature end, and vice versa. The TPO profiles of the spent catalysts from both NTP-O_2

and COA are significantly lower than the spent catalyst from the control condition. Not only the overall coke was reduced, but also the amount of the harder coke was significantly lowered compared to the control condition; as a result, the loss of surface area was significantly decreased compared to the control condition. The result from glycerol conversion, TPO profile, the weight increase of spent catalyst and the percentage surface loss consistently showed the trend that the NTP-O_2 suppressed coking more than COA.

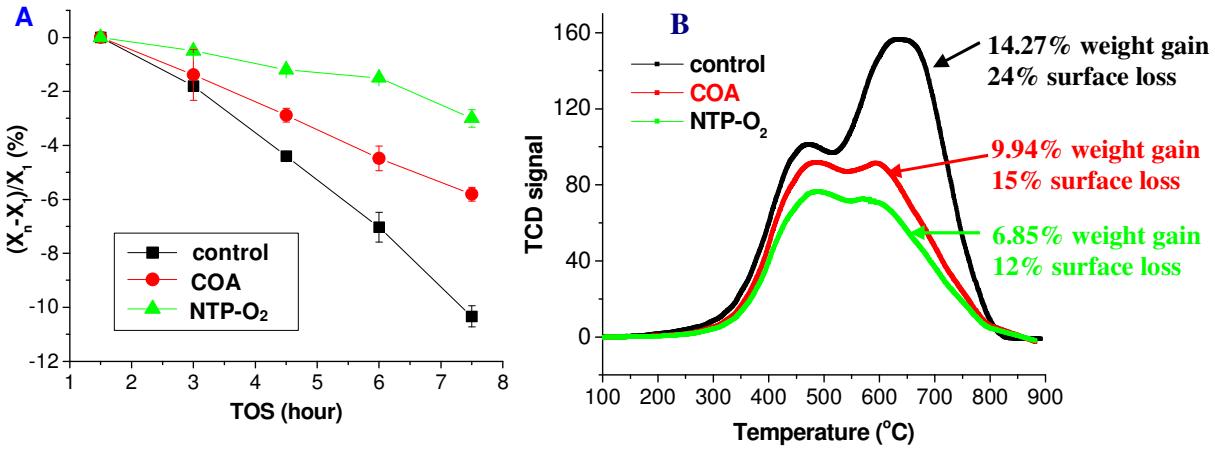

Figure 5-3: The decrease percentage of glycerol conversion (defined as the difference between glycerol conversion at longer TOS (X_n) and glycerol conversion at 1.5 hours (X_1) divided by X_1) as functions of time (A); the TPO profiles of the spent HSiW-Si catalyst after three different reaction conditions (B)

5.3.2 Offline coke removal and catalyst regeneration

The X-ray diffraction results (Figure 5-4) showed no difference between the fresh HSiW-Si and the spent HSiW-Si, which agreed with the previous publications [127, 129, 144] in that the deposited coke was amorphous and would not change the crystalline structure of the catalyst which it deposited on.

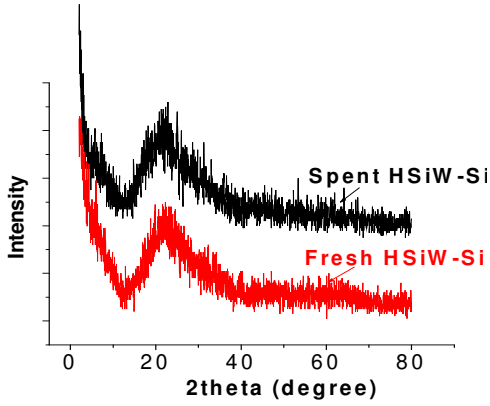

Figure 5-4: XRD patterns of fresh HSiW-Si and spent HSiW-Si

This section presents the results obtained from the study of the catalyst regeneration. Three major effects were investigated, including 1) the NTP field strength, 2) the operation temperature, and 3) the discharge gas. The first two major effects were examined from two perspectives (Section 5.3.2.1): 1) monitoring the decoking process allowed us to understand what was happening in the NTP-O_2 cell based on the TCD signal change during the regeneration treatment period; 2) the TPO characterization of the catalyst after the treatment allowed us to evaluate the effectiveness of coke removal by comparing the profile of coke distribution on the catalyst surface before and after the regeneration treatment. Section 5.3.2.2 presents the regeneration result evaluated based on the kinetic parameters of glycerol dehydration after periodic regeneration; the comparison in the regeneration influence of background gas was conducted in this manner.

5.3.2.1 Direct investigation of coke removal

The effect of NTP field strength

The effect of NTP field strength was first studied by monitoring the decoking process. Here an explanation is given of how the real-time TCD monitoring served the function of examining coke removal from the baseline signal. Figure 5-5 displays the baseline signal obtained using fresh HSiW-Si with different field strengths of non-thermal plasma. The background collected on the fresh catalyst with pure helium showed no baseline shift

regardless of how large of NTP discharge field strength was applied. This observation suggests that the excited helium species were transient and vanished as soon as they left the discharge zone. On the contrary, the background collected on the fresh catalyst with O_2-containg gas showed some signal changes when the NTP was applied. Each background curve of NTP-O_2 displayed the characteristic behavior of an initial overshoot followed by a plateau at an intermediate signal value (i.e., a stabilized baseline). An increasing trend of the stabilized baseline was observed as the field strength of the plasma increased from 3.0 kV/cm to 8.4 kV/cm.

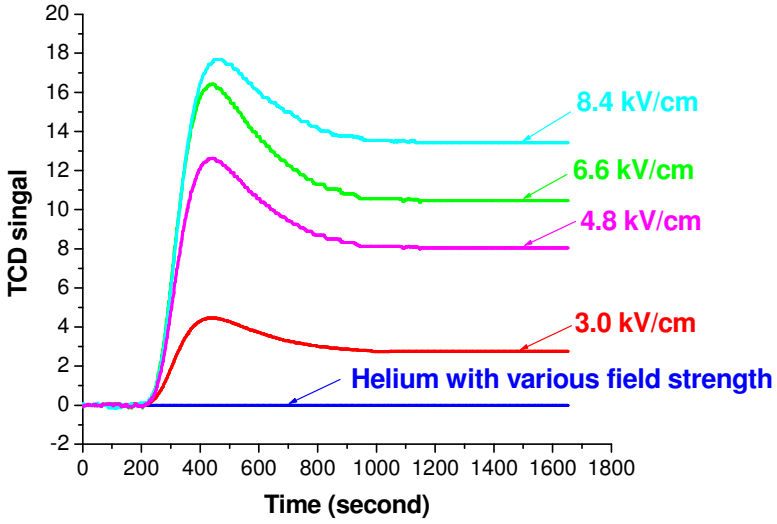

Figure 5-5: The baselines conducted using fresh catalyst under various conditions. 3.0 kV/cm, 4.8 kV/cm, 6.6 kV/cm, and 8.4 kV/cm depict the field strength of NTP-O_2 with the gas composition of 5% O_2 in He.

NTP discharge excited molecular oxygen into new species, such as ozone, O (^{1}D), O (^{3}P) and other surface oxygen species. Except for ozone, all the other strong oxidants were short-lived species. As soon as these short-lived oxygen species left the discharge zone, they recombined to molecular oxygen. O_3 has a lifetime of over a day at room temperature, so it would not convert back to molecular oxygen in the effluent after leaving the discharge zone. Therefore, the gaseous effluent after the discharge cell packed with the fresh catalyst was

composed of O_2, O_3 and He. However, O_3 was condensed, which could be observed as a layer of navy blue liquid condensed in the liquid nitrogen trap, and could not be detected by TCD. Therefore, essentially what TCD could detect was the consumption of oxygen. The initial overshoot was probably caused by the presence of porous materials (HSiW-Si).

Figure 5-6 illustrates the mechanism of the process. Before the NTP application (denoted as t_0), the system inside of the cell was in an equilibrium state of adsorption-desorption of O_2 (denoted as E1). The catalyst bed was already saturated with molecular oxygen, which was marked as ad-O_2 in Figure 5-6. The same amount of molecular oxygen entered and left the cell. When NTP was switched on, the active oxygen species, such as O_3 and atomic oxygen O^*, were generated in the electric field. With the increased concentration of the new oxygen species and decreased concentration of molecular oxygen in the gas phase, the equilibrium E1 was disturbed. The new species O_3 and O^* started to interact with the catalyst surface via physisorption and/or chemisorption. The loss of the plasma species in the adsorption drove the forward reactions from molecular oxygen to these species. As a result, the consumption of oxygen was maximized. As the catalyst gradually became saturated, the consumption of the plasma oxygen species in the adsorption decreased. Therefore, the gas phase reactions between molecular oxygen and the plasma oxygen species were approaching equilibrium, and oxygen consumption decreased to a constant value. At t_2, a new equilibrium in the gas phase was established, as was the equilibrium between the gas-phase and the catalyst surface. An increasing trend of the stabilized baseline was observed as the field strength of the plasma increased from 3.0 kV/cm to 8.4 kV/cm, suggesting that the ozone yield increased with the increase of the NTP field strength.

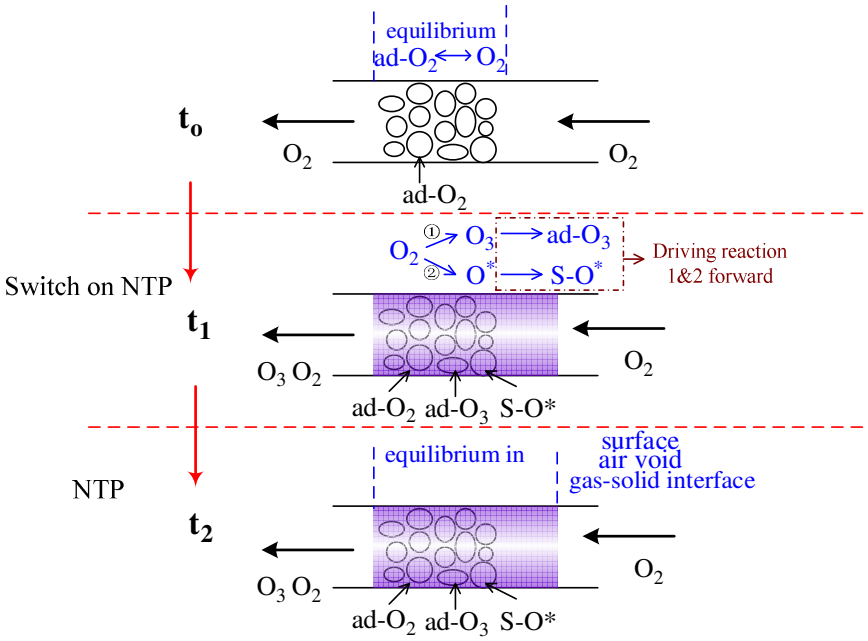

Figure 5-6: Illustration of the transition from "NTP off" to the stabilized "NTP on" status on the NTP treatment cell loaded with fresh catalyst. "ad-" denotes physically-adsorbed species, "S-O*" denotes surface oxygen species, and O* denotes excited oxygen species except for O_3.

For a given condition, the ozone concentration should be a constant. Therefore, after subtracting the raw signal obtained during the NTP-O_2 treatment of the spent HSiW-Si from the baseline, which was at least 8-fold smaller than the raw signal, any signal change would be caused by the ongoing reaction with the surface carbonaceous species. Figure 5-8 exhibits the result of monitoring the decoking process under the various discharge field strengths after the subtraction of the corresponding stabilized baseline. There was an equilibrium among the distribution of molecular oxygen, which could be detected by TCD, and other O species generated by NTP. When the reactive O species (oxygen is inert to coke at room temperature) reacted with some surface carbonaceous species, the consumption of these species drove forward the reactions of O_2 to the active species, such as ozone and O radical, causing the consumption of O_2. Upon each plasma application, the signal jumped to the maximum; at that moment, the active oxygen species reacted with all the surface carbonaceous species that could possibly be reacted at various rates determined by the hardness of the carbonaceous species with which they were reacting. Consequently, the O_2 consumption was maximized. Coke was the limiting reactant while oxidative species formed in NTP-O_2 were in excess. As the portion of softer coke was consumed, the reaction became more difficult, and the

oxidation rate became increasingly slow. In other words, the consumption of the active oxygen species, and ultimately O_2, decreased, as reflected in the TCD profile as the signal not only decreased, but also decreased at a slower rate.

Therefore, Figure 5-7 implies that the effectiveness of coke removal increased with increasing NTP field strength; the effectiveness was ascending in the order of 3.0 kV/cm < 4.8 kV/cm < 6.6 kV/cm < 8.4 kV/cm. In particular, at the field strength of 3.0 kV/cm, there was barely any coke removal. From 3.0 kV/cm to 4.8 kV/cm, there was a drastic change in coke removal. From 4.8 kV/cm to 6.6 kV/cm, there was also a significant change in coke removal, but not as much as the difference between 3.0kV/cm and 4.8kV/cm. The increase in coke removal continuously became smaller when the applied field strength increased from 4.8 kV/cm to 6.6 kV/cm and from 6.6 kV/cm to 8.4 kV/cm. Coke removal increased with increasing NTP field strength, however, the increment in coke removal was reduced as NTP field strength increased further. The power calculated via a Lissajous figure using Equation 2-3 was 0.05 W, 0.43 W, 0.84 W, and 1.27 W corresponding to 3.0 kV/cm, 4.8 kV/cm, 6.6 kV/cm and 8.4 kV/cm, respectively (Appendix VI).

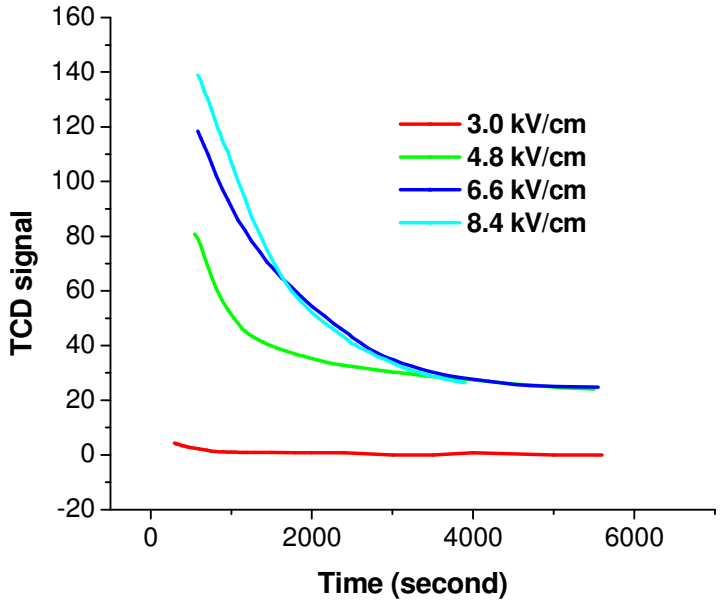

Figure 5-7: Monitoring the decoking process under various NTP field strengths at room temperature. (The signal rising part was omitted for more straightforward presentation). 3.0 kV/cm, 4.8 kV/cm, 6.6 kV/cm, and 8.4 kV/cm depict the field strength of NTP-O_2 with the gas composition of 5% (volumetric ratio) oxygen in helium.

Figure 5-8 presents the TPO characterization result of the spent catalyst without treatment, and after 1.5 hours of NTP-O_2 treatment with different NTP field strengths. The result agrees well with the real-time monitoring. No significant change in the TPO profile was observed between the untreated spent catalyst and the spent catalyst after 1.5 hours treatment by NTP-O_2 at the field strength of 3.0 kV/cm NTP. For the rest of the investigated field strengths, the TPO curves showed a decreasing trend as compared to the spent catalyst treated at a higher field-strength NTP. Although the reduction of signal intensity was more significant in the softer coke region (1st peak zone), the reduction was also observed in the harder coke region (2nd peak zone).

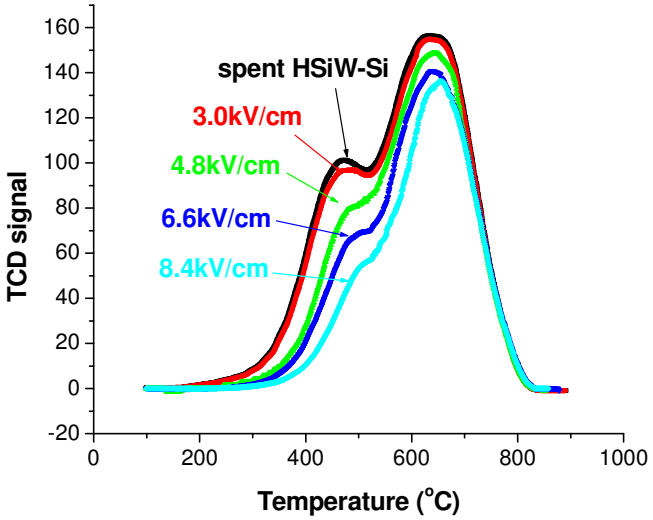

Figure 5-8: TPO characterization of the spent catalyst without NTP-O_2 treatment and that after regeneration with NTP-O_2 at different field strengths

Both evaluation approaches (monitoring the decoking process and TPO characterization of the coke profile) showed that the coke removal was more effective at higher field-strength NTP applications. The field strength of 8.4 kV/cm, under which the maximum coke removal was observed, was employed for the following tests.

The effect of operation temperature

The determined optimal field strength (8.4 kV/cm) from the previous subsection for coke removal at room temperature was used to study the temperature influence in O_2-NTP coke removal. Figure 5-9 depicts the results of monitoring the decoking process. The stabilized baseline (Figure 5-9 B) of NTP operation decreased in the order 25°C> 100°C > 150°C > 200°C, and the stabilized baseline at 200°C was nearly zero. The relative positions of the stabilized baselines at different operation temperatures suggests that ozone concentration decreased as the operation temperature increased. In other words, ozone decomposed faster at higher temperatures; nearly no O_3 existed at 200°C. Figure 5-9 A displays the signal profile during NTP-O_2 treatment at different temperatures. The signal magnitude was descending in the order of 150°C > 100°C > 200°C> 25°C, suggesting that the effectiveness of the coke removal descended in such an order. Therefore, the order of coke removal effectiveness does not quite obey the sequence of the ozone concentration as suggested by the relative levels of the stabilized baselines. This inconsistency suggests that the ozone concentration was not the only factor that determined the coke removal effectiveness.

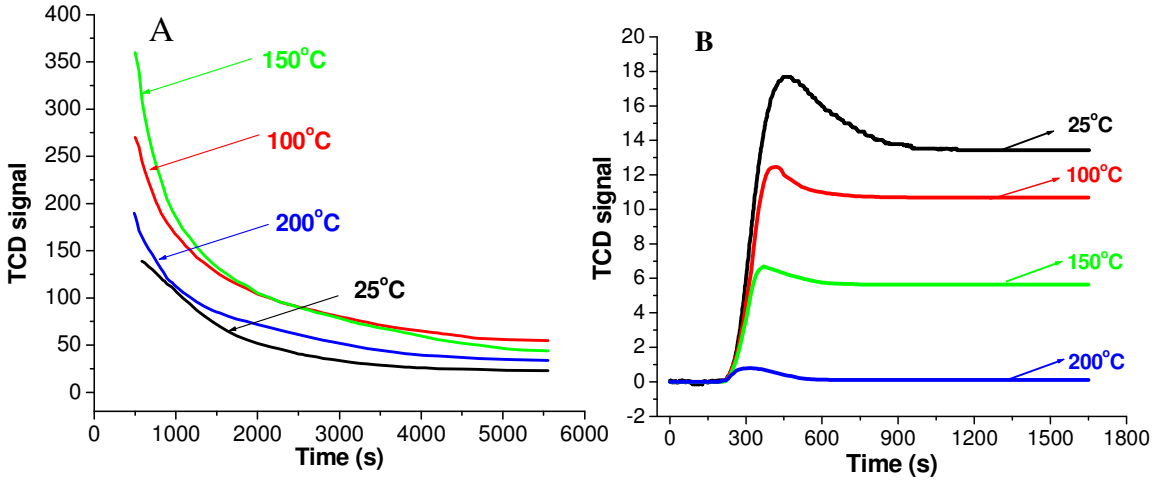

Figure 5-9: Monitoring the decoking process with 8.4 kV/cm NTP-O_2 at various temperatures (A)(the signal rising part was omitted for more straightforward presentation); the baseline profiles collected using fresh catalyst (B). The gas composition was 5% (volumetric ratio) oxygen in helium.

A consistent trend was exhibited by TPO characterization of the spent HSiW-Si after the 8.4 kV/cm NTP treatment at different temperatures, as shown in Figure 5-10. Coke was greatly reduced after the NTP-O_2 treatment at 100°C, and more so at 150°C. However, the trend reversed as the temperature further increased to 200°C, and more coke, especially hard coke, remained on the catalyst compared to those being treated at 100°C and 150°C, respectively. Also, the results confirmed that the reactive oxygen species formed under NTP discharge were able to react with hard coke, especially when the NTP regeneration was operated under a proper temperature. The peak in hard coke region (around 700°C) was decreasing from the catalyst after the treatment at 25°C to the one at 100°C and to the one at 150°C, indicating more "hard" coke was removed or deconstructed. Among the temperatures investigated, the most effective coke removal occurs at 150°C.

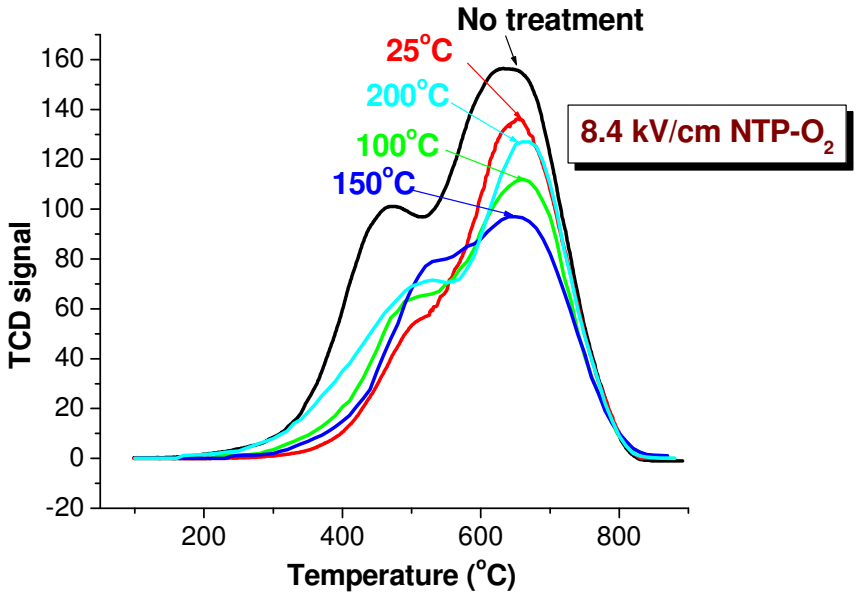

Figure 5-10: TPO characterization of the spent catalyst and that after regeneration with NTP-O_2 of 8.4 kV/cm at different temperature conditions after 1.5 hours

Both evaluation approaches (monitoring the decoking process and TPO characterization of the coke profile) consistently showed that operating the NTP-O_2

regeneration at 150°C provided more effective coke removal than any other temperatures investigated.

Time dependence of coke removal

Figure 5-11 shows the time dependence of the coke removal under the regeneration condition of 8.4 kV/cm NTP discharge at 150° C. The carbon-deposit percentage was defined as the weight difference between the fresh catalyst and the coked catalyst divided by the weight of fresh catalyst. Although the strong oxidizing species could react with the hard coke, the reaction rate is very likely to be much smaller in comparison to the oxidants reacting with the soft coke. Therefore, the decrease of the catalyst weight was greatly dependent on the reacting process of the soft coke. The consumption rate of the soft coke was much higher than the formation rate of soft coke converted from hard coke. Therefore, as the treatment proceeded, one reactant in the oxidation reaction (the amount of soft coke) decreased, resulting in a reduction of the reaction rate. This is one reason that the weight decrease in Figure 5-11 became slower at the longer treatment time. Also, the diffusion of the strong oxidant into the pores was an issue as previously discussed, so when the more exposed surface coke was consumed, the process would become more difficult. The residual coke, after partial NTP-O_2 decoking, contains oxidized components that can continue to be oxidized in a step-by-step fashion until complete removal (every carbon in the original coke was converted into CO_2 effluent). Although NTP-O_2 could react with both soft and hard coke simultaneously, it is possible that large differences existed between the reaction rate of NTP-O_2 oxidizing soft coke and that of NTP-O_2 oxidizing hard coke. When the very "soft" coke was oxidized, CO_2 was formed and flushed off the surface, directly resulting in the weight decrease of the spent catalyst. In contrast, for oxidation of hard coke, the reaction rate was very slow, and the oxidation of hard coke started from converting it to an oxygen-rich intermediate, or breaking it down into a smaller structure. In other words, oxidizing hard coke most likely did not generate CO_2, leaving the total mass barely changed. These reasons conceivably explain why the coke removal rate slowed with time even though NTP-O_2 could react with hard coke. The coke removal rate decreased with regeneration time.

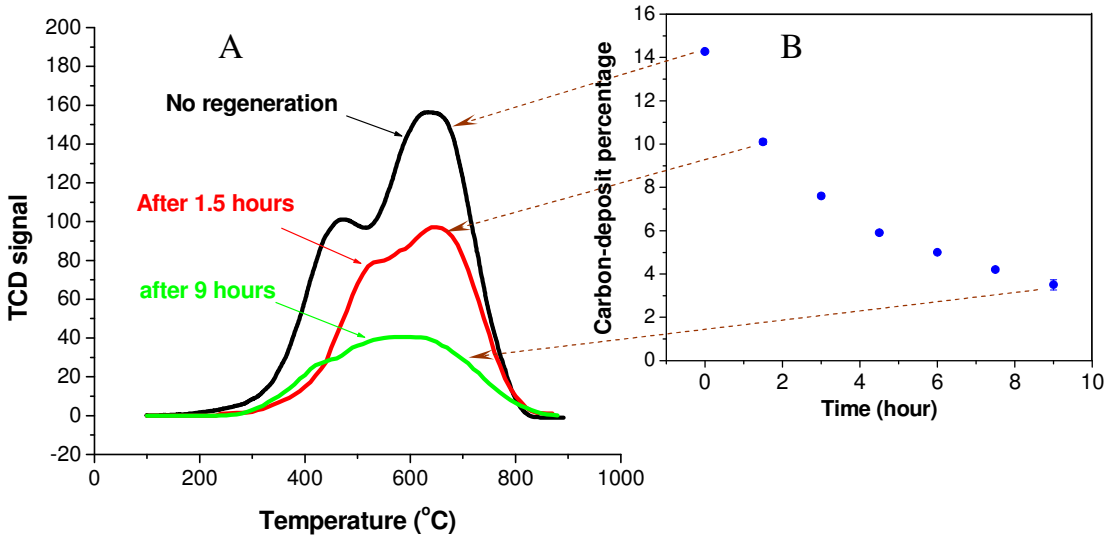

Figure 5-11: TPO characterization of the spent catalyst after regeneration at 150°C using 8.4 kV/cm NTP-O_2 for different regeneration time periods (A); carbon-deposit percentage as a function of time (B)

5.3.2.2 Direct evaluation of catalyst regeneration

The effect of discharge gas

The NTP-O_2 effect in coke removal has already been discussed in Section 5.3.2.1. Coke removal usually resulted in catalyst regeneration, but not always: for example, if some catalyst active sites were damaged during coke removal, catalytic performance would not be regained. The NTP-O_2 effect in catalyst regeneration was directly tested via periodic online regeneration. The results of periodic regeneration using 20% oxygen blended with argon, 20% oxygen blended with nitrogen, and pure oxygen are presented in Figure 5-12 A, B, and C, respectively. As a comparison, a control test is presented in Figure 5-12 D, for which there was no NTP application during the 2 hours of flushing the reactor with 20% O_2 in argon. NTP application regenerated the catalyst, showing as the rebound of the glycerol conversion after each session of the regeneration. The NTP with 20% O_2 in argon showed the better effectiveness in regeneration than NTP-O_2 under the nitrogen and pure oxygen atmospheres. The effectiveness of coke removal by NTP-O_2 in different discharge gases was descending in the order of NTP-O_2 in argon > NTP-O_2 in O_2 > NTP-O_2 in N_2. From the results shown

earlier (Figure 5-11), it is already known that 2 hour NTP treatment could not completely remove surface coke. The results here show that the catalytic activity could be regained even with only partial regeneration. However, because of the fact that coke was not thoroughly removed, the catalyst after partial regeneration may be prone to deactivate somewhat faster. This explains why overall a slightly decreasing trend in glycerol conversion was observed after each regeneration in the figures. Nevertheless, the purpose of this experiment (to examine the influence of the discharge gas on the regeneration) was achieved.

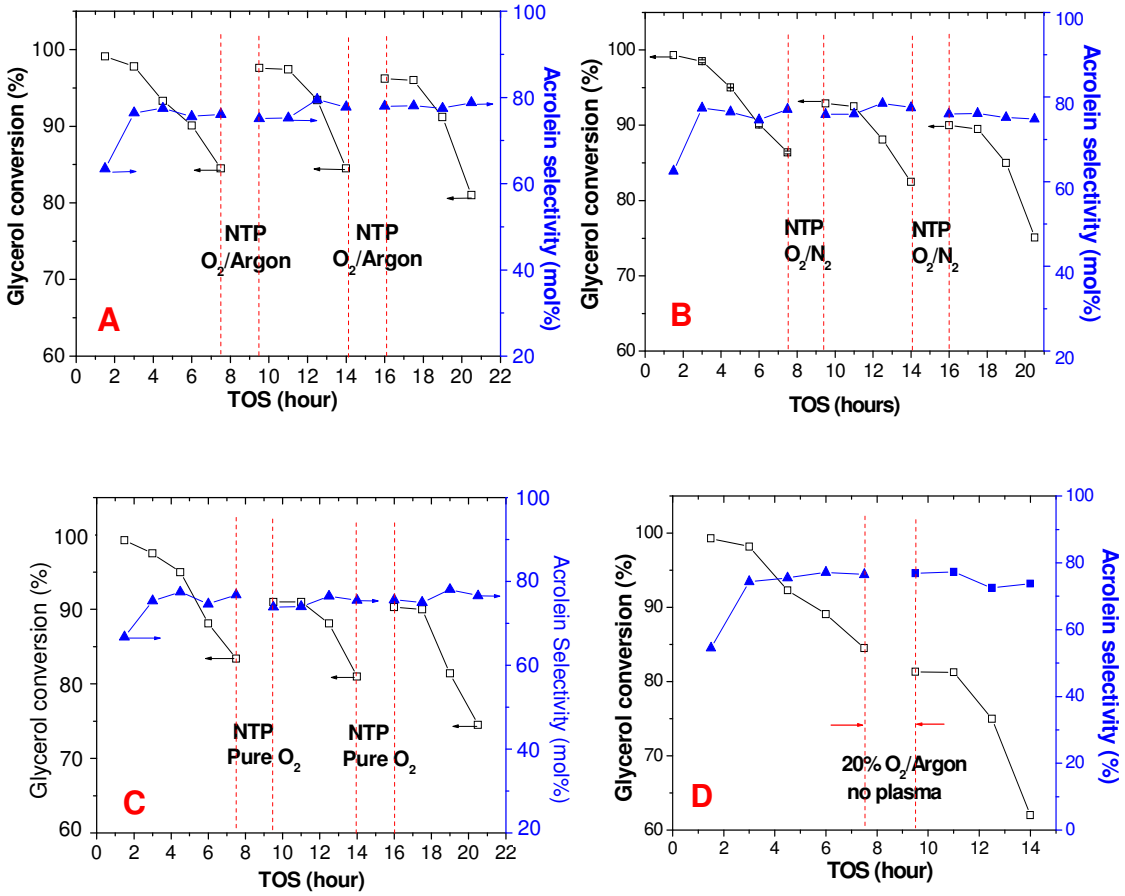

Figure 5-12: Periodic regeneration using non-thermal plasma (8.4 kV/cm) using (A) 20% O_2 in argon, (B) 20% O_2 in nitrogen, and (C) pure oxygen; and (D) no plasma application with 20% O_2 in argon flushing for 2 hour. Each data point was the average of two repetitive measurements of a sample from a kinetic run. Dehydration condition: reaction temperature: 275°C, gas-hourly-space-velocity: 84.4 h^{-1}, carrier gas argon flow rate: 60 mL/min

Better regeneration can always be achieved by extending the treatment time. A more detailed investigation with economic analyses can be conducted in a scale-up practice to find the most cost-efficient schedule, since the coke removal became slower and required longer

treatment time, which would lead to more energy consumption, slower productivity, and less profit.

5.3.3 Combining online coking suppression and offline catalyst regeneration (coke removal)

Usually, if the coke formed on the catalyst surface is less hard, its removal is less difficult and the regeneration is more effective. As is shown earlier, using oxygen-containing carrier gas in the reaction shifted the coke distribution to the "soft coke" region, which might facilitate the NTP regeneration process. Figure 5-13 shows the TPO profile of the spent catalyst from an NTP-O_2 kinetic run before and after 1.5-hour treatment (5%O_2 in He, 8.4 kV, 150^o C); the spent catalyst from the control kinetic run was listed as a reference. The weight reduction of the surface carbonaceous species by NTP treatment on the spent catalyst from the NTP-O_2 run was 46.8% (obtained by (6.85%-3.64%)/6.85%), which was significantly larger than the reduction by the same NTP treatment on the spent catalyst from a control run (29.2%, calculated by (14.27%-10.1%)/14.27%, refer to Figure 5.12). This showed that effectiveness of coke removal by NTP-O_2 treatment greatly depended on the characteristics of the coke that deposited on the catalyst surface.

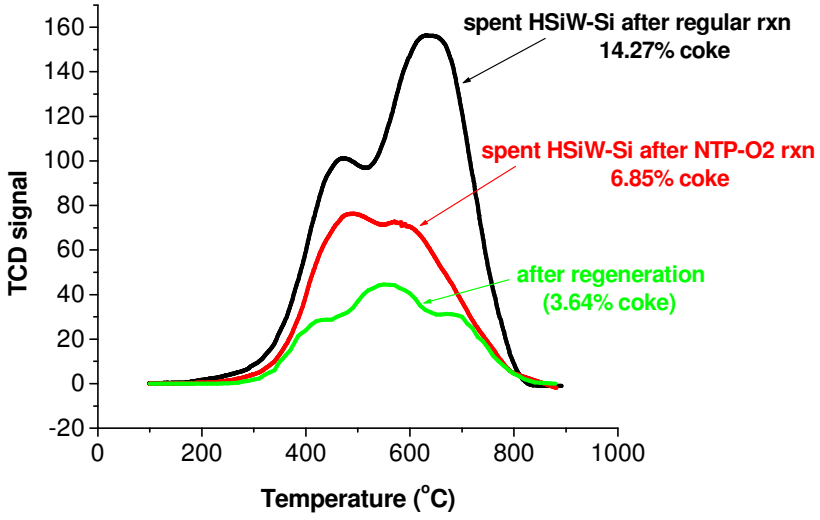

Figure 5-13: TPO profiles of the spent catalyst (coked in a NTP-O_2 applied glycerol dehydration reaction) before and after NTP-O_2 off-line treatment, in comparison to TPO of the spent catalyst from control condition

Figure 5-14 displays the periodic regeneration using 20% oxygen in argon applied to the kinetic reaction under the NTP-O_2 condition. Compared with Figure 5-12 A (the more deactivated process), the catalytic activity could be fully regained after periodic regeneration. The result showed that the characteristic of coke formed on the catalyst significantly affected the regeneration effectiveness.

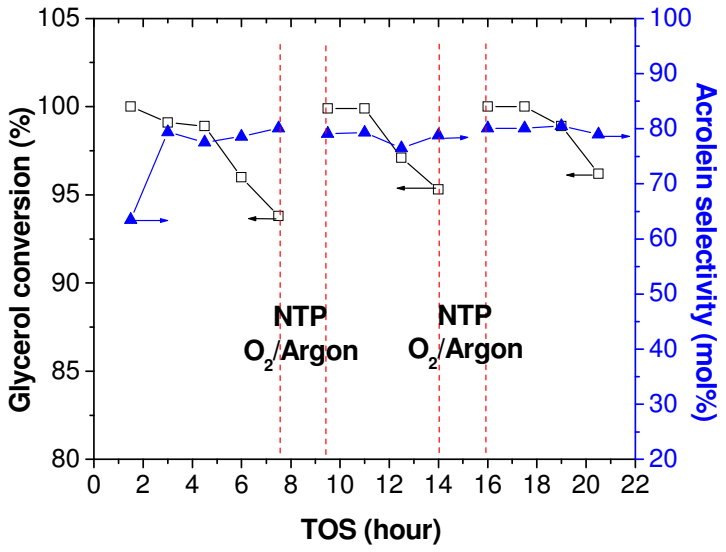

Figure 5-14: Periodic regeneration using 8.4 kV/cm NTP-O_2 in argon (2 hours). Dehydration condition: reaction temperature, 275°C; gas-hourly-space-velocity, 84.4 h^{-1}; carrier gas, 5% O_2 in argon; argon flow rate, 60 mL/min; field strength, 4.58 kV/cm.

5.4 Discussion

5.4.1 Online coking suppression

The presence of oxidant(s) kept the products or intermediates in their oxidized state, which inhibited the hydrogen abstraction and thus suppressed coke formation. However, the oxidant oxidized some products (including acrolein) as well. Propionaldehyde could be oxidized into propionic acid, and also could undergo deeper oxidation to CO_2 and/or CO (CO_x). Also, the oxidant prevented the hydrogenation reaction from occurring, and thus suppressed propionaldehyde formation from acrolein (as shown in Figure 4-13) [144]; hence propionaldehyde was significantly reduced in selectivity. The existence of the oxidants (molecular O_2 in the case of COA; molecular O_2, excited O_2*, O and possibly OH radicals in

the case of NTP-O_2) kept the substances in the system at the oxidation state, preventing coking [144]. Coke could be formed via condensation/oligomerization of the reactant glycerol; therefore, suppression of this part of coke formation resulted in more reactant available for acrolein formation. Coke could also be formed via the condensation/addition of acrolein; and the suppression of this part of coke formation resulted in that more acrolein could be collected as product. The coke suppression was another benefit provided by the conditions of COA and NTP-O_2.

However, the presence of the oxidant could impose a negative effect in acrolein production by oxidizing acrolein into acrylic acid and CO_x. Usually, it is easier to oxidize aldehyde than ketone, which would imply that acrolein is more prone to oxidation than acetol. Therefore, it was not surprising that there was a relatively larger loss for acrolein selectivity than acetol selectivity under COA condition compared to the control condition. However, the result did not quite follow this rule in NTP-O_2 condition. A couple of factors might have contributed to this result.

Previous studies proved that Brønsted acid sites favor acrolein production, while Lewis acid sites favor acetol formation [136]. HSiW has pure Brønsted acid sites, and most, if not all, Lewis acid sites are located on the support. The exposed $^{+}SiO_3$, a type of "structure defect", acts as a Lewis acid site (Figure 5-15). Oxygen is electronegative, so it is very likely to attach to the Si^{4+}, reducing the number of Lewis acid sites. Since the acetol formation is more sensitive to the reduction of Lewis acid sites than is the acrolein formation, the oxygen addition "selectively" lowered acetol formation. Under the NTP condition, some oxygen was present in the form of O atom via the electron dissociation, which is more readily accessible to the defect due to the steric effect. As the result, the presence of O_2, especially NTP-O_2, during the reaction affected the selectivity of acetol more than that of acrolein. Therefore, acetol selectivity decreased in the sequence of NTP-O_2 > COA > control. Then these defect sites could be further converted to surface hydroxyl group, which acted as weak Brønsted acids, in favor of acrolein formation. Acetol formation was partially suppressed by oxygen occupation of the Lewis acid sites, which left a larger proportion of glycerol taking the path to form acrolein, since the presence of oxygen would not lower, if not increase, the Brønsted acid sites. This could be one benefit to acrolein selectivity.

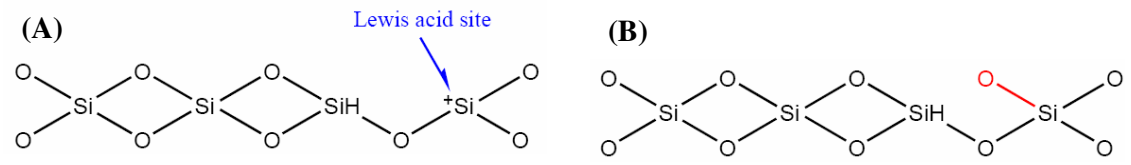

Figure 5-15: The structure of silica with the "defect site" (A); elimination of the Lewis acid site by oxygen occupation (B).

As discussed in the previous chapter, the presence of NTP discharge would induce the formation of hydronium ions under high humidity, which provided some additional Brønsted acidity to the system, favoring acrolein production. This so-called "non-resonant charge exchange" initiated by the formation of a significant amount of positively charged argon ions, Ar^+, via the efficient electron collision mechanism (Equation 5-1), and the subsequent ionization process of argon could induce the formation of water ions, $H_2O.^+$ (Equation 5-2). Water ions then passed the charge to neutral water molecules, and the hydronium ions were thus formed (Equation 5-3). The charged water molecule (even if present in only a small amount) could initiate the protonation of some glycerol molecules even prior to its contact with the acid sites of the catalyst. It would render an accumulative enhancement to the acrolein formation.

$$Ar + e^- \rightarrow Ar.^+ + 2\,e^- \qquad \textbf{Equation 5-1}$$

$$Ar.^+ + H_2O \rightarrow H_2O.^+ + Ar \qquad \textbf{Equation 5-2}$$

$$H_2O.^+ + H_2O \rightarrow H_3O^+ + .OH \qquad \textbf{Equation 5-3}$$

These factors offset the acrolein loss due to oxidation in the NTP-O_2 condition, and testify to the fact that NTP-O_2 did not cause a significant change in acrolein selectivity compared to the control condition, while COA caused a significant loss of selectivity to acrolein.

5.4.2 Offline coke removal/catalyst regeneration

Regarding the issue that partial coke removal could already restore catalytic activity to a large degree, the "indirect deactivation mechanism" [262] was probably the predominant

mechanism causing the deactivation of the HSiW-Si catalyst during the glycerol dehydration process. Figure 5-16 illustrates this "indirect deactivation mechanism". Silica had relatively small pores (average ~11 nm). Some coke formed near the mouth of the pore, narrowing or blocking the entrance of the pores, wherein lots of active sites were located (Figure 5-16C). All of these active sites became inaccessible if the pore entrance was blocked. Similarly, once these "entrance blockers" were removed or partially removed, a significant amount of active sites became accessible again for the reactant to contact with. Therefore, even partial coke removal greatly brought back the catalytic activity.

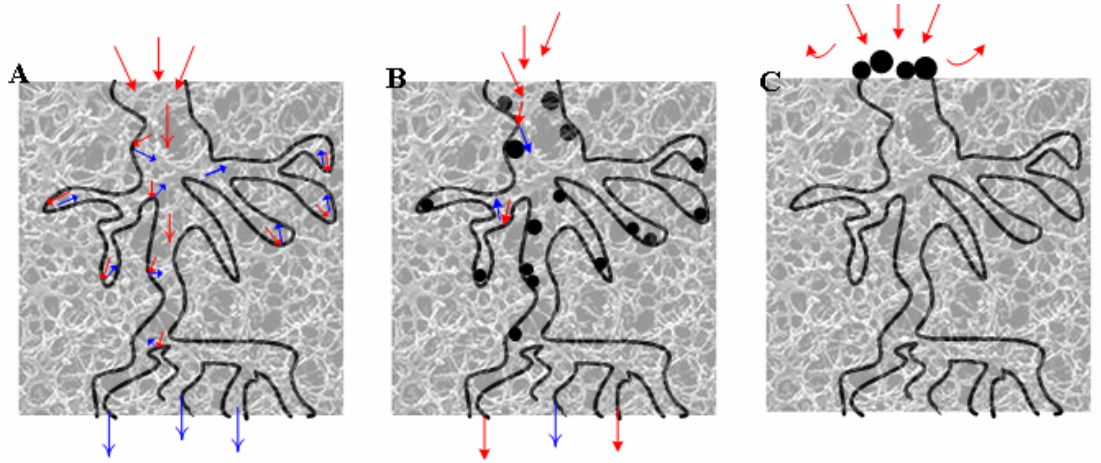

Figure 5-16: The illustration of the catalyst pores (A) fresh catalyst; (B) coke relatively even-distributed on the active site, and glycerol molecules only could not reach the active site covered by coke (direct deactivation); (C) coke deposit on the mouth of the main pore entrance, and glycerol molecules could not reach the active sites that were still "available" (indirect deactivation). Red arrows denote the path of glycerol, blue arrows denote the path of product (acrolein), and the black dots denote the coke particles

There is no doubt that NTP-O_2 produced some strong oxidizing agents, since otherwise there would be no coke removal under low temperature conditions. The situation of *in-situ* NTP-O_2 with the presence of the catalyst is very complex, and to my best knowledge, such a situation has barely been discussed in the past. In the NTP-O_2 plasma system, the possibly existing oxygen species include ozone (O_3), O_2 molecules in the ground state ($O_2(X^3\Sigma^-)$), O_2 molecules in the excited state ($O_2(a^1\square^-)$ and $O_2(b^1\Sigma_g^+)$, atomic oxygen in the ground state ($O(^3P)$), the atomic oxygen in the excited state ($O(^1D)$), and oxygen ions (O_2^+, O^+, and O^-). Among them, the most effective oxidants are ozone and atomic oxygen. Since non-thermal plasma is an electron-driven process [166], atomic oxygen is most likely to be firstly generated via dissociation in the Schumann-Runge band (Equation 5-4) and in the Herzberg

band (Equation 5-5) [276]. Herzberg-band dissociation has a higher efficiency than Schumann-Runge-band dissociation [276], because the ground-state oxygen atom $O(^3P)$ is relatively more stable than the excited-state oxygen atom $O(^1D)$, and also because $O(^1D)$ could be easily quenched into $O(^3P)$ (Equation 5-6); $O(^3P)$ was possibly the most predominant atomic oxidant [277, 278].

$$O_2 + e \rightarrow O(^3P) + O(^1D) \quad k_1=5.0*10^{-8}\exp(-8.4/T_e) \quad [277] \qquad \textbf{Equation 5-4}$$

where T_e is electron temperature, and k is the reaction rate constant.

$$O_2 + e \rightarrow O(^3P) + O(^3P) \quad k_2=4.23*10^{-9}\exp(-5.56/T_e) \quad [277] \qquad \textbf{Equation 5-5}$$

$$O(^1D) + M \rightarrow O(^3P) + M \quad [278] \qquad \textbf{Equation 5-6}$$

where M is any other types of molecule, T_e is electron temperature, and k is the reaction rate constant.

It was proved that atomic oxygen could rapidly react with carbonaceous species [279-281]. Some researchers claimed that the atomic oxygen was a stronger oxidant than ozone, and could provide a faster rate when reacting with carbonaceous species [282] [272, 276, 283]. Some plausible overall reactions are listed in the following equations 5-7 through 5-9 [283]. The very detailed mechanism was not quite clear; however, it was generally thought that the O attacked the carbonaceous compound preferentially via the delocalized π bonds.

$$C_xH_yO_z + O + e \rightarrow C_{x-1}H_yO_z + CO + e \qquad \textbf{Equation 5-7}$$

$$C_xH_yO_z + O + e \rightarrow C_{x-1}H_{y-1}O_z + H + CO + e \qquad \textbf{Equation 5-8}$$

$$CO + O + e \rightarrow CO_2 + e \qquad \textbf{Equation 5-9}$$

Ozone is another effective strong oxidant that has been previously reported as being reactive with carbonaceous species [176, 269, 270, 282, 284]. Ozone is generated via three-body collisions (Equation 5-10), involving the molecular oxygen, the ground-state atomic oxygen, and another gas molecule M; ozone is decomposed via Equation 5-11. Both processes consume some atomic oxygen. The general process of ozone reacting with carbonaceous species is summarized in Equation 5-12 [282].

$O_2 + O(^3P) + M \rightarrow O_3 + M \qquad k_3 = 8.6*10^{-31}T^{-1.25}$ [277] **Equation 5-10**

$O_3 + O(^3P) \rightarrow 2\,O_2 \qquad k_2 = 9.5*10^{-12}\exp(-2300/T)$ [277] **Equation 5-11**

where T is the overall gas temperature

$C_n \xrightarrow{O_3}$ **Functional groups (-COOH, -C-OH, -C=O)** $\longrightarrow \cdots \longrightarrow CO_2$ **Equation 5-12**

Figure 5-17 more specifically illustrates the plausible ways that ozone molecule attacked the surface coke species, and initiated the breakdown of the surface coke [269, 270, 282]. For example, if a C-C double bond was located on the end of an aliphatic carbon chain, the ozone addition could directly reduce the number of carbons and release a mole of CO_2. If the C-C double bond was located within an aromatic carbonaceous compound, then the ozone insertion opened up the ring structure, significantly lowering its stability and thus lowering the activation energy for further oxidization and increasing the reactivity. The process could have continued via a step-by-step fashion, breaking the larger molecule into smaller molecules, and eventually converted all to CO_x, which could be pumped out of the system.

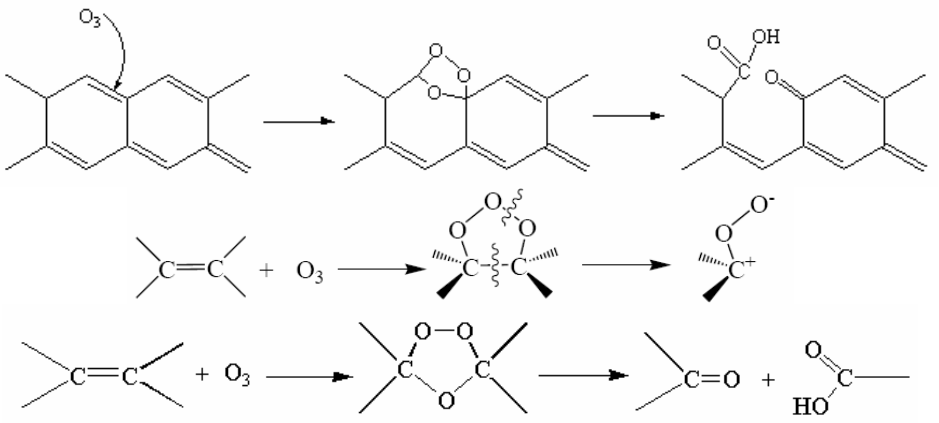

Figure 5-17: Possible mechanisms of ozone reaction with the functional groups of coke [269, 270, 282]

Some of the oxidizing species could also chemically bind to the catalyst surface, existing as surface oxidizing species. The active surface species are assigned to three categories: surface atomic oxygen (denoted as O-S), adsorbed excited oxygen (O_2^*-S) and adsorbed ozone (O_3-S) (Equation 5-13 to Equation 5-15). It is possible that the reaction with the carbonaceous species proceeded via two different pathways: first, the active O species in

the gas phase directly attacked the surface coke, which would be O_3, O or O* directly interacting with coke; second, the reactive surface O species (O-S, O_2^*-S, and O_3-S) were migrating on the surface and were reacting with the neighboring coke. Due to the complexity, these processes are not shown in details here.

$$O_3 + S \rightarrow O_3\text{-}S \qquad \textbf{Equation 5-13}$$

$$O_2(^1\Delta P) + S \rightarrow O_2(^1\Delta P)\text{-}S \ \ (O_2^*\text{-}S) \qquad \textbf{Equation 5-14}$$

$$O(^3P) + S \rightarrow O(^3P)\text{-}S \ \ \text{or} \ \ O(^1D) + S \rightarrow O(^1D)\text{-}S \qquad \textbf{Equation 5-15}$$

Effect of NTP field strength (further discussion of Figure 5-7 and Figure 5-8)*:* As the field strength increased, the electron became more energetic and a larger amount of energized electrons were generated in the system. The dissociation of the molecular oxygen was facilitated as the result, and more atomic oxygen was formed. Ozone was generated via the three-body-collision and atomic oxygen was the limiting substrate. Therefore, if all other parameters remained the same, the ozone concentration was most likely to increase as the field strength increased [285]. Under the application of a more intense plasma field, more reactive oxygen species were generated, and more energy was available in the system that could be efficiently transferred to the oxidation processes. As the result, coke removal effectiveness increased along with the field strength as was observed in the experiments. However, there were also the decomposition/recombination reactions that converted the reactive oxygen species to inert O_2, as shown in Equation 5-16 and Equation 5-17. As a result, the density (or concentration) of ozone and oxygen atoms would not monotonously increase as the plasma field strength increased, and it was more likely to be an asymptotic function of field strength increasing toward a saturation point. This statement agrees with a previous finding made by Sung *et al.* that a study of the ozone concentration in an atmosphere of oxygen increased with the increase of the discharge power, approaching a saturated point (equilibrium) of the concentration of these oxygen species [286]. This explained the result that the increasing increment of the removal effectiveness deceased as the NTP field strength increased.

$$O_3 + O\ (^3P) \rightarrow 2\ O_2 \qquad \textbf{Equation 5-16}$$

$O\ (^3P) + O\ (^3P)\ (+ M) \rightarrow O_2 + e\ (+ M)$ **Equation 5-17**

Effect of Operation temperature (further discussion of Figure 5-9 and Figure 5-10)***:*** The result showed that operating the NTP-O_2 regeneration at 150°C provided more effective coke removal than any other temperatures investigated. The most important oxidizing species were ozone and atomic oxygen, and maybe some .OH. The kinetic equations of ozone shows that low temperature favors ozone formation (Equation 5-10), while high temperature favors ozone decomposition (Equation 5-11); both processes consume some atomic oxygen. At higher temperatures, less ozone is formed; since the ozone concentration is eliminated in the first place, there is a limited amount of atomic oxygen that would be consequently consumed according to Equation 5.11. Although few ozone molecules could exist under temperature conditions above 200^o C (as shown in Figure 5-9 B), atomization of oxygen molecules is not an issue under 300^o C [287]. Some people believed that atomic oxygen was an even stronger oxidizing species than ozone [272, 273, 276, 283]. Atomic oxygen is a short-lived species, and it is possibly unable to diffuse deeply into a pore within its lifetime. Higher temperature increased the kinetic velocity of atomic oxygen, facilitating deeper penetration into the catalyst and increasing the collision probability with more carbonaceous molecules [283]. Consequently, the reaction of atomic oxygen with coke was enhanced in this sense. However, when the oxygen atoms moved faster under elevated temperatures, the odds of their collision with another oxygen atom increased, increasing the possibility of recombination to inert molecular oxygen (Equation 5-18). As the temperature increased, the rate of oxidation with carbonaceous species by atomic oxygen and/or ozone significantly increased. All these factors interacting/counteracting with each other resulted in the optimal operation occurring at a mildly elevated temperature, and in the study, coke removal at 150^oC showed the most effectiveness than other investigated temperatures.

$O\ (^3P) + O\ (^3P) \rightarrow O_2$ **Equation 5-18**

Time dependence (further discussion of Figure 5-11): The residual coke, after partial NTP-O_2 decoking, contains oxidized components that can continue to be oxidized in a step-

by-step fashion until every carbon in the original coke is converted into CO_x, or total elimination. Although NTP-O_2 could react with both soft and hard coke simultaneously, it is most likely that large differences between the reaction rate of NTP-O_2 oxidizing soft coke and that of NTP-O_2 oxidizing hard coke were very likely to exist. When the very "soft" coke was oxidized, CO_2 was formed and flushed off the surface, directly resulting in the weight decrease of the spent catalyst. On the contrary, in the case of oxidation of hard coke, the reaction rate could be very slow, and the oxidation of hard coke possibly started from converting it to an oxygen-rich intermediate, or breaking it down into a smaller structure. Oxidizing hard coke would not necessarily generate CO_2, so the total mass would be barely changed. It is rather difficult for the short-lived species ($O(^3P)$, $O(^1D)$ and OH) generated in the gas-phase and/or catalyst surface to diffuse deeply into the catalyst pore due to their short lifetimes. Ozone would have easily diffused into the pores within its relatively long lifetime [288]; however, ozone is much larger in molecular size than atomic oxygen, and its steric hindrance is therefore larger than that of atomic oxygen. Therefore, ozone would not diffuse into pores as easily as atomic oxygen considering the steric effect [270]. As the result, the diffusion of the highly reactive oxidant into the porous catalyst might be another important issue limiting the rate of further coke removal, slowing down the removal as the coke on the top of the surface was consumed. These reasons conceivably explain why the coke removal rate slowed down with time, even though NTP-O_2 could react with hard coke. The coke removal rate decreased with regeneration time. These reactions would continue as long as the basic graphitic structure and the C-C double bond still existed [271], although the reaction rate varied.

Effect of discharge gas (further discussion of Figure 5-12): The plausible reactions under NTP with different background gases are listed in Table 5-3. The metastable states of argon (Ar), formed from Ar radical, Ar*, via radioactive decays, had very small transition probability for further decays, and instead, they were more likely to transfer energy to oxygen molecules via collisions, generating O atoms and thus ozone. Also, the presence of the large number of Ar atoms created an inhibiting "wall" between oxygen atoms, and oxygen atoms and ozone, prevented these active oxygen species from recombining into inert oxygen. As the

result of these two factors, the density of O and ozone in the presence of the background gas argon might be higher than the density of oxidizing species in pure O_2. In this sense, the background N_2 could have served the same "wall-effect" function. However, N_2 and the N species could react with the active oxygen species, forming NO_x, most of which do not have oxidative capability. These reactions competitively consumed part of the highly reactive oxygen species, resulting in a decrease in the regeneration effectiveness. In general, a noble gas, such as argon, can be ionized most easily. Therefore, at a given field strength, the electron energy and the number of electrons were significantly higher in the argon-mixture system than the two other systems [289, 290]. Forming atomic nitrogen costs a large amount of energy [166], and the dissociation of nitrogen competitively consumed a certain amount of energy available in the system. The presence of nitrogen added to the complexity of the gaseous-electron processes and downgraded the electron energy density. A study showed that the rate of atomic oxygen produced in the argon gas mixture was an order of magnitude more than the rate of atomic oxygen produced in the nitrogen gas mixture [289, 291]. These factors might account for the result in that the trend in regeneration effectiveness decreased as NTP-O_2 in Ar > NTP-O_2 > NTP-O_2 in N_2. All the discussion associated with argon should be presumably applicable to any noble gas, such as helium.

Table 5-3: The relevant reactions [166, 292, 293] in the oxygen non-thermal plasma (NTP-O_2) conditioned with different discharge gases

Discharge gas*	Relevant reactions in the specific NTP-O_2
O_2	$e + O_2 \rightarrow 2\,O + e$ $\quad e + O_2 \rightarrow O_2^+ + 2e$ $\quad e + O_2^+ \rightarrow 2\,O^*$
Argon(Ar)	$e + Ar \rightarrow Ar^* + e$ where Ar* is the excited state, or Ar radical $Ar^* \rightarrow Ar^M$ where Ar^M is the metastable states of Ar from Ar $Ar^M + O_2 \rightarrow Ar + O + O$ $\quad Ar^M + O \rightarrow Ar + O^*$ $Ar^+ + O_2 \rightarrow O_2^+ + Ar$ $\quad O_2^+ + e \rightarrow O + O$
N_2	$e + N_2 \rightarrow 2\,N + e$ $\quad e + N_2 \rightarrow N_2^+ + 2e$ $O^+ + N_2 \rightarrow NO^+ + N$ $\quad O_2^+ + N_2 \rightarrow NO^+ + NO$ $N_2^+ + O_2 \rightarrow NO^+ + NO$

*The gas component present in the flow in a larger percentage than O_2. To be specific, O_2 (2^{nd} row) relates to the case of using pure oxygen, which was be viewed as 20% O_2 blended in 80% oxygen; Ar (3^{rd} row) related to the case of using 20% O_2 blended in argon; N_2 (4^{th} row) relates to the case of using 20% O_2 blended in N_2.

The conventional combustion method of a substance with molecular oxygen is an exothermal process. The operation requires a very strict temperature controlling and heat releasing system to avoid temperature runoff, which would result in the permanent deactivation of the catalyst (such as sintering), and, more importantly, potential safety issues for a plant. Regeneration with NTP-O_2 at a mild temperature condition could best preserve the catalyst properties. The overheating in the conventional combustion possibly causes irreversible sintering of even the catalyst support [294]; therefore, in general, it is thought that it would be very beneficial if any endothermic processes could be utilized and/or a process that can remove coke at a low temperature is developed. The deactivated catalyst from acid catalysis was more difficult than in the other studies reported using an ozone-based approach, most of which included metal functional groups on the surface. The metal sites could launch oxygen spillover, allowing oxidation to occur at a less demanding condition [295]. Also, because of the dilemma of the diffusion issue for the atomic oxygen and ozone, it is believed that the fluidized bed reactor would facilitate the catalyst regeneration process.

5.4.3 Combining online coking suppression and offline catalyst regeneration (coke removal)

Coke deposited acid sites, especially strong acid sites, usually are less hydrogenated than those on metal sites, and thus difficult to remove. The coke on the acid catalyst HSiW-Si from glycerol dehydration was more distributed toward the harder coke region compared to most spent cracking metal catalysts [106, 296]. Therefore, the concept proved for a more difficult model compound (coked acid catalyst HSiW-Si) is very likely to be applicable to metal catalysts, which are sensitive to the sintering problem. Some modifications to the catalyst, such as doping of palladium metals [115], may significantly modify the coke distribution (to the softer end) and lead to more efficient regeneration.

5.5 Conclusions

Silicotungstic acid (HSiW) is one of the best acid catalysts ever reported for acrolein production via glycerol dehydration. This study integrated non-thermal plasma into the

process, and showcased how NTP could possibly play a positive role in process. This study proved the concept of using non-thermal oxygen plasma in the coke suppression during the dehydration reaction and in regeneration of the deactivated catalyst.

Our results showed that application of NTP-O_2 (NTP field strength 4.58 kV/cm and 5% O_2 in argon) could significantly suppress coke formation and thus slow down the decrease of glycerol conversion during the reaction time course. Unlike oxygen alone, this process overall did not decrease acrolein yield. The catalyst deactivated in the glycerol dehydration process under the NTP-O_2 condition could be regenerated much more effectively, compared to the one deactivated under the control condition; this is because the coke removal effectiveness was greatly dependent on the deposited coke characteristics (hardness distribution).

More importantly, this study proved that NTP-O_2 was a viable method to regenerate supported silicotungstic acid, which could not be accomplished by the conventional method due to its low thermal stability. The existence of strong oxidizing agents produced in the gas-phase discharge (O_3, atomic oxygen and active surface oxygen species) on the catalyst surface made it possible to oxidize coke at a much lower temperature compared to the conventional combustion method. NTP-O_2 at higher field strengths was more effective in coke removal; however, the improvement in the coke removal showed an asymptotic tendency. Among the investigated field strengths and temperature conditions, operating NTP-O_2 (8.4 kV/cm) at 150ºC provided the most effective coke removal among those investigated. Longer NTP-O_2 treatment times of the spent catalyst would certainly regenerate the catalyst more thoroughly; however, a balance needs to be found since the removal became slower, while more time means more energy consumption and slower overall acrolein production.

It is most likely that HSiW-Si was deactivated via an indirect mechanism, since partial decoking NTP-O_2 can regenerate the catalyst to a large degree. NTP-O_2 with argon as the background gas showed better regeneration effectiveness than using nitrogen as background gas; also, diluting oxygen with argon showed better regeneration than using pure oxygen. This comparison is presumably applicable to the noble gas helium as well.

NTP-O_2 coke removal was non-selective; it can react with both soft coke and hard coke. For the much softer coke, it is very likely to directly form CO/CO_2, which would directly leave the catalyst surface; while for the harder coke species, the active oxidants reacted with them and formed some intermediate oxygenated surface compound, shifting the distribution to the soft-coke end on the TPO profile. Non-thermal plasma discharge of oxygen containing gas could significantly lower the coke removal temperature; this method is presumably applicable to all catalysts that suffer a coking deactivation where their thermal stability is an issue.

Chapter 6

A feasibility study of non-thermal plasma induced acid catalyst fabrication

Abstract

The feasibility of fabricating better acid catalysts for bio-based acrolein production is discussed in Chapter 6. Non-thermal plasma (NTP) discharge exposure was integrated during catalyst fabrication under both air and argon atmospheres. The fabricated catalysts were evaluated by BET, TPD, XRD, and FTIR techniques in comparison to regularly prepared catalysts as a control. In the end, the kinetic results collected via the glycerol dehydration kinetic runs were compared, and improvement in acrolein selectivity was displayed when using the NTP-argon prepared catalyst, but not when the NTP-air prepared catalyst was used.

Keywords: Catalyst fabrication, non-thermal plasma, Brønsted acid site, Lewis acid site, FTIR-pyridine, TPD, XRD.

6.1 Introduction

It is known that plasma has desirable capabilities in the area of surface modification. In the past, its applications in changing material surface properties have been observed, such as the improvement of adhesion strength and coating, the generation of ultra-fine particles, the deposition of catalytically active species, the reduction of metal during metal-catalyst preparation, etc [297, 298].

Non-thermal plasma (NTP) assisted fabrication has been used in preparing supported metal catalysts. For example, Halverson and Cocke prepared Ru/Al_2O_3 with highly dispersed metallic particles by impregnation on the plasma-grown alumina under NTP with an oxygen and water vapor environment [299]. Al_2O_3 supported $LaMO_x$ (M denotes one of Co, Mn, or Ni) films were developed by radio frequency plasma spray deposition, and different catalytic activities were found as compared to the regularly prepared ones [300]. Vissokov found that plasma could help produce ultra-dispersed catalysts due to changes in the nano-structural and physicochemical properties; as a result, 15-20% higher activity was achieved [301]. Usually, better dispersion of the active compound on the catalyst support leads to better catalysts [297].

NTP treatment has been reported as a substitute for the thermal calcination process. Significant reduction in treatment temperature and time and chemical activation were some of the major advantages of this novel approach [302]. Microwave NTP was mostly applied for heat treatment, since it could introduce a certain level of local heating compared to other NTP techniques. For example, Sugiyama *et al.* used microwave NTP heat treatment to anneal the catalyst, and this catalyst improved the selectivity to the desired product, as compared to conventional calcination [302]. This NTP annealing process also showed the advantage in reducing treatment time [303]: it provided similar or better reduction of metal oxide as compare to hours of conventional calcination. Zhang *et al.* found that using NTP glow discharge could activate Ni/α-Al_2O_3 and greatly improve its activity and stability; better syngas production from methane was achieved using this catalyst [304]. The zeolite template could be removed when it was treated by a radio-frequency NTP [305]. Usually high-temperature treatment would cause the separation of the metal phase [306], the agglomeration into large metal particles [307, 308], or the framework destruction, which would negatively affect catalytic activities [297]. NTP treatment has been found as a solution to these problems.

Plasma exposure has also been found as a cause of surface modification. Guo *et al.* found that the exposure to plasma discharge enhanced the specific surface area of the catalyst (manganese oxide/alumina/nickel foam). It was found that the granularity of the catalyst surface becomes smaller, and the distribution is more uniform after discharge exposure [309]. Discharge exposure increased the surface area, and as the result, adhesive strength increased [310]. Studies of treated resins have revealed that plasma discharge can be the cause of a change in the surface oxygen content, surface morphologies, and surface energy [208]. Plasma exposure caused the granularity of the surface of manganese oxide/alumina/nickel catalyst to become smaller and the distribution more uniform [185]. A claim was made in Veprek's review on non-thermal plasma [311] that the radiation damage caused by ion implantation increases the area of the internal surfaces. Ion implantation with high energy was found able to modify a layer of nitrided steel up to several micrometers thick [311]. Yagofocskaya *et al.* used NTP glow discharge to avoid the undesired segregation of the metal phase in zeolites during calcination. Amorphous Fe_2O_3 with a well-structured and enlarged surface was developed under oxygen or argon glow discharge [306]. Atsushi *et al.* suggested

that NTP could directly activate lattice oxygen and the surface OH group on TiO_2 catalyst in their study of the decomposition of $CClF_3$ [312].

Proton exchanges and acid-base reactions could occur at the interface between the plasma phase and the aqueous or solid target [313]. The enhancement in acidity by NTP treatment has been reported by Yu *et al.*, in that the Brønsted acidity of the Fe-Mo/HZSM-5 zeolite catalyst was greatly increased [314]. NTP glow discharge treatment approximately doubled both Brønsted and Lewis acid sites on HZSM-5 catalysts, and thus improved the interaction between PdO and HZSM-5, and also improved the dispersion of PdO [315].

Several factors are critical to the gas-phase dehydration of glycerol to acrolein. 1) Large surface area is preferred, since it usually positively associates with more active sites. 2) Good dispersion of acid on the support surface and homogeneous distribution of active compounds would contribute to the catalytic selectivity and a decreased sensitivity to poisons [297]. 3) Brønsted acid sites are preferred over Lewis acid sites for acrolein formation. Improvement in each of these factors by NTP has been observed in the previous studies [297] on NTP applications in catalyst preparation. Consequently, the questions become whether these effects can be attained for the supported acid catalysts and whether NTP can help the acid catalyst achieve better catalytic performance in glycerol dehydration to acrolein. To my best knowledge, there have been no studies conducted on the NTP modification of acid catalysts for dehydration reactions. A pioneering study would contribute to further interest in the NTP application in catalysis area. The objective of this study is to discover how NTP can modify the properties of solid acid catalysts in terms of surface area, the acid strength, the acid dispersion, the type of acid sites, and, eventually its catalytic activity in the glycerol dehydration reaction.

6.2 Materials and Methods

Fabrication apparatus

The plate-to-plate discharge was utilized in this dielectric barrier discharge (DBD) device. As illustrated in Figure 6-1, two Pyrex glass plates (4''×4'' ×1/16'') were separated by a thin-sliced glass tube (large glass ring, 3.5'' OD, 1 mm thickness and 10mm height). A round surface coating was made using copper tape (2.5'' in diameter), and this was fixed to the outside surface of each plate (in the center), thus serving as two electrodes. The round shape was used to prevent possible spark generation at a sharp edge of the electrode (such as right angles of a square). The discharge zone was therefore a cylinder with the dimension of 2.5'' in diameter and 1mm in height. Two glass tubes (5 mm i.d., 6 mm o.d.) were fixed on the opposite side of the large glass ring; one was connected to a gas tank (gas inlet), and one was connected to the wall vacuum supply (gas outlet). Another thin-sliced glass tube (small glass ring, 2.5'' ID, 1 mm thickness and 7 mm height) was placed inside the chamber to keep the catalyst particles within the NTP discharge. The chamber was sealed under vacuum. The flow rate of gas supply (20 mL/min) was controlled by a rotameter. Two discharge gases were used in this study: argon (industrial grade, 99.99%) and air (breathing grade). The NTP field strength used in the study was 9 kV/cm.

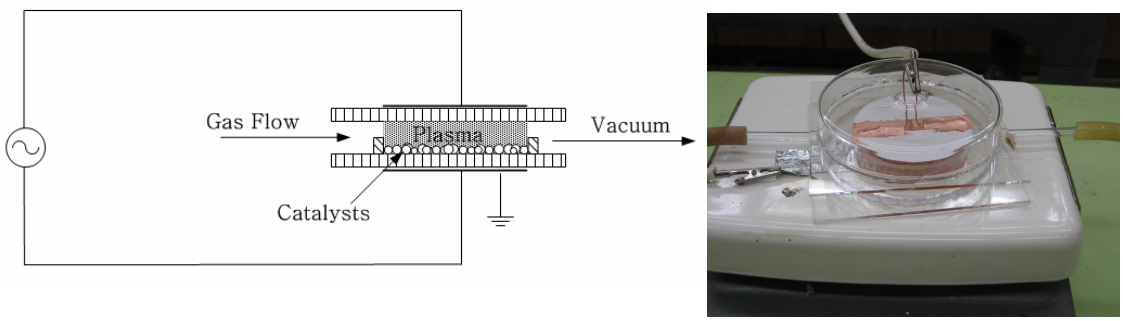

Figure 6-1: The NTP fabrication apparatus

NTP applied catalyst fabrication procedure

Both Alumina 2700 (Al) and Silica 1252 (Si) supports were calcined at 300^{o}C for 2 hours before use. HSiW was loaded on the catalyst support using the impregnation method. In this procedure, HSiW was dissolved (10% of the weight of the support) in deionized water to make 0.04 g/mL solution. The calcined support was added to the HSiW solution. Constant stirring was applied to the mixture at room temperature for 24 hours to attain the adsorption-desorption equilibrium. After the 10 wt% loading, the catalysts were dried in the 55^{o}C convection oven until the majority of water was evaporated and the catalysts were covered

only by a thin sheet of liquid. The damp catalysts were then transported to the NTP discharge chamber, and arranged in a single layer (no stacking of the particles). The catalysts were then exposed to NTP discharge for 5 hours under specific conditions (NTP field strength, type of carrier gas), and then the catalysts (usually dry, visually) were sent back to the convection oven, set at 105^{o}C, for complete dryness before the next 10mol% loading increment. This procedure was repeated until 30 wt% of HSiW was loaded onto the alumina support, or 20 wt% of HSiW was loaded onto the silica support. "The NTP-argon fabrication" is used in the following text to refer to the fabrication procedure with the application of NTP using argon as the discharge gas; and the catalyst prepared via the NTP-argon fabrication is referred to "the NTP-argon fabricated" catalyst hereafter. "The NTP-air fabrication" is used to refer to the fabrication procedure with the application of NTP using air as the discharge gas, and the catalyst prepared in this manner is referred to as "the NTP-air fabricated" catalyst. "The regular fabrication" is used to refer to the regular wet-impregnation procedure, which was detailed in Chapter 3, Materials and Methods; the catalyst prepared via the regular fabrication is referred to as "the regular" catalyst.

Catalyst characterization

The single-point BET measurement of the surfaces was conducted on a Pulsar ChemBET TPR/TPR station obtained from Quantachrome Instrument (Boynton Beach, FL, USA). The catalyst (0.100g) was degassed at 300^{o}C in a nitrogen atmosphere. The physisorption was initiated when the sample cell was immersed into a liquid nitrogen bath, and then desorption occurred at room temperature. Both processes were displayed as peaks on the thermal conductivity detector (TCD) output on a computer screen. The detailed protocol is provided in the manual of Pulsar ChemBET TPR/TPR [316]. Then nitrogen amount was calibrated by injecting a known volume of pure nitrogen gas (ultra purity) until the peak area of the injected volume was equivalent to the peak area of the desorption peak. In this way, the absorbed nitrogen volume was known based on the monolayer nitrogen adsorption and the calculation in Equation 6-1 [317]. The surface area of the probed catalyst could be obtained, and was expressed with units of square meters per gram (m^2/g):

$$SA = {SA_{total}}/{w} = \frac{P \cdot V \cdot N \cdot A_{cs} \cdot (1 - P/P_o)}{R \cdot T \cdot w}$$ **Equation 6-1**

where *SA* is surface area, *P* is the operating pressure, *V* is the total volume of the adsorbed (or desorbed) nitrogen, *N* is Avogadro's number ($6.023*10^{23}$ molecules/mol), A_{cs} is the cross-sectional area of the N_2 molecule (0.162 nm^2), *R* is gas constant, *T* is the temperature at which desorption takes place, and *w* is the weight of the catalyst in the glass cell [316].

With the knowledge of the specific surface area, the surface coverage of HSiW on Si1252 and Al can be calculated via Equation 6-2 [101]. This parameter provides a general idea of how much coverage of the active acid sites is on a given catalyst surface [20][101].

$$D_{surface} = \frac{L\%}{(1 - L\%) \cdot M_{HSiW} \cdot A_{BET}}$$ **Equation 6-2**

where D_{surf} denotes the surface density of HSiW on the support, *L%* is the acid loading weight percentage, M_{HSiW} is the molecular weight of HSiW (3310.66 g/mol) loaded on the silica, and A_{BET} is the surface area of the support, respectively [20].

The acid strengths of the solid catalysts were evaluated via temperature programmed desorption (TPD). The principle of this method is explained as follows. The gaseous base molecules NH_3 are absorbed on the catalyst surface, and the base molecule adsorbed on stronger acid sites will be more difficult to desorb and will only do so when a higher temperature is applied. As the result, as the temperature elevates, the amount of the preferentially-evacuated base will provide a measure of acid strength of the solid catalyst. Ammonia is the gaseous base that was used, and TPD measurements were conducted on the Pulsar ChemBET TPR/TPR system. Prior to the TPD studies, the samples were pretreated at 100°C for 1 hr. in a flow of ultra-pure helium gas (70 mL min^{-1}). The temperature was high enough to fully remove the physisorption of gaseous particles (mainly air), while it was also low enough not to affect the subsequent chemisorption. After pretreatment, the sample was saturated with anhydrous ammonia gas (70 mL min^{-1}) at 100°C for 30 min, and subsequently flushed with He (70 mL min^{-1}) at 100°C for 2 hr. to remove the physisorbed ammonia. Then heating was applied to ramp the temperature up to 600°C at the rate of 10°C min^{-1}. A profile

figure is thus obtained with temperature as the x-axis and the TCD signal as the y axis, which is proportional to the amount of evacuated NH_3.

Powder X-ray diffraction (XRD) patterns were recorded on a Philips X'Pert PRO PW3050 X-ray diffractometer using Cu $K\ \alpha$ radiation (0.154 nm) and a graphite generator. The tube voltage and the current were 45 kV and 40 mA, respectively. The scan rate was 0.5º/min, and the scan range was 2º–80º with the step size of 0.04º.

Fourier transform infrared spectroscopy (FTIR)-pyridine adsorption, was conducted using a Varian 3100 spectrometer equipped with a high-sensitivity linearized mercury cadmium telluride detector (Varian, USA). The diffuse reflectance FTIR technique was achieved using a DiffusIR™ cell (PIKE Technologies, USA). The cell, fitted with ZnSe windows, was capable of operation at a wide range of pressure and temperature, the latter of which was accurately controlled by PID with rapid temperature elevation. Spectra were obtained at a resolution of 8 $cm^{-1}$and with an average of 256 co-additions. The catalyst sample was finely ground so that it could be tightly packed, and a flat and smooth surface could be achieved. These procedures not only made the sampling more representative and more repeatable, but also ensured that the maximum diffuse reflectance signal was returned to the detector. The sample cup, with the catalyst sample already loaded, was calcined at 300°C for 1 hour to evacuate any undesired gas molecules (mainly air) that had been adsorbed on the catalyst surface and would interfere with the spectroscopic evaluation. The cell was cooled in a vacuumed desiccator, and then placed back into the DiffusIR Environmental Chamber (PIKE Technologies, USA.) with helium (He) flowing through at 100 mL/min; then the background spectrum of the fresh catalyst was collected at 25°C. After this, the cell was transferred to a furnace and calcined at 300°C for another hour before placing it in a pre-vacuumed chamber that was saturated with pyridine vapor. The sample was left within the pyridine atmosphere for 8 hours to ensure that it was saturated with pyridine molecules. The cell was transferred again back to the diffuse reflectance FTIR chamber. The catalyst was purged under helium flow (100 mL min^{-1}) at 150°C for 1 hour to exclude any physical adsorption. Then the PID controlled temperature was lowered to 25°C, and the spectrum was collected for the catalyst sample that fully chemisorbed with pyridine. Lowering the temperature to 25°C to collect the spectrum was to ensure that the sample

spectrum was taken at the same temperature as the background, in order to prevent the interference caused by the temperature variation.

6.3 Results

BET surface area

The measured BET surface areas are listed Table 6-1, where the trend that NTP discharge enlarged the surface area is observed. The surface areas of both the NTP-argon fabricated and the NTP-air fabricated catalysts were somewhat larger, when compared to the original support. For the supported catalysts (HSiW-Al or HSiW-Si), both NTP-argon fabrication and NTP-air fabrication displayed the tendency of increasing the surface area, compared to the regularly fabricated catalysts. In particular, the NTP-argon fabricated ones appeared to have a larger surface area than the NTP-air fabricated counterparts.

Table 6-1: BET surface area of the support and the catalyst after different treatments

	Support (m^2/g)			Supported HSiW (m^2/g)		
	Original	**NTP-Argon**	**NTP-Air**	**Regular**	**NTP-Argon**	**NTP-Air**
Al	148 [1] ±3.5 [2]	155 ± 0	153 ± 3.5	140 ± 3	150 ± 0	145 ±7
Si	393+4.2	405 ± 7	405 ± 0	300 ± 10	325±14	310 ±7

[1] Mean of two measurements. [2] Standard error calculated from two measurements.

XRD experiment

Usually, a material with a mesoporous structure would show a large peak in the low angle (0^o-2^o) region of the XRD graph [318-320]. Although the XRD scan could only start from 2^o (due to the instrument limitations), there would be a sharper decline around 2^o, if there was a large peak in the low angle. The declines of NTP fabricated catalysts were sharper than the regular ones. Also, the declines of NTP-argon fabricated catalysts were shaper than those of NTP-air fabricated ones. This could indicate that there was a more distinct mesoporous structure occurring after NTP exposure, or that the mesoporous structure of the support was better retained after acid loading if NTP was applied during the process. This tendency was more obvious on silica supported materials. This can be explained, most

likely, by assuming that the electron bombardment etched the surface of the catalyst, opening up some micropores, and converting some of them into mesopores. Since silica has narrower pores, the existence of the NTP field facilitated the acid particles to diffuse into the pores instead of clustering at the mouth. The results implied that, after NTP exposure, the mesoporous structure was preserved to a large degree while reducing the surface area loss due to the acid loading.

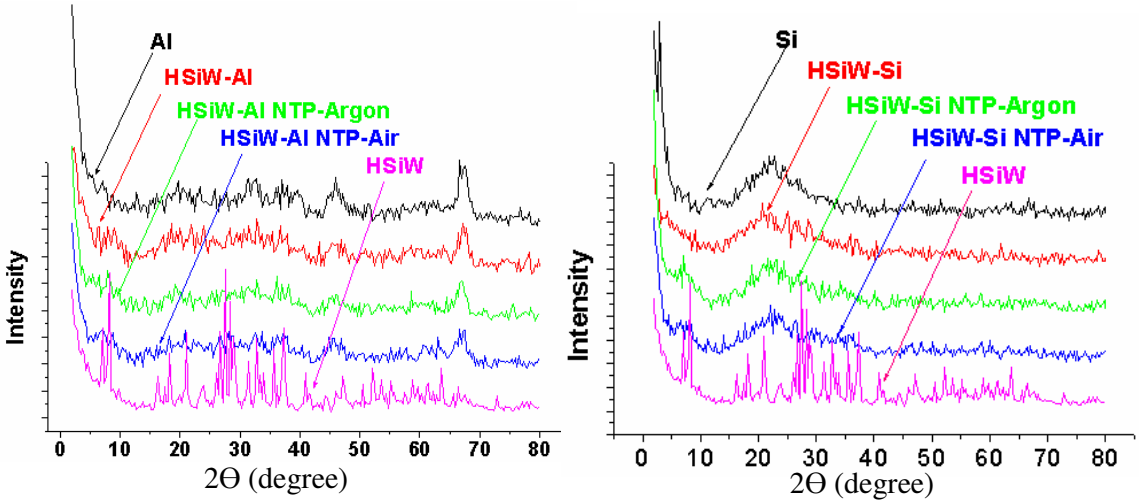

Figure 6-2: XRD patterns of silicotungstic acid (HSiW) and different supported HSiW

TPD-NH_3 experiments for the acid strength

The results obtained via TPD-NH_3 are shown in Figure 6-3. Higher X-value indicates higher acid strength; and higher Y-value indicates higher amount of the acid sites with a specific acid strength. The trend that the acid strength of the catalyst descended in the order of NTP-argon fabrication > regular fabrication > NTP-air fabrication was observed for both HSiW-Al (Figure 6-3 A) and HSiW-Si (Figure 6-3 B).

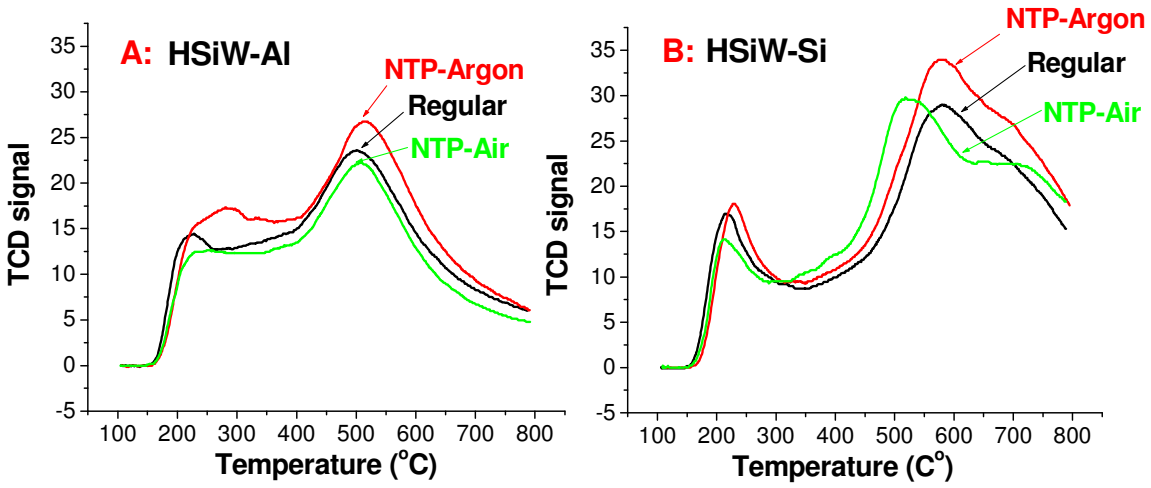

Figure 6-3: TPD-NH_3 profiles of differently fabricated HSiW-Al (A) and HSiW-Si (B)

Diffuse reflectance FTIR

TPD-NH_3 measures the total acid strength, but it is very likely that some Brønsted acid sites and some Lewis acid sites could have the same acid strength. In other words, TPD cannot differentiate the Brønsted acids and Lewis acids, and cannot assess their amounts independently. The proportion of these two types of acid sites plays an important role in determining the distribution of dehydration products of glycerol conversion. The FTIR-pyridine adsorption technique provides a viable measurement in this regard. Pyridine forms a coordinately bonded complex with a Lewis acid, while it forms pyridinium ion with Brønsted acid sites (as summarized in the table imbedded in Figure 6-4). In both cases, N shares the lone pair of electrons with acids that have an electron vacancy. Pyridine can also be weakly adsorbed to surface hydroxyl groups via hydrogen bonding. Figure 6-4 shows the FTIR spectra of pyridine adsorption on HSiW-Al and HSiW-Si, in comparison to those of the corresponding supports (Al and Si). Two peaks (around 1445 cm^{-1} and 1545 cm^{-1}) marked on the graph are commonly acknowledged as the indicators of Lewis acid sites and Brønsted acid site, respectively [106]. For both Al and Si, the signal around 1545 cm^{-1} was hardly differentiated from the baseline noise, indicating that neither of these two supports had Brønsted acidity. The hydrogen-bonded pyridine peak (1580-1600 cm^{-1}) [106] was much more distinguished on Si and HSiW-Si, as compared to Al and HSiW-Al. Al showed a small peak while Si showed no peak around 1480 cm^{-1}; according to the summary table in Figure 6-

4, the IR signal around 1480 cm^{-1} could be attributed to both Brønsted acid and Lewis acid. Al displayed a relatively larger peak than Si around 1445 cm^{-1}, which indicated Lewis acidity. Putting all these consideration together, the conclusion can be reached that both Si and Al had no Brønsted acid sites, and that Al has more Lewis acid sites than Si. Si has more hydrogen-bonded pyridine, which might be because its surface area was over 2.5 times of that of Al; thus the total number of surface hydroxyl groups was larger in Si than Al. The relative amounts of Brønsted acid sites were significantly increased by loading HSiW on Si and Al, which was indicated by the occurrence of the 1545 cm^{-1} peak in the spectra of HSiW-Al and HSiW-Si. As a result of the increase in Brønsted acidity, the 1580 cm^{-1} peak (accumulation of both Brønsted and Lewis acidity) also increased accordingly in the spectra of HSiW-Al and HSiW-Si.

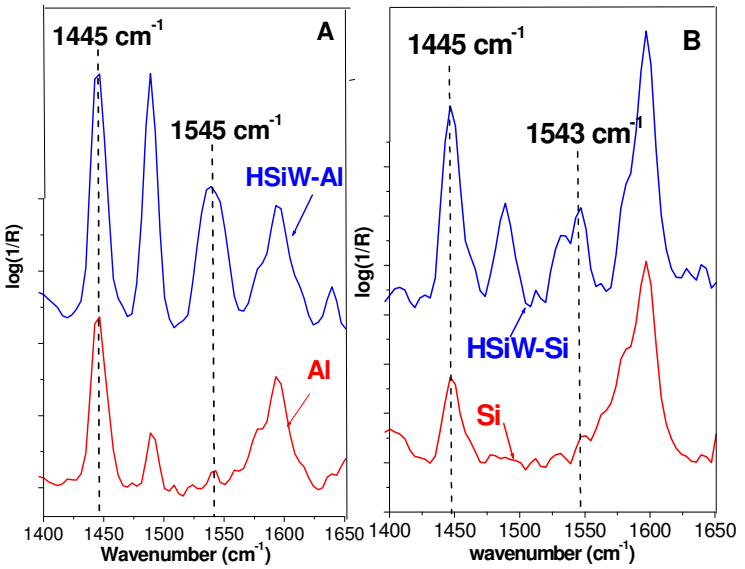

Hydrogen bonded pyridine
1400-1447 (vs); 1580-1600 (s); 1485-1490 (w);
Coordinately bonded pyridine
1447-1460 (vs); 1488-1503 (v), to 1580 (v) 1600-1633 (s)
Pyridinium ion
1485-1500 (vs); 1540 (s), to 1620 (s), to 1640 (s)

Figure 6-4: The FTIR spectra of pyridine adsorption on Al and HSiW-Al (30 wt% acid loading) (A), and on Si and HSiW-Si (20 wt% acid loading) (B). The responsive peak information is summarized in the imbedded table. [106] (vs: very strong; s: strong; v: variable; w: weak)

Figure 6-5 shows the FTIR spectra of pyridine adsorption for HSiW-Al and HSiW-Si prepared via NTP-argon fabrication and NTP-air fabrication, compared to those of the regularly fabricated HSiW-Al and HSiW-Si. The ratio of the signal intensity of the peak around 1540 cm^{-1} to that of the peak around 1445 cm^{-1} could be used as a measure of the relative amount of Brønsted acid sites to Lewis acid sites on the catalyst surface [321-323].

This ratio was calculated and marked as B/L in Figure 6-5. For both HSiW-Al and HSiW-Si, the B/L ratio descended in the order of the NTP-argon fabricated > NTP-air fabricated > regular. The results suggested that the NTP application to catalyst preparation either induced some Brønsted acidity or converted some Lewis acidity to Brønsted acidity, and that the NTP-argon fabrication was more effective in such a function than the NTP-air fabrication.

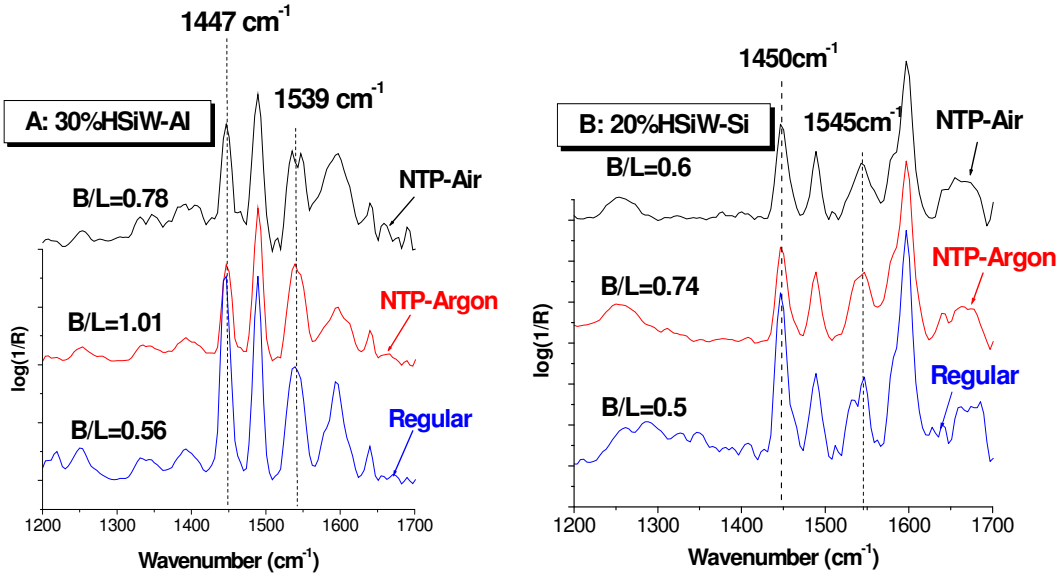

Figure 6-5: The FTIR spectra of pyridine adsorption on the differently fabricated HSiW-Al (30 wt% acid loading) (A) and on differently fabricated HSiW-Si (20 wt% acid loading) (B)

Glycerol dehydration kinetics

The kinetic results obtained in the regular glycerol dehydration processes using the NTP-argon and NTP-air fabricated catalysts are shown in Table 6-2; the results obtained with the regular catalysts were also provided as the comparison. The NTP-argon treated catalysts showed a marginal improvement in glycerol conversion and acrolein selectivity. The NTP-air treated catalysts did not show a significant difference (if any were present, it was worse), as compared to the performance of the regular catalyst in terms of acrolein selectivity.

Table 6-2 Kinetics data of the glycerol dehydration at 275° C over differently fabricated alumina supported silicotungstic acid (HSiW-Al) and silica supported silicotungstic acid (HSiW-Si)

		Conversion (%)	Selectivity (mol%)				Coke [2]	Carbon balance (%)[3]
			Acrolein	Acetaldehyde	Propionaldehyde	Acetol		
HSiW-Al	Regular	96.2[1] ± 0.3	77.0 ± 0.9	1.9 ± 0.1	1.4 ± 0.1	10.6 ± 0.9	8.65% ±0.92%	96.3 ± 0.2
	NTP-Argon	98.9 ± 1.8	80.3 ± 1.1	1.9 ± 0.4	1.5 ± 0.1	10.2 ± 0.7	8.48% ±0.35%	97.4 ± 0. 9
	NTP-Air	96.8 ± 0.9	76.8 ± 1.5	1.7 ± 0.2	1.2 ± 0.1	11.4 ± 1.2	8.06% ±0.89%	95.0 ± 1.3
HSiW-Si	Regular	92.9 ± 0.6	79.5 ± 0.2	1.1 ± 0.2	1.1 ± 0.0	7.6 ± 0.3	14.27% ± 0.5%	96.0 ± 2.0
	NTP-Argon	93.5 ± 1.8	84.1 ± 0.9	1.2 ± .0.2	1.1 ± 0.1	6.9 ± 0.9	11.67 ± 1.13%	95.7± 1.1
	NTP-Air	94.8 ±1.2	78.7 ± 1.4	1.1± 0.3	0.9 ± 0.1	7.5 ± 0.4	11.23% ±0.56%	93.7 ± 2.8

1: Average of the conversion (selectivity) averaged over 1.5-7.5 hours time-on-stream of two kinetic repetitions.
2. Calculated by the catalyst weight gain after 7.5 hour reaction divided by the fresh catalyst weight.
3. Calculated via Equation 3-8 in Chapter 3.

Both NTP-air treated and NTP-argon treated HSiW-Si somewhat improved the glycerol conversion. Compared to the regularly prepared catalyst, a decrease in the amount of coke formed during 7.5-hour TOS was observed for both NTP-argon fabricated HSiW-Si and the NTP-air fabricated HSiW-Si; such a decrease in coke formation made by using the NTP fabrication was not as significant with HSiW-Al as that with HSiW-Si. NTP-argon fabricated catalysts did lead to the improvement in acrolein selectivity, which well agreed with TPD and FTIR results in that Brønsted acidity and stronger acid strength favored acrolein formation. The preservation of pore shrinkage during acid loading and the enlargement of the surface area are possibly the cause of less coke formation, especially for HSiW-Si.

6.4 Discussion

The interaction between HSiW and the support might not be the same for silica and alumina, due to the difference in the pore structure and especially surface hydroxylation, which might have played an important role in the HSiW adsorption. Since Si has no surface basicity and very weak surface acidity, the coordination mechanism [324] might have predominated the HSiW adsorption on silica; in this mechanism, an outer-sphere surface complex, $(SiOH_2)^+(SiW)^-$, was formed between the protonated surface hydroxyl and the heteropolyanion, denoted as $(SiW)^-$ (Equation 6-2). With its hydroxylation characteristic, Al has both surface acidity and basicity to certain degree, providing some ionic interaction with HSiW, and thus stronger immobilization of HSiW on its surface, as compared to that on Si surface. The two-step ligand exchange mechanism [324] occurred on the Al surface, where the protons of strong Brønsted-acidic HSiW first transfer to the Al surface hydroxyl group (Equation 6-3), and then the protonated surface hydroxyl group reacted with the heteropolyanion, forming a monolayer neutral surface compound Al(SiW) (Equation 6-4). The coordination mechanism could also exist in the interactions between HSiW and Al surface [325], and $(AlOH_2)^+(SiW)^-$ was formed as shown in Equation 6-2 .

Coordination mechanism:

$M\text{-}OH_2^+{}_{(s)} + (SiW)^-{}_{(aq.)} \rightarrow (MOH_2)^+(SiW)^-$ **where M is either Al or Si** **Equation 6-2**

Ligand exchange mechanism:

$$Al\text{-}OH_{(s)} + H^{+}_{(aq.)} \rightarrow AlOH_2^{+}{}_{(s)} \qquad \textbf{Equation 6-3}$$

$$Al\text{-}OH_2^{+}{}_{(s)} + (SiW)^{-}_{(aq.)} \rightarrow Al(SiW)_{(s)} + H_2O_{(l)} \qquad \textbf{Equation 6-4}$$

NTP fabricated catalysts tended to have larger surface area (Table 6-1) and better preserved mesoporous structures (Figure 6-2). NTP exposure preserved the mesoporous structure to a large degree while reducing the surface area loss due to the acid loading. Such results could be understood as follows: 1) the continuous electron (or maybe Ar^{+}) bombardment broke the long intact chain of Si-O-Si or Al-O-Al. Some defect sites (either electron-rich or electron-deficient) may link with some neighboring "defect" sites, resulting in "migration". Such "migration" would possibly cause the conversion of micropores into mesopores. 2) The application of NTP might have increased the interaction between the HSiW molecules and the support (Al or Si), and consequently shortened the distance between HSiW and the support surface. As a result, the pores did not shrink as much as compared to the regular loading. 3) During the vaporization of excessive water in the regular fabrication process, the mass transport of water molecules from the liquid bulk to the surface possibly pushed some HSiW molecules outward to the liquid surface, resulting in some degree of agglomeration at the mouth of the micropores instead of deeply within the pores. Such an event might have been minimized in the presence of NTP. An additional electrical field thus existed along with the NTP discharge; this electrostatic force contributed to keeping the HSiW molecules close to the surface (both the very outside surface and the wall inside all of the pores).

Some plausible mechanisms regarding the increase of acid strength (Figure 6-3) and Brønsted acidity (Figure 6-5) are provided as follows. Usually, each surface OH group is a potential Brønsted acid site, since it is available to be protonated. NTP exposure caused "defects" on the support surface; such "defects" usually are associated with surface OH groups. As the result, these newly formed surface OHs by NTP application potentially could introduce extra Brønsted acid sites in the presence of water. As previously discussed, NTP could induce some Brønsted acidity in the presence of the water molecules, producing protons (or hydronium ions). These protons countered some of the basic sites on the alumina, resulting in a decrease in the interaction with HSiW. This decreased interaction possibly led to better preservation of the Keggin structure. This interaction resulted in a more

protonated surface. The protonated surface attracted HPA anions, stoichiometrically resulting in some free hydroxonium. This free hydroxonium formerly bonded to HPA anions, but now they were localized near the surface. As a result, FTIR showed some increase in the ratio of Brønsted-pyridine peak intensity to Lewis-pyridine peak intensity; the TPD-NH_3 results showed higher acid strength for the NTP-argon fabricated catalysts; and acrolein selectivity obtained with NTP-argon fabricated HSiW-Al was somewhat increased, compared to the selectivity obtained with regular HSiW-Al.

Regarding the observations that the NTP-air fabrication did not show much positive contribution, if not negative, in the abovementioned aspects, the following reasons are provided as the explanations. 1) It is more difficult to breakdown air than to breakdown argon; the energy and the amount of the electrons in the NTP-air fabrication were smaller than in the NTP-argon fabrication. As the result, the performance in electron bombardment and NTP acidity induction was reduced. 2) As illustrated in the process A in Figure 6-6, dehydroxylation occurred on the hydroxyl aluminum during the calcination in the regular catalyst fabrication procedure. Some dehydroxylated sites were rehydroxylated (the process B in Figure 6-6) when they were again exposed to water during the subsequent loading step, resulting in some Brønsted acid sites. However, during the NTP-air fabrication, some novel surface bond (Al-O*) was formed [326, 327] (the process C). Al-O* was not able to undergo the dehydroxylation-rehydroxylation process; instead it converted back to the surface hydroxyl group and released oxygen (the process D) in the subsequent acid loading. As the result, Brønsted acid sites could not be generated in processes (C and D). The released oxygen could either occupy the surface acid sites, blocking HSiW's interaction, or push outwards the acid via the "degassing" motion, which was originally attracted towards the alumna surface. 3) The O atoms formed in NTP were electrophilic. In some sense, all the electrophiles can be considered as acids. These electrophiles have a tendency to be attracted to the catalyst surface due to the electrostatic field. Some surface adsorptive sites could be preoccupied by these O atoms, which behaved as a competitive process to the adsorption of SiW anion. As the result, the binding between HSiW and the support was weakened. During the calcinations, temperature elevation pushed the oxygens off the catalyst surface and they subsequently recombined to molecular O_2. Therefore, overall the NTP-air fabrication did not show any improvement, or maybe even a hint of a negative effect, toward acrolein selectivity.

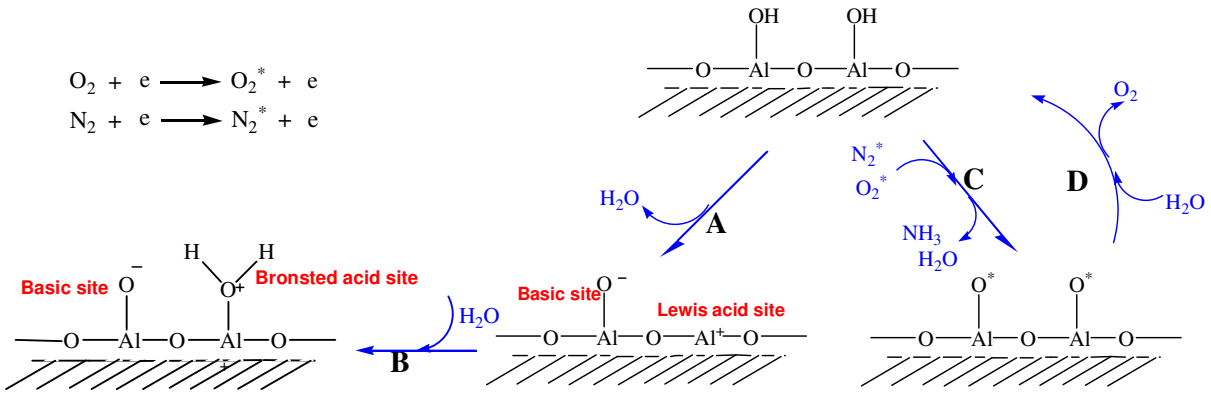

Figure 6-6: The surface reactions when the support (Al as an example) is dehydrated, hydrated, or exposed to NTP-air

The redox capability of NTP-air fabricated catalysts was not evident in the kinetics results as had been desired, possibly because the calcinations at 300°C evacuated the active O species off the surface, and the discharge conditions used this study were not able to implant the O as lattice oxygen.

I am certainly aware of the limited achievements in this chapter. Although more NTP discharge configurations and more advanced characterizations were not conducted due to the time constraint and equipment restrictions, I want to share some ideas that are worth studying in the future.

1. More electrons with higher energy can be produced under the application of a more intense discharge (larger field strength). It is reasonable to deduce that more significant improvement can be achieved by using a more intense NTP-argon discharge. However, this study could not proceed with this idea due to the constraint of my plasma generation system. Nevertheless, the application of more intense NTP is certainly an interesting direction to go.

2. No significant advantage was shown in terms of the acid dispersion, since the acid was already well-dispersed on the catalyst surface. With the enhanced electrostatic attraction by NTP fabrication, the loading limit is possibly able to be pushed higher, which would enhance the Brønsted acidity.

3. In the fabrication procedure, NTP was not applied until the majority of

water was evaporated; therefore, how the interaction between the support and HSiW when they first contacted could be altered by the NTP has not yet been examined. It would be interesting to examine the NTP application at the onset of wet impregnation. This impregnation protocol may not be appropriate for such an investigation. Isometric impregnation is recommended as the acid-loading protocol for this examination purpose.

4. NTP discharge could strengthen the bonding between the catalyst support and HSiW, which could be used as a replacement for calcinations. Microwave NTP would be the best candidate for this purpose.

6.5 Conclusions

The application of NTP to catalyst fabrication demonstrated the potential of modifying the supported silicotungstic acid (HSiW). The modifications include increasing the surface area, preserving the mesoporous structure, increasing the acid strength, and increasing the proportion of Brønsted acid sites.

Regarding the modifications, NTP-argon fabrication (9 kV/cm) caused relatively more significant improvements to the supported HSiW than did the NTP-air fabrication (9 kV/cm). As a result, some improvement in acrolein yield was observed with the NTP-argon fabricated catalysts, but not with the NTP-air fabricated catalysts. NTP-air fabrication with a 9 kV/cm field strength could not impose permanent redox properties, as was desired, which was suggested by observing no significant coking suppression.

Overall summary

This study simultaneously examined two interesting areas: 1) converting glycerol, biodiesel byproduct, to the value-added product acrolein; 2) applying non-thermal plasma (NTP) to a dehydration process. Several contributions were made by this study in developing sustainable acrolein production and in understanding plasma chemistry in dehydration.

First, a comprehensive review was provided on the acrolein synthesis methods. This study demonstrated that the bio-based acrolein production from glycerol was the most viable production alternative to the current propylene-based manufacturing method, both technologically and economically. Based on the assessment, the price of acrolein produced from crude glycerol was lowered compared to the current acrolein price. Even the production from refined glycerol may be worthwhile, because it is renewable and sustainable, and yet it does not increase the price much. Such a comprehensive comparative review, especially with the economical assessment included, had never been conducted before; it is definitely valuable and meaningful in directing the industrial processes and future research thrusts.

Second, the catalysts were fabricated using commercially available components (acid and the support). As a result, the reproduction by industry or other end users is straightforward and convenient. To date, most, if not all, acrolein research was conducted in small-scale, which minimized many engineering problems, such as axial heat transfer, pressure drop, etc. Compared to those small-scale reactors, my reactor was much larger in scale, and yet the results in acrolein production were among the best results ever published to date. The support effect and the temperature effect were studied for the catalytic acrolein production from glycerol. The optimal acrolein production occurred at 275°C, and the acrolein yields were 73.86 mol% (92.9% conversion and 79.5 mol% selectivity) and 74.05 mol% (96.2% conversion and 77.0 mol% selectivity) for alumina (Al2700®) supported silicotungstic acid (HSiW-Al) and silica (Si1252®) supported silicotungstic acid (HSiW-Si), respectively.

Third, NTP was studied in a dehydration reaction for the first time. On one side, NTP served as an effective energy source. Some similarities as well as interactions could be found between the temperature effect and the NTP field-strength effect. One example of NTP in the energy aspect was that glycerol conversion was improved with the NTP application. On the other side, NTP induced additional Brønsted acidity, in that acrolein selectivity could be improved and activation energies of glycerol conversion to acrolein were lowered,

compared to the control conditions. The "acidity" function was selective to acrolein formation but the "energy" function was not; therefore, NTP field strength needed to be carefully configured to ensure that NTP played a positive role in acrolein production. The optimal discharge conditions for the maximal acrolein yields were 3.78 kV/cm for HSiW-Al and 4.58 kV/cm for HSiW-Si. The acrolein yield achieved accordingly was 83.6 mol% (98.7 % conversion, 84.7 mol% selectivity) and 83.1 mol% (94.4% conversion, 88.0 mol% selectivity), respectively, which was almost a 10 mol% improvement, compared to the optimal acrolein production under the control conditions.

Fourth, this study also opened up a novel pathway of solving the catalyst deactivation problem, which was very tough for the supported HSiWs in that their thermal stability rejected the conventional combustion treatment. The results showed that NTP-O_2 was an effective approach to regenerate the supported HSiW. It was found that the coke removal effectiveness increased with NTP field strength but with a decreasing increment. Among the temperatures that were studied (25ºC, 125ºC, 150ºC and 200ºC), the most effective coke removal occurred at 150°C. Also, this study found that argon was a better discharge gas for NTP-O_2 catalyst regeneration, compared to nitrogen or oxygen itself. NTP-O_2 proved to be reactive to the carbonaceous species with various hardness degrees, although the removal rate varied. The indirect deactivation mechanism was most likely to be the case for the easily-deactivated HSiW-Si; as a result, even partial coke removal could regain the catalytic activity to large degree. Co-feeding small amounts of oxygen (5% volumetric percentage) with the presence of non-thermal plasma discharge during the dehydration reaction could greatly suppress the coke formation without affecting acrolein selectivity, as compared to the control reaction. This attempt also resulted in a different coke distribution: not only less amount of coke, but also the composition prone to the soft-coke end compared to the profile obtained from the control reaction. Not surprisingly, the spent catalyst from such a reaction was more readily to be regenerated; complete recovery of catalytic activity was achieved multiple times.

Last, this study explored the possibility of modifying the supported silicotungstic acid by applying NTP during the catalyst fabrication. NTP fabrication showed some capabilities in enlarging surface area, preserving mesopores, enhancing acid strength, and increasing the proportion of Brønsted acid sites. Using argon as the discharge gas provided relatively more

significant results in the abovementioned functions than using air as the discharge gas.

Eventually, the end product of glycerol conversion to acrolein is acrylic acid. Therefore, the next step of this research would be to develop the process to convert acrolein to acrylic acid. The calculation in Chapter 1 shows that using crude glycerol as the starting material is much more economical than using refined glycerol; the studies in literature that used crude glycerol in gas-phase acrolein production are difficult to find. Many technical issues, such as the tolerance of the solid catalyst to the impurities in glycerol, need to be addressed and resolved. Therefore, developing an efficient bio-based acrolein production using crude glycerol as the raw material is a practical and meaningful study to be conducted next.

This study demonstrated the NTP capability in improving the glycerol dehydration to acrolein. NTP capability in dehydration needs to be further verified with other reaction cases. The reason that the achieved improvement in acrolein production was limited was due to the existence of many side reactions. It is thus hypothesized that the acid-catalytic capability function of NTP will stand out when the dehydration reaction system does not contain many side reactions. For example, acid hydrolysis of sugars may be a good research candidate.

Doping platinum group metals may help further improve the NTP-O_2 regeneration capability. The research needs to be focused on whether doping platinum group metal would influence the acrolein yield in the glycerol dehydration and how much improvement in catalyst regeneration can be achieved in combination with NTP-O_2.

As discussed in the end of Chapter 6, there are many options to extend the research of NTP assisted fabrication of solid acid catalysts to a greater depth. First, applying more intense NTP-argon discharge during catalyst fabrication needs to be studied in the future. Second, the possibility of increasing the acid loading and still maintaining good acid dispersion on the support is high because of the enhanced electrostatic attraction by NTP. The hypothesis of such a possibility needs to be validated. Third, it would be interesting to examine the NTP application at the onset of wet impregnation using isometric impregnation as the acid-loading protocol. Fourth, whether NTP discharge could be used as the replacement for calcination by strengthening the bonding between the catalyst support

and HSiW is also a worthwhile research topic.

Appendices

Appendix I
Vaporization of glycerol solution

Glycerol decomposition started at 290°C [328, 329]; usually above 350°C, pyrolysis was the primary reaction occurring in the system [108]. The boiling point of pure glycerol is 290°C, while dilution in water can lower its partial vapor pressure. Therefore, it is necessary to determine where is the low-end temperature limit to conduct the glycerol dehydration while ensuring it remains a gas-phase reaction.

The Antoine equation describes the relationship between vapor pressure and temperature for a pure substance, as shown in Equation I-1. The constants and the applicable temperature range of the equation for water and glycerol are listed in Table I.

$$\log_{10} P = A - \frac{B}{C + T} \qquad \textbf{Equation I-1}$$

where P is the vapor pressure (mm Hg), T is the temperature (°C), A, B, and C are the constant parameters fitted to each substance.

Table I: Antoine coefficients and the temperature range over which they are applicable [330, 331].

	A	B	C	T_{min} (°C)	T_{max} (°C)
Water	8.14019	1810.94	244.485	99	374
Glycerol	7.01621	1448.81	62.4928	96	576.85

Based on Antoine equation, the vapor pressure of pure substance glycerol or water can be calculated for each temperature. Figure I-1 shows the plot of vapor pressure of glycerol and water as a function of temperature.

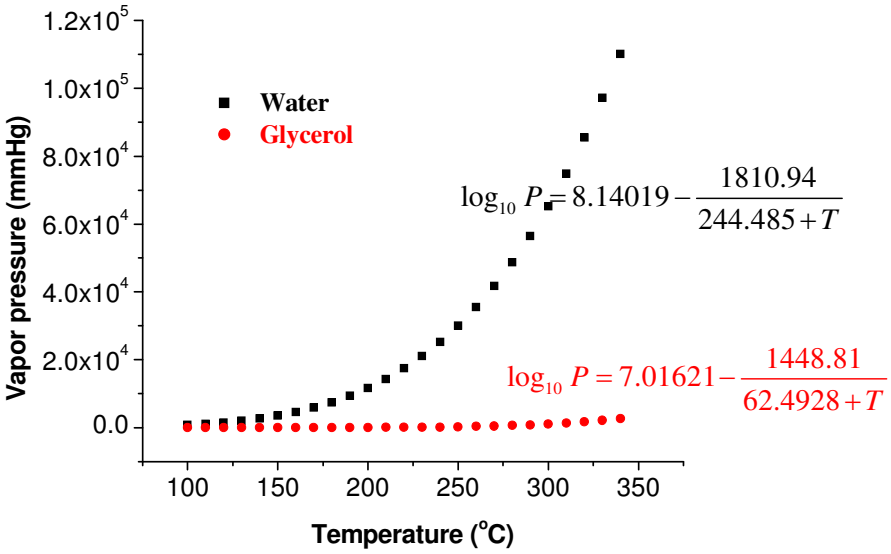

Figure I-1: Vapor pressure as a function of temperature for water and glycerol calculated via Antoine Equation.

Considering the 20 wt% glycerol solution (equivalent to the molar percentage of 4.6632%) as an ideal solution, then according to Raoult's law, there is the following relationship for the two-component system (Equation 8-2 and Equation 8-3):

$$p_t = p^*_{water} \cdot x_{water} + p^*_{glycerol} \cdot x_{glycerol} \qquad \textbf{Equation I-2}$$

$$p_{water} = p^*_{water} \cdot x_{water} \quad p_{glyceorl} = p^*_{glycerol} \cdot x_{glycerol} \qquad \textbf{Equation I-3}$$

where p_t is the total vapor pressure in the two-component system, p^* is the vapor pressure of the pure component (water or glycerol, as specified by the subscript), and p is the partial vapor pressure of each component (specified by the subscript). x is the molar percentage of each component (x_{water} =95.3368% and x_{water} =4.6632%) in the liquid phase, or the composition in the feed solution.

To ensure that the two-component solution can be completely evaporated, the total vapor pressure of the glycerol-water solution needs to be 760 mm Hg. The following steps detail the approach to solving this problem. 1) Assume a temperature (100°C -290°C), so that the partial vapor pressure can be calculated for both glycerol and water using the Antoine

equation; therefore, the total vapor pressure can be expressed as a function of only one variable, $X_{glyceol}$. 2) Let the total vapor pressure be equal to 760 mm Hg, then solve the equation for $X_{glyceol}$. 3) The gas-phase molar composition is then calculated via Equation 8-4 by combining Dalton's law (Equation 8-5) and Raoult's law (Equation 8-2&3). 4) Temperature is varied to cover more data points within the range of 100-290°C.

$$y_{glycerol} = \frac{p^*_{glycerol} \cdot x_{glycerol}}{p^*_{water} \cdot x_{water} + p^*_{glycerol} \cdot (1 - x_{water})} \qquad \textbf{Equation I-4}$$

$$p_{water} = p_t \cdot y_{water} \quad \textbf{and} \quad p_{glycerol} = p_t \cdot y_{glycerol} \qquad \textbf{Equation I-5}$$

The *T-x-y* diagram of the glycerol water system can be therefore plotted; it is displayed in Figure I-2, which displays the boiling point for the solution of a certain glycerol molar concentration and the corresponding glycerol molar percentage in the vapor phase can be found. Based on this diagram, the temperature obtained from the *T-x-y* graph for a vapor with 4.6632% glycerol molar ratio is 210°C. Therefore, if the reaction temperature is maintained above 210°C, the 20 wt% glycerol solution is completely vaporized. This justifies my lowest temperature of interest.

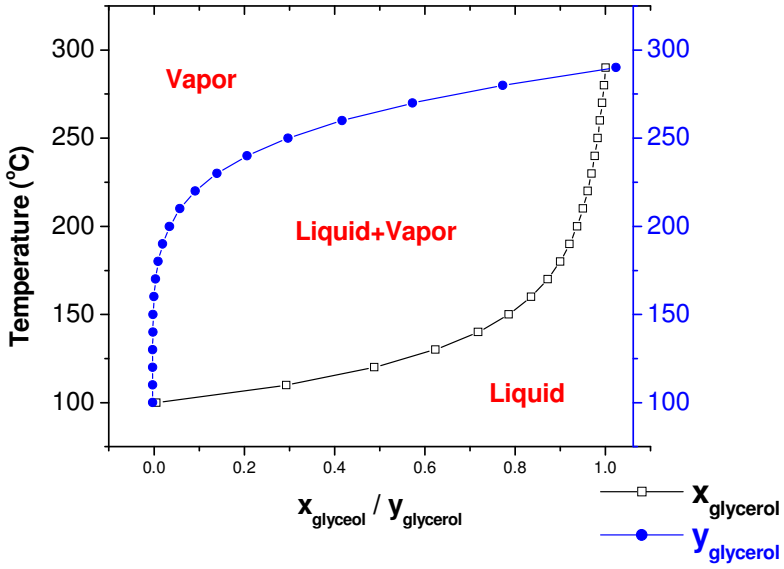

Figure I-2: *T-x-y* diagram for the glycerol-water two-component system at 760 mm Hg.

Appendix II
Thermodynamics information

Enthalpy of reaction is a state function, regardless of whether or not and which catalysts are used. Therefore, only the overall reaction equation of glycerol dehydration to acrolein is necessary.

$$C_3H_8O_3 \rightarrow C_3H_4O + 2\ H_2O$$

The thermodynamic properties of the relevant compounds are listed in Table II.

Table II: Thermodynamic properties of the chemical compounds of the feed and the products of gas-phase glycerol dehydration, and the calculated heat of reaction at each reaction temperature used in the study

Temperature		$\Delta_f H^o$ (kJ· mol^{-1})			$\triangle H_{rxn}$	Endothermic?
in ºC	in K	Glycerol [1]	H_2O [2]	Acrolein [1]	(kJ· mol^{-1})	
220ºC	493K	-594.0	-234.9	-86.63	37.57	Yes
235ºC	508K	-594.7	-234.3	-86.93	39.17	Yes
250ºC	523K	-595.4	-233.8	-87.22	40.58	Yes
275ºC	548K	-596.4	-232.8	-87.67	43.13	Yes
290ºC	563K	-597.1	-232.3	-87.91	44.59	Yes
305ºC	578K	-597.7	-231.7	-88.16	46.14	Yes
320ºC	593K	-598.3	-231.1	-88.37	47.73	Yes

1: Data were obtained from Chemical property handbook [332].

2: Calculated based on $\Delta H^o_{f,T} = \Delta H^o_{f,25C} + \int_{298}^{T} C_{p,water}\,dT$ **, where** $\Delta H^o_{f,25C}$ **for water (g) is -241.8 kJ· mol^{-1}, and $C_{p,water(g)}$= 33.933 – 0.0084186T + 0.000029906T^2 [332]**

Appendix III
Activation energy calculated for glycerol dehydration to acrolein with/without non-thermal plasma

For the given reaction, the reaction rate is defined as in Equation III-1.

$$-r_j''' = \frac{\text{mole of "j" species reacted or formed}}{\text{(unit catalyst bed volume)(unit time)}} = \pm\frac{dN_j}{V_s dt}\left\langle\frac{mol}{m^3 s}\right\rangle \qquad \textbf{Equation III-1}$$

Therefore, for the reactant glycerol, the reaction rate is expressed in Equation III-2:

$$-r_{glycerol} = \frac{\text{mole of glycerol reacted}}{\text{(unit catalyst bed volume)(unit time)}} = \pm\frac{dN_{glycerol}}{V_s dt} \qquad \textbf{Equation III-2}$$

$$\Rightarrow \qquad -r_{glycerol} = \frac{dX}{d(V/F_{glycerol})}$$

For a continuous system, conversion is defined as

$$F_j = F_{j0}\left(1 - X_j\right)$$

Anywhere in the reaction zone, the components are:

Glycerol: $F_{glycerol,0}\left(1-X\right)$ where $F_{glycerol,0}$ is the molar flow rate of glycerol before entering the catalyst bed.

Products (acrolein & water): $F_{glycerol,0}\left(1+\varepsilon\right)X$

Solvent (water in feed): $F_{glycerol,0}\cdot\beta$ where β is the ratio of the moles of solvent to the moles of glycerol.

So the total molar flow rate F_T can be expressed as follows

$$F_T = F_{glycerol,0}\left(1-X\right) + F_{glycerol,0}\left(1+\varepsilon\right)X + F_{glycerol,0}\beta = F_{glycerol,0}(1+\varepsilon X+\beta)$$

Where β is the ratio of the moles of solvent to the moles of glycerol, and ε is the expansion factor. The expansion factor ε is a measure of the variation of the reacting system volume, along the reaction path, by totally transforming a given reactant into products. The calculation is depicted as follows.

$$\varepsilon = \frac{V_{X_j=1} - V_{X_j=0}}{V_{X_j=0}}$$

Similarly, the total molar concentration (including glycerol, acrolein and water) can be obtained.

$$C_T = C_{glycerol,0}(1+\varepsilon X+\beta)$$

The relationship can be developed among glycerol concentration ($C_{glycerol}$), total molar concentration (C_T), and glycerol conversion (X).

$$X = \frac{1-\dfrac{C_j}{C_{j0}}}{1+\varepsilon\,\dfrac{C_j}{C_{jo}}} \quad \Leftrightarrow \quad C_{glycerol} = C_{glycerol,o}\frac{1-X}{1+\varepsilon\,X} = C_T\frac{1-X}{1+\varepsilon\,X+\beta}$$

C_T can be calculated based on the ideal gas law. $P=C_TRT$, where P is the atmospheric pressure ($1.01*10^5$ pa), R is the gas constant 8.315 m^3 Pa K^{-1} mol^{-1}, and T is the reaction temperature.

Mechanism of glycerol dehydration is

$$C_3H_8O_3 \rightarrow C_3H_4O + 2\,H_2O \quad \text{so} \quad \varepsilon = 2$$

Differential method is used to obtain the reaction rate equation, assuming the reaction can be expressed in the form shown in Equation III-3.

$$-r_{glycerol} = k_{glycerol} C_{glycerol}^{n} \quad \Leftrightarrow \quad -\frac{dC_{glycerol}}{dt} = k_{glycerol} C_{glycerol}^{n} \qquad \textbf{Equation III-3}$$

$$\log(-r_{glycerol}) = \log k_{glycerol} + n \log C_{glycerol} = \log k_{glycerol} + n \log C_{glycerol,o} + n \log(\frac{1-X}{1+\varepsilon \cdot X + \beta})$$

Now the task is to obtain -$r_{glcyerol}$, and (1-X)/(1+εX), so that when *log($dC_{glcyerol}/dt$)* is plotted versus *log((1-X)/(1+εX))*, the slope of the straight line yields the reaction order n, and the rate constant can be calculated from the intercept. In order to obtain -$r_{glcyerol}$, we need to have the dependence of glycerol conversion X versus $V/F_{glycerol}$. This was approached by obtaining the conversions using different glycerol feed flow rate. Figure II-1 is the plot of X versus $V/F_{glycerol}$ for HSiW-Al and HSiW-Si, respectively. Quadratic functions were fit to the data with the R-square equal to 1. The rate at each flow rate and temperature can be calculated by evaluating the 1st derivative of the corresponding quadratic equation at a given $V/F_{glycerol}$. The calculated rates were listed in Table III-1.

$$-r_{glycerol} = \frac{dX}{d(V/F_{glycerol})}$$

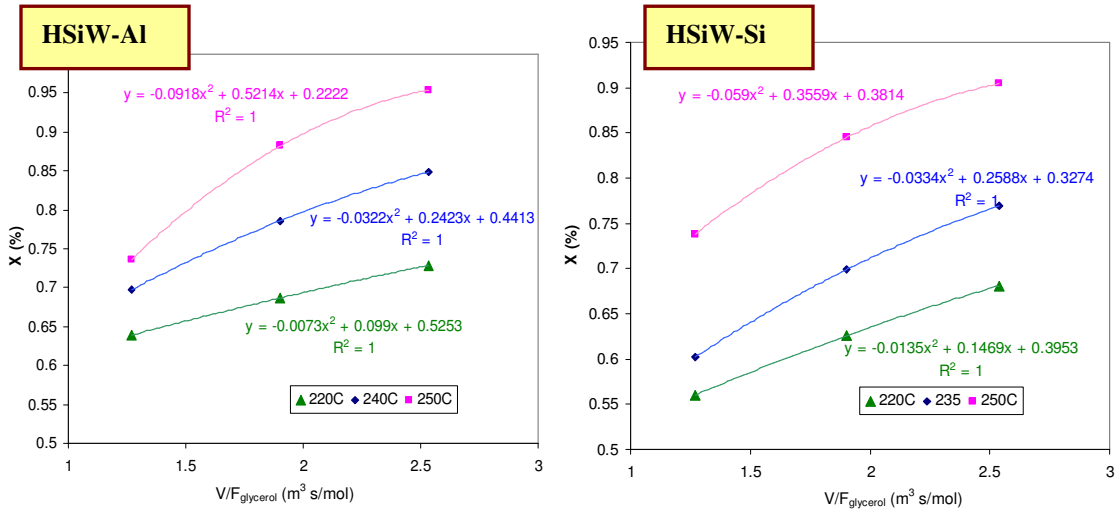

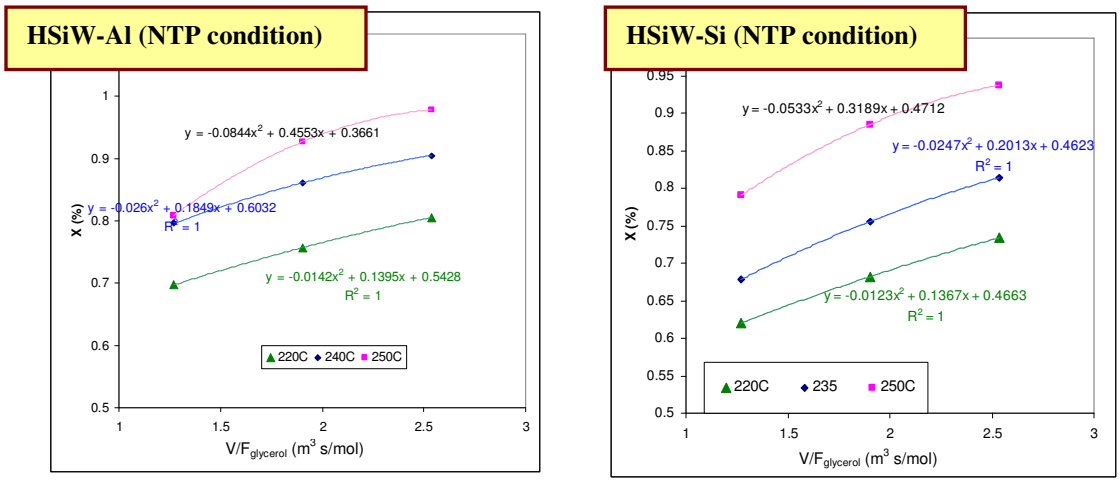

Figure III-1:The plot of conversion X versus $V/F_{glycerol}$

Table III-1: The calculated reaction rate at each temperature and feed rate

		HSiW-Al		HSiW-Si	
		control	NTP	control	NTP
Temperature (°C)	$F_{glycerol}$(mol/s)	$r_{glycerol}$ (mol s^{-1} m^{-3})			
220	2.76E-06	0.062	0.011	0.081	0.074
220	**3.68E-06**	0.071	0.053	0.093	0.090
220	5.52E-06	0.080	0.096	0.106	0.105
235	2.76E-06	0.079	0.026	0.096	0.075
235	**3.68E-06**	0.120	0.088	0.129	0.108
235	5.52E-06	0.161	0.151	0.161	0.141
250	2.76E-06	0.056	0.038	0.065	0.049
250	**3.68E-06**	0.172	0.148	0.118	0.116
250	5.52E-06	0.288	0.258	0.172	0.184

With the availability of $-r_{glycerol}$, we now can plot $\log(-r_{glycerol})$ versus $\log((1-X)/(1+\varepsilon X+\beta)$, and the resulted plots are shown in Figure 8-4. It confirmed that glycerol dehydration is 1st order reaction, since all the sloped rounded up to 1. Also k could be obtained at the same time; their values are listed in Table 2. Then After plotting lnk versus 1/T, activation energy could be obtained by multiply the slope by ideal gas constant R. The calculated E_as are listed in Table 8-5 as well.

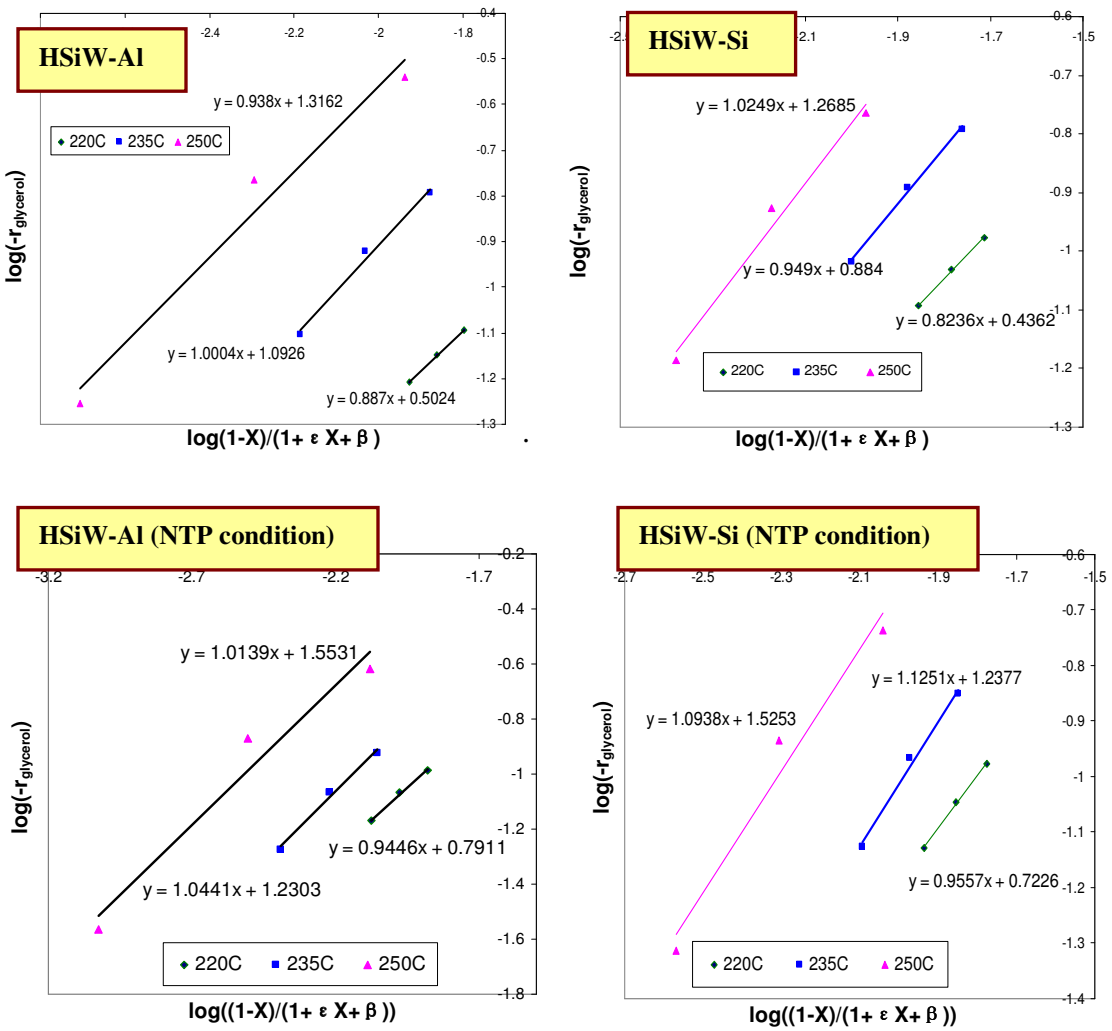

Figure III-2: The plot of log($-r_{glycerol}$) versus log((1-X)/(1+εX+β)

Table III-3: The calculated reaction rate constant k and activation energy E_a

		HSiW-Al		HSiW-Si	
		control	NTP	control	NTP
Temperature	$F_{glycerol}$(mol/s)	k (s^{-1})			
220	2.76E-06	10.64	22.38	8.38	19.58
235	3.68E-06	49.81	72.68	28.68	79.42
250	5.52E-06	78.54	150.94	79.61	158.6
Activation energy (J/mol) E_a		1.435E05	1.367E05	1.610E05	1.499E05

Appendix IV
Comparison of Energy Consumption between the control condition and the NTP condition

Table IV lists the energy requirement for the system corresponding to each temperature increment (in the first row). The numbers were obtained exclusively from heating the substance. We did not include the energy required to heat up the reactor or the energy loss to the environment, which would account for much larger actual energy consumption using regular heating. Based on Figures 4.4B and 4.5B in Chapter 4, under the optimal NTP conditions, the acrolein yield reached equal or higher values as compared to that without NTP at temperatures over 15^{o} C higher. According to energy calculations via the Lissajous figure under the optimal NTP condition (3.78kV/cm for HSiW-Al, 4.58 kV/cm for HSiW-Si), every hour the input energy by NTP was 158.4 J and 225 J for HSiW-Al and HSiW-Si, respectively, which were smaller as compared to the minimal energy requirement for regular heating. These two numbers were calculated from the discharge power, which was calculated via Lissajous figure (Appendix VI).

Table IV: The minimal energy required to heat the substance in the PBR system corresponding to each temperature increment

	Heat capacity J mol^{-1} K^{-1}	**10 ° C** J h^{-1}	**15 ° C** J h^{-1}	**20 ° C** J h^{-1}	**25 ° C** J h^{-1}	**30 ° C** J h^{-1}	**35 ° C** J h^{-1}
Glycerol	218.9	28.36	42.55	56.73	70.91	85.09	99.27
Water	33.6	90.94	136.42	181.89	227.36	272.83	318.30
Argon	20.8	30.53	45.79	61.05	76.31	91.58	106.84
Silica	0.703	24.61	36.91	49.21	61.51	73.82	86.12
Alumina	0.88 **	30.8	46.2	61.6	77	92.4	107.8
Total (in HSiW-Al system)		180.63	270.95	361.27	451.58	541.90	632.22
Total (in HSiW-Si system)		174.44	261.66	348.88	436.10	523.31	610.53

**:http://www.matweb.com/search/datasheet.aspx?matguid=0654701067d147e88e8a38c646dda195&ckck=1

Appendix V
Keggin Structure of Silicotungstic acid

Silicotungstic acid, $H_4SiW_{12}O_{40}$, is a pure Brønsted acid falling within the super-acid category (a super acid is defined as an acid with strength greater than that of 100% H_2SO_4 [113]). It features a so-called Keggin structure, which is the structural form of the Keggin anion (Figure V A). The formula of Keggin anion is $[XM_{12}O_{40}]^{n-}$, where X is the heteroatom (most commonly P^{5+}, Si^{4+}, or B^{3+}) and M is the addenda atom (most commonly Mo or W). Figure V B shows the secondary structure of silicotungstic acid [114].

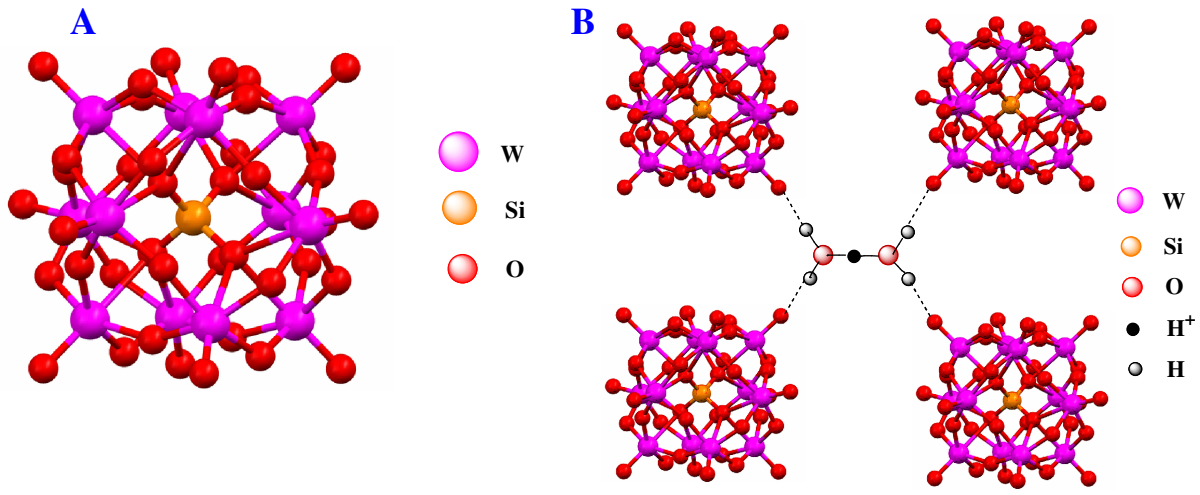

Figure V: Heteropoly anion $SiW_{12}O_{40}^{4-}$ with Keggin structure (A); Secondary structure of silicotungstic acid. Each H_5O_{2+} bridges four Keggin anions (B)

Appendix VI
NTP power calculation based on Lissajous figures

Figure VI-1 is the Lissajous figure for the optimized non-thermal plasma (NTP) for HSiW-Al catalyzed and HSiW-Si catalyzed glycerol dehydration. The calculation of the power calculation is shown as follows.

$$P = C_M f \oint U dU_c = C_M f \cdot Area$$

where f is the frequency, C_M is the capacitance of the capacitor, U is the voltage across the discharge area, U_c is the voltage across the capacitor, and Area is the integrated area of the Lissajous closed loop.

Field strength 3.78 kv/cm:
$$P_1 = C_M f \oint U dU_c = C_M f \cdot Area$$
$$= (2\times10^{-9}\ F)\cdot(1000Hz)\cdot(22.05\times10^{3}V^{2}) = 0.044W$$

Field strength 4.58 kv/cm:
$$P_2 = C_M f \oint U dU_c = C_M f \cdot Area$$
$$= (2\times10^{-9}\ F)\cdot(1000Hz)\cdot(31.35\times10^{3}V^{2}) = 0.063W$$

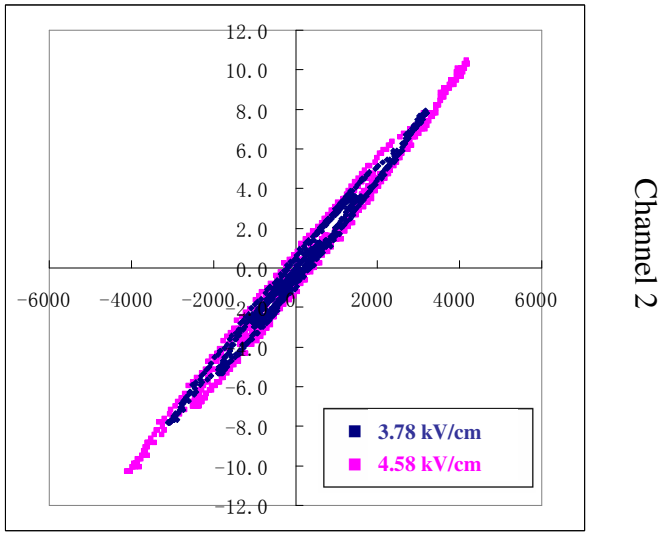

Figure VI-1: Lissajous figure of the non-thermal plasma: optimal conditions for alumina

(3.78 kV/cm) and silica (4.58 kV/cm).

Figure VI-2 is the Lissajous figures for NTP-O_2 coke removal study in the effect of plasma field strength. The calculation of the power calculation is shown as follows. P1', P2', P3', and P4' are related to the field strength of 3.0 kV/cm, 4.8 kV/cm, 6.0 kV/cm and 8.4 kV/cm. respectively.

$$P_1' = C_M f \oint U dU_c = C_M f \cdot Area$$
$$= (2\times10^{-9} F)\cdot(2000Hz)\cdot(1.35\times10^4 V^2) = 0.054W$$
$$P_2' = C_M f \oint U dU_c = C_M f \cdot Area$$
$$= (2\times10^{-9} F)\cdot(2000Hz)\cdot(106.36\times10^3 V^2) = 0.43W$$
$$P_3' = C_M f \oint U dU_c = C_M f \cdot Area$$
$$= (2\times10^{-9} F)\cdot(2000Hz)\cdot(209.38\times10^3 V^2) = 0.84W$$
$$P_4' = C_M f \oint U(U_c) dU_c = C_M f \cdot Area$$
$$= (2\times10^{-9} F)\cdot(2000Hz)\cdot(319.16\times10^3 V^2) = 1.27W$$

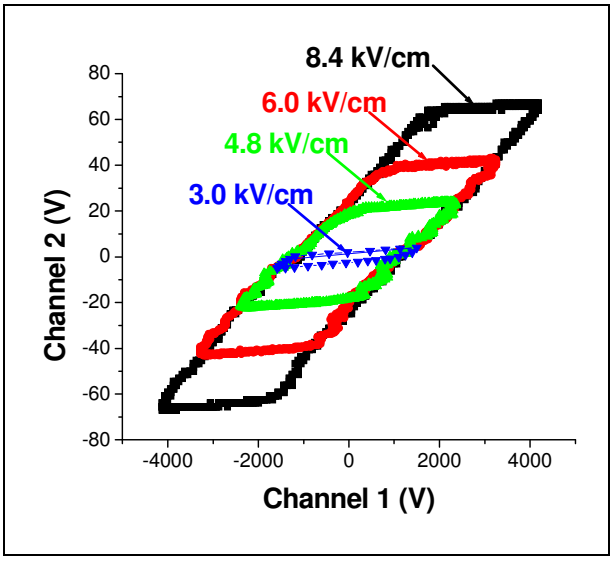

Figure VI-2: Lissajous figure of the non-thermal plasma (NTP) applied to the regeneration study of the NTP field strength

Appendix VII
Flow diagram for ChemBET Pulsar TPR/TPD Analyzer

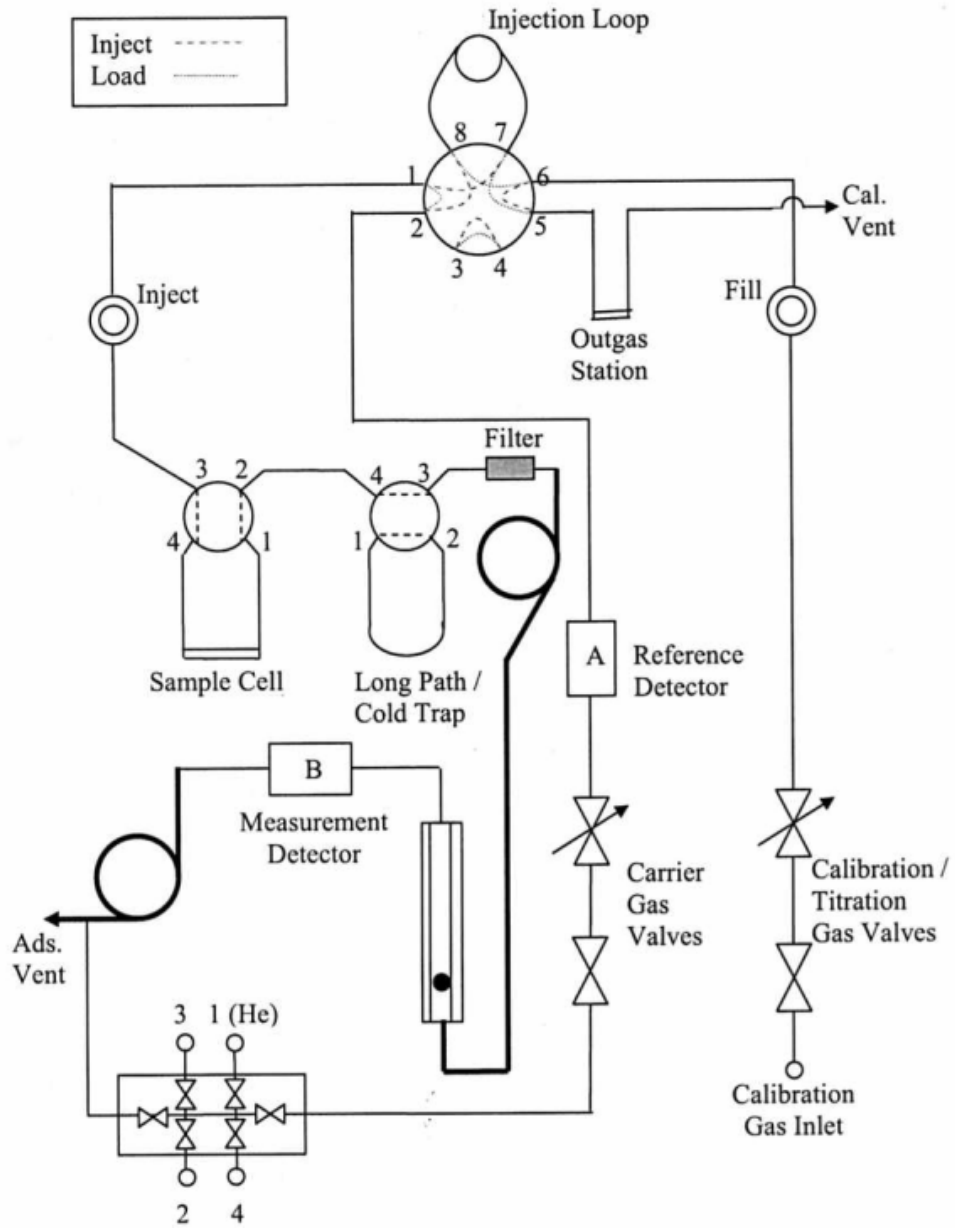

Figure VII: Flow diagram of ChemBET Pulsar TPR/TPD Analyzer [333]

References

1. Etzkorn, W.G., S.E. Pedersen and T.E. Snead, *Acrolein and Derivatives*. 2002, John Wiley & Sons, Inc.
2. Enonik Industries. *Methionine - a success story*. Available from: http://history.evonik.com/sites/geschichte/en/chemicals/inventions/degussa/methionine/pages/default.aspx.
3. JCN Newswire. *Sumitomo chemical doubles production of feed additive methionine*. 2003 [cited 2011 Feburary]; Available from: http://www.japancorp.net/Article.Asp?Art_ID=5235.
4. National Research Council, *Formaldehyde and other aldehydes.* 1981: National Research Council (U.S.). Committee on Aldehydes.
5. Bowmer, K.H. and G.H. Smith, *Herbicides for injection into flowing water: acrolein and endothal-amine.* Week Research, 2006. **24**(3): p. 201 - 211.
6. Szmant, H.H., *Organic building blocks of the chemical industry*. 1989: John Wiley & Sons, Inc. .
7. Ai, M., *Formation of acrolein by the reaction of formaldehyde with ethanol.* Applied Catalysis, 1991. **77**(1): p. 123-132
8. Voisenet, E., *Formation d'acroleine dans la maladie de I'amertume des vins.* Comptes Rendus (Acad. Sci.), 1910. **150**: p. 1614-1616.
9. Serjak, W.C., W.H. Day, J.M. Van Lanen and C.S. Boruff, *Acrolein production by bacteria found in distillery grain mashes.* Applied and Enviromental Microbiology, 1953. **2**(1): p. 14-20.
10. Bauer, R., M. du Toit and J. Kossmann, *Influence of environmental parameters on production of the acrolein precursor 3-hydroxypropionaldehyde by Lactobacillus reuteri DSMZ 20016 and its accumulation by wine lactobacilli.* International Journal of Food Microbiology. **137**(1): p. 28-31.
11. Vollenweider, S. and C. Lacroix, *3-Hydroxypropionaldehyde: applications and perspectives of biotechnological production.* Applied Microbiology and Biotechnology, 2004. **64**(1): p. 16-27.
12. Redtenbacher, J., *Über die Zerlegungsprodukte des Glycerinoxydes durch trockene Destillation.* Ann Chem Pharm, 1843. **47**: p. 113–148.

13. Ai, M., *Formation of acrolein by the reaction of acrolein by the reaction of formaldehyde with ethanol.* Applied Catalysis, 1991. **77**(1): p. 123-132.
14. Brazdil, J.F., *Strategies for the selective catalytic oxidation of alkanes.* Topics in Catalysis, 2006. **38**(4): p. 289-294.
15. Morita, T., M. Konishi, T. Fukuoka, T. Imuraa and D. Kitamoto, *Microbial conversion of glycerol into glycolipid biosurfactants, mannosylerythritol lipids, by a basidiomycete yeast, Pseudozyma antarctica JCM 10317.* Journal of Bioscience and Bioengineering, 2007. **104**(1): p. 78-81
16. Rahmat, N., A.Z. Abdullah and A.R. Mohamed, *Recent progress on innovative and potential technologies for glycerol transformation into fuel additives: A critical review.* Renewable and Sustainable Energy Reviews, 2010. **14**(3): p. 987-1000
17. Morais, S., A.A. Martins and T.M. Mata, *Comparison of allocation approaches in soybean biodiesel life cycle assessment.* Journal of the Energy Institute, 2010. **83**(1): p. 48-55.
18. F.O. Licht Analysts, *F.O. Licht, World Ethanol and Biofuels Report*. 2008. p. 29.
19. F.O. Licht Analysts, *F.O. Licht, World Ethanol and Biofuels Report*. 2009. p. 288.
20. ENERS Energy Concept. *Production of biofuels in the world in 2009*. 2009; Available from: http://www.plateforme-biocarburants.ch/en/infos/production.php?id=biodiesel.
21. Palion, W.J. and S. Malinowski, *Solid catalysts containing silica and alumina.* Reaction Kinetics and Catalysis Letters, 1974. **1**(4): p. 461-465.
22. Ai, M., *Formation of acrylaldehyde by vapor-phase aldol condensation I. Basic oxide catalysts.* Bulletin of Chemical Society of Japan., 1991. **64**: p. 1342-1345.
23. Dumitriu, E., V. Hulea, N. Bilba, G. Carja and A. Azzouz, *Synthesis of acrolein by vapor phase condensation of formaldehyde and acetaldehyde over oxides loaded zeolites.* Journal of Molecular Catalysis, 1993. **79**: p. 175-185.
24. Dumitriu, E., V. Hulea, C. Chelaru, C. Catrinescu, D. Tichit and R. Durand, *Influence of the acid-base properties of solid catalysts derived from hydrotalcite-like compounds on the condensation of formaldehyde and acetaldehyde.* Applied Catalysis A: General, 1999. **178**: p. 145-157.
25. Azzouz, A., D. D. Messad, D. Nistor, C. Catrinescu, A. Zvolinschi and S. Asaftei, *Vapor phase aldol condensation over fully ion-exchanged montmorillonite-rich catalysts.* Applied Catalysis A: General, 2003. **241**(1-2): p. 1-13.
26. Cobzaru, C., S. Oprea, E. Dumitriu and V. Hulea, *Gas phase aldol condensation of lower aldehydes over clinoptilolite rich natural zeolites.* Applied Catalysis A: General, 2008. **351**(2): p. 253-258.
27. Howard, R.F., *Handbook of commercial catalysts: heterogeneous catalysts*. 2000, Boca Raton, Florida: CRC Press LLC.
28. Salehalhamed, Y.A., R.R. Hudgins and P.L. Silveston, *Investigations of catalytic mechanisms for selective propene oxidation in the presence of steam.* Applied Catalysis A: General, 1995. **127**(1-2): p. 177-199.
29. Xie, E.H., Q.L. Zhang and K.T. Chuang, *Role of steam in partial oxidation of*

propylene over a Pd/SDB catalyst. Applied Catalysis A: General, 2001. **220**(1-2): p. 215-221.
30. Redlingshofer, H., O. Krocher, W. Bock, K. Huthmacher and G. Emig, *Catalytic wall reactor as a tool for isothermal investigations in the heterogeneously catalyzed oxidation of propene to acrolein.* Industrial & Engineering Chemistry Research, 2002. **41**(6): p. 1445-1453.
31. Kashiwabara, H. and Y. Nakamura, *Catalysts for oxidation of propylene to acrolein or acrylic acid*. 1968, Asahi Electro-Chemical Co., Ltd.: JP 43024645. p. 8 pp.
32. *Acrolein from propylene*. 1968, (Montecatini Edison S.p.A.). FR 1524744. p. 3 pp.
33. Takayama, Y. and T. Ikeda, *Oxidation catalysts containing tellurium for the preparation of acrolein from propylene*. 1969, Mitsubishi Rayon Co., Ltd.: JP 44013130. p. 4 pp.
34. Tokutaniyama, A., T. Kato and K. Baison, *Acrolein from vapor-phase catalytic oxidation of propylene*. 1969, Asahi Chemical Industry Co., Ltd.: JP 44013130. p. 5 pp.
35. Ikeda, T., H. Ishii and T. Nakano, *Acrolein*. 1969, Mitsubishi Rayon Co., Ltd.: JP 44027202. p. 3 pp.
36. Ito, H., H. Inoue and Y. Nakamura, *Catalytic oxidation of propylenes to acroleins*. 1969, Toa Gosei Chemical Industry Co., Ltd.: JP 44025047. p. 7 pp.
37. Koberstein, E., T. Luessling, E. Noll, H. Suchsland and W. Weigert, *Catalyst for the oxidation of alkenes*. 1970, Deutsche Gold- und Silber-Scheideanstalt vorm. Roessler: ZA 6906179. p. 12 pp.
38. Takenaka, S. and G. Yamaguchi, *Acrolein by propylene oxidation*. 1969, Nippon Kayaku Co., Ltd.: JP 44006245. p. 4 pp.
39. Takenake, S., Y. Kido, T. Shimabara and M. Ogawa, *Oxidation catalyst for propylene*. 1970, Nippon Kayaku Co., Ltd.: DE 2020791. p. 13 pp.
40. Takenaka, S., Y. Kido, T. Shimabara and M. Ogawa, *Catalysts for the oxidation of propylene to acrolein*. 1971, Nippon Kayaku Co., Ltd.: DE 2038749. p. 13 pp.
41. Koshikawa, T., *Acrolein and acrylic acid from propylene*. 1974, Mitsubishi Petrochemical Co., Ltd.: JP 49030308. p. 6 pp.
42. Takenaka, S. and G. Yamaguchi, *Acrolein by catalytic oxidation of propylene*. 1974, Nippon Kayaku Co., Ltd.: JP 49003510. p. 3 pp.
43. Sakakibara, K., I. Abe and K. Matsuoka, *Acrolein from propylene*. 1974, Daicel Ltd.: JP 49075514. p. 6 pp.
44. Ono, T. and Y. Kubokawa, Bulletin of the Chemical Society of Japan, 1982. **55**: p. 1748.
45. Nagai, I., I. Yanagisawa, M. Ninomiya and T. Oohara, *Oxidation of propylene*. 1976, Nippon Shokubai Kagaku Kogyo Co., Ltd., Japan. JP 51004113. p. 4 pp.
46. Fattore, V. and B. Norari, *Acrolein production by the oxidation of propylene*. 1976, Snamprogetti SpA, Italy: DE 2365733 . p. 20 pp Division of Ger. Offen..
47. *Acrolein*. 1980, Ube Industries, Ltd., Japan. JP 55157529. p. 6 pp.

48. *Acrolein*. 1980, Ube Industries, Ltd., Japan. JP 55160737. p. 5 pp.
49. Takata, M., R. Aoki and T. Sato, *Catalyst for oxidation of propylene*. 1983, Nippon Shokubai Kagaku Kogyo Co., Ltd., Japan: DE 3300044. p. 23 pp.
50. Kieser, H., K. Ohl, R. Thaetner, R. Feldhaus and K. Anders, *Selective oxidation catalysts*. 1983, VEB Leuna-Werke "Walter Ulbricht", German Democratic Republic. DD 204406. p. 11 pp.
51. Shiotani, T. and T. Kuroda, *Molybdenum-bismuth-iron-based cylindrical catalysts and their use for synthesis of unsaturated aldehydes and carboxylic acids*. 1994, Mitsubishi Rayon Co, Japan: JP 06210183. p. 5 pp.
52. Shiotani, T. and T. Kuroda, *Manufacture of catalysts for synthesis of unsaturated aldehydes and carboxylic acids*. 1995, Mitsubishi Rayon Co, Japan: JP 07016464. p. 5 pp.
53. Shiotani, T., T. Kuroda and Y. Taniguchi, *Manufacture of oxidation catalysts based on molybdenum, bismuth and iron oxides*. 1996, Mitsubishi Rayon Co, Japan: JP 08024652. p. 6 pp.
54. Tanaka, Y., *Preparation of acrolein from propylene and of mixed metal oxide catalysts used in the preparation of acrolein*. 1996, Daicel Chem, Japan: JP 08040969. p. 5 pp.
55. Chang, T.S., D.H. Cho and D.K. Lee, *Oxidation process and catalyst system for the manufacture of acrolein from propylene*. 2002, Korea Research Institute of Chemical Technology, S. Korea: US 6410800. p. 4 pp.
56. Liu, G., P. Liu, H. Sun and H. Wu, *Catalyst for production of acrolein by direct oxidation of propylene*. 2009, Hefei Haili Scientific Development Co., Ltd., Peop. Rep. China: CN 101402044. p. 7pp.
57. Creten, G., D.S. Lafyatis and G.F. Froment, *Transient kinetics from the tap reactor system - application to the oxidation of propylene to acrolein.* Journal of Catalysis, 1995. **154**(1): p. 151-162.
58. Salehalhamed, Y.A., R.R. Hudgins and P.L. Silveston, *Periodic operation studies on the partial oxidation of propylene to acrolein and acrylic-acid.* Chemical Engineering Science, 1992. **47**(9-11): p. 2885-2890.
59. Bondareva, V.M., T.V. Andrushkevich and Y.D. Pankratiev, *Bond-energy of surface oxygen in multicomponent oxide catalysts for propylene oxidation to acrolein.* Reaction Kinetics and Catalysis Letters, 1986. **32**(1): p. 171-175.
60. Fansuri, H., G.H. Pham, S. Wibawanta, D.K. Zhang and D. French, *The relationship between structural and catalytic activity of alpha and gamma-bismuth-molybdate catalysts for partial oxidation of propylene to acrolein.* Surface Review and Letters, 2003. **10**(2-3): p. 549-553.
61. Hanna, T.A., *The role of bismuth in the SOHIO process.* Coordination Chemistry Review, 2004. **248**: p. 429-440.
62. Patience, G.S. and P.L. Mills, *Modeling of propylene oxidation in a circulating fluidized-bed reactor* in *New Developments in Selective Oxidation II* V.C. Corberan and S.V. Bellon, Editors. 1994. p. 1-18.
63. Leib, T.M., P.L. Mills and J.J. Lerou, *Fast response distributed parameter*

fluidized bed reactor model for propylene partial oxidation using feed-forward neural network methods. Chemical Engineering Science, 1996. **51**(10): p. 2189-2198.
64. Song, K.H., S.E. Han and K.H. Park, *Heat transfer effect of inert gas on multi-tubular reactor for partial oxidation reaction.* Korean Journal of Chemical Engineering, 2001. **18**(2): p. 184-189.
65. Han, S.E., J. Choe, K.H. Song and I.W. Kim, *An influence of the inert gas on the operation and design of a multi-tubular reactor.* Journal of Industrial and Engineering Chemistry, 2003. **9**(3): p. 301-305.
66. Redlingshofer, H., A. Fischer, C. Weckbecker, K. Huthmacher and G. Emig, *Kinetic modeling of the heterogeneously catalyzed oxidation of propene to acrolein in a catalytic wall reactor.* Industrial & Engineering Chemistry Research, 2003. **42**(22): p. 5482-5488.
67. O'Neill, C.M. and E.E. Wolf, *Yield improvements in membrane reactors for partial oxidation reactions.* Industrial & Engineering Chemistry Research, 2006. **45**(8): p. 2697-2706.
68. Yi, X.D., X.B. Zhang, W.Z. Weng and H.L. Wan, *Studies on the reaction pathways for the selective oxidation of propane to acrolein over MoPO/SiO_2 catalyst by IR spectroscopy.* Journal of Molecular Catalysis A: Chemical, 2007. **277**(1-2): p. 202-209.
69. Sinev, M.Y. and O.V. Udalova, *Propane partial oxidation to acrolein over combined catalysts.* Catalysis Letters, 2000. **69**: p. 203-206.
70. Lin, M.H., T.B. Desai, F.W. Kaiser and P.D. Klugherz, *Reaction pathways in the selective oxidation of propane over a mixed metal oxide catalyst.* Catalysis Today, 2000. **61**(1-4): p. 223-229.
71. Conner, J., M. NMontague, S.L. Soled, N.J. Madison, A.J. Signorelli, N.J. Succasunna, B.A. DeRites and N.J. Wayne, *Bismuth-containing mixed oxides of perovskite structure in oxidation of acyclic hydrocarbons.*, in *United States Patent*. 1980, Allied Corportation, Morris Township, Morris County, N.J.: US.
72. Kaddouri, A., C. Mazzocchia and E. Tempesti, *The synthesis of acrolein and acrylic acid by direct propane oxidation with Ni-Mo-Te-P-O catalysts.* Applied Catalysis A: General, 1999. **180**(1-2): p. 271-275.
73. Zhang, X., H.L. Wan and W.Z. Weng, *Reaction pathways for selective oxidation of propane to acrolein over Ce-Ag-Mo-P-O catalysts.* Applied Catalysis A: General, 2009. **353**(1): p. 24-31.
74. Fu, G., X.D. Yi, C.J. Huang, X. Xu, W.Z. Weng, W.S. Xia and H.L. Wan. *Developing selective oxidation catalysts of light alkanes: From fundamental understanding to rational design.* 2007.
75. Zhang, C. and C.R.A. Catlow, *The mechanism of propane oxidation over iron antimony oxide.* Journal of Physical Chemistry C, 2008. **112**(26): p. 9783-9797.
76. Stern, D.L. and R.K. Grasselli, *Reaction network and kinetics of propane oxydehydrogenation over nickel cobalt molybdate.* Journal of Catalysis, 1997. **167**(2): p. 560-569.

77. Savary, L., G. FCOstentin, M.M. Bettahar, A. FGrandin, M. Gubelmann-Bonneau and J.C. Lavalley, *Effects of the structural and cationic properties of $AV_2P_2O_{10}$ solids on propane selective oxidation.* Catalysis Today, 1996. **32**: p. 305-306.
78. Kim, Y.-C., W. Ueda and Y. Moro-oka, *Selective oxidation of propane to acrolein over Ag-doped bismuth vanadomolybdate catalysts.* Journal of the Chemical Society, Chemical Communications 1989: p. 652 - 653.
79. Kim, Y.C., W. Ueda and Y. Moro-oka, *Catalytic Activity of Mixed Metal Oxides for Selective Oxidation of Propane to Acrolein.* Chemistry Letters, 1989. **18**(4): p. 531-534.
80. Kim, Y.-C., Y. Uragami and Y. Moro-oka, *Selective oxidation of propane involving homogeneous and heterogenous steps over multicomponent metal oxide catalysts.* Applied Catalysis, 1991. **70**: p. 175-187.
81. Jiang, H.C., W.M. Lu and H.L. Wan, *Effect of different dopant in the Mo-V-Te-O catalyst on the performance of selective oxidation propane to acrolein.* Chinese Chemical Letters, 2004. **15**(8): p. 977-980.
82. Zhu, Y.H., W.M. Lu, H. Li and H.L. Wan, *Selective modification of surface and bulk V^{5+}/V^{4+} ratios and its effects on the catalytic performance of Mo-V-Te-O catalysts.* Journal of Catalysis, 2007. **246**(2): p. 382-389.
83. Huang, C.J., W. Guo, Y.X. Jin, X.D. Yi, W.Z. Weng and H.L. Wan, *Study on structures and performances of $MoVTeO/SiO_2$ catalysts for selective oxidation of propane to acrolein.* Acta Chimica Sinica, 2004. **62**(18): p. 1701-1705.
84. Huang, C.J., Y.X. Jin, F. Ying and H.L. Wan, *Formation of acrolein in the propane oxidation over $VTeO/SiO_2$ catalysts.* Chemistry Letters, 2006. **35**(6): p. 606-607.
85. Huang, C.J., W. Guo, X.D. Yi, W.Z. Weng and H.L. Wan, *Effect of preparation condition on the performance of silica-supported MoVTeO catalysts for selective oxidation of propane to acrolein.* Catalysis Communications, 2007. **8**(2): p. 162-166.
86. He, Y.M., X.D. Yi, C.J. Huang, F. Ying, X.B. Zhang, W.Z. Weng and H.L. Wan, *Role of Te on selective oxidation of propane to acrolein over $MoBiTeO/SiO_2$ catalysts.* Acta Physico-Chimica Sinica, 2007. **23**(6): p. 851-855.
87. Giordano, J.C., J. Bart, P. Vitarelli and S. Cavallaro, Oxidation Communincations, 1984. **7**: p. 99.
88. Komatsu, T., Y. Uragami and K. Otsuka, *Partial oxidation of propane over B-P oxide catalysts.* Chemisty Letters, 1988: p. 1903-1906.
89. Finocchio, E., G. Busca, V. Lorenzelli and R.J. Willey, *The activation of hydrocarbon C-H bonds over transition-metal oxide catalysts - A FTIR study of hydrocarbon catalytic combustion over $MgCr_2O_4$.* Journal of Catalysis, 1995. **151**(1): p. 204-215.
90. Yang, H.P., Y.N. Fan, J.M. Wu and Y. Chen, *Structure and properties of BiCeVMoO mixed metal oxides catalysts for selective oxidation of propane.* Journal of Molecular Catalysis A: Chemical, 2005. **227**(1-2): p. 279-283.
91. Xin, Z., W. Hui-Lin, W.Z. Weng, L.F. Yang and X.D. Yi, *Role of Ce on selective*

oxidation of propane to acrolein over Ce-Ag-Mo-P-O catalysts. Acta Physico-Chimica Sinica, 2003. **19**(6): p. 492-497.
92. Ulgen, A. and W. Hoelderich, *Conversion of glycerol to acrolein in the presence of WO_3/ZrO_2 catalysts.* Catalysis Letters, 2009. **131**(1-2): p. 122-128.
93. Wohl, A. and B. Mylo, *Preparation of Acrolein.* Berichte der Deutschen Chemischen Gesellschaft, 1912. **45**: p. 2046-54.
94. Bergh, G.F., *Preparation of Acrolein.* 1910. **79**: p. 351-7.
95. Senderens, J.B., *Preparation of Acrolein.* 1910. **151**: p. 530-2.
96. Moureu, C. and A. Lepape, *Acrolein*. 1920: GB.
97. Ramayya, S., A. Brittain, C. DeAlmeida, W. Mok and M.J. Antal, Jr., *Acid-catalyzed dehydration of alcohols in supercritical water.* Fuel, 1987. **66**(10): p. 1364-71.
98. Buhler, W., E. Dinjus, H.J. Ederer, A. Kruse and C. Mas, *Ionic reactions and pyrolysis of glycerol as competing reaction pathways in near- and supercritical water.* Journal of Supercritical Fluids, 2002. **22**(1): p. 37-53.
99. Ott, L., M. Bicker and H. Vogel, *Catalytic dehydration of glycerin to acrolein in near- and supercritical water.* Chemie Ingenieur Technik, 2004. **76**(9): p. 1292.
100. Watanabe, M., T. Iida, Y. Aizawa, T.M. Aida and H. Inomata, *Acrolein synthesis from glycerol in hot-compressed water.* Bioresource Technology, 2006. **98**(6): p. 1285-1290.
101. Atia, H., U. Armbruster and A. Martin, *Dehydration of glycerol in gas phase using heteropolyacid catalysts as active compounds.* DGMK Tagungsbericht, 2008. **2008-3**(Preprints of the DGMK-Conference "Future Feedstocks for Fuels and Chemicals", 2008): p. 177-184.
102. Tsukuda, E., S. Sato, R. Takahashi and T. Sodesawa, *Production of acrolein from glycerol over silica-supported heteropoly acids.* Catalysis Communications, 2007. **8**(9): p. 1349-1353.
103. Yan, W. and G.J. Suppes, *Low-pressure packed-bed gas-phase dehydration of glycerol to acrolein.* Industrial & Engineering Chemistry Research, 2009. **48**(7): p. 3279-3283.
104. Hoyt, H.E. and T.H. Manninen, *Acrolein from glycerol.* 1951, U. S. Industrial Chemicals, Inc.: US.
105. Suzuki, N. and M. Takahashi, *Preparation of acrolein by dehydration of glycerin using acidic solid catalysts in solvents*. 2006, Kao Corp., Japan: JP 2006290815. p. 7pp.
106. Tanabe, K., M. Misono, M. Ono and H. Hattori, *New solid acids and bases. Their catalytic properties*. Studies in surface science and catalysis. Editors: B. Delmon and J.T. Yates. 1989, Tokyo, JP: Elsevier.
107. Li, X., C. Zhang, C. Qin, C. Chen and J. Shao, *Process for preparing acrolein via dehydration of glycerol*. 2007, Shanghai Huayi Acrylic Acid Co., Ltd., Peop. Rep. China: CN 101070276. p. 10pp.
108. Corma, A., G.W. Huber, L. Sauvanaud and P. O'Connor, *Biomass to chemicals: Catalytic conversion of glycerol/water mixtures into acrolein, reaction network.*

Journal of Catalysis, 2008. **257**(1): p. 163-171.
109. Goehlich, M., K. Raeuchle, H. Toufar and W. Reschetilowski, *From biomass to value-added chemicals: conversion of glycerol over modified zeolites.* DGMK Tagungsbericht, 2008. **2008-3**(Preprints of the DGMK-Conference "Future Feedstocks for Fuels and Chemicals", 2008): p. 209-215.
110. Kim, Y.T., K.-D. Jung and E.D. Park, *Gas-phase dehydration of glycerol over ZSM-5 catalysts.* Microporous and Mesoporous Materials, 2010. **131**(1-3): p. 28-36.
111. Okuno, M., E. Matsunami, T. Takahashi, H. Kasuga, M. Okada and M. Kirishiki, *Production method of acrolein by dehydration reaction of glycerin*. 2007, Nippon Shokubai Co., Ltd., Japan: WO 2007132926. p. 55 pp.
112. Arita, Y., T. Takahashi, M. Okada and T. Moriguchi, *Method for production of acrolein*. 2008, Nippon Shokubai Co., Ltd., Japan: WO 2008140118. p. 29pp.
113. Timofeeva, M.N., *Acid catalysis by heteropoly acids.* Applied Catalysis A: General, 2003. **256**: p. 19-35.
114. Wu, Y., X.K. Ye, X.G. Yang, X.P. Wang, W.L. Chu and Y.C. Hu, *Heterogenization of heteropolyacids: A general discussion on the preparation of supported acid catalysts.* Industrial & Engineering Chemistry Research, 1996. **35**(8): p. 2546-2560.
115. Kozhevnikov, I.V., *Sustainable heterogeneous acid catalysis by heteropoly acids.* Journal of Molecular Catalysis A: Chemical, 2007. **262**(1-2): p. 86-92.
116. Kozhevnikov, I.V., *Catalysis by heteropoly acids and multicoponent polyoxometalates in liquid-phase reactions.* Chemical Reviews, 1998. **98**: p. 171-198.
117. Bardin, B.B. and R.J. Davis, *Effect of water on silica-supported phosphotungstic acid catalysts for 1-butene double bond shift and alkane skeletal isomerization.* Applied Catalysis A: General, 2000. **200**(1-2): p. 219-231.
118. Chu, W.L., X.G. Yang, Y.K. Shan, X.K. Ye and Y. Wu, *Immobilization of the heteropoly acid (HPA) $H_4SiW_{12}O_{40}$ (SiW_{12}) on mesoporous molecular sieves (HMS and MCM-41) and their catalytic behavior.* Catalysis Letters, 1996. **42**(3-4): p. 201-208.
119. Michel J. Verhoefa, P., J. Kooyman, J.A. Peters and H.v. Bekkum, *A study on the stability of MCM-41-supported heteropoly acids under liquid- and gas-phase esterification conditions.* Microporous and Mesoporous Materials, 1999. **27**(2-3): p. 365-371.
120. Izumi, Y., R. Hasebe and K. Urabe, *Catalysis by heterogeneous supported heteropoly acid.* Journal of Catalysis, 1983. **84**(2): p. 402-409
121. Nowinska, K., R. Field and J. Adamiec, *Catalytic activity of supported heteropoly acids for reactions requiring strong acid centres.* Journal of the Chemical Society, Faraday Transactions, 1991. **87**(5): p. 749-753.
122. Ning, L., Y. Ding, W. Chen, L. Gong, R. Lin, Y. Lu and Q. Xin, *Glycerol dehydration to acrolein over activated carbon-supported silicotungstic acids.* Cuihua Xuebao, 2008. **29**(3): p. 212-214.

123. Kozhevnikov, I.V., *Catalysis by heteropoly acids and multicomponent polyoxometalates in liquid-phase reactions.* Chemical Reviews, 1998. **98**(1): p. 171-198.
124. Dubois, J.-L., Y. Magatani and K. Okumura, *Production of acrylic acid from acrolein prepared by dehydration of glycerol in the presence of heteropoly acid catalysts.* 2009, Arkema France, France: WO 2009128555. p. 26pp.
125. Dubois, J.-L., Y. Magatani and K. Okumura, *Process for manufacturing acrolein from glycerol in the presence of heteropoly acid catalysts*. 2009, Arkema France, France: WO 2009127889. p. 25pp.
126. Chai, S.-H., H.-P. Wang, Y. Liang and B.-Q. Xu, *Sustainable production of acrolein: Preparation and characterization of zirconia-supported 12-tungstophosphoric acid catalyst for gas-phase dehydration of glycerol.* Applied Catalysis A: General, 2009. **353**(2): p. 213-222.
127. Alhanash, A., E.F. Kozhevnikova and I.V. Kozhevnikov, *Gas-phase dehydration of glycerol to acrolein catalysed by caesium heteropoly salt.* Applied Catalysis A: General, 2010. **378**(1): p. 11-18.
128. Chai, S.-H., H.-P. Wang, Y. Liang and B.-Q. Xu, *Sustainable production of acrolein: Gas-phase dehydration of glycerol over Nb_2O_5 catalyst.* Journal of Catalysis, 2007. **250**(2): p. 342-349.
129. Wang, F., J.-L. Dubois and W. Ueda, *Catalytic dehydration of glycerol over vanadium phosphate oxides in the presence of molecular oxygen.* Journal of Catalysis, 2009. **268**(2): p. 260-267.
130. Suprun, W., M. Lutecki, T. Haber and H. Papp, *Acidic catalysts for the dehydration of glycerol: Activity and deactivation.* Journal of Molecular Catalysis A Chemical, 2009. **309**(1-2): p. 71-78.
131. Liu, Q., Z. Zhang, Y. Du, J. Li and X. Yang, *Rare earth pyrophosphates: effective catalysts for the production of acrolein from vapor-phase dehydration of glycerol.* Catalysis Letters, 2009. **127**(3-4): p. 419-428.
132. Cheng, L. and X.P. Ye, *A DRIFTS Study of Catalyzed Dehydration of Alcohols by Alumina-Supported Heteropoly Acid.* Catalysis Letters, 2009. **130**(1-2): p. 100-107.
133. Yoda, E. and A. Ootawa, *Dehydration of glycerol on H-MFI zeolite investigated by FT-IR.* Applied Catalysis A: General, 2009. **360**(1): p. 66-70.
134. Pathak, K., K.M. Reddy, N.N. Bakhshi and A.K. Dalai, *Catalytic conversion of glycerol to value added liquid products.* Applied Catalysis A: General, 2010. **372**(2): p. 224-238.
135. Kuba, M. and J.-L. Dubois, *Glycerol to acrolein - as fast as possible.* Speciality Chemicals Magazine, 2009. **29**(7): p. 42-43.
136. Chai, S.-H., H.-P. Wang, Y. Liang and B.-Q. Xu, *Sustainable production of acrolein: investigation of solid acid-base catalysts for gas-phase dehydration of glycerol.* Green Chemistry, 2007. **9**(10): p. 1130-1136.
137. Chai, S.-H., H.-P. Wang, Y. Liang and B.-Q. Xu, *Sustainable production of acrolein: Gas-phase dehydration of glycerol over Nb_2O_5 catalyst.* Journal of

Catalysis, 2007. **250**(2): p. 342-349.
138. Zhou, C.-J., C.-J. Huang, W.-G. Zhang, H.-S. Zhai, H.-L. Wu and Z.-S. Chao, *Synthesis of micro- and mesoporous ZSM-5 composites and their catalytic application in glycerol dehydration to acrolein.* Studies in Surface Science and Catalysis, 2007. **165**(Recent Progress in Mesostructured Materials): p. 527-530.
139. Chai, S.-H., H.-P. Wang, Y. Liang and B.-Q. Xu, *Sustainable production of acrolein: gas-phase dehydration of glycerol over 12-tungstophosphoric acid supported on ZrO_2 and SiO_2.* Green Chemistry, 2008. **10**(10): p. 1087-1093.
140. Li, X., C. Qin, C. Chen and J. Shao, *Method for preparation of acrolein by catalytic dehydration of glycerol with macroporous Al_2O_3 as catalyst*. 2009, Shanghai Huayi Acrylic Acid Co., Ltd., Peop. Rep. China: CN 101580461. p. 10pp.
141. Deleplanque, J., J.L. Dubois, J.F. Devaux and W. Ueda, *Production of acrolein and acrylic acid through dehydration and oxydehydration of glycerol with mixed oxide catalysts.* Catalysis Today, 2010.
142. Jia, C.-J., Y. Liu, W. Schmidt, A.-H. Lu and F. Schueth, *Small-sized HZSM-5 zeolite as highly active catalyst for gas phase dehydration of glycerol to acrolein.* Journal of Catalysis, 2010. **269**(1): p. 71-79.
143. Dubois, J.-L., *Process for manufacturing acrolein from glycerol.* 2010, Arkema France, Fr.: WO 2010046227. p. 27pp.
144. Wang, F., J.-L. Dubois and W. Ueda, *Catalytic performance of vanadium pyrophosphate oxides (VPO) in the oxidative dehydration of glycerol.* Applied Catalysis A: General, 2010. **376**(1-2): p. 25-32.
145. Atia, H., U. Armbruster and A. Martin, *Dehydration of glycerol in gas phase using heteropolyacid catalysts as active compounds.* Journal of Catalysis, 2008. **258**(1): p. 71-82.
146. Arita, Y., H. Tsuneki, H. Kasuga, M. Okada and M. Kirishiki, *Environment-friendly method for producing acrolein and glycerin-containing composition*. 2008, Nippon Shokubai Co., Ltd., Japan: WO 2008066082. p. 46 pp.
147. Ohara, T., H. Sato, N. Shimizu, G. Prescher, H. Schwind and O. Weiberg, *Acrolein and methacrolein*, in *Ullmann's Encyclopedia of Industrial Chemistry*, W. Gerhartz, et al., Editors. 1985, VCH.
148. Matar, S. and L.F. Hatch, *Chemistry of petrochemical processes*. 1994, Houston, TX: Gulf Publishing Company.
149. *Acrolein and derivatives*, in *Kirk-Othmer Encyclopedia of Chemical Technology*. 1978, Wiley-interscience.
150. Weissermel, K., *Industrial organic chemistry: Important raw materials and intermediates*. 1978: Verlag Chemie, Weinheim, New York.
151. Hess, L.G., A.N. Kurtz and D.B. Stanton, *Kirk-Othmer Encyclopedia of chemical technology*. 3rd ed. Acrolein and derivatives, ed. G.J. Bushey and A. Klingsberg. Vol. 1. 1978: John Wiley & Sons.
152. Hermann, B.G. and M. Patel, *Today's and tomorrow's bio-based bulk chemicals from white biotechnology - A techno-economic analysis.* Applied Biochemistry

and Biotechnology, 2007. **136**(3): p. 361-388.
153. ICIS. *Propylene prices and pricing information*. 2011 [cited 2011 March, 2011]; Available from: http://www.icis.com/v2/chemicals/9076454/propylene/pricing.html.
154. ICIS. *Sample report: Glycerin (US Gulf)*. 2010 [cited 2011 March 2011]; Available from: http://www.icispricing.com/il_shared/Samples/SubPage170.asp.
155. Johnson, D.T. and K.A. Taconi, *The glycerin glut: Options for the value-added conversion of crude glycerol resulting from biodiesel production.* Environmental Progress, 2007. **26**(4): p. 338–348.
156. Voegele, E., *Legislating an Incentive*, in *Biorefining*. November 03, 2010.
157. Dubois, J.-L., *Acrolein Preparation Method*. 2007, Arkema France US
158. Bertolini, N. and N. Ferlazzo, *Supported catalyst for the oxidation of acrolein into acrylic acid*. 1981, Euteco Impianti S.p.A., Milan, Italy: US. p. 6pp.
159. Hammon, U., K. Herzog and H.-P. Neumann, *Catalytic gas-phase oxidation of acrolein to acrylic acid*. 1993, BASF Aktiegesellschaft, Ludwigshafen, Germany: US. p. 4pp.
160. Ruppel, W., U. Wegerle, A. Tenten and U. Hammon, *Catalytic gas-phase oxidation of acrolein to acrylic acid*. 1998, BASF Aktiengesellschaft, Ludwigshafen, Germany: US. p. 4pp.
161. Unverricht, S., H. Arnold, A. Tenten and U. Hammon, *Method for the catalytic gas phase oxidation of acrolein into acrylic acid*. 2002, BASF Aktiengesellschaft, Ludwifshafen, (DE): US. p. 9pp.
162. Reisch, M.S., *Advancing Biomaterials* Chemical & Engineering News, 2010. **88**(11): p. 12.
163. Reisch, M.S., *Arkema Pushes Into Biobased Acrylics---French chemical firm ramps up effort to commercialize acrylic acid based on glycerin.* Chemical & Engineering News, 2010. **88**(21): p. 20-21.
164. Coons, R., *Arkema Finds Glycerol-to-Acrylic Acid Catalysts; Demo-Scale Plant Possible*, in *Chemical Week*. April 10, 2009.
165. Alperowicz, N., *Shokubai Advances Glycerine-to-Acrylic Acid Process*, in *Chemicalweek*. December 1, 2009.
166. Fridman, A., *Plasma Chemistry*. 2008: Cambridge University Press.
167. Naidu, M.S. and V. Kamaraju, *High Voltage Engineering, 2nd ed.* 1995: McGraw Hill.
168. Eliasson, B. and U. Kogelschatz, *Modeling And Applications Of Silent Discharge Plasmas.* IEEE Transactions on Plasma Science, 1991. **19**(2): p. 309-323.
169. Konelschatz, U., B. Eliasson and W. Egli, *Dielectric-Barrier Discharges. Principle and Applications.* Journal de Physique, 1997. **IV**(7).
170. Nehra, V., A. Kumar and H.K. Dwivedi, *Atmospheric non-thermal plasma sources.* International Journal of Engineering, 2008. **2**(1): p. 53-64.
171. Borcia, G., A. Chiper and I. Rusu, *Using a He + N2 dielectric barrier discharge for the modification of polymer surface properties.* Plasma Sources Science and Technology 2006. **15**(4): p. 849.

172. Bromberg, L., D.R. Cohn, A. Rabinovich and N. Alexeev, *Plasma catalytic reforming of methane.* International Journal of Hydrogen Energy, 1999. **24**(12): p. 1131-1137.
173. Esena, P., C. Riccardi, S. Zaninia, M. Tontini, G. PolettiF and F. Orsini, *Surface modification of PET film by a DBD device at atmospheric pressure.* Surface and Coatings Technology, 2005. **200**(1-4): p. 664-667.
174. Kraus, M., B. Eliasson, U. Kogelschatz and A. Wokaun, *CO_2 reforming of methane by the combination of dielectric-barrier discharges and catalysis.* Physical Chemistry Chemical Physics, 2001. **3**(3): p. 294-300.
175. Manley, T.C., *The electric characteristics of the ozonator discharge.* Transactions of the Electrochemical Society, 1943. **84**(1): p. 12.
176. Subrahmanyam, C., D.A. Bulushev and L. Kiwi-Minsker, *Dynamic behaviour of activated carbon catalysts during ozone decomposition at room temperature.* Applied Catalysis B: Environmental, 2005. **61**(1-2): p. 98-106.
177. Altimir, N., P. Kolari, J.P. Tuovinen, T. Vesala, J. Back, T. Suni, M. Kulmala and P. Hari, *Foliage surface ozone deposition: a role for surface moisture?* Biogeosciences, 2006. **3**(2): p. 209-228.
178. Shoyama, T. and Y. Yoshioka, *Theoretical study of methods for improving the energy efficiency of NO_x removal from diesel exhaust gases by silent discharge.* Electrical Engineering in Japan, 2007. **161**(3): p. 1-9.
179. Zhu, T., J. Li, Y.Q. Jin, Y.H. Liang and G.D. Ma, *Gaseous phase benzene decomposition by non-thermal plasma coupled with nano titania catalyst.* International Journal of Environmental Science and Technology, 2009. **6**(1): p. 141-148.
180. Liu, C.J., G.H. Xu and T.M. Wang, *Non-thermal plasma approaches in CO_2 utilization.* Fuel Processing Technology, 1999. **58**(2-3): p. 119-134.
181. Liu, C.-j., G.-h. Xu and T. Wang, *Non-thermal plasma approaches in CO_2 utilization.* Fuel Processing Technology, 1999. **58**(2-3): p. 119-134.
182. Kogelschatz, U. *Twenty years of Hakone symposia: From basic plasma chemistry to billion dollar markets*. 2007: Wiley-V C H Verlag Gmbh.
183. Suhr, H., *Application of nonequilibrium plasmas in organic chemistry.* Plasma Chemistry and Plasma Processing, 1983. **3**(1): p. 1-61.
184. Chen, H.L., H.M. Lee, S.H. Chen, Y. Chao and M.B. Chang, *Review of plasma catalysis on hydrocarbon reforming for hydrogen production-Interaction, integration, and prospects.* Applied Catalysis B: Environmental, 2008. **85**(1-2): p. 1-9.
185. Van Durme, J., J. Dewulf, C. Leys and H. Van Langenhove, *Combining non-thermal plasma with heterogeneous catalysis in waste gas treatment: A review.* Applied Catalysis B: Environmental, 2008. **78**(3-4): p. 324-333.
186. Khoshtinat, M., N.A.S. Amin and I. Noshadi, *A review of methanol production from methane oxidation via non-thermal plasma reactor.* World Academy of Science, Engineering and Technology, 2010. **62**: p. 354-358.
187. Indarto, A., *A review of direct methane conversion to methano by dielectric*

barrier discharge. IEEE Transactions on Dielectrics and Electrical Insulation, 2008. **15**(4): p. 1038-1043.
188. Pietruszka, B. and M. Heintze, *Methane conversion at low temperature: the combined application of catalysis and non-equilibrium plasma.* Catalysis Today, 2004. **90**(1-2): p. 151-158.
189. Petitpas, G., J.D. Rollier, A. Darmon, J. Gonzalez-Aguilar, R. Metkemeijer and L. Fulcheri, *A comparative study of non-thermal plasma assisted reforming technologies.* International Journal of Hydrogen Energy, 2007. **32**(14): p. 2848-2867.
190. Yang, Y., *Methane conversion and reforming by nonthermal plasma on pins.* Industrial & Engineering Chemistry Research, 2002. **41**(24): p. 5918-5926.
191. Istadi and N.A.S. Amin, *Co-generation of synthesis gas and C2C hydrocarbons from methane and carbon dioxide in a hybrid catalytic-plasma reactor: A review.* Fuel, 2006. **85**: p. 577–592.
192. Rajanikanth, B.S., D. Sinha and P. Emmanuel, *Discharge plasma assisted adsorbents for exhaust treatment: A comparative analysis on enhancing NO_x removal.* Plasma Science & Technology, 2008. **10**(3): p. 307-312.
193. Kwak, J.H., C.H.F. Peden and J. Szanyi, *Non-thermal plasma-assisted NO_x reduction over Na-Y zeolites: the promotional effect of acid sites.* Catalysis Letters, 2006. **109**(1-2): p. 1-6.
194. McAdams, R., P. Beech and J.T. Shawcross, *Low temperature plasma assisted catalytic reduction of NOx in simulated marine diesel exhaust.* Plasma Chemistry and Plasma Processing, 2008. **28**(2): p. 159-171.
195. Miessner, H., K.P. Francke, R. Rudolph and T. Hammer, *NO_x removal in excess oxygen by plasma-enhanced selective catalytic reduction.* Catalysis Today, 2002. **75**(1-4): p. 325-330.
196. Hammer, T., *Non-thermal plasma application to the abatement of noxious emissions in automotive exhaust gases.* Plasma Sources Science & Technology, 2002. **11**(3A): p. A196-A201.
197. Locke, B.R., M. Sato, P. Sunka, M.R. Hoffmann and J.S. Chang, *Electrohydraulic discharge and non-thermal plamsma for water treatment.* Industrial and Engineering Chemistry Research, 2006. **45**: p. 882-905.
198. Lyubochko, V.A., V.V. Malikov, O.G. Parfenov and N.V. Belousova, *Reduction of aluminum oxide in a nonequilibrium hydrogen plasma.* Journal of Engineering Physics and Thermodynamics, 2000. **73**(3): p. 568-572.
199. Bullard, D.E. and D.C. Lynch, *Reduction of titanium dioxide in a nonequilibrium hydrogen plasma.* Metallurgical and Materials Transactions B, 1997. **28**(6): p. 1069-1080.
200. Getty, J.D., *How Plasma-Enhanced Surface Modification Improves the Production of Microelectronics and Optoelectronic.* Chip Scale Review, 2002: p. 72-73.
201. Sekimoto, H., T. Uda, Y. Nose, S. Sato, H. Kakiuchi and Y. Awakura, *Reduction of titanium oxide in the presence of nickel by nonequilibrium hydrogen gas.*

Materials Research Society, 2009. **24**(7): p. 2391-2399.
202. Watanabe, T., M. Soyama, A. Kanzawa, A. Takeuchic and M. Koike, *Reduction and separation of silica-alumina mixture with argon–hydrogen thermal plasmas.* Thin Solid Films, 1999. **345**(1): p. 161-166.
203. Kim, S.-S., H. Lee, B.-K. Na and H.K. Song, *Plasma-assisted reduction of supported metal catalyst using atmospheric dielectric-barrier discharge.* Catalysis Today, 2003. **89**(1-2): p. 193-200.
204. Song, H.K., H. Lee, J. Choi, G. Yang, S. Kim and B. Na, *Reduction method of catalysts using non-thermal plasma*. 2005, Korea Institute of Science and Technology, Seoul, KR: US 20050032626. p. 5 pp.
205. Liu, C.J., D.G. Cheng, Y.P. Zhang, K.L. Yu, Q. Xia, J.G. Wang and X.L. Zhu, *Remarkable Enhancement in the Dispersion and Low-Temperature Activity of Catalysts Prepared via Novel Plasma Reduction-Calcination Method.* Catalysis Surveys from Asia, 2004. **8**(2): p. 111-118.
206. Liu, C.J., G.P. Vissokov and B.W.L. Jang. *Catalyst preparation using plasma technologies*. 2002: Elsevier Science Bv.
207. Kizling, M.B. and S.G. Jaras, *A review of the use of plasma techniques in catalyst preparation and catalytic reactions.* Applied Catalysis A: General, 1996. **147**(1): p. 1-21.
208. Morent, R., N. De Geyter, J. Verschuren, K. De Clerck, P. Kiekens and C. Leys, *Non-thermal plasma treatment of textiles.* Surface & Coatings Technology, 2008. **202**(14): p. 3427-3449.
209. Wu, H., Y. Guo, J. Zhang and J. Yu, *Study on surface modification of soybean protein fiber with dielectric barrier discharge plasma.* Fangzhi Xuebao, 2004. **25**(5): p. 15-16.
210. Liu, C., N. Cui, N.M.D. Brown and B.J. Meenan, *Effects of DBD plasma operating parameters on the polymer surface modification.* Surface and Coatings Technology, 2004. **185**(2-3): p. 311-320.
211. Pappas, D.D., A.A. Bujanda, J.A. Orlicki and R.E. Jensen, *Chemical and morphological modification of polymers under a helium-oxygen dielectric barrier discharge.* Surface and Coatings Technology, 2008. **203**(5-7): p. 830-834.
212. Park, W.J., S.G. Yoon, W.S. Jung and D.H. Yoon, *Effect of dielectric barrier discharge on surface modification characteristics of polyimide film.* Surface and Coatings Technology, 2007. **201**(9-11): p. 5017-5020.
213. Ren, C.-s., H. Yu, J.-l. Zhang, D.-z. Wang and T.-c. Ma, *Surface energy modification of polyethylene by dielectric barrier discharge (DBD).* Dalian Ligong Daxue Xuebao, 2004. **44**(1): p. 31-34.
214. Seebock, R., H. Esrom, M. Charbonnier, M. Romand and U. Kogelschatz, *Surface modification of polyimide using dielectric barrier discharge treatment.* Surface and Coatings Technology, 2001. **142-144**: p. 455-459.
215. Tang, X., Q. Gao and X. Feng, *Atmospheric dielectric barrier discharge and its application to surface modification of blood-filtering nonwoven fabrics.* Indian Journal of Fibre & Textile Research, 2006. **31**(3): p. 432-438.

216. Upadhyay, D.J., N.-Y. Cui, B.J. Meenan and N.M.D. Brown, *The effect of dielectric barrier discharge configuration on the surface modification of aromatic polymers.* Journal of Physics D Applied Physics, 2005. **38**(6): p. 922-929.
217. Wang, C. and X. He, *Polypropylene surface modification model in atmospheric pressure dielectric barrier discharge.* Surface and Coatings Technology, 2006. **201**(6): p. 3377-3384.
218. Alexandrov, S.E. and M.L. Hitchman, *Chemical vapor deposition enhanced by atmospheric pressure non-thermal non-equilibrium plasmas.* Chemical Vapor Deposition, 2005. **11**(11-12): p. 457-468.
219. Meichsner, J., M. Schmidt, R. Schneider and H. Wagner, *Non-thermal Plasma Chemistry and Physics.* 2007.
220. Ge, Y.J., G.Q. Zhang, Y.M. Liu, X.G. Guo and Z.F. Zhao, *Study on the surface modification of nanometer carbon particles in atmospheric plasma.* Acta Metallurgica Sinica (English Letters), 2002. **15**(2): p. 177-181.
221. Gessner, C., V. Bartels, T. Betker, U. Matucha, C. Penache and C.-P. Klages, *Surface modification for biomedical purposes utilizing dielectric barrier discharges at atmospheric pressure.* Thin Solid Films, 2004. **459**(1-2): p. 118-121.
222. Bai, M., X. Bai, Z. Zhang and M. Bai, *Synthesis of Ammonia in a Strong Electric Field Discharge at Ambient Pressure.* Plasma Chemistry and Plasma Process, 2000. **20**(4): p. 511-520.
223. Panteleev, V.I., *Electro-Ionization Synthesis of Chemical Compounds*. 1978, Lebedev Physical Institute of USSR Academy of Sciences: Moscow.
224. Rusanov, V.D., Fridman, A., *Physics of Chemically Active Plasma*. 1984, Moscow. Nauka (Science).
225. Tsyganenko, A.A., E.N. Storozheva, O.V. Manoilova, T. Lesage, M. Daturi and J.-C. Lavalley, *Brønsted acidity of silica silanol groups induced by adsorption of acids.* Catalysis Letters, 2000. **70**: p. 159-163.
226. Levchenko, A.A., P. Jain, O. Trofymluk, P. Yu, A. Navrotsky and S. Sen, *Nature of molecular rotation in supercooled glycerol under nanoconfinement.* Journal of Physical Chemistry, 2010. **114**(8): p. 3070–3074.
227. Tomin, V.I. and K. Hubis, *Instantaneous emission spectra and molecular rotation of n-dimethylaminobenzonitrile fluorescing in the long-wavelength spectral range.* Optics and Spectroscopy, 2005. **100**(1): p. 65-74.
228. Hao, L. and D.G. Leaist, *Large soret effect for silicotungstic acid in a supporting electrolyte: 9% Change in concentration per degree.* Journal of Physical Chemistry, 1994. **98**: p. 13741-13744.
229. Wolf, E.E. and E.E. Petersen, *Catalysts deactivation by coking* Catalysis Reviews: Science and Engineering,. **24**(3): p. 329 - 371.
230. Tanabe, K., *Solid acids and bases: their catalytic properties.* Studies in surface sciences and catalysis. 1989, Tokyo: Elsevier.
231. Holzer, F., F.D. Kopinke and U. Roland, *Influence of ferroelectric materials and catalysts on the performance of non-thermal plasma (NTP) for the removal of air*

pollutants. Influence of ferroelectric materials and catalysts on the performance of non-thermal plasma (NTP) for the removal of air pollutants, 2005. **25**(6): p. 595-611.
232. Holzer, F., F.D. Kopinke and U. Roland, *Influence of ferroelectric materials and catalysts on the performance of non-thermal plasma (NTP) for the removal of air pollutants.* Plasma Chemistry and Plasma Processing, 2005. **25**(6): p. 595-611.
233. Song, H.K., H. Lee, J.-W. Choi and B.-k. Na, *Effect of Electrical Pulse Forms on the CO_2 Reforming of Methane Using Atmospheric Dielectric Barrier Discharge.* Plasma Chemistry and Plasma Processing, 2004. **24**(1): p. 57-72.
234. Lee, H., C.-H. Lee, J.-W. Choi and H.K. Song, *The Effect of the Electric Pulse Polarity on CO_2 Reforming of CH4 Using Dielectric Barrier Discharge.* Energy & Fuels, 2007. **21**(1): p. 23-29.
235. Cormier, J.M., I. Rusu and A. Kaminska, *On the use of electric discharge reactors for the syngas production by steam reforming.* High Temperature Material Processes, 2002. **6**(4): p. 421-429.
236. Nair, S.A., T. Nozaki and K. Okazaki, *Methane oxidative conversion pathways in a dielectric barrier discharge reactor-Investigation of gas phase mechanism.* Chemical Engineering Journal (Amsterdam, Netherlands), 2007. **132**(1-3): p. 85-95.
237. Sarmiento, B., J.J. Brey, I.G. Viera, A.R. Gonzalez-Elipe, J. Cotrino and V.J. Rico, *Hydrogen production by reforming of hydrocarbons and alcohols in a dielectric barrier discharge.* Journal of Power Sources, 2007. **169**(1): p. 140-143.
238. Lanz, D.P., *DBD (dielectric barrier discharge) NTP (nonthermal plasma) apparatus for treatment of volatile organic compounds (VOC) in industrial air emission*. 2008, Air Phaser Environmental Ltd., CA. WO. p. 51pp.
239. Kim, H.H., A. Ogata and S. Futamura, *Atmospheric plasma-driven catalysis for the low temperature decomposition of dilute aromatic compounds.* Journal of Physics D-Applied Physics, 2005. **38**(8): p. 1292-1300.
240. Kim, H.H., S.M. Oh, A. Ogata and S. Futamura, *Decomposition of benzene using Ag/TiO_2 packed plasma-driven catalyst reactor: influence of electrode configuration and Ag-loading amount.* Catalysis Letters, 2004. **96**(3-4): p. 189-194.
241. Kim, H.H., S.M. Oh, A. Ogata and S. Futamura, *Decomposition of gas-phase benzene using plasma-driven catalyst (PDC) reactor packed with Ag/TiO2 catalyst.* Applied Catalysis B: Environmental, 2005. **56**(3): p. 213-220.
242. Kim, S.C. and Y.N. Chun, *Reforming characteristics for hydrogen production using plasmatron.* Journal of Industrial and Engineering Chemistry, 2007. **13**(4): p. 523-529.
243. Martin, L., S. Ognier, E. Gasthauer, S. Cavadias, S. Dresvin and J. Amouroux, *Destruction of Highly Diluted Volatile Organic Components (VOCs) in Air by Dielectric Barrier Discharge and Mineral Bed Adsorption.* Energy & Fuels, 2008. **22**(1): p. 576-582.
244. Keras, A.D., *Dielectric barrier discharge cell with hermetically sealed electrodes,*

apparatus and method for the treatment of odor and volatile organic compound contaminants in air emissions, and for purifying gases and sterilizing surfaces. 2006, Iono2X Engineering, L.L.C., Woodland, WA, US: US 20060251550. p. 19pp.
245. Ognier, S., S. Cavadias and J. Amouroux, *Aromatic VOC removal by formation of microparticles in pure nitrogen discharge barrier discharge.* Plasma Processes and Polymers, 2007. **4**(5): p. 528-536.
246. Yamagata, Y., K. Niho, K. Inoue, H. Okano and K. Muraoka, *Decomposition of volatile organic compounds at low concentrations using combination of densification by zeolite adsorption and dielectric barrier discharge.* Japanese Journal of Applied Physics, Part 1 Regular Papers, Brief Communications & Review Papers, 2006. **45**(10B): p. 8251-8254.
247. Sakoda, T., K. Imagawa and K. Furukawa, *Surface modification of molding silica gel using dielectric barrier discharge.* Transactions of the Materials Research Society of Japan, 2003. **28**(2): p. 209-213.
248. Sakoda, T., S. Maeda, K. Nishihara and K. Furukawa, *Surface treatment of powdery silica gel using a dielectric barrier discharge.* Transactions of the Materials Research Society of Japan, 2002. **27**(3): p. 483-486.
249. Nimlos, M.R., S.J. Blanksbby, X. Qian, M.E. Himmel and D.K. Johnson, *Mechanisms of glycerol dehydration* Journal of Physic and Chemistry A., 2006. **110**: p. 6145-6156.
250. Duquenne, C., A. Ulgen, S. Sabater, W.F. Holderich, J.L. Dubois and J. Kervennal, *A new process for glycerol transformation to acrolein.* Abstracts of Papers, 234th ACS National Meeting, Boston, MA, United States, August 19-23, 2007, 2007: p. IEC-020.
251. McMurry, J., *Organic Chemistry*. 2nd ed. 1988, Belmont: Brooks/Cole Publishing Companry.
252. Liu, C.-j. and J.-j. Zou, *Hydrolysis of starch catalyzed by dielectric barrier discharge plasma and the definition of plasma acid.* Journal of Tianjin University, 2004. **37**(3): p. 189-192.
253. Zou, J.-j. and C.-j. Liu, *Acidic characteristic of plasma chemistry.* 中国科技论文在线, 2004: p. 1-11.
254. Nimlos, M.R., S.J. Blanksby, X.H. Qian, M.E. Himmel and D.K. Johnson, *Mechanisms of glycerol dehydration.* Journal of Physical Chemistry A, 2006. **110**(18): p. 6145-6156.
255. Kiselev, V.D., E.A. Kashaeva, A.V. olotov, I.I. Shakirova and A.I. Konovalov, *Energy and volume activation parameters of the retro-Diels-Alder reaction in different solvents.* Russian Chemical Bulletin, International Edition, 2009. **58**(1): p. 21-24.
256. Malz, R.E., *Catalysis of Organic Reaction*. 1996, New York: Marcel Dekker, Inc.
257. Gayubo, A.G., A.T. Aguayo, A. Atutxa, R. Aguado, M. Olazar and J. Bilbao, *Transformation of oxygenate components of biomass pyrolysis oil on a HZSM-5 zeolite. II. Aldehydes, ketones, and acids.* Industrial & Engineering Chemistry

Research, 2004. **43**(11): p. 2619–2626.
258. Locke, B.R., M. Sato, P. Sunka, M.R. Hoffmann and J.S. Chang, *Electrohydraulic discharge and nonthermal plasma for water treatment.* Industrial & Engineering Chemistry Research, 2006. **45**(3): p. 882-905.
259. Guo, Y., X. Liao and D. Ye, *Detection of hydroxyl radical in plasma reaction on toluene removal.* Journal of Environmental Sciences, 2008. **20**(12): p. 1429-1432.
260. Decroocq, D., *Catalytic cracking of heavy petroleum fractions*. 1984, Houston, Texas: Gulf Publishing Company.
261. Dubois, J.-L., C. Duquenne and W. Hoelderlich, *Preparation of acrolein by dehydrating glycerol in the presence of molecular oxygen*. 2006, Arkema France, Fr.: WO 2006087083. p. 25pp.
262. Tanabe, K., *Solid Acids and Bases: their catalytic properties*. Studies in Surface Sciences and Catalysis. 1989, Tokyo: Elsevier.
263. Khan, M.A. and A.A. Al-Jalal, *Enhanced decoking of a coked zeolite catalyst using a glow discharge in Al-O_2 gas mixture.* Applied Catalysis A: General, 2004. **272**: p. 141-149.
264. Blin-Simiand, N., P. Tardiveau, A. Risacher, F. Jorand and S. Pasquiers. *Removal of 2-heptanone by dielectric barrier discharges - The effect of a catalyst support*. 2005: Wiley-V C H Verlag Gmbh.
265. Demidiouk, V. and J.O. Chae, *Decomposition of volatile organic compounds in plasma-catalytic system.* IEEE Transactions on Plasma Science, 2005. **33**(1, Pt. 2): p. 157-161.
266. Francke, K.P., H. Miessner and R. Rudolph, *Plasmacatalytic processes for environmental problems.* Catalysis Today, 2000. **59**(3-4): p. 411-416.
267. Subrahmanyam, C., A. Renken and L. Kiwi-Minsker. *Novel catalytic non-thermal plasma reactor for the abatement of VOCs*. 2007: Elsevier Science Sa.
268. Cha, M.S., S.M. Lee, K.T. Kim and S.H. Chung, *Soot suppression by nonthermal plasma in coflow jet diffusion flames using a dielectric barrier discharge.* Combustion and Flame, 2005. **141**(4): p. 438-447.
269. Mawhinney, D.B. and J.T. Yates, *FTIR study of the oxidation of amouphous carbon by ozone at 300K --Direct COOH formation.* Carbon, 2001. **39**: p. 1167-1173.
270. Deitz, V.R. and J.L. Bitner, *Interaction of ozone with adsorbent charcoal.* Carbon, 1973. **11**(6): p. 681-681.
271. Takeuchi, T. and T. Itoh, *Removal of ozone from air by activated carbon treatment.* Separation Science and Technology, 1993. **3**: p. 168-175.
272. Pieck, C.L., C.R. Vera, C.A. Querini and J.A. Parera, *Differences in coke burning-off from Pt-Sn/Al_2O_3 catalyst with oxygen or ozone.* Applied Catalysis A: General, 2005. **278**(2): p. 173-180.
273. Silva, A.O.S., M.J.B. Souza, J.M.F.B. Aquino, V.J. Fernandes and A.S. Araújo, *Coke removal of the HZSM-12 zeolite with different silica/alumina ratio.* Journal of Thermal Analysis and Calorimetry, 2004. **75**(2): p. 699-704.
274. Hammon, U., J. Meschke, U. Rauh, K.J. Müller-engel, P. Schlemmer and V.

Schliephake, *Safe operation of a continuous heterogeneously catalyzed gas-phase partial oxidation of at least one organic compound*. 2004, BASF, Aktiengesellschaft, Ludwigshafen, DE: US 20040015012. p. 9 pp.
275. Bayraktar, O. and E.L. Kugler, *Characterization of coke on equilibrium fluid catalytic cracking catalysts by temperature-programmed oxidation.* Applied Catalysis A: General, 2002. **233**(1-2): p. 197-213.
276. Falkenstein, Z., *Effects of the O2 concentration on the removal efficiency of volatile organic compounds with dielectric barrier discharges in Ar and N_2.* Journal of Applied Physics, 1999. **85**(1): p. 81-89.
277. Mok, Y.S., D.J. Koh, D.N. Shin and K.T. Kim, *Gaseous ozone decomposition using a nonthermal plasma reactor with adsorbent and dielectric pellets.* Korean Journal of Chemical Engineering, 2009. **26**(6): p. 1613-1619.
278. Bogaerts, A., *Effects of oxygen addition to argon glow discharges: A hybrid Monte Carlo-fluid modeling investigation.* Spectrochimica Acta Part B: Atomic Spectroscopy, 2009. **64**(11-12): p. 1266-1279.
279. Marsh, H., E. O'HAIR, R. Reed and W.F.K. Wynne-Jones, *Reaction of Atomic Oxygen with Carbon.* Nature, 1963. **198**: p. 1195 - 1196
280. Pattabiraman, P., N.M. Rodriguez, B.Z. Jang and R.T.K. Baker, *A study of the interaction of atomic oxygen with various carbonaceous materials.* Carbon, 1990. **28**(6): p. 867-878.
281. Blackwood, J.D. and F.K. McTaggart, *The oxidation of carbon with atomic oxygen.* Australian Journal of Chemistry, 1958. **12**(2): p. 114-121.
282. Smith, D.M. and A.R. Chughtai, *The surface structure and reactivity of black carbon.* Colloids and Surfaces A: Physicochemical and Engineering Aspects, 1995. **105**(1): p. 47-77.
283. Khan, M.A. and A.M. Al-Jalal, *Cumulative contributions of 3s-np (n >= 3) transitions in comparing O atom densities in low-pressure Ar-O_2 and He-O_2 glow discharges.* Applied Physics Letters, 2006. **89**(171501): p. 1-3.
284. Dusenbury, J.S. and F.S. Cannon, *Advanced oxidant reactivity pertaining to granular activated carbon beds for air pollution control.* Carbon, 1996. **34**(12): p. 1577-1589.
285. Teranishi, K., N. Shimomura, S. Suzuki and H. Itoh, *Development of dielectric barrier discharge-type ozone generator constructed with piezoelectric transformers: effect of dielectric electrode materials on ozone generation.* Plasma Sources Science & Technology, 2009. **18**(4): p. 10.
286. Sung, Y.M. and T. Sakoda, *Optimum conditions for ozone formation in a micro dielectric barrier discharge.* Surface & Coatings Technology, 2005. **197**(2-3): p. 148-153.
287. Khan, M.A. and A.A. Al-Jalal, *Enhanced decoking of a coked zeolite catalyst using a glow discharge in Ar-O2 gas mixture.* Applied Catalysis A: General, 2004. **272**: p. 141-149.
288. Holzer, F., U. Roland and F.D. Kopinke, *Combination of non-thermal plasma and heterogeneous catalysis for oxidation of volatile organic compounds Part 1.*

Accessibility of the intra-particle volume. Applied Catalysis B: Environmental, 2002. **38**(3): p. 163-181.
289. Snyder, H.R. and G.K. Anderson, *Effect of air and oxygen content on the dielectric barrier discharge decomposition of chlorobenzene.* IEEE Transactions on Plasma Science, 1998. **26**(6): p. 1695-1699.
290. Okumoto, M.H.H.K.T., K. Katsura, S. Mizuno, A. , *Reactivity of methane in nonthermal plasma in the presence of oxygen and inert gases at atmospheric pressure.* IEEE Transactions on Industry Applications, 2001. **37**(6): p. 1618-2001.
291. Khan, M.A. and A.M. Al-Jalal, *Cumulative contributions of 3s-np (n >= 3) transitions in comparing O atom densities in low-pressure Ar-O_2 and He-O_2 glow discharges.* Applied Physics Letters, 2006. **89**(17).
292. Khan, M.A. and A.M. Al-Jalal, *Dissociation of O_2 in low pressure glow discharges in He-O_2, Ne-O_2, and Ar-O_2 gas mixtures.* Journal of Applied Physics, 2008. **104**(12).
293. Al-Jalal, A.M. and M.A. Khan, *Optical Emission and Raman Spectroscopy Studies of Reactivity of Low-Pressure Glow Discharges in Ar-O_2 and He-O_2 Gas Mixtures with Coked Catalysts.* Plasma Chemistry and Plasma Processing, 2010. **30**(1): p. 173-182.
294. Pieck, C.L., E.L. Jablonski and J.M. Parera, *Regeneration of coked Pt-Re/Al_2O_3 catalyst by burning with oxygen and ozone*, in *Catalyst Deactivation*, B. Delmon and G.F. Froment, Editors. 1994, Elsevier Science Publ B V: Amsterdam. p. 289-295.
295. Parera, J.M., E.M. Traffanoa, J.C. Mussoa and C.L. Pieck, *Hydrogen and Oxygen Spillover on Pt/Al_2O_3 During Naphtha Reforming.* Studies in Surface Science and Catalysis, 1983. **17**(101-108).
296. Li, C.e. and T.C. Brown, *Temperature-programmed oxidation of coke deposited by 1-octene on cracking catalysts.* Energy and Fuels, 1999. **13**(4): p. 888–894.
297. Liu, C.J., G.P. Vissokov and B.W.L. Jang, *Catalyst preparation using plasma technologies.* Catalysis Today, 2002. **72**(3-4): p. 173-184.
298. Kizling, M.B. and S.G. Jaras, *A review of the use of plasma techniques in catalyst preparation and catalytic reactions.* Applied Catalysis A: General, 1996. **147**: p. 1-21.
299. Halverson, D.E. and D.L. Cocke, *Ruthenium impregnation of plasma grown alumina films.* Journal of Vacuum Science & Technology A, 1989. **7**(1): p. 40-49.
300. Khan, H.R. and H. Frey, *RF plasma spray deposition of LaMOx (M-equivalent-to-Co, Mn, Ni) films and the investigations of structure, morphology and the catalytic-oxidation of CO and C_3H_8.* Journal of Alloys and Compounds, 1993. **190**(2): p. 209-217.
301. Vissokov, G.P., *On the plasma-chemical synthesis and/or regeneration of ultradispersed catalysts for ammonia production.* Catalysis Today, 2002. **72**(3-4): p. 197-203.
302. Sugiyama, K., G. Anan, T. Shimada, T. Ohkoshi and T. Ushikubo, *Catalytic ability of plasma heat-treated metal oxides on vapor-phase Beckmann*

rearrangement. Surface & Coatings Technology, 1999. **112**(1-3): p. 76-79.
303. Sugiyama, K., Y. Nakano, H. Aoki, Y. Takeuchi and T. Matsuda, *High-speed preparation of metal oxide fine powders by microwave cold plasma heating.* Journal of Materials Chemistry, 1994. **4**: p. 1497-1501.
304. Zhang, Y., W. Chu, W. Cao, C. Luo, X. Wen and K. Zhou, *A plasma-activated Ni/α-Al_2O_3 catalyst for the conversion of CH_4 to syngas.* Plasma Chemistry and Plasma Processing, 2000. **20**(1): p. 137-144.
305. Maesen, T.L.M., D.S.L. Bruinsma, H.W. Kouwenhoven and H. Van Bekkum, *Use of radiofrequency plasma for low-temperature calcination of zeolites.* Journal of the Chemical Society. Chemical communications, 1987. **17**: p. 1284-1285.
306. Yagodovskaya, T.V. and V.V. Lunin, *Surface modification of cements and zeolite catalysts by glow discharge.* Zhurnal Fizicheskoi Khimii 1997. **71**(5): p. 775-786.
307. Davis, R.J. and M. Boudart, *Structure of supported PdAu clusters determined by X-ray absorption spectroscopy.* Journal of Physical Chemistry, 1994. **98**(21): p. 5471-5477.
308. Diamy, A.-M., Z. Randriamanantenasoa, J.-C. Legrand, M. Polisset-Thfoin and J. Fraissard, *Use of a dihydrogen plasma afterglow for the reduction of zeolite-supported gold-based metallic catalysts.* Chemical physics Letters, 1997. **269**: p. 327-332.
309. Guo, Y.F., D.Q. Ye, K.F. Chen, J.C. He and W.L. Chen, *Toluene decomposition using a wire-plate dielectric barrier discharge reactor with manganese oxide catalyst in situ.* Journal of Molecular Catalysis A: Chemical, 2006. **245**(1-2): p. 93-100.
310. Krump, H., M. Simor, I. Hudec, M. Jasso and A.S. Luyt, *Adhesion strength study between plasma treated polyester fibres and a rubber matrix.* Applied Surface Science, 2005. **240**(1-4): p. 268-274.
311. Veprek, S., *Preparation of inorganic materials, surface treatment, and etching in low pressure plasmas: present status and future trends.* Plasma Chemistry and Plasma Processing, 1989. **9**(1, Suppl.): p. 29S-54S.
312. Ogata, A., H.-H. Kim and S. Futamura, *Direct activation of catalyst-surface by nonthermal plasma.* Catalysts & Catalysis, 2005. **47**(6): p. 491-493.
313. Amouroux., *interaction between a condensed target and a non-equilibrium plasma: acid-base reactions at the interface.* Scanning Microscopy, 1987. **1**(4): p. 1575-1592.
314. Yu, K.-L., Q. Xia, C.-J. Liu, G. Li, B. Eliasson and B. Xue. *On the plasma enhanced Bronsted acidity of solid acids*. in *Proceedings of 4th International Symp. On Green Chem. In China (Prt 1)*. 2001. Jinan.
315. Liu, C.J., K.L. Yu, Y.P. Zhang, X.L. Zhu, F. He and B. Eliasson, *Characterization of plasma treated Pd/HZSM-5 catalyst for methane combustion.* Applied Catalysis B: Environmental, 2004. **47**(2): p. 95-100.
316. Quantachrome, *User manual for ChemBET Pulsar TPR/TPD*. 2008, Quantachrome Instrument (Boynton Beach, Florida, USA). p. 94-96.
317. Lowell, S., J.E. Shields, M.A. Thomas and M. Thommes, *Characterization of*

porous solids and powders: Surface area, pore size and density Particle Technology Series, ed. B. Scarlett. 2004, Dordrecht, the Netherlands: Springer.
318. Varisli, D., T. Dogu and G. Dogu, *Novel mesoporous nanocomposite WO_x-silicate acidic catalysts: Ethylene and diethylether from ethanol.* Industrial & Engineering Chemistry Research, 2009. **48**: p. 9394-9401.
319. Baca, M., E.d.l. Rochefoucauld, E. Ambroise, J.-M. Krafft, R. Hajjar, P.P. Man, X. Carrier and J. Blanchard, *Characterization of mesoporous alumina prepared by surface alumination of SBA-15.* Microporous and Mesoporous Materials, 2007. **110**(2-3): p. 232-241.
320. Yan, X.-M. and a. Jia-Heng Lei, , Dan Liua, Yang-Chun Wua and Wei Liu, *Synthesis and catalytic properties of mesoporous phosphotungstic acid/SiO_2 in a self-generated acidic environment by evaporation-induced self-assembly.* Materials Research Bulletin, 2007. **42**(11): p. 1905-1913.
321. Chakraborty, B. and B. Viswanathan, *Surface acidity of MCM-41 by in situ IR studies of pyridine adsorption.* Catalysis Today, 1999. **49**: p. 253-260.
322. Sakthivel, R., H. Prescotta and E. Kemnitz, *WO_3/ZrO_2: a potential catalyst for the acetylation of anisole.* Journal of Molecular Catalysis A: Chemical, 2004. **223**(1-2): p. 137-142.
323. Musthofa, M., A.H. Karim, N.A. Fadzlillaah, N.H.R. Annuar, A.A. Jalil and S. Triwahyono, *Determination of Lewis and Brönsted acid sites by gas flow-injection technique.* Journal of Fundamental Sciences, 2010. **6**(2): p. 127-131.
324. Wu, Y., X.K. Ye, X.G. Yang, X.P. Wang, W.L. Chu and Y.C. Hu, *Heterogenization of heteropolyacids: A general discussion on the preparation of supported acid catalysts.* Industrial & Engineering Chemistry Research, 1996. **35**(8): p. 2546-2560.
325. Wang, X., X. Ye and Y. Wu, *Interaction between 12-Silicotungstic acid (SiW_(12)) and γ-Al_2O_3 surface.* Chinese Journal of Catalysis, 1996. **17**(2): p. 149-152.
326. Gieshoff, J. and J. Lang, *Process for the plasma-catalytic production of ammonia*. 2002, Degussa-Huls Aktiengesellschaft (Frankfurt am Main, DE) United States.
327. Kameoka, S., M. Kuroda, K. Aoyagi, S. Ito and K. Kunimori, *Formation of novel Al_2O_3 surface (Al-O-star) by plasma-excited nitrogen and its catalytic application - production of ammonia and oxygen from nitrogen and water.* Applied Surface Science, 1997. **121**: p. 351-354.
328. Industries. *Material Safety Data Sheet*. Available from: www.stewartsusa.com/index_files/GlycerinMSDS.pdf.
329. Industries. *Material Safety Data Sheet.*; Available from: http://www.biodieselgear.com/documentation/MSDS_Glycerol.pdf.
330. Yaws, C.L., P. Narasimhan and C. Gabbula, *Yaws' Handbook of Antoine Coefficients for Vapor Pressure (2nd Electronic Edition)*. 2009.
331. *The Dortmund Data Bank*. [cited 2010] ; Available from: *<http://www.ddbst.com/en/online/Online_Calc_vap_Form.php?component=Water>*.
332. Yaws, C.L., *Chemical Properties Handbook*. 1999, McGraw-Hill. p. 288-313.

333. Quantachrome, *User manual for ChemBET Pulsar TPR/TPD*. 2008, Quantachrome Instrument (Boynton Beach, Florida, USA). p. 36.

Vita

Lu Liu (Shirley) was born in Fuzhou, Fujian, China, where she received her early education prior to college. In 2000, she was admitted by one of the top universities in China, Tongji University, Shanghai. She received her Bachelor's degree in Applied Chemistry in 2004. Afterwards, she took an internship position at the Institute of Biotechnology in Fuzhou University and began preparing for the application of overseas study. In Fall of 2005 she started her graduate study in Biosystems Engineering at the University of Tennessee, Knoxville. She completed a Master's degree in December 2007, and generated the thesis "Applied Fourier Transform Near-Infrared Techniques for Biomass Compositional Analysis". She has been working towards her PhD since 2008, and this dissertation is the output of her PhD work.